UNIVERSIDAD COMPLUTENSE DE MADRID
FACULTAD DE CIENCIAS QUÍMICAS

TESIS DOCTORAL

A Mechanical Insight into the Stability of the Chemical Bond

Una perspectiva mecánica sobre la estabilidad del enlace químico

MEMORIA PARA OPTAR AL GRADO DE DOCTOR

PRESENTADA POR

Álvaro Lobato Fernández

Directores

Valentín García Baonza
Mercedes Taravillo Corralo

Madrid

A Mechanical Insight into the Stability of the Chemical Bond

Una perspectiva mecánica sobre la estabilidad del enlace químico

Álvaro Lobato Fernández

Facultad de Ciencias Químicas
Dpto. de Química-Física
Universidad Complutense de Madrid
Madrid 2019

Directores:
Valentín García Baonza
Mercedes Taravillo Corralo

Universidad Complutense de Madrid
Facultad de Ciencias Químicas
Dpto. de Química-Física

Madrid 2019

A Mechanical Insight into the Stability of the Chemical Bond

Una perspectiva mecánica sobre la estabilidad del enlace químico

Memoria para optar al grado de Doctor presentada por

Álvaro Lobato Fernández

Directores:
Valentín García Baonza
Mercedes Taravillo Corralo

Acknowledgments

The author is fully grateful to the “Ministerio of Educación, Cultura y deporte” for the financial support from FPU grant no. FPU13/ 05731. This work was also supported by MICINN and MINECO through the following projects: CTQ2015-67755-C2-R and MAT2015-71070-REDC. The Grant UCM-GR17-910481 from the Universidad Complutense de Madrid is also acknowledged.

Index

Abstract

This PhD was devoted to demonstrating that the nature and intrinsic features of a given pairwise interaction (covalent, electrostatic, van der Waals, etc.) defines a suitable framework to relate both molecular and bulk properties. To reach this goal, we have considered classical, well-established concepts from the field of condensed matter and translated them into the molecular realm, and vice versa.

Pairwise interactions rest on the idea that the physical and chemical properties of a system can be accurately described considering only the potential energy curve between the neighbor atoms or, in other words, how the energy changes with the distance between the interacting particles. Several authors have demonstrated that the shape of the potential energy curve can be considered universal regardless that we consider a molecule or a crystal, implying that its general characteristics are also universally applicable and transferable from one system to the others. This procedure has been profusely applied in chemistry and physics of the solid state, but it has important the important limitation that to transfer the characteristic parameters it is required to fit specific experimental properties. In other words, the shape of the interaction potential is universal, but the characteristic parameters are not. Developing a methodology capable of providing truly universal parameters is one of the major challenges of this PhD thesis and one of its underlying motivations.

Commonly used potential functions include those classical of Lennard-Jones, Born-Mayer and Mie-Grüneisen, or others borrowed from spectroscopy, like Rydberg, Morse and Sutherland. And an example of the success of considering the universality of the potential energy curve was provided in the introduction chapter of this PhD memo with the model relating the stretching force constant of diatomic molecules with the bulk modulus of their ionic, metallic and covalent counterpart crystals. The key ideas to put forward such relationship were: to assume that the distance dependence of the diatomic stretching force constant can be universally described, and that they can accurately describe the interaction between the same atoms in the crystal. These two assumptions can be only fulfilled if the pairwise potential shape is universal and its parameters can be universally transferred between molecules and crystals.

The previous observations constitute by themselves quite a striking result and indicate that some well-established concepts in the field of condensed matter at high-pressure can be translated into the molecular realm. Special attention deserves the idea that under tensile conditions (negative pressure) the

interaction in a liquid or solid suddenly vanishes due to a mechanical instability, which is consequence of the intrinsic anharmonicity of the interaction potential. In this regard, our group has extensively demonstrated along two decades that such rupture conditions, also called the spinodal instability, represents an excellent reference to describe the thermodynamic equation of state and the mechanical behavior of crystals and liquids under pressure (positive and negative). Polymers, metals, covalent and ionic crystals have been analyzed under this approach, showing that their pressure-volume (p-V) data can be accurately and universally represented through the so-called spinodal equation of state. From the point of view of Thermodynamics, the spinodal limit is defined by the condition of a zero second derivative of the energy respect to the volume (zero bulk modulus or divergence of the isothermal compressibility) and corresponds to the maximum negative pressure which the systems can withstand before breaking.

In condensed systems, approaching the spinodal limit requires the application of a homogeneous and simultaneous expansion of the system in all three dimensions. Although this is a very challenging experimental task, it is still feasible to induce tensions in liquids and local superheating in crystals. However, it is somewhat surprising that, being experimentally much simpler to produce stresses in mono- and two-dimensional systems (graphene and nanotubes are the most fashionable examples) the spinodal condition has not been considered so far as a reference in this scenario. In the course of this PhD Thesis, two related studies have been carried out on two-dimensional systems in order to validate our ideas in a different context: i) the limit of mechanical stability associated with the friction between graphene layers and ii) the effect of negative pressure (stress) in laminar materials. Nevertheless, these are not included here in order to preserve the scope of this PhD Thesis.

In any case, since the properties of bulk systems can be represented by summing up pairwise interactions -by virtue of the Clausius' virial theorem- the characteristics and properties of the (energy-volume) curve must recall those of the one-dimensional potential energy curve. Under this simplified view, the rupture limit of a one-dimensional interaction must be determined by the same conditions than in the bulk, but considering the distance, force and stretching force constant instead of the volume, pressure and bulk modulus, respectively.

This hypothesis was corroborated analyzing the temperature dependence of the longitudinal optical phonon ω_{LO} (*i.e.* the temperature dependence of the spring force constant) of some diatomic solids. The value of ω_{LO} is mainly

determined by the spring force constant of the diatomic like atoms involved in the vibration, and therefore can be determined by the one-dimensional pair potential energy function between them. In terms of a pairwise interaction the stretching force constant can be expressed as the ratio between the spinodal force and distance difference between the equilibrium and the spinodal values. We assume a Mie-Grüneisen type potential, although the formalism is equivalent in other functional forms. In order to evaluate the temperature dependence, we refer all the frequencies to a given value and assume that the spinodal force and distance temperature dependence was the same as their bulk spinodal pressure and volume analogs which are described by the equation of state developed in our group. Nicely our model was not only able to reproduce the temperature softening of ω_{LO}, but also to separate the so called intrinsic and extrinsic contributions, which was a controversial problem in solid state physics.

These results had a profound impact on this PhD thesis, because the idea that a one-dimensional potential energy curves display a rupture (spinodal) point, means that chemical bonds -or other bonding interactions of any kind- also break at a given distances that can be straightforwardly determined from the potential energy functions. To the best of our knowledge, this idea has never been considered so far, despite its evident implications in the understanding of reactive processes as well as to determine the stability range of potential novel materials and new molecular compounds. We should not forget that we are facing the possibility of establishing a criterion for defining the conditions under which bonds are formed or broken, and under what conditions these bonds will or will not be stable from a mechanical point of view and, according to the conclusions of this PhD Thesis, also from an electronic and chemical points of view.

At this point, it should be mentioned that despite the suitability of the spinodal criterion as a reference in condensed phases, its existence is nothing more than a conjecture, since the spinodal conditions cannot be reached experimentally (with the notable exception of the critical point in fluids) due to nucleation phenomena. For this reason, the few known data on spinodal parameters so far are based on extrapolation of experimental results in supercooled liquids or in superheated solids using pulsed laser techniques.

But the above situation is even worse in the molecular field. Indeed, one of the main difficulties of this PhD thesis concerned the compilation of data able to corroborate our ideas. Along the manuscript we will see how it has been necessary to dive into spectroscopic, mechanochemical and reactivity data, as

well as to perform computational and topological analysis of the electron density, with the sole purpose to confirm that the models developed here accurately describe the chemical properties of the systems studied. For these reasons, only a few examples, although very relevant from the chemical point of view, could be analyzed in depth.

In any case, the assumption that a given interatomic interaction has a limit of stability raises interesting implications, because the effect of pressure (positive or negative) must match with that resulting from chemical interactions, or in other words, the mechanical and chemical pressures can drive the same phenomena; and this is the underlying idea in most mechanochemical studies. In fact, the analogy between mechanical and chemical pressure (forces) has influenced, and sometimes dominated, the field of Solid State Chemistry, in which the substitution of one elemental atom or ion by another (structurally compatible) induces a compression or expansion in the original unit cell, leading to development of some well-established, well-known structure-property rules. In this regard, in recent years, our group, in collaboration with the University of Oviedo, has been involved in the development and interpretation of a new quantum formalism named as DFT-Chemical Pressure. Up to now several studies has been performed showing the potential application of this methodology to study intermetallic phases, vibrational modes and chemical bonds. However, the DFT-Chemical Pressure formalism has been not so far applied to characterize molecules or high-pressure effects.

In this PhD Thesis we have used the above methodologies to show that the existence of a limit of stability for a given bond is reflected in electron density reorganizations (for instance, in covalent bonds, there is a transition between a bonding share-electron regime to a radical-type state). Furthermore, by describing chemical bonds are pairwise interactions, we have shown that bond stability limits can be calculated from available experimental data of dissociation energies and stretching force constants at equilibrium. Moreover, the study of the C-C bond evidenced that bond stability limits are indeed an intrinsic property governed by the type and nature of its main bonding interaction, and therefore it is not strongly dependent either on the external chemical effects (e.g. dispersive or negative hyperconjugation) or the stretching/compressive mechanism (chemical or mechanical).

We follow up with an analysis of non-covalent interactions to analyze whether the spinodal criterion still holds when the nature of the interaction is changed. This analysis leads us to propose the Chained Interaction conjecture, which

essentially establishes that the stability conditions of the successive interactions (covalent–>electrostatic–>van der Waals) overlap, giving rise to a natural sequence of mechanical (and electronic) instabilities close to the respective spinodal conditions. The most interesting conclusion derived from this study is that the spinodal criterion may serve to classify the type of bonding interaction present in a molecule or crystal according to the interatomic distances observed in the experiment or derived from first principles calculations.

Finally, applying again our mechanical-chemical analogy through the DFT-Chemical Pressure formalism, we have shown that the negative pressure (attractive) and positive pressure (repulsive) regions in a molecule define a picture of the molecular bonding structure which is fully compatible with the classical separation into bonds and lone pairs. This formalism also allowed us to quantify the chemical activity of the lone pairs and relate it to the electronegativity of the host atom. As a consequence, we have been able to introduce a stress-redox equivalence principle that explains two well-established phenomena typical of Solid State Chemistry, namely: (i) that a metal sublattice is expanded or contracted after hosting a non-metallic element, but maintains its original topology/structure and (ii) that during the formation of an inorganic compound, an increase or decrease of the effective charge of the anion is produced with respect to the charge already present in the interstices of the metal sublattice. Both are intrinsic mechanisms to the metal sublattice resulting from a electronegativity equalization between the host metal sublattice and the guest anions, in the line of the 1980's principle of Sanderson and Pearson.

Let us conclude this summary by emphasizing that the work developed in this PhD thesis has provided us with a unique insight into how pairwise interactions can be used to describe the main types of chemical interactions and several high-pressure phenomena. We have shown that a given chemical bond has a defined range of stability and that a limit of stability must exist, or at least it can be univocally defined. In addition, we have demonstrated that the existence of such a limit of bond stability -mechanical, chemical or both- enables us to define a convenient reference for a true universal behavior of chemical bonds.

Resumen

El objetivo central de Tesis Doctoral ha sido demostrar que las características intrínsecas de una interacción entre pares de átomos dada (covalente, electrostático, van der Waals, etc.) permite establecer un marco interpretativo excelente para relacionar las propiedades mecánicas y químicas de las moléculas y los sólidos cristalinos caracterizadas por dicho tipo de enlace. Para alcanzar este objetivo, hemos tomado como base conceptos clásicos y ampliamente aceptados en materia condensada y los hemos trasladado al campo molecular; pero en otras ocasiones hemos recorrido el camino inverso, con el objetivo de demostrar que dichos conceptos pueden ser -y lo son de hecho- intercambiables entre sistemas materiales muy dispares.

Las interacciones entre pares de átomos se fundamental en la idea de que las propiedades físicas y químicas de un sistema pueden describirse con precisión considerando sólo la curva de energía potencial entre los átomos vecinos; en otras palabras, cómo cambia la energía con la distancia entre las partículas que interaccionan. Algunos autores han demostrado en las últimas décadas que la forma de la curva de energía potencial puede considerarse universal, independientemente de que consideremos una molécula o un cristal, lo que implica que las características generales del potencial de interacción son también universalmente aplicables y transferibles de un sistema a otro. A pesar de que esta metodología se ha aplicado de forma exitosa y extensa en las áreas de la Química y la Física del Estado Sólido, tiene la limitación de que para transferir los parámetros característicos entre dos sistemas es necesario ajustar los parámetros característicos del potencial de interacción a propiedades experimentales específicas. En otras palabras, la forma del potencial de interacción es universal, pero los parámetros característicos no lo son. En consecuencia, uno de los mayores retos de esta Tesis Doctoral y una de sus motivaciones originales ha sido el de desarrollar una metodología capaz de proporcionar parámetros verdaderamente universales.

Los potenciales de interacción más comúnmente utilizados incluyen los clásicos de Lennard-Jones, Born-Mayer y Mie-Grüneisen, y otros provenientes del campo de la espectroscopia, como el Rydberg, el de Morse o el de Sutherland. Un ejemplo del éxito de considerar la universalidad de la curva de energía potencial es el descrito en el capítulo introductorio de esta memoria con el desarrollo del modelo que relaciona la constante de fuerza de moléculas diatómicas con el módulo de compresión volumétrico de sólidos cristalinos iónicos, metálicos y covalentes. Las ideas clave para justificar dicha relación estaban basadas en dos premisas: 1) que la dependencia de la distancia de la constante de la fuerza en una molécula diatómica puede ser descrita

universalmente, y 2) que se puede describir con precisión la interacción entre los mismos átomos en el sólido cristalino. Pero es importante recalcar que ambas premisas sólo pueden cumplirse si la forma potencial entre pares es universal y sus parámetros son universalmente transferibles entre moléculas y cristales.

Las observaciones anteriores constituyen por sí mismas un resultado muy relevante, y sugieren que algunos conceptos bien establecidos en el campo de la materia condensada -en concreto, aquellos empleados en el área de las altas presiones- podrían ser trasladados al campo molecular. Merece especial atención la idea de que, bajo condiciones de tensión (presión negativa) creciente, llega un momento en el que se pierde a cohesión en un líquido o sólido debido a una inestabilidad puramente mecánica, consecuencia de la naturaleza anarmónica del potencial de interacción. Dicho esto, es preciso recordar que nuestro grupo ha demostrado ampliamente – y a lo largo de más de dos décadas- que dicho límite de estabilidad mecánica, conocido como inestabilidad espinodal, representa una excelente referencia para describir la ecuación de estado termodinámica y el comportamiento mecánico de cristales y líquidos bajo presión (positiva y negativa). El estudio de polímeros, metales, cristales covalentes e iónicos utilizando este original enfoque ha demostrado que los resultados experimentales presión-volumen (p-V) pueden ser representados de manera precisa y universal a través de la denominada ecuación de estado espinodal. Desde el punto de vista de la Termodinámica, el límite espinodal está definido por la anulación de la segunda derivada de la energía con respecto al volumen (anulación del módulo de compresión volumétrico o divergencia de la compresibilidad isotérmica) y corresponde a la presión negativa máxima que los sistemas pueden soportar antes de disgregarse.

En sistemas condensados, acercarse al límite espinodal requiere la aplicación de una expansión homogénea y simultánea del sistema en las tres dimensiones. Si bien ésta es una tarea experimental muy complicada, sí es factible inducir tensiones en líquidos y sobrecalentamientos locales en sólidos. No deja de ser curioso que, siendo experimentalmente mucho más sencillo inducir tensiones en sistemas mono- y bi-dimensionales -el grafeno y los nanotubos son los sistemas de moda- la condición espinodal no ha sido considerada hasta ahora como una referencia en dichos sistemas. En el transcurso de esta Tesis Doctoral se han llevado a cabo dos estudios relacionados con sistemas bidimensionales para comprobar estas ideas en diferentes contextos: i) límite de estabilidad mecánica en relación con la fricción entre capas del grafeno y

ii) efecto de presión negativa (tensión) en materiales laminares. No obstante, estos dos estudios no se han incluido en esta memoria para mantener el enfoque de esta Tesis Doctoral.

En cualquier caso, dado que las propiedades de los sistemas volumétricos pueden obtenerse sumando interacciones por pares -en virtud del Teorema del Virial de Clausius- las características y propiedades de la curva (energía-volumen) deben ser idénticas a las de la curva de energía potencial unidimensional. En esta visión simplificada, el límite de ruptura de una interacción unidimensional debe ser determinado imponiendo las mismas condiciones que en el caso volumétrico, pero considerando ahora la distancia, la fuerza y la constante de fuerza, en lugar del volumen, presión y el módulo de compresión volumétrico, respectivamente.

Esta hipótesis fue corroborada analizando del fonón óptico longitudinal ω_{LO} de algunos sólidos diatómicos. Conviene recordar que el valor de ω_{LO} está determinado principalmente por la constante de la fuerza de los dos átomos involucrados en la vibración, y por lo tanto viene determinado por la forma funcional del potencial de interacción entre pares de átomos. Teniendo en cuenta esta aproximación, la constante de la fuerza depende de la ratio la fuerza espinodal y la diferencia entre las distancias de equilibrio y espinodal. Con el fin de simplificar al máximo el tratamiento, se utilizó un potencial de interacción de tipo Mie-Grüneisen, aunque se puede demostrar fácilmente que el formalismo es equivalente para otras formas funcionales. Para evaluar la dependencia de la temperatura de ω_{LO}, simplemente se toma el valor a una temperatura de referencia y se considera que la dependencia con la temperatura de la fuerza espinodal y la distancia interatómica era la misma que la presión espinodal y el volumen, que pueden ser calculados fácilmente mediante la ecuación de estado espinodal desarrollada en nuestro grupo. Pues bien, nuestro modelo no sólo fue capaz de reproducir fielmente la disminución de ω_{LO} al aumentar la temperatura, sino que también se pudieron discriminar las denominadas contribuciones intrínseca y extrínseca, hecho este último muy relevante, dado que la separación de ambas contribuciones constituye un tema bastante controvertido en Física del Estado Sólido.

Los dos ejemplos descritos en los párrafos precedentes tuvieron un impacto muy profundo y determinante a la hora de plantear los objetivos de esta Tesis Doctoral, puesto que la comprobación de que una curva de energía potencial unidimensional muestra un punto espinodal, significa que los enlaces químicos -o interacciones de enlace de cualquier otro tipo- también deben romperse a una distancia dada, y que debe poder determinarse directamente si se conocen

los parámetros del potencial de interacción. Hasta donde sabemos, esta idea nunca había sido considerada hasta ahora, a pesar de sus evidentes implicaciones en la comprensión de muchos procesos reactivos o en la determinación del rango de estabilidad de nuevos materiales o nuevas entidades moleculares. No olvidemos que estamos ante la posibilidad de establecer un criterio para decidir las condiciones en las que se forman o rompen enlaces y en qué condiciones dichos enlaces van a ser o no estables desde el punto de vista mecánico y, de acuerdo con las conclusiones de esta Tesis Doctoral, desde el punto de vista electrónico y químico.

Llegados a este punto, debemos reconocer que, a pesar de la idoneidad del criterio espinodal para referir el comportamiento fases condensadas, su existencia no es más que una conjetura, ya que las condiciones espinodales no se pueden alcanzar experimentalmente (con la notable excepción del punto crítico en fluidos) debido a la nucleación de la nueva fase de equilibrio, dado que estamos en un régimen de inestabilidad termodinámica o simplemente energética. En definitiva, los escasos datos de parámetros espinodales conocidos hasta el momento se basan en la extrapolación de resultados experimentales en líquidos subenfriados (bajo tensión) o sólidos sobrecalentados localmente mediante técnicas de láser pulsado.

Pero la situación anterior es aún peor en el campo molecular. De hecho, una de las principales dificultades a la hora de abordar esta Tesis Doctoral era la recopilación de datos, experimentales o computacionales, que pudieran corroborar nuestras premisas. A lo largo del manuscrito veremos cómo ha sido imprescindible analizar cuidadosamente muchos datos espectroscópicos, mecanoquímicos y de reactividad, así como realizar complejos cálculos computacionales y análisis topológicos de la densidad electrónica, con el único propósito de confirmar que los modelos desarrollados aquí describen con precisión las propiedades de los sistemas elegidos para nuestro estudio. Por ello, sólo ha sido posible analizar unos pocos ejemplos en profundidad, aunque afortunadamente se de sistemas muy relevantes desde el punto de vista químico.

En cualquier caso, la suposición de que cada interacción interatómica tiene un límite de estabilidad único y definido tiene muchas implicaciones interesantes, porque las presiones (positivas o negativas) deben tener su equivalencia en determinadas interacciones químicas; en otras palabras, las presiones mecánicas y químicas den conducir a los mismos fenómenos, y ésta es precisamente la idea subyacente en la mayoría de los estudios mecanoquímicos. De hecho, la analogía entre la presión (o fuerza) mecánica y

química ha influido, y a veces dominado, el campo de la Química de Estado Sólido, en el que la sustitución de un átomo elemental o un ion por otro (compatible estructuralmente), induce una compresión o una expansión de la celda unidad original, lo que ha permitido establecer una serie de reglas "estructura-propiedades" ampliamente utilizadas en Química. En este sentido, en los últimos años, nuestro grupo, en colaboración con la Universidad de Oviedo, ha participado en el desarrollo e interpretación de un nuevo formalismo mecano-cuántico denominado Presión Química-DFT. Hasta ahora se habían realizado varios estudios que demostraban el potencial de la aplicación de esta metodología en el estudio de fases intermetálicas, modos vibracionales y el enlace químico. Sin embargo, el formalismo de la Presión Química-DFT no había sido aplicado hasta ahora para estudiar moléculas o los efectos de alta presión.

En esta Tesis Doctoral hemos utilizado esta metodología para demostrar que la existencia de un límite de estabilidad para un enlace dado se refleja en una reorganización de la densidad electrónica (por ejemplo, en los enlaces covalentes, hay una transición desde un régimen de compartición de electrones hacia un estado de tipo radical). Además, la descripción de los enlaces químicos como interacciones entre pares nos ha permitido demostrar que los límites de estabilidad de los enlaces pueden calcularse directamente a partir de datos experimentales de las energías de disociación y de constantes de fuerza en las condiciones de equilibrio. Además, el estudio del enlace simple C-C puso de manifiesto que los límites de estabilidad de dicho enlace son una propiedad intrínseca que viene dictada únicamente por el tipo y la naturaleza del enlace (en este caso una interacción covalente). Por lo tanto, los límites de estabilidad no experimentan variaciones significativas por la presencia de interacciones químicas externos (por ejemplo, fuerzas de dispersión o hiperconjugación negativa) ni dependen del mecanismo a través del cual se produce la elongación/compresión del enlace (químico o mecánico).

Continuamos nuestro estudio con un análisis de las interacciones no-covalentes con para comprobar si el criterio espinodal sigue siendo válido cuando se cambia la naturaleza de la interacción. Este análisis nos ha llevado a proponer la conjetura de Interacciones Encadenadas que, en esencia, establece que las condiciones de estabilidad para sucesivas interacciones (covalente>electrostático>van der Waals) se superponen, dando lugar a una secuencia natural de inestabilidades mecánicas (y electrónicas) que coinciden aproximadamente con las respectivas condiciones espinodales. La conclusión más interesante de este estudio es que el criterio espinodal puede servir para

clasificar el tipo de interacción presente en un determinado enlace de una molécula, o de un cristal, tomando como único criterio de clasificación las distancias interatómicas, que pueden obtenerse de medidas estructurales o a partir de cálculos de primeros principios.

Nuestra última aportación resulta de aplicar nuevamente la analogía mecano-química a través del formalismo de la Presión Química-DFT. Así, hemos demostrado que las regiones de presión negativa (atractiva) y positiva (repulsiva) en una molécula delinean una imagen de la estructura molecular que es totalmente compatible con la separación clásica en enlaces y pares solitarios. Este formalismo también nos ha permitido cuantificar la actividad química de los pares solitarios y relacionarla con la electronegatividad del átomo huésped. Una consecuencia inmediata de estos resultados es que hemos sido capaces de introducir un principio de equivalencia "estrés-redox" capaz de explicar dos fenómenos bien establecidos en Química del Estado Sólido, a saber: i) que una subred metálica se expande o contrae después de alojar un elemento no metálico, pero mantiene su topología/estructura original, y ii) que durante la formación de un compuesto inorgánico se produce un aumento o disminución de la carga efectiva del anión con respecto a la carga ya presente en los intersticios de la subred metálica. Ambos son mecanismos intrínsecos a la subred metálica resultantes de una ecualización de la electronegatividad entre la subred metálica huésped y los aniones huésped, y que corrobora el principio de Sanderson y Pearson establecido en la década de los 1980s.

Finalizaremos este resumen haciendo especial énfasis en que el trabajo desarrollado en esta Tesis Doctoral nos ha proporcionado una visión única de cómo las interacciones entre pares pueden utilizarse para describir los principales tipos de interacciones químicas y algunos fenómenos de alta presión. Hemos demostrado que un determinado enlace químico tiene un rango de estabilidad bien definido y, además, que siempre debe existir un límite de estabilidad (o al menos se puede definir unívocamente). Además, hemos demostrado que la existencia de tal límite de estabilidad del enlace -mecánico, químico o ambos- nos permite definir una magnífica referencia para definir un verdadero comportamiento universal de los enlaces químicos.

Chapter 1

Introduction

Preliminaries

The field of application of this PhD thesis lies at the boundary between Physics and Chemistry, with the notion that pressure, positive or negative, is a fundamental magnitude for understanding and rationalizing the behavior of material systems.

Our goal is to develop interpretative models on the nature of the chemical bond in molecules, prototypical chemical reactions, and crystalline solids, by applying two basic principles: 1) the existence of a universal behavior in the conditions of stability for an interaction between two atoms (pairwise interaction), and 2) there exists a direct correspondence between mechanical (physical) and chemical pressures, both at macroscopic and microscopic levels.

From the methodological point of view, we wanted to reconcile and translate some classical ideas about pair interactions and the mechanical stability of condensed phases to the field of chemical reactivity, which is understood in terms of rupture and bond formation. However, it has often been necessary to follow the opposite reasoning. This dynamics in the rationale very likely constitutes the biggest obstacle for sorting the arguments and the results collected in this PhD thesis, but at the same time it also represents one of its most important contributions.

The Limit of Mechanical Stability

Underlying our reasoning scheme is the concept of spinodal instability, which establishes that the limit of mechanical stability can be taken as a reference to reproduce and to predict the behavior of the system when it is subjected to an external pressure, either positive or negative. This is a very well-established concept in our research group, as we have successfully used it over two decades for the development of predictive models of thermodynamic properties and the equation of state of liquids and solids. Polymers, metals, covalent and ionic crystals have been analyzed under this approach, showing that their pressure-volume (p-V) data can be accurately and universally represented through the so-called spinodal equation of state. From the point of view of Thermodynamics, the spinodal limit is defined by the condition of a zero second derivative of the energy respect to the volume (zero bulk modulus or divergence of the isothermal compressibility) and corresponds to the maximum negative pressure which the system can withstand before breaking. In condensed systems, approaching the spinodal limit requires the

application of a homogeneous and simultaneous expansion in all three dimensions. Although this is a very challenging experimental task, it is still feasible to induce tensions in liquids and local superheating in crystals. However, it is somewhat surprising that, being experimentally much simpler to produce stresses in mono- and two-dimensional systems (graphene and nanotubes are the most fashionable examples) the spinodal condition has not been considered so far as a reference in this scenario. In the course of this PhD Thesis, two related studies have been carried out on two-dimensional systems in order to validate our ideas in a different context: i) the limit of mechanical stability associated with the friction between graphene layers and ii) the effect of negative pressure (stress) in laminar materials. Nevertheless, these are listed at the end of this chapter, but are not included here in order to preserve the scope of this PhD Thesis.

But along this PhD thesis the spinodal concept reaches a renewed value when it is extended to analyze the stability limit of a chemical bond. In such scenario, the limit of stability can be determined by applying the same conditions than in the bulk, but considering the distance, force and stretching force constant instead of the volume, pressure and bulk modulus, respectively. A couple of examples demonstrating this analogy are given the next section and constitute the first genuine results in this dissertation. We advance here that these results had a profound impact on the development of this PhD thesis, because they confirm that the spinodal concept may be used to study the bonding parameters in diatomic molecules.

The notion that a diatomic potential energy curve also presents a rupture (spinodal) point can be generalized to any chemical bond in a molecule or a crystal. To the best of our knowledge, this idea has never been considered so far, despite its evident implications in the understanding of reactive processes as well as to determine the stability range of potential novel materials and new molecular compounds. Unfortunately, it must be emphasized that the spinodal conditions cannot be reached experimentally (with the notable exception of the critical point in fluids) because it implies deep metastable states and nucleation of the stable phase takes place before reaching the spinodal. Only few data on spinodal parameters have been reported so far and are based on the extrapolation of experimental results in supercooled liquids or superheated solids. The situation is even worse in the molecular field, because the highly reactive species generated after breaking a bond.

Thus, one of the main difficulties of this PhD thesis concerned the compilation of data able to corroborate our ideas. In the particular case of molecular data,

we seek for specific spectroscopic, mechanochemical and reactivity results to confirm the suitability of the models developed here. That is why a significant number of the results included in this dissertation come from rigorous quantum-mechanical calculations, modern topological analyses of the electronic density, and novel formalisms such as the DFT-Chemical Pressure. In addition, this formalism has allowed us to verify in this PhD thesis the scope and applicability of the models based on the spinodal instability as well as to put into context our results in the scope of the stability of the chemical bond and its chemical reactivity, structural inorganic chemistry, and several phenomena in the field of high pressures.

Some Supporting Results

As stated in previous sections of this introductory chapter, there are not previous results to show that the spinodal instability criterion can be applied to chemical bonds. Therefore, in this section we are summarizing two preliminary studies which demonstrate that we can translate some ideas concerning the spinodal instability that are grounded in condensed matter to the molecular field.

The first example concerns the correlation between the bulk modulus of diatomic crystals and the spring force constant derived from an interatomic potential for diatomic molecules. Let us emphasize here that many models have been put forward for correlating molecular and bulk properties through decades with different degrees of success, and that simple models considering only nearest neighbor interactions and effective pair potentials are thought to be incorrect. However, we will demonstrate below that the spinodal force (the one-dimensional analogous to the spinodal pressure) follows the same potential law in diatomics and crystals.

The spinodal pressure in bulk systems is defined as:

$$p_{sp} = -\beta \frac{B_{T0}}{B'_{T0}} \tag{1.1}$$

where p_{sp} is the spinodal pressure β is universal exponent that characterizes the divergence of the isothermal bulk modulus B_{T0} and B'_{T0} is its pressure derivative.

In the linear (molecular) case, the spinodal condition is equivalent to the definition:

$$F_{sp} = -\beta \frac{B_{T0L}}{B'_{T0L}} \tag{1.2}$$

where F_{sp} is the force defined at the inflection point of the energy-distance curve of the bond, β is a universal scaling constant, and B_{T0L} and B'_{T0L} are, respectively, the linear compression modulus and its derivative with respect to the force:

$$B_{TL} = r\frac{d^2E}{dr^2} = rk(r) \rightarrow B_{T0L} = r_e k_e \tag{1.3}$$

$$B'_{TL} = \frac{dB_{TL}}{dF} = \frac{dB_{TL}}{dr}\frac{dr}{dF} = \frac{dB_{TL}}{dr}\frac{1}{k(r)} \rightarrow B'_{T0L} = 1 + \frac{k'_e r_e}{k_e} \tag{1.4}$$

where r_e is the equilibrium distance, k_e is the spring constant, and k'_e is the derivative of the spring constant with respect to the force. Now, we may write F_{sp} as:

$$F_{sp} = -\beta \frac{r_e k_e^{\,2}}{k_e + k'_e r_e} \tag{1.5}$$

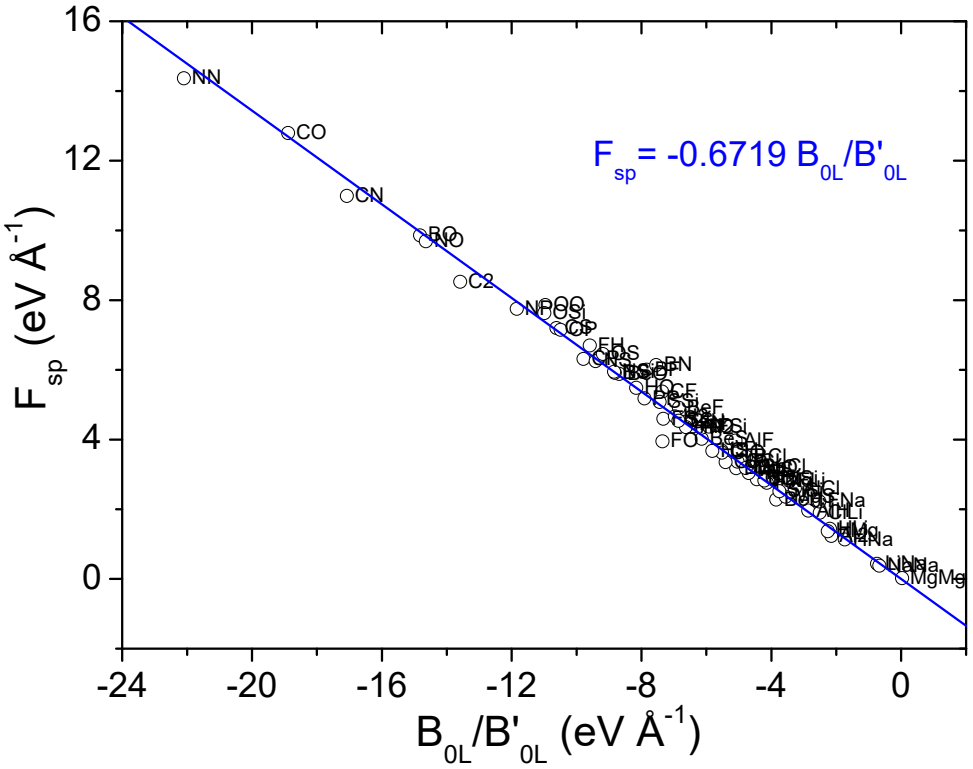

Figure 1.1. Correlation between the spinodal force and the mechanical coefficients for diatomics

Using available data for the RKR potential of diatomics as a reference, we obtain the correlation scheme shown in Figure 1.1, that demonstrates that the value of β is constant with a value close to 0.67, in excellent agreement with the value obtained in crystalline solids[1-3].

The second example deals with the temperature dependence of the longitudinal optical phonon, ω_{LO}, of diatomic solids. The value of ω_{LO} is determined by the spring force constant of the diatomic-like atoms involved in the vibration, and therefore it can be determined from a known pair potential energy function.

We will assume a Mie-Grüneisen type potential for simplicity as an effective anharmonic model for vibrations [4], although the formalism is equivalent in other functional forms. Our procedure involves linking the potential parameters to the limit of mechanical stability, a concept that has been often referred to in the literature as the Born spinodal instability condition [5]. The temperature dependencies of the characteristic potential parameters are evaluated within the Mie-Grüneisen formalism using a standard procedure borrowed from equation of state studies [6].

The generalized Mie potential is usually written as a function of the interatomic distance, r, in the form:

$$U(r) = D\frac{mn}{n-m}\left[\frac{1}{n}\left(\frac{r_e}{r}\right)^n - \frac{1}{m}\left(\frac{r_e}{r}\right)^m\right] \tag{1.6}$$

where n and m are constants characterizing the repulsive and attractive parts of the potential, respectively, D is the dissociation energy, and r_{e} is the equilibrium distance. And the quasi-harmonic frequency for the Mie potential can be written as:

$$\omega = \left(\frac{nmD}{{r_e}^2\mu}\right)^{1/2} \tag{1.7}$$

where μ is the reduced mass.

If we apply the instability condition to the Mie potential, $\mathrm{d}^2U/\mathrm{d}r^2 = 0$, which is illustrated in Figure 1.2 for the Mie (12,6) potential, the following relationship is obtained:

$$r_{sp} = r_e\left(\frac{n+1}{m+1}\right)^{\frac{1}{n-m}} \tag{1.8}$$

where r_{sp} is the internuclear distance at the limit of stability.

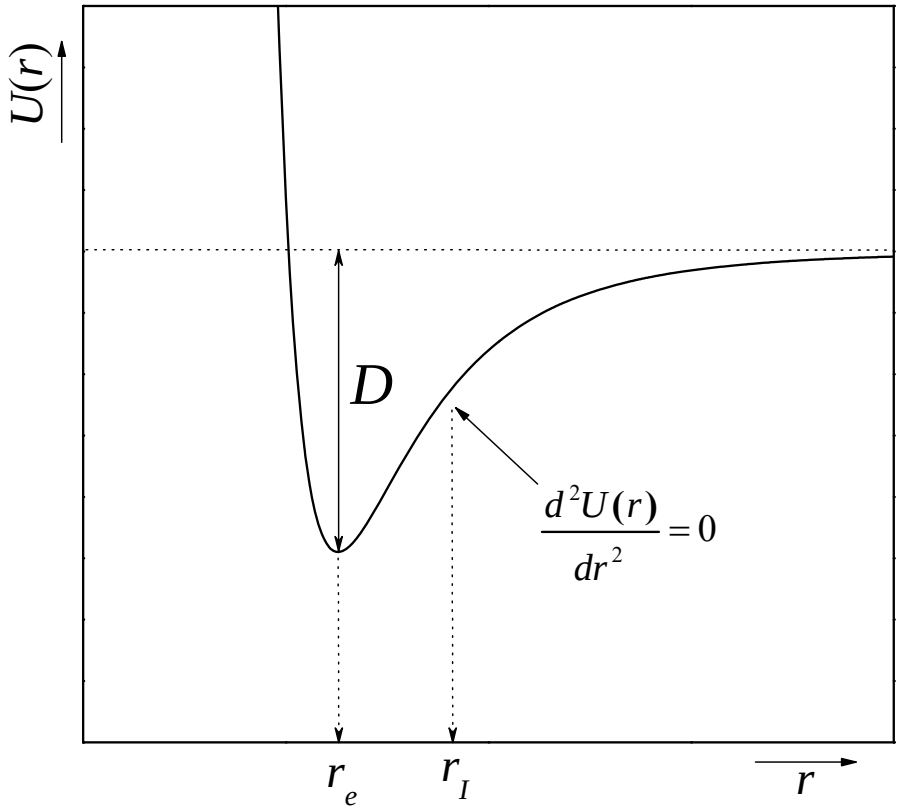

Figure 1.2. Schematic representation of the stability limit from the Mie potential. N and m has been assumed equal to 6 and 12 respectively. (See text for discussion)

The dissociation energy can be related to the force (in tension) acting on the system at the limit of stability, defined as $F_{sp} = -[dU(r)/dr]_{r=rsp}$, through the following relation,

$$F_{sp} = \frac{D}{r_e} f(n,m) \tag{1.9}$$

where $f(n,m)$ is a rather complex function of n and m whose details are of little interest here. Actually, the interesting point is that the temperature dependence of D is modulated by the changes in F_{sp} and r_e and the above expression confirms that the thermal expansion of the crystal has a two-fold effect in changing the phonon frequency. This recalls the widely assumed approximation that the temperature dependence of each phonon frequency consists of two additive contributions: the implicit contribution due to the thermal expansion of the lattice, and the explicit contribution that arises from anharmonic interactions between phonons. However, our approach accounts for both contributions simultaneously.

In order to evaluate the temperature dependence of ωLO in diamond we refer all the frequencies to a given value and assume that the spinodal force and distance temperature dependence was the same as their bulk spinodal pressure and volume analogs which are described by the spinodal equation of state[7]. Thus, the frequency can be calculated from the expression:

$$\omega(T) = \omega_{ref}\left[\frac{D(T)}{D(T_{ref})}\right]^{1/2}\left(\frac{r_e(T_{ref})}{r_e(T)}\right) \tag{1.10}$$

The force at the instability F_{sp} is the linear analog to the spinodal pressure p_S in the bulk crystal[8] and we shall use this analogy to account for the temperature dependence of F_{sp}, and the predicted values of $\omega LO(T)$ in diamond as an example of diatomic solid. Our results are compared to the experiment in Figure 1.3.

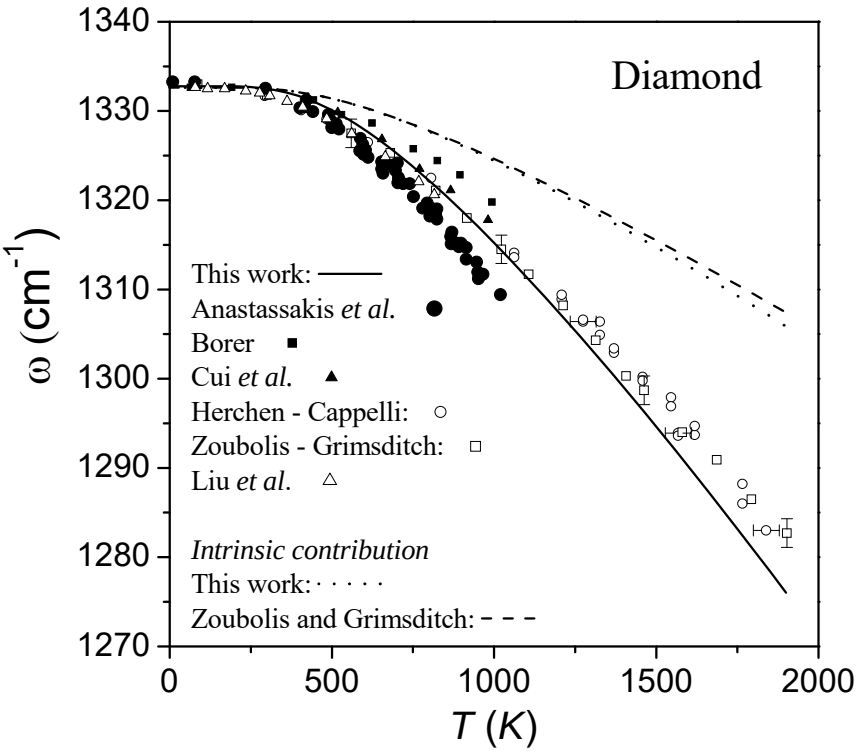

Figure 1.3. Solid line: prediction of the temperature dependence of the triply degenerate Raman-active phonon of diamond (see text). The intrinsic contribution is represented by the dashed lines.

Our model gives an excellent prediction considering the discrepancies between different experimental sources. In any case, or results demonstrate the validity of using the spinodal criterion to account for the spring force constant in diatomics.

Aims and Objectives

The aim of this PhD Thesis is demonstrating that the nature and intrinsic features of a given pairwise interaction (covalent, electrostatic, van der Waals, etc.) defines a suitable framework to relate both molecular and bulk properties. To reach this goal, we have considered classical, well-established concepts from the field of condensed matter and translated them into the molecular realm, and vice versa. Such an approach can lead to the understanding of different chemical phenomena such as bond nature, reactivity and even a pressure description of chemical interactions. More specifically, we pursue the following specific goals:

- Introduce and provide theoretical evidences that the spinodal concept can constitute an accurate reference to understand the distance range where interactions are stable.
- Provide experimental evidences of bond stability limits as well as to explore its chemical implications to detect interaction changes and reactive models.
- Demonstrate that the analogy between force and pressure can be a useful tool to understand chemical phenomena and high-pressure experiments.

Organization of this Dissertation

We have organized this dissertation into eight chapters.

This first chapter is focused on establishing the main principles on which the PhD thesis develops and summarizes some key results that support our premises.

In chapter 2, we analyze the spinodal concept in a framework of pairwise interaction and how it can be considered as a reference for defining the stability of the chemical bond in a generic manner. Both topological analyses of the electron density and electron localization function have been carried out along the (stretching) potential energy curves in order to relate the mechanical instability limit with changes in the electronic properties. In addition, considering that bonds are pairwise interactions, we will demonstrate how these limits can be determined from experimentally accessible equilibrium properties: the dissociation energy and the stretching force constant at the equilibrium distance.

Chapters 3 and 4 explore the chemical implications of the bond stability limits in two archetypical chemical bonds: C-C (Chapter 3) and OH (Chapter 4). Transition state distances, vibrational frequencies and histograms derived from structural data (equilibrium distances) for the C-C bond are used to provide some clues about the implication of our ideas into mechanochemistry and reactivity -including synthetic chemistry- since our model can be used to anticipate the stability conditions where a compound can be (meta)stable or not. Our analysis of the C-C bond finalizes evidencing the applicability of the bond stability limits as a tool to detect and to classify interaction changes and anticipates the Chained Interaction conjecture discussed in Chapter 4 using the O-H bond as a working example.

Chapters 5 and 6 are devoted to demonstrating that the recently developed formalism known as DFT-Chemical Pressure provides a reliable basis to understand some relevant chemical phenomena in molecules and crystals. More specifically, in Chapter 5 we explore what the DFT-Chemical Pressure formalism can tell us about chemical bonds and lone pairs. We provide the pressure distributions in prototypical molecules, classified according to the Valence Shell Electron Pair Repulsion (VSERP) theory where we show how chemical concepts such as lone pair activity and nucleophilic/electrophilic behavior can be quantified in terms of attractive and repulsive forces. In Chapter 6 we see how the effects of the pressure can be related to a chemical interaction to explain the formation and structural stability of inorganic solids. We introduce the equivalence between mechanical and chemical pressures to study two several phenomena with implications in Solid State Chemistry.

The main contributions of the PhD thesis are summarized in Chapter 7, and we have added Chapter 8 to elucidate and discuss some emerging directions of work in which we are already engaged and that follow the core ideas settled out of this PhD thesis.

Supplementary results and data are included in each chapter and in the amended Appendixes.

Related Publications

Manuscripts published:

- **Chemical pressure–chemical knowledge: squeezing bonds and lone pairs within the valence shell electron pair repulsion model.**

A. Lobato, H.H. Osman, M.A. Salvadó, M. Taravillo, V.G. Baonza and J.M. Recio.
Phys. Chem. Chem. Phys. 21, 12585-12596 (2019). DOI: 10.1039/C9CP00913B

- **Generalized Stress-Redox Equivalence: A Chemical Link between Pressure and Electronegativity in Inorganic Crystals**
A. Lobato, H.H. Osman, M.A. Salvadó, P. Pertierra, A. Vegas, V.G. Baonza and J.M. Recio.
Inorg. Chem. (2019). Published in ASAP. DOI: 10.1021/acs.inorgchem.9b01470

Manuscripts in preparation:

- **Bond Stability Limits: A Dual Mechanical and Electronic Perspective**
A. Lobato, J.M. Recio, M. Taravillo and V. G. Baonza.
- **Universality in the Rupture Distances of C-C Single Bonds**
A. Lobato, M. Taravillo and V. G. Baonza.
- **A Chained-Interactions Conjecture for the Chemical Bond: The Case of Hydrogen Bonding**
A. Lobato, M. Taravillo and V. G. Baonza.

The following publications are devoted to support the fundamental ideas of this thesis, but these are not included in this PhD dissertation in order to preserve the scope of the PhD Thesis.

- **Computational Modeling of Tensile Stress Effects on the Structure and Stability of Prototypical Covalent and Layered Materials**
H. Chorfi, A. Lobato, F. Boudjada, M.A. Salvadó , R. Franco , V.G. Baonza and J.M. Recio.
Nanomaterials. Manuscript ID: nanomaterials-608869.
- **Temperature effects on the friction-like mode of graphite.**
C. Menéndez, A. Lobato, V.G. Baonza and J.M. Recio.
Theor. Chem. Acc. 136, 40 (2017). DOI: 10.1007/s00214-017-2072-4
- **Anharmonicity effects in the frictionlike mode of graphite.**
C. Menéndez, A. Lobato, D. Abbasi-Pérez, J. Fernández-Núñez, V.G. Baonza and J.M. Recio.
Phys. Rev. B 93, 144112 (2016). DOI: 10.1103/PhysRevB.93.144112

References

[1] J. Ferrante, J. R. Smith, and J. H. Rose, Diatomic Molecules and Metallic Adhesion, Cohesion, and Chemisorption: A Single Binding-Energy Relation. *Physical Review Letters*, *50*, 1385-1386, **1983**. DOI: https://doi.org/10.1103/PhysRevLett.50.1385.

[2] J. R. Smith, H. Schlosser, W. Leaf, J. Ferrante, and J. H. Rose, Connection between energy relations of solids and molecules. *Physical Review A*, *39*, 514-517, **1989**. DOI: https://doi.org/10.1103/PhysRevA.39.514.

[3] J. H. Rose, J. R. Smith, and J. Ferrante, Universal features of bonding in metals. *Phys. Rev. B*, *28*, 1835-1845, **1983**. DOI: 10.1103/PhysRevB.28.1835.

[4] P. M. Morse, Diatomic Molecules According to the Wave Mechanics. II. Vibrational Levels. *Physical Review*, *34*, 57-64, **1929**. DOI: https://doi.org/10.1103/PhysRev.34.57.

[5] M. Born and K. Huang, *Dynamical Theory of Crystal Lattices*, London: Oxford University Press, **1954**.

[6] S. Eliezer, A. Ghatak, and H. Kotari, *An Introduction to Equations of State: Theory and Applications* Cambridge: Cambridge University Press, **1986**.

[7] V. G. Baonza, M. Taravillo, M. Caceres, and J. Nuñez, Universal features of the equation of state of solids from a pseudospinodal hypothesis. *Phys. Rev. B*, *53*, 1-9, **1996**. DOI: https://doi.org/10.1103/PhysRevB.53.5252.

[8] M. Taravillo, V. N. G. A. Baonza, J. E. F. Rubio, J. Núñez, and M. Cáceres, The temperature dependence of the equation of state at high pressures revisited: a universal model for solids. *Journal of Physics and Chemistry of Solids*, *63*, 1705-1715, **2002**. DOI: 10.1016/s0022-3697(01)00257-8.

Chapter 2

Bond Stability Limits

Introduction

Interaction or bond distances have been stablished as one of the mainly parameters to describe chemical interactions. Its relationship with bond dissociation energies, bond orders or bond strengths reflects the well-known chemical interconnection between geometry and properties [1,2]. However, whereas equilibrium distances have been widely studied, characterized and therefore tabulated, bond breaking distances has been little explored. A simple question such as, when a bond breaks or forms is still controversial [3,4], even though it is crucial to understand and define chemical interactions and so chemical reactivity [5-7].

Although fundamental in nature, this question is continuously repeated in different ways trough the chemical bibliography. For example, in the case of covalent chemistry it is manifested as what are the longest C-C distance? or equivalently, what is it the maximum C-C distance which can be reached without breaking its bond? [8,9]. In chemical reactions, bond ruptures distances are considered as the main parameters to characterize the mechanism along where the reaction takes places. They usually define the transition state geometry, and consequently chemical modifications can be performed to reduce the activation energy barrier, improving the reaction rate. The relevance of the bond formation and bond breaking distances also extends to supramolecular chemistry. Hydrogen bond lengths are continuously revisited trying to figure out what are the main characteristics of this union and consequently where are the distances between the covalent and weak interactions.

Of course, bond breaking (forming) processes or equivalently bond stability limits, leads the molecule to be in an unstable state, and consequently are difficult to characterize. Unstable processes generally occur in short periods of time, making its experimental detection limited [10,11]. In addition, from the point of view of theoretical chemistry, bond breaking (formation) requires an accurate description of multireference states [12,13] which sometimes are not easily accessible. Up to now, several approaches have been used to define the bond breaking and interaction distances. Specifically, the capability of electron density and related scalar fields to fully characterize intermolecular effects have shown that changes in the charge distribution can be related to bond type transitions and consequently with rupture and interactions points [refs]. recovering the chemical idea that bond breaking involves a transition from shared bonding electrons to atoms or ions.

In the same way, bond ruptures have been also studied in terms of the mechanical characteristics of the bonds. In this approach, bond breaking is defined in terms of the maximum force supported on the bond, either applied externally as in the case of the mechanochemistry [14,15] or by chemical interactions [16,17]. Accordingly, equilibrium properties and bond strength define also the unstable molecular states. To cite a few examples, through a systematic study of the potential energy stretching curves of the several molecules, Beyer demonstrates that the maximum forces and therefore breaking distances at which a given covalent bond in a molecule becomes unstable, directly depends on their dissociation energy and stretching force constant [18,19]. Likewise, Torro-Labbe introduced the idea of reaction force, realizing that the maximum force exerted on the molecule along a chemical reaction corresponds to a highly molecular distorted state where some bonds can be broken or formed [20,21]. Such a maximum force state allows the electronic reorganization and clearly depends on the equilibrium bond strength characteristics of the reactive. This view supports the chemical idea that equilibrium properties and bond strength define also the unstable molecular states.

The aforementioned approaches have evidenced that interaction and bond ruptures are produced at characteristic distances which depends on the atoms involved, as the case of the equilibrium distances. However, regardless its success, a general relationship between bond unstable states and bond properties is still lacking. In this work, we will apply a different approach to bond ruptures. Based on the analysis of the potential stretching energy curves we will show that bond stability limits are intrinsically determined in terms of the energetic characteristics of the bond. Accordingly, we define the minimum and maximum distances at which any covalent interaction could extend. Moreover, assuming a simple analytical model we provide strong evidences that unstable distances depends on the bond strength characteristics of the bond, which are universally applicable. Finally, an electronic analysis in the bond stability range of several covalent bonds let us to depict a clear connection between the unstable points of the potential energy and the chemical picture of bond ruptures based on the idea of an electron density transference form the internuclear region to the atoms.

Computational Details

All the molecular calculations has been carried out with the gaussian09 (g09) [22]. code at the CCSD level using Dunning's cc-pVTZ basis set [23].

Geometry optimizations were carried out using analytical gradients [24], according to the Berny algorithm [25]. Dissociation curves were always performed fixing the bond length and partial optimizing the rest of the coordinates. For each partial optimization we use as a guest the previous step, up to the first where the optimized geometry was used as an input. The keyword stable during the optimization was used in order to check and ensure the sanity and stability of the wavefunction.

Electron density analysis was performed using AIMALL package [26]. Electron localization function and topology was calculated using CRITIC2 code [27]. The visualization of the results was carried out with VESTA [28] and Chimera [29] software.

Equilibrium bond lengths, dissociation energies and equilibrium stretching force constants for all the optimized states are presented in Table S.2.1 of the supplementary material.

Defining Bond Stability Limits

Definition of bond stability limits requires a general criterion able to relate an energetically unstable state with some characteristic structural parameter such as the rupture distance. In this regard, all the energetic changes which characterizes a given bond are represented through their potential energy curves (PECs), and therefore its stability conditions must be somehow reflected within them. The question remains if these unstable points can be accurately determined in terms of physical and chemical backgrounds.

Let us consider a diatomic molecule, a test-bed example of a bond PEC. In this case, the bond energy depends only on the interatomic distance. At equilibrium, the bond displays a potential energy minimum and is in a stable configuration defined by its equilibrium distance (r_e) and its dissociation energy (D_e). When the bond is compressed, the energy steeply increases up to the zero–energy crossing, where it changes from negative to positive (see Figure 2.1).

In as much as, stable interactions must have a negative potential energy, if not, only the repulsive term to the energy will drive the interaction, this point can be considered as the compression stability limit of the bond. In analogy with the hard sphere potentials used in thermodynamics, we have named this zero–energy crossing distance as the hard sphere distance (r_{hs}) and can be interpreted as the closest interatomic distance at which the atoms can approach maintaining their potential energy negative. On contrary, when the

bond distance is increased, the potential energy approaches to zero asymptotically up to the limit of infinite internuclear distance, where has a value of zero.

Usually this limit has been considered as the point where the bond is totally broken and therefore no interaction between the atoms exits. Nonetheless this is not an unstable point in the PEC, but a stable configuration between two non-interacting atoms. Indeed, as manifested in typically chemical reactions, bond ruptures occur at lower distances than infinite atom separation. Hereof the stretching bond instability must occur at intermediate distances between equilibrium point and the infinitely separated atoms.

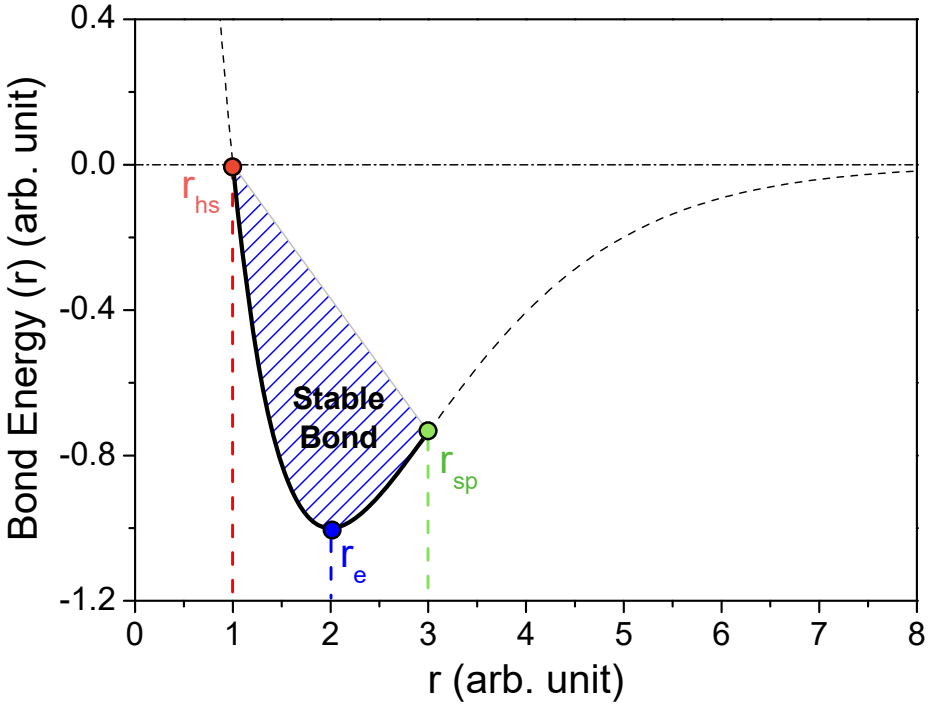

Figure 2.1. PEC of a generic diatomic bond potential. The hard sphere and the spinodal points are represented by red and green dots respectively. The stability region of the bond is displayed by the blue shaded area.

Suppose that we exert a tensile force along the diatomic bond which, for instance, can be produced by an AFM tip or an attractive chemical interaction. Under this external force, the diatomic state will move along its potential energy curve up to a distance $r > r_e$ given by the condition of total null force. To be stable, the stretched diatomic bond requires that its hessian must be positive definite, otherwise under a slight perturbation the bond internal force will not balance the external one and the system will evolve to another state with lower energy. The latter condition implies that the second

derivative of the energy respect to the distance, the stretching force constant $k(r)$, must be positive. In Figure 2.2 we have represented the force and the stretching force constant as a function of the interatomic distance for a generalized diatomic PEC. Notice that the force represented is the tensile external one and is equal to minus the internal force on the bond. As the interatomic distance increases the force increases up to a point where it is maximum. Here, the bond force constant has a value of zero and becomes negative if the bond is further elongated. This point, which corresponds to the inflexion/turning point of the PEC, represents the limit where the attractive interactions such as the nuclei-electron ones cannot balance the external tensile effects, i.e. the bond is broken.

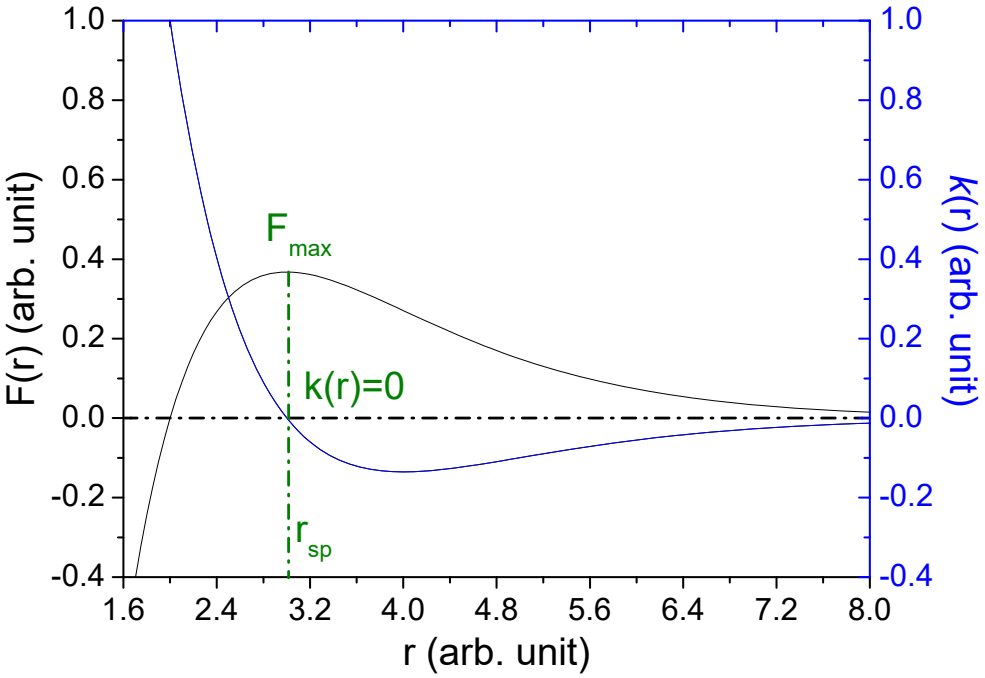

Figure 2.2. External Force (black) and stretching force constant (blue) as a function of the internuclear separation for a generic diatomic bond potential. The condition of mechanical stability limit is represented in green by the maximum force (F_{max}) and zero stretching force constant, $k(r) = 0$ condition occurring at the spinodal distance r_{sp}.

Again, a clear resemblance with the thermodynamic realm can be provided. In this field, for a one component with fix number of particles, the limit of stability, also known as the spinodal locus, is defined by the condition of zero second derivative of the internal energy respect to the volume. At this point the system is said to be mechanically unstable. The one–dimensional bond analogs of the volume and the internal energy can be considered the distance and the bond stretching energy represented by its PEC. In this regard, the

condition of zero stretching force constant must be understood as the mechanical stability limit between the stable and unstable stretching regimens. For this reason, henceforth we will refer to the diatomic rupture energy and distance as the spinodal energy, E_{sp}, and spinodal distance, r_{sp}.

In the case of a molecule, the PECs are n-dimensional representations of the energy respect to the all internal coordinates, thus bond stretching curves depends on the spatial atomic rearrangement. Nonetheless those effects can be included in the stretching potential energy curve. Accordingly, bond stability conditions in a molecule or a solid can be determined analogously as we have done to diatomic bonds giving to our model a general applicability.

Finally, it is worth to mention, that during the last decade several examples have evidenced that the spinodal point can be related to bond ruptures, although it has not been defined as it. A clear example is provided through the mechanochemistry reactions. The measured dissociation reaction forces of covalent bonds provided by force spectroscopy experiments have demonstrated that the maximum tensile effect which can be exerted on the bond is related to the maximum force obtained by the analysis of the stretching PEC.[18] However, not only force effects have been related with the spinodal constrain but also chemical processes. For instance, Toro-labbe et al [16,17] introduced the concept of reaction force and reaction force constant to study different chemical phenomena such as isomerization processes, cycloadditions and dissociation reactions. The key feature of their analysis recall in the idea that during a chemical reaction the reactive attains a maximum force state allowing the electronic rearrangement necessary to form the product. Such a maximum force state involves at least a one normal mode zero force constant and it is related with a highly distorted molecular state. Under this perspective, during a chemical process an unstable molecular state is obtained which can be interpreted as its bond stability limit.

From Bond Strengths to Bond Stability Limits

Once we have defined the stability region, it is interesting to check quantitatively the critical distances and energies displayed by the prototypical bonds. To this end, we have calculated the hard sphere and spinodal limits of the potential energy curves of 70 diatomic molecules determined from its spectroscopic parameters according to the RKR procedure[30,31]. This data covers almost any interaction type. They include single, multiple, polar covalent and ionic bonds as well different ground state multiplicities. In Table 2.1, we have summarized the critical bond stability limit distances and

energies of some representative diatomic molecules which cover the full range of interactions studied. All the computed data along with the parameters used in the RKR potentials are shown in the supplementary material 2. Critical parameters display a wide broad range of values. For instance, hard sphere and spinodal distances spreads from 1.17 to 3.21 Å and from 1.91 to 3.91 Å respectively, whereas the spinodal energies are almost 10 eV different from the lower to the highest energetically bond. The variety across the bond stability limit parameters is in concordance with the disparity in their equilibrium values and reflects the different nature of bonds studied. Nonetheless, when critical parameters are compared with their own equilibrium ones, the percentage of variation in energy and distance is roughly constant and equal to the 25 % for each bond.

Table 2.1. Equilibrium and bond stability limit distances for different diatomic molecules obtained from the RKR data.

Bond	$\mathbf{r_e}$ **(Å)**	r_{sp}**(Å)**	r_{hs}**(Å)**	$\mathbf{E_{sp}}/D\mathbf{e}$	$r_{sp}/\mathbf{r_e}$
BCl	1.7159	2.223	1.209	0.715	1.29
C_2	1.243	1.538	0.954	0.740	1.24
CH	1.1199	1.492	0.759	0.771	1.33
Cl_2	1.9879	2.354	1.634	0.741	1.19
SiCl	2.058	2.564	1.573	0.791	1.25
CN	1.1718	1.459	0.893	0.747	1.25
LiF	1.5639	2.295	0.945	0.728	1.47
H_2	0.7414	1.130	0.377	0.762	1.52
OH	0.9696	1.288	0.661	0.720	1.32
MgO	1.749	2.157	1.285	0.754	1.23
O_2	1.2075	1.48773	0.941	0.696	1.23
SiO	1.5097	1.89014	1.129	0.768	1.25
P_2	1.8934	2.28922	1.510	0.750	1.21
Si_2	2.246	2.75463	1.754	0.768	1.22

A similar relationship between the equilibrium properties and the mechanical stability limit was also observed in the reaction force analysis performed by Murray et al. [32] during diatomic dissociation reactions. These authors also study the spectroscopic RKR potentials of a reduced group of 13 diatomic, aiming to probe that the distance dependence of the force stretching constant it is related with the electronic changes during the dissociation path. They observed that the energy and distance needed to transit between a diatomic

and an atom like state was about 22% of its equilibrium value in clear agreement with our spinodal analysis.

Either way, given the variety of bond types included in our study it is surprising that multiple, single, polar covalent and ionic bonds present equal relative stability limits. Considering the different dissociation energies and equilibrium stretching force constants included in our analysis, one could expect that different bonds will exhibit different energetic and mechanical ratios at the unstable points of the PEC. It seems that, regardless the bond type, bond ruptures occur when all bonds are distorted a given amount from its equilibrium conditions. Under this perspective, bond breaking and forming processes does not depend on the stretching mechanism, either produced by an external force or by a chemical interaction but are an intrinsic bond property.

To further explore the latter relationship, it is useful to assume an analytically potential energy function which may allow us to derive a close expression between the bond strength equilibrium parameters and bond stability limits. In this regard, we have assumed the potential developed by Ferrante, Smith and Rose [33] as an analytical functional form for bond the stretching PECs. Such a function been used as an universal binding energy relationship (UBER) due its capability to describe the distance dependence of diatomic molecules, covalent, and metallic solids as well as chemisorption processes [34,35], and therefore it can be considered as a reference to proof the validity of the bond stability limit model across different chemical interactions.

As defined by Ferrante et al., UBER relationship is based on a scaled Rydberg type potential:

$$E/D_e = -(1 + a^*)e^{-a^*} \tag{2.1}$$

where a^* is a scaled distance defined in terms of the dissociation energy, D_e, and the equilibrium stretching force constant k_e :

$$a^* = \frac{r - r_e}{(D_e/k_e)^{1/2}} \tag{2.2}$$

Equating this potential to zero one obtains that the hard sphere distance is defined through the condition $a^* = -1$ and therefore,

$$r_{hs} = \ r_e - (D_e/k_e)^{1/2} \tag{2.3}$$

Likewise, the scaled distance at which the second derivative of the energy respect to the distance is zero has a value of one, thus the spinodal distance read as,

$$r_{sp} = r_e + (D_e/k_e)^{1/2} \tag{2.4}$$

Interestingly, in the UBER potential, the bond stability limits are symmetrically disposed around the equilibrium position spaced by a constant

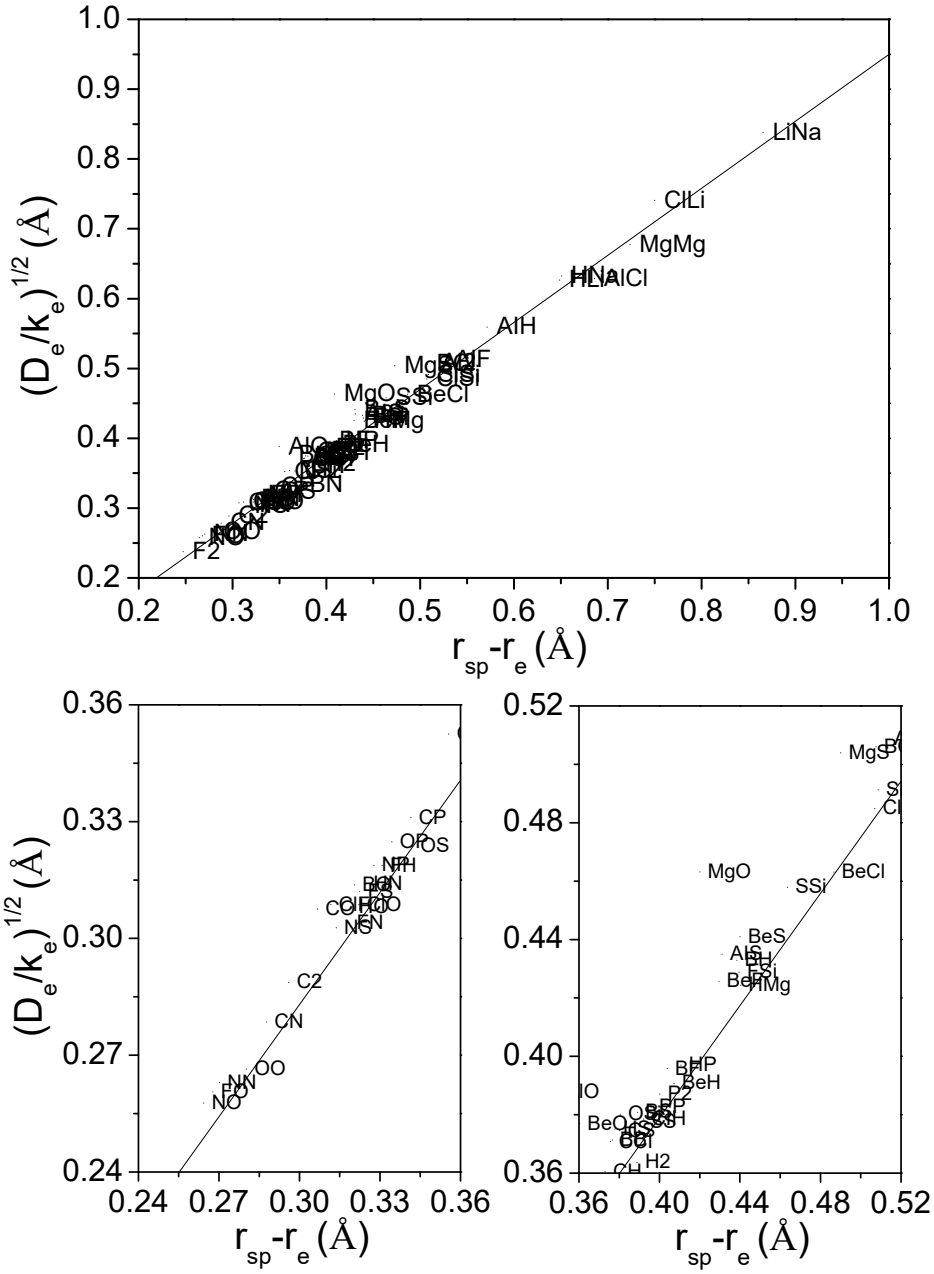

Figure 2.3. $(D_e/k_e)^{1/2}$ scaled parameter of the UBER potential against the difference between the spinodal and the equilibrium distances for several diatomic molecules.

Two extensions of the graph are shown in the bottom. The straight line is defined by $(D_e/k_e)^{1/2} = 0.96(r_{sp} - r_e)$.

quantity which depends on the dissociation energy and the bond stretching force constant, the two typical chemical measurements of the bond strength.

In order to confirm the latter relationship, we have plotted in Figure 2.3 the difference between r_{sp} and r_e obtained from the spectroscopically RKR data against the scaling parameter $(D_e/k_e)^{1/2}$. Most of the bonds display a spinodal–equilibrium distance difference grouped in the range between 0.3 and 0.5 Å pointing towards the observed constancy in the relative bond stability limits. A detailed analysis also shows that as the ionic character of the bond is increased the distance difference to the stability limits also increases (see Figure 2.3 extensions) in agreement with the expected long-range character of the ionic electrostatic interactions. Indeed, a nice linear correlation between our calculated values and the RKR ones is obtained with a slope of 0.96 evidencing the connection between the equilibrium bond characteristics and the bond stability limits. A similar plot is obtained when we represent the hard sphere distance in agreement with our UBER potential analysis where these two points are opposite defined.

According to our results, the amount of distortion which can be exerted on a given bond is determined by its equilibrium properties. Consequently, bond ruptures are produced at particular distances which depend on the bond strength characteristics. In this regard, rigid bonds with highly stretching force constants and low dissociation energies will display rupture distances closer to its equilibrium one. From this point of view, a clear connection with the Hammond postulate will be provided. More reactive bonds are those which its rupture distance is closer to their equilibrium one.

This view is confirmed when we realize that the diatomic molecules with the smaller distance differences between the spinodal and the equilibrium distance are those with multiple and halogen bonds such as C_2, O_2, F_2 and FO. If bond in diatomic molecules can be assimilated with bond in molecules those are the ones which commonly appears in organic reactions.

At this point, it should be mentioned that the spinodal relationship provided in the analysis of the UBER potential also holds for other analytical energy functions. Indeed, the so claimed universality of pair–wise interactions demonstrated by the spectroscopic relationships given by Parr et al., the bond softness constant of the Morse potential or the bond valence potentials are based on reduced potential energy functions with a scaled distance involving

the square ratio between the dissociation energy (D_e) and the equilibrium force constant (k_e) [36-39]. These potentials lead to similar expressions for the bond stability limits, and therefore the relationship between the bond equilibrium properties and bond ruptures can be consider as a general principle. These results support us in using the bond stability limits in what follows as a reference to define bond ruptures along chemical processes.

An Electronic–Mechanical Perspective of Covalent Bond Ruptures

So far, we have demonstrated that bond stability limits in diatomic molecules may constitute a reliable criterion to bond ruptures which can be defined in terms of the energetic and mechanical properties of the bond. Nonetheless, our ultimate goal is to seek for a relationship between the energetic–mechanical instabilities and the traditional chemical electronic picture depicted for bond ruptures.

According to the latter, when the bond ruptures are produced, a quite dramatic change occurs in the electronic distribution of the molecule. The bonding shared electrons migrates from the internuclear axis to the cores giving as a result two interacting, but non–bonded atoms. In the same way, when the molecule is compressed up to the limit where the electronic repulsion dominates, the electrons are confined in a really tiny space, the cores began to interact and formally, the bond disappear forming an inner valence shells interaction with the electrons highly localized along the internuclear axis. Under this traditional view, unstable states are completely different for bonds and therefore, if bond stability limits are actually and energetic-mechanical indicator of this processes we must expect that the electronic rearrangements occurs at similar distances at which bond stability limits are produced.

Among all the electronic criteria developed to detect interaction changes, the topological analysis of the electron density and the electron localization function (ELF), are perhaps the ones which have provided more fruitful chemical interpretations of electronic rearrangements in terms of the reliable basis of quantum mechanics [40-43]. Bond ruptures, chemical reactions, intermolecular processes or even the appearance of highly localized electrons has been defined and rationalized in terms of the topological characteristics of this scalar fields. Therefore both, the electron density and the ELF analysis can be considered as a reference to characterize electronic changes, and a framework to validate our bond stability limits from a chemical electron perspective.

As we are interested in rupture and highly accumulations of the electron density due to core interactions, we have selected the typical indicators used in this scalar fields to detect such processes. In the case of the electron density analysis, we have chosen the Laplacian sign change and the signature change of the electron density at the bond at the bond critical point as a bond rupture and highly localized electron criteria respectively. The Laplacian sign change evidences a transition from a shared to a closed shell regime which is interpreted as a depletion of electron density along the internuclear axis. For pure covalent bonds, this topological change can be related with the covalent bond rupture; the shared bonding electrons (shared shell) are transferred to the atoms, closed shell entities. It must be emphasized that when the ionic character of the bond is increased such a criterion not necessary hold. As the partial charge of the atoms is increased, their electronic distributions resemble more to the ions, which formally are closed shell entities. On the other hand, the signature change of electron density at the bond critical point reflect the changes in the curvatures of the electron density. Typically, upon compression a transition from a saddle point to a non–nuclear maxima (NNM) is produced reflecting the presence of highly localized e^- along the internuclear region [44].

Analogously, in the case of the ELF function their topology along the stretching curves, can be analyzed terms of the bonding evolution theory (BET) [45,46]. This theory recovers Lewis's picture of the bonding [43,47] and defines different stability structural domains in which the electronic rearrangements are revealed as topological catastrophes classified according to the Thom´s theory [48]. Within this framework, both homolytic and heterolytic bond ruptures can be differentiated. Homolytic ruptures are defined as a dual cusp catasthrophes, where the ELF maxima representing the two shared bonding electrons annihilates and transform into two new maxima and one saddle point. In this process a disynaptic basin transform into two monosynaptic basins which identifies the radical character of the atoms. On contrary, heterolytic ruptures are identified as a fold type catastrophe where the disypnatic bond pair basin evolves to a monosypnatic basin with the creation of two new critical points.

Let us start discussing the electronic changes in the bond compressive regimen. As it can be seen in Table 2, for all homonuclear bonds studied, the appearance of NNM seems to coincide with the hard sphere distance. The signature change of the electron density at the bond critical point occurs at distances lower than 0.1-0.15 Å from the one predicted at the hard sphere point. As expected by our analysis of the PECs, the latter similarity on the

distances reflects that, at the compression limit, the cores began to interact producing a highly electronic accumulation along the internuclear region which results in an overall repulsive effect.

This behavior contrast with the results displayed for heteroatomic bonds. Not any of them display this topological feature, even at shorter distances than our compression limit. However, does not mean that core interactions and highly electron accumulation cannot be produced in those bonds. The hard sphere distance is intrinsically a repulsive state and therefore it is produced regardless the atoms involved in the bond. As stated by Pendás et al. [44] the appearance of NNM in heteronuclear diatomic molecules it is very unlikely due to the narrow convex region of electron density tails which difficulties the fulfillment of negative parallel curvature in a non–fixed critical point. In these cases, the expected core effects do not lead to a NNM maxima but they must be produced in a similar way as in homonuclear bonds.

Table 2.2. Bond stability Limits and electron instabilities distances for the bonds studied. r_{Lap}, r_{NNM}, r_{BET} and $r_{BET\text{-}Hs}$ stands for the distance at which is produced the sign change at the bond critical point, the non–nuclear maxima, the bond rupture catastrophe and the catastrophe in the highly compressed state respectively. All unit are in Å.

Bond	r_{sp}	r_{Lap}	r_{BET}	r_{hs}	r_{NNM}	$r_{BET\text{-}hs}$
C-Cl (CH_3Cl)	2.20	2.15	2.20	1.30	--	1.20
C-Br (CH_3Br)	2.40	2.30	2.40	1.50	--	1.40
C-C (CH_3CH_3)	1.95	2.20	2.00	1.00	1.10	0.95
C-N (CH_3NH_2)	1.85	1.95	1.90	1.05	--	1.00
C-O(CH_3OH)	1.85	1.85	1.85	1.00	--	0.90
Cl-Cl (Cl_2)	2.40	2.05	2.40*	1.65	1.55	1.45
Si-Cl (SiH_3Cl)	2.65	2.80	2.70	1.60	--	1.50
O=O (O_2)	1.55	1.40	1.55*	0.95	0.85	0.85
N≡N (N_2)	1.45	1.65	1.40	0.85	0.95	0.75
C=C (CH_2CH_2)	1.70	2.15	1.60	0.95	1.15	1.00
C=O (H_2CO)	1.60	1.75	1.60	0.90	--	0.85

*These distances are those at which two valence shell are completely formed. See text for explanation.

An example of this situation is shown in Figure 2.4, where the ELF isosurfaces and the position of the ELF bond attractors for the CH_3OH molecule in this highly compressed state are represented. Notice that a cusp catastrophe where the bond ELF maxima transform into a saddle point and two new attractors has occurred. Each ELF basing yields $0.8e^-$ for the bond attractors, and a

substantial increment of the number of electrons associated with the lone pair ($3.4e^-$) and hydrogens ($1.9e^-$). Similar situations with topological changes in the index of the ELF bond attractor and high e^- populations in the bond axis are obtained for the other molecules. In the light of these results the hard sphere limit corresponds to the point where the cores began to interact giving as a result a highly electronic localization in the internuclear axis. Not surprisingly, the unstable points of the PEC are associated with bonding electronic changes according to the intuitive chemical idea.

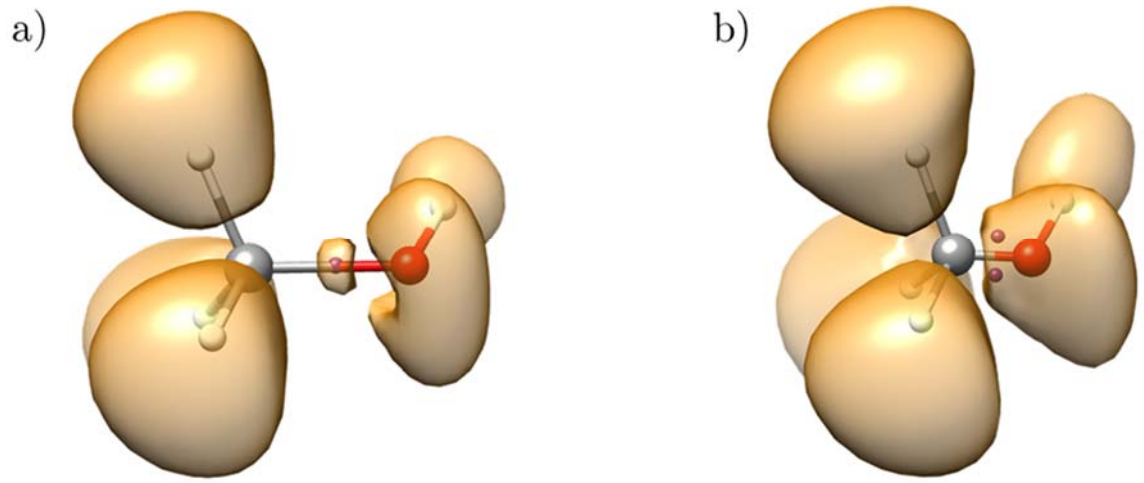

Figure 2.4 ELF isosurfaces for the CH_3OH (ELF isovalue 0.78) along with bond attractor represented as purple spheres at C-O distances a) 1.45 Å and b) 0.95 Å.

This connection becomes even more evident in the analysis of the rupture distances. For single covalent bonds, we can see an excellent agreement with the distances at which the mechanical and electronical rupture is predicted.

Whereas the Laplacian change sign is produced always within 0.1-0.15 Å around mechanical stability limit, the distance difference between BET catastrophe (cusp or fold), which results in the annihilation of the bond disypnatic basin, and the spinodal point is smaller than 0.05 Å or in the majority of the cases almost coincident. The only exception is the Cl_2 molecule where the cusp catastrophe has already occurred at the equilibrium distance and, neither the Laplacian, nor the homolytic BET indicator are suitable to reveal the rupture process.

This molecule constitutes an example of a homopolar charge–shift bonding where the covalent contribution induces a destabilizing effect to the bond energy as a result of a covalent-ionic fluctuation of the electron-pair density[49]. The ionic contribution to the wavefunction is the responsible for

the disynaptic basin at equilibrium configuration and for the positive value of the Laplacian electron density at the critical point.

Upon elongation, the charge shift character increases resulting in a bond electron density transference to the lone pairs. (see figure 2.5) In this case, a heterolytic rupture of the bond cannot be produced as in other charge shift bonds, where there is a substantial electronegativity difference between the atoms. In contrast, this process continues up to the formation of two unique valence shells in each Cl atom. Interestingly, in the Cl_2 molecule such process occurs at 2.40 Å, again the same as the spinodal distance, and is accompanied by a topological change from two attractors to two (3,+1) critical points,

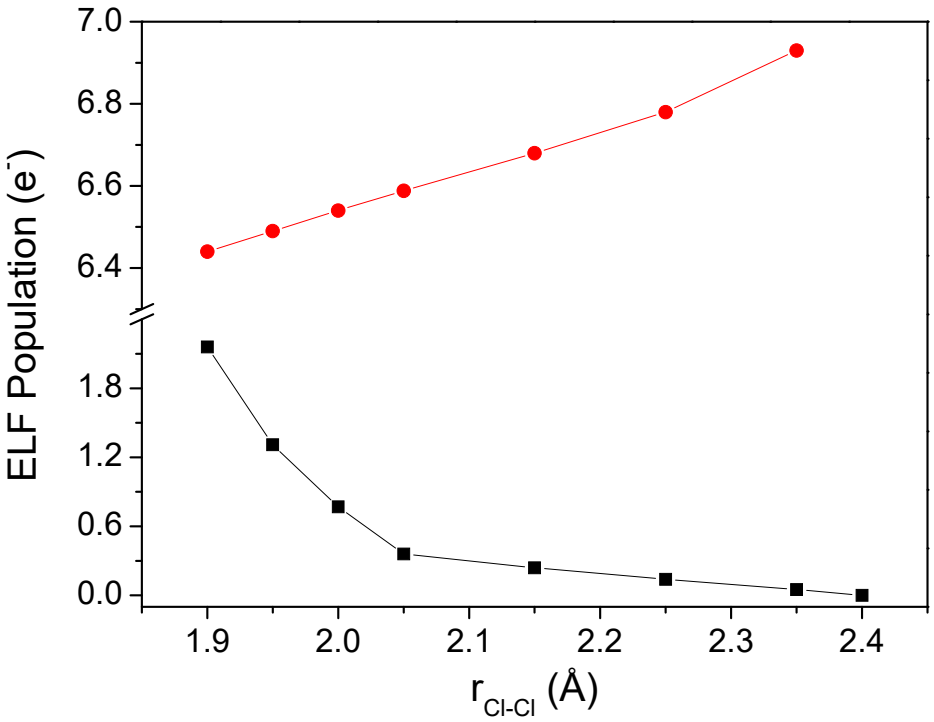

Figure 2.5 Populations of the bond pair basin(s) and lone pair basins at difference Cl-Cl distances.

highlighting once again that spinodal criteria it is a general chemical principle which also holds for homopolar charge shift bonds.

Similar results are obtained for multiple bonds. Again, the spinodal distances coincides with the BET cusp catastrophe. However, the Laplacian of electron density criterion differs from the BET and spinodal criteria. Although the π-bonds can be broken, a σ contribution is still joining the atoms and an amount of electron density still accumulated along the internuclear axis producing a negative value for the Laplacian of electron density. Also, if the charge shift character is elevated, even before the π rupture, the Laplacian is positive.

This is the case of the O_2 molecule. The cusp catastrophe occurs at 1.30Å, however as in the case of the Cl_2 where the disynaptic bond basin is already at the equilibrium conditions, such a topological feature does not necessary implies an unstable bond, but a stabilized one by a covalent-ionic resonance energy. Again, a gradually transference of electrons from the internuclear axis to the atoms is produced up to the spinodal point (1.55Å), where the two O valence shells are formed.

This remarkable agreement between electronic and mechanical criteria cannot be accidental. The spinodal mechanical instability indeed corresponds to intuitive chemical picture of electron density transference from the internuclear region to the atoms. Both the electronic and mechanical instability occurs simultaneously, and bond ruptures cannot be considered as dependent on the bond stretching mechanism but an intrinsic bond property which are produced at specific distances. A clear example is provided, through the analysis of the rupture distances in C-X bonds (X=Cl,Br). The pure stretching ruptures occur at 2.20 and 2.40 Å for C-Cl and C-Br respectively, whereas the ruptures along the symmetrical SN_2 reactions [50] are 2.201 and 2.398 Å. Bonds are unstable because its own properties not because the way they are elongated. According to these results, *not* a*ny covalent interaction can be extended far beyond its single bond spinodal distance because is both mechanically an electronically unstable.* Notice that such a statement is indeed a quite restrictive one. Chemical reactions where one and only one single covalent bond is broken or formed, cannot take places before the mechanical stability limit is produced.

Moreover, in the previous section we empirically determine that reactive bonds are rigid and energetically unfavored because the spinodal distance depends on the square root ratio between D_e and k_e. Now, under this electronic-mechanical perspective we can set some theoretical background for our previous conclusions. Covalent bond ruptures are produced as a result of an electron density transference from the internuclear region to the atoms. In general, this process is favored when the orbital overlapping is decreased, or when a covalent-ionic fluctuation of the pair density is increased. Therefore, in rigid bonds, where the electron density is effectively and extensively concentrated around the internuclear axis as a result of an extended orbital overlapping, an increase of the internuclear produces a substantial orbital enlargement. As a result, the orbital overlapping is dramatically reduced and ant the electron density is more effectively migrated to the nuclei. Likewise, the covalent-ionic fluctuation increases by the presence of lone pairs. The

latter ultimately lead to lower dissociation energies as a result of the repulsion between the lone pairs and the bonding electrons. Under this view the bonding characteristics determine the bond ruptures. Therefore, multiple and halogen bonds, where these two effects play a dominant role, are those where its bond ruptures are closer to the equilibrium distance.

References

[1] M. Kaupp, D. Danovich, and S. Shaik, Chemistry is about energy and its changes: A critique of bond-length/bond-strength correlations. *Coord. Chem. Rev.*, *344*, 355-362, **2017**. DOI: https://doi.org/10.1016/j.ccr.2017.03.002.

[2] L. Pauling, The Nature of the Chemical Bond and the Structure of Molecules and Crystals: An Introduction to Modern Structural Chemistry, Cornell University Press, 3rd ed., **1960**.

[3] L. Zhao, M. Hermann, W. H. E. Schwarz, and G. Frenking, The Lewis electron-pair bonding model: modern energy decomposition analysis. *Nature Reviews Chemistry*, *3*, 48-63, **2019**. DOI: https://doi.org/10.1038/s41570-018-0060-4.

[4] J. Grunenberg, The Weakness of B-Hpi Interactions: Much Softer than a Hydrogen Bond. *Chem. Eur. J.*, *22*, 18678-18681, **2016**. DOI: 10.1002/chem.201603535.

[5] S. Pratihar, X. Ma, Z. Homayoon, G. L. Barnes, and W. L. Hase, Direct Chemical Dynamics Simulations. *J Am Chem Soc*, *139*, 3570-3590, **2017**. DOI: https://doi.org/10.1021/jacs.6b12017.

[6] G. J. Cheng, X. Zhang, L. W. Chung, L. Xu, and Y. D. Wu, Computational organic chemistry: bridging theory and experiment in establishing the mechanisms of chemical reactions. *J Am Chem Soc*, *137*, 1706-1725, **2015**. DOI: https://doi.org/10.1021/ja5112749.

[7] B. K. Carpenter, Energy disposition in reactive intermediates. *Chem Rev*, *113*, 7265-7286, **2013**. DOI: https://doi.org/10.1021/cr300511u.

[8] P. R. Schreiner, L. V. Chernish, P. A. Gunchenko, E. Y. Tikhonchuk, H. Hausmann, M. Serafin, S. Schlecht, J. E. Dahl, R. M. Carlson, and A. A. Fokin, Overcoming lability of extremely long alkane carbon-carbon bonds through dispersion forces. *Nature*, *477*, 308-311, **2011**. DOI: https://doi.org/10.1038/nature10367.

[9] R. Isea, What is the maximum stretching for the C-C single bond? *J. Mol. Struct.*, *540*, 131-138, **2001**. DOI: https://doi.org/10.1016/S0166-1280(00)00721-1.

[10] T. Bredtmann, M. Ivanov, and G. Dixit, X-ray imaging of chemically active valence electrons during a pericyclic reaction. *Nat Commun*, *5*, 5589, **2014**. DOI: https://doi.org/10.1038/ncomms6589.

[11] K. Black, P. Liu, L. Xu, C. Doubleday, and K. N. Houk, Dynamics, transition states, and timing of bond formation in Diels-Alder reactions. *Proc Natl Acad Sci U S A*, *109*, 12860-12865, **2012**. DOI: https://doi.org/10.1073/pnas.1209316109.

[12] A. Ghosh, R. K. Chaudhuri, and S. Chattopadhyay, Relativistic state-specific multireference coupled cluster theory description for bond-breaking energy surfaces. *J. Chem. Phys.*, *145*, 124303, **2016**. DOI: https://doi.org/10.1063/1.4962911.

[13] C. A. Gaggioli, L. Belpassi, F. Tarantelli, J. N. Harvey, and P. Belanzoni, Spin-Forbidden Reactions: Adiabatic Transition States Using Spin-Orbit Coupled Density Functional Theory. *Chem. Eur. J.*, *24*, 5006-5015, **2018**. DOI: https://doi.org/10.1002/chem.201704608.

[14] J. Ribas-Arino, M. Shiga, and D. Marx, Understanding covalent mechanochemistry. *Angew Chem Int Ed Engl*, *48*, 4190-4193, **2009**. DOI: https://doi.org/10.1002/anie.200900673.

[15] J. Ribas-Arino and D. Marx, Covalent mechanochemistry: theoretical concepts and computational tools with applications to molecular nanomechanics. *Chem Rev*, *112*, 5412-5487, **2012**. DOI: https://doi.org/10.1021/cr200399q.

[16] A. Toro-Labbe, S. Gutierrez-Oliva, J. S. Murray, and P. Politzer, The reaction force and the transition region of a reaction. *J Mol Model*, *15*, 707-710, **2009**. DOI: https://doi.org/10.1007/s00894-008-0431-8.

[17] A. Toro-Labbé, S. Gutiérrez-Oliva, J. S. Murray, and P. Politzer, A new perspective on chemical and physical processes: the reaction force. *Molecular Physics*, *105*, 2619-2625, **2010**. DOI: https://doi.org/10.1080/00268970701604663.

[18] M. K. Beyer, The mechanical strength of a covalent bond calculated by density functional theory. *J. Chem. Phys.*, *112*, 7307-7312, **2000**. DOI: http://dx.doi.org/10.1063/1.481330.

[19] M. Frei, S. V. Aradhya, M. Koentopp, M. S. Hybertsen, and L. Venkataraman, Mechanics and chemistry: single molecule bond rupture forces correlate with molecular backbone structure. *Nano Lett*, *11*, 1518-1523, **2011**. DOI: https://doi.org/10.1021/nl1042903.

[20] S. Giri, E. Echegaray, P. W. Ayers, A. S. Nunez, F. Lund, and A. Toro-Labbe, Insights into the mechanism of an S(N)2 reaction from the reaction force and the reaction electronic flux. *J. Phys. Chem. A*, *116*, 10015-10026, **2012**. DOI: https://doi.org/10.1021/jp3076707.

[21] E. Echegaray and A. Toro-Labbe, Reaction Electronic Flux: A New Concept To Get Insights into Reaction Mechanisms. Study of Model Symmetric Nucleophilic Substitutions. *J. Phys. Chem. A*, *112*, 11801–11807, **2008**. DOI: https://doi.org/10.1021/jp805225e.

[22] G. W. T. M. J. Frisch, H. B. Schlegel, G. E. Scuseria, M. A. Robb, J. R. Cheeseman, G. Scalmani, V. Barone, G. A. Petersson, H. Nakatsuji, X. Li, M. Caricato, A. Marenich, J. Bloino, B. G. Janesko, R. Gomperts, B. Mennucci, H. P. Hratchian, J. V. Ortiz, A. F. Izmaylov, J. L. Sonnenberg, D. Williams-Young, F. Ding, F. Lipparini, F. Egidi, J. Goings, B. Peng, A. Petrone, T. Henderson, D. Ranasinghe, V. G. Zakrzewski, J. Gao, N. Rega, G. Zheng, W. Liang, M. Hada, M. Ehara, K. Toyota, R. Fukuda, J. Hasegawa, M. Ishida, T. Nakajima, Y. Honda, O. Kitao, H. Nakai, T. Vreven, K. Throssell, J. A. Montgomery, Jr., J. E. Peralta, F. Ogliaro, M. Bearpark, J. J. Heyd, E. Brothers, K. N. Kudin, V. N. Staroverov, T. Keith, R. Kobayashi, J. Normand, K. Raghavachari, A. Rendell, J. C. Burant, S. S. Iyengar, J. Tomasi, M. Cossi, J. M. Millam, M. Klene, C. Adamo, R. Cammi, J. W. Ochterski, R. L. Martin, K. Morokuma, O. Farkas, J. B. Foresman, and D. J. Fox, *Gaussian 09*, I. Gaussian, Wallingford CT, 2016

[23] T. H. Dunning, Gaussian basis sets for use in correlated molecular calculations. I. The atoms boron through neon and hydrogen. *J. Chem. Phys.*, *90*, 1007-1023, **1989**. DOI: https://doi.org/10.1063/1.456153.

[24] G. E. Scuseria, Analytic evaluation of energy gradients for the singles and doubles coupled cluster method including perturbative triple excitations: Theory and applications to FOOF and Cr2. *J. Chem. Phys.*, *94*, 442-447, **1991**. DOI: https://doi.org/10.1063/1.460359.

[25] Energy-Represented Direct Inversion in the Iterative Subspace within a Hybrid Geometry Optimization Method. *J. Chem. Theory Comput.*, *2*, 835-839, **2006**. DOI: https://doi.org/10.1021/ct050275a.

[26] Todd A. Keith, *AIMAll (Version 19.02.13)*, O.P.K. TK Gristmill Software, USA, aim.tkgristmill.com, 1995

[27] A. Otero-De-La-Roza, E. R. Johnson, and V. Luaña, Critic2: A program for real-space analysis of quantum chemical interactions in solids. *Computer Physics Communications*, *185*, 1007-1018, **2014**. DOI: https://doi.org/10.1016/j.cpc.2013.10.026.

[28] K. M. a. F. Izumi, VESTA 3 for three-dimensional visualization of crystal, volumetric and morphology data. *J. Appl. Cryst.*, *44*, 1272-1276, **2011**. DOI: https://doi.org/10.1107/S0021889811038970.

[29] E. F. Pettersen, T. D. Goddard, C. C. Huang, G. S. Couch, D. M. Greenblatt, E. C. Meng, and T. E. Ferrin, UCSF Chimera--a visualization system for exploratory research and analysis. *J Comput Chem*, *25*, 1605-1612, **2004**. DOI: https://doi.org/10.1002/jcc.20084.

[30] P. Huxley and J. N. Murrel, Ground-state Diatomic Potentials. *J. Chem. Soc., Faraday Trans.*, *79*, 323-328, **1983**. DOI: 10.1039/F29837900323.

[31] P. Huxley, D. B. Knowles, J. N. Murrell, and J. D. Watts, Ground-state diatomic potentials. Part 2.—Van der Waals molecules. *J. Chem. Soc., Faraday Trans. 2*, *80*, 1349-1361, **1984**. DOI: 10.1039/f29848001349.

[32] J. S. Murray, A. Toro-Labbe, T. Clark, and P. Politzer, Analysis of diatomic bond dissociation and formation in terms of the reaction force and the position-dependent reaction force constant. *J Mol Model*, *15*, 701-706, **2009**. DOI: https://doi.org/10.1007/s00894-008-0400-2.

[33] J. Ferrante, H. Schlosser, and J. R. Smith, Global expression for representing diatomic potential-energy curves. *Physical Review A*, *43*, 3487-3494, **1991**. DOI: https://doi.org/10.1103/PhysRevA.43.3487.

[34] J. R. Smith, H. Schlosser, W. Leaf, J. Ferrante, and J. H. Rose, Connection between energy relations of solids and molecules. *Physical Review A*, *39*, 514-517, **1989**. DOI: https://doi.org/10.1103/PhysRevA.39.514.

[35] J. Ferrante, J. R. Smith, and J. H. Rose, Diatomic Molecules and Metallic Adhesion, Cohesion, and Chemisorption: A Single Binding-Energy Relation. *Physical Review Letters*, *50*, 1385-1386, **1983**. DOI: https://doi.org/10.1103/PhysRevLett.50.1385.

[36] V. S. Urusov, Semi-Empirical Groundwork of the Bond-Valence Model. *Acta Cryst. B*, *51*, 641-649, **1995**. DOI: https://doi.org/10.1107/S0108768195003417.

[37] J. L. Graves and R. G. Parr, Possible universal scaling properties of potential-energy curves for diatomic molecules. *Physical Review A*, *31*, 1-4, **1985**. DOI: https://doi.org/10.1103/PhysRevA.31.1.

[38] S. Adams, Practical Considerations in Determining Bond Valence Parameters in Bond Valences, 91-128 2013.

[39] G. V. Hooydonk, A Universal Two-Parameter Kratzer-Potential and Its Superiority over Morse's for Calculating and Scaling First-Order Spectroscopic Constants of 300 Diatomic Bonds. *Eur. J. Inorg. Chem.* , 1617-1642, **1999**. DOI: https://doi.org/10.1002/(SICI)1099-0682(199910)1999:10.

[40] R. F. W. Bader, *Atoms in Molecules A Quantum Theory*, Oxford University Press, New York, **1994**.

[41] R. F. W. Bader, Definition of Molecular Structure: By Choice or by Appeal to Observation? *J. Phys. Chem. A*, *114*, 7431–7444, **2010**. DOI: https://doi.org/10.1021/jp102748b.

[42] M. Rahm and K. O. Christe, Quantifying the nature of lone pair domains. *Chem. Phys. Chem.*, *14*, 3714-3725, **2013**. DOI: https://doi.org/10.1002/cphc.201300723.

[43] A. Savin, R. Nesper, S. Wengert, and T. E. Fassler, ELF: The Electron Localization Function. *Angew. Chem. Int. Ed. Engl.*, *36*, 1808-1832, **1997**. DOI: https://doi.org/10.1002/anie.199718081.

[44] A. M. Pendás, M. A. Blanco, A. Costales, P. M. Sánchez, and V. Luaña, Non-nuclear Maxima of the Electron Density. *Phys. Rev. Lett.*, *83*, 1930-1933, **1999**. DOI: https://doi.org/10.1103/PhysRevLett.83.1930.

[45] X. Krokidis, S. Noury, and B. Silvi, Characterization of Elementary Chemical Processes by Catastrophe Theory. *J. Phys. Chem. A*, *101*, 7277-7282, **1997**. DOI: https://doi.org/10.1021/jp9711508.

[46] J. Andres, S. Berski, and B. Silvi, Curly arrows meet electron density transfers in chemical reaction mechanisms: from electron localization function (ELF) analysis to valence-shell electron-pair repulsion (VSEPR) inspired interpretation. *Chem. Commun.*, *52*, 8183-8195, **2016**. DOI: 10.1039/c5cc09816e.

[47] B. Silvi, The Relevance of the ELF Topological Approach to the Lewis, Kossel, and Langmuir Bond Model in The Chemical Bond II213-247 2015.

[48] R. Thom, Structural stability and morphogenesis: an outline of a general theory of models., ed. R. Benjamin, **1975**

[49] S. Shaik, D. Danovich, B. Silvi, D. L. Lauvergnat, and P. C. Hiberty, Charge-shift bonding--a class of electron-pair bonds that emerges from valence bond theory and is supported by the electron localization function approach. *Chem. Eur. J.*, *11*, 6358-6371, **2005**. DOI: https://doi.org/10.1002/chem.200500265.

[50] V. Polo, P. Gonzalez-Navarrete, B. Silvi, and J. Andres, An electron localization function and catastrophe theory analysis on the molecular mechanism of gas-phase identity SN_2 reactions. *Theoretical Chemistry Accounts*, *120*, 341-349, **2008**. DOI: https://doi.org/10.1007/s00214-008-0427-6.

Supplementary Material Chapter 2

Table S.2.1. Equilibrium values for the molecules calculated in this work.

Bond	r_e (Å)
C-Cl (CH_3Cl)	1.78
C-Br (CH_3Br)	1.95
C-C (CH_3CH_3)	1.54
C-N (CH_3NH_2)	1.47
C-O(CH_3OH)	1.42
Cl-Cl (Cl_2)	2.05
Si-Cl (SiH_3Cl)	2.10
O=O (O_2)	1.20
N≡N (N_2)	1.10
C=C (CH_2CH_2)	1.35
C=O (H_2CO)	1.20

Table S.2.2. RKR parameters for the 70 diatomic molecules studied.

Bond	*D*e (eV)	r_e (Å)	k_e (N/m)	r_{sp}(Å)	r_{hs}(Å)
Al_2	1.572	2.466	97.3	2.978	1.957
AlCl	5.15	2.1301	208.7	2.816	1.501
AlF	6.94	1.6544	422.7	2.181	1.141
AIH	3.163	1.6478	162.0	2.219	1.088
AlO	5.33	1.6179	567.3	1.967	1.229
AlS	3.878	2.029	328.3	2.460	1.593
B_2	3.085	1.589	358.4	1.965	1.217
BCl	5.552	1.7159	347.3	2.223	1.209
BeCl	4.052	1.7971	302.6	2.283	1.333
BeF	6.337	1.361	560.3	1.790	0.935
BeH	2.161	1.3426	226.8	1.749	0.951
BeO	6.659	1.3309	751.3	1.691	0.954
BeS	5.007	1.7415	412.5	2.171	1.300
BF	7.896	1.2626	807.3	1.666	0.866
BH	3.565	1.2324	304.7	1.670	0.799
BN	5.793	1.281	833.0	1.652	0.947
BO	8.396	1.2045	1366.1	1.525	0.890
BS	6.083	1.6092	672	1.998	1.228

C_2	6.325	1.243	1216.1	1.538	0.954
Bond	De (eV)	r_e (Å)	k_e (N/m)	r_{sp}(Å)	r_{hs}(Å)
CCl	3.393	1.645	395.4	2.020	1.274
CF	5.751	1.2718	741.4	1.627	0.919
CH	3.631	1.1199	447.6	1.492	0.759
Cl_2	2.514	1.9879	322.7	2.354	1.634
ClF	2.666	1.6283	448.2	1.940	1.319
HCl	4.617	1.2745	516.3	1.666	0.895
LiCl	4.88	2.0207	142.4	2.770	1.279
ClO	2.803	1.5696	471.3	1.891	1.260
SiCl	3.855	2.058	262.7	2.564	1.573
CN	7.888	1.1718	1629.2	1.459	0.893
CO	11.226	1.1283	1901.9	1.435	0.820
CP	5.357	1.5622	783.1	1.903	1.231
CS	7.434	1.5349	848.9	1.915	1.160
F_2	1.658	1.4119	470.2	1.659	1.174
HF	6.123	0.9168	965.7	1.247	0.598
LiF	5.966	1.5639	250.1	2.295	0.945
MgF	4.794	1.75	316.3	2.154	1.257
NF	3.57	1.317	618.7	1.635	1.012
NaF	5.363	1.9259	176	2.854	1.227
OF	2.294	1.326	541.4	1.593	1.065
P_2	4.652	1.5897	497.4	1.989	1.202
SF	3.563	1.6006	586.3	1.923	1.288
SiF	5.623	1.6011	489.8	2.040	1.172
H_2	4.747	0.7414	575.1	1.130	0.377
LiH	2.515	1.5957	102.5	2.244	0.968
MgH	1.432	1.7297	127.4	2.170	1.305
NH	3.671	1.0361	596.7	1.360	0.722
NaH	1.952	1.8874	78.1	2.538	1.254
OH	4.621	0.9696	780.4	1.288	0.661
PH	3.165	1.4223	321.7	1.832	1.025
SH	3.716	1.3409	423.2	1.718	0.965
LiNa	0.916	2.81	20.8	3.675	1.971
Mg_2	0.053	3.8905	1.8	4.614	3.213

MgO	4.666	1.749	348.4	2.157	1.285
MgS	3.578	2.1425	225.7	2.615	1.638
Bond	De (eV)	r_e (Å)	k_e (N/m)	r_{sp}(Å)	r_{hs}(Å)
MgS	3.578	2.1425	225.7	2.615	1.638
Na_2	2.234	3.0789	364	3.910	2.765
N_2	9.905	1.0977	2294.8	1.367	0.834
NO	6.614	1.1508	1595.1	1.41514	0.893
PN	6.443	1.4909	1016	1.81864	1.172
SN	4.875	1.494	852.1	1.8077	1.191
SiN	5.701	1.5718	728.8	1.93239	1.217
O_2	5.213	1.2075	1176.6	1.48773	0.941
PO	6.226	1.4759	945.3	1.81032	1.151
SO	5.43	1.4811	829.6	1.82314	1.157
SiO	8.337	1.5097	924.2	1.89014	1.129
P_2	5.081	1.8934	556.2	2.28922	1.510
Si_2	3.242	2.246	215.2	2.75463	1.754
S_2	4.414	1.8892	495.9	2.2804	1.511
SiS	6.466	1.9293	494	2.39291	1.510

Chapter 3

Universal Rupture of C-C Bonds

Introduction

In the last years, new organic compounds showing anomalous distances have been synthesized, pushing the chemical knowledge of what chemical bonds are, and confirming that the classical conception of a C-C single bond length of ~ 1.54 Å was long ago overcome. Kaupp and Boy in 1997 showed that highly strained or steric congested structures present overlong C-C bonds with values ranging from 1.60 to 1.67 Å [1]. Since then, the quest to produce untypically long C-C bonds has continued[2]. Dispersion forces and steric crowding have been able to generate new molecules with C-C bond lengths up to 1.80 Å[3,4]. Peculiar electronic effects such as negative hyperconjugation have also played a key role stretching the limits of these bonds, so distances up to 1.93 Å in Diamino-o-carboranes compounds have been reported[5], blurring the boundary between covalent and non-covalent interactions[6].

Nonetheless, not only extremely long C-C bonds have been studied, but also highly compressed ones. As demonstrated by Huntley et al. [7], confinement and Van der Waals (repulsive) forces can reduce the C-C single bond lengths to 1.31 Å, very close to the standard equilibrium distance of the C-C double bond in ethene. Such abnormal distances have evidenced again that the question What are the C-C bond stability limits? is still controversial, even though it is crucial to understand and to define chemical interactions, and so chemical reactivity.

In this regard modern electron density analysis has been extensively applied to study C-C bond limits. For instance, Isea [8] observed a change from closed shell to open shell regime during the stretching curve of the ethane molecule evidencing that the covalent limit of this molecule occurs around 2 Å. Remarkably, in the aforementioned study of the diamino- o-carborane compounds the authors claimed the existence of a bond path between the longest C-C bonds that disappeared also at 2 Å. Moreover, Costales et al. [9] demonstrated that C-C bonds obeys a universal sequence of non-nuclear maxima (NNM) open shell closed shell regime with their transition points at the same distances of their diatomic counterparts, *i.e.* 1.15 Å and 1.9 Å.

It is also remarkable that molecular dynamics, time resolved ultrafast spectroscopy, and electron density studies have shown that in Diels-Alder reactions both symmetrical and unsymmetrical transition states involve constant C-C bond distances distributions between 1.9 to 2.2 Å [10-12]. Moreover, Cope rearrangements which involves an aromatic chairlike C_{2h}-symmetry transition structure has also an inter-allylic bond length between

forming C-C bonds of 2.0 Å [13,14]. In summary, it appears that bond stability limit constitutes an underlaying, yet unexplored, universal chemical characteristic.

Motivated by these observations, we seek to provide a general chemical model able to define the stability limits of the single C-C bond, showing that the maximum and minimum distances at which a bond can be distorted are deeply related to its bonding properties/features, and therefore they are intimately linked to its chemical reactivity. The discovery of such a general principle will undoubtedly have a huge impact on new chemical structural predictions, which will enable to define the boundaries within which novel compounds can be synthesized (stable) or not.

Computational Details

All the molecular calculations has been carried out with the gaussian09 (g09) [15]. code at the B3LYP level using Dunning's cc-pVTZ basis set [16]. Geometry optimizations were carried out using analytical gradients [17], according to the Berny algorithm [18]. Dissociation curves were always performed fixing the bond length and partial optimizing the rest of the coordinates. The keyword stable during the optimization was used in order to check and ensure the sanity and stability of the wavefunction.

Electron density analysis was performed using AIMALL package [19]. Electron localization function and topology was calculated using CRITIC2 code [20]. The visualization of the results was carried out with VESTA [21] and Chimera [22] software.

Potential energy curves, equilibrium bond lengths, dissociation energies and equilibrium stretching force constants for all the optimized states are presented in Table S.3.1 of the supplementary material.

Rupture Distances in C-C Bonds. Linking the reactive processes and bond stabilities

Different criteria such as distance histograms, electron density laplacian sign change at the critical point during the C-C stretching of the ethane molecule, and C-C distances in the transitions states of typical C-C forming reactions, indicate that C-C covalent interactions are broken or formed at a similar distance (~ 2Å). This means that there may be an upper distance limit at which the C-C covalent bond in no longer stable. Such a stability limit, if

any, implies that the rupture of a C-C bond does not depend on how it is produced and, therefore, the maximum distance at which it can be elongated must be similar to that at which the reactive processes do occur. To the best of our knowledge, the idea of a C-C bond stability limit has not been reported so far and, as stated above, we believe it requires further exploration, because it may provide a link between the equilibrium energetics, mechanical, and electron density characteristics of a stable bond and its potential reactive behaviour.

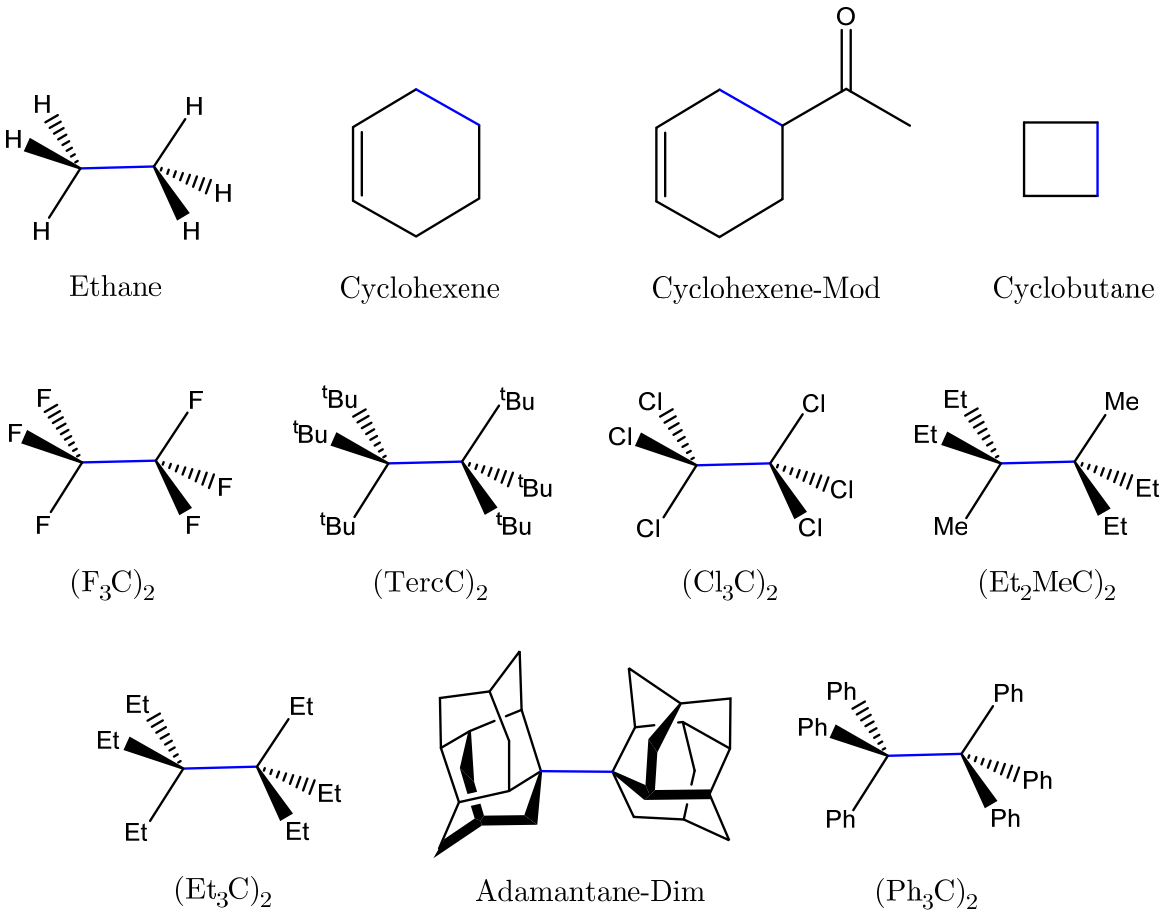

Figure 3.1. Single C-C bond studied in this work (blue) and their respective compounds. Single C-C bonds used in calculations are labelled in blue.

In this regard, it has been shown that the bond stability conditions can be accurately defined in terms of the bond stretching potential energy curve characteristics (See Chapter 2). Accordingly, the maximum elongation that a bond can withstand is governed by the so-called spinodal condition, which is defined as the distance at which the stretching force constant vanishes and determines the maximum external force that the bond can withstand without breaking. In other words, the spinodal condition represents the limit of

mechanical stability of the bond. In the case of covalent bonds, such mechanical instability coincides with a transition between a shared electron regime to a radical-like state. Therefore, if the universal covalent bond stability limit does exist, C-C bonds affected by different effects (electronic, mechanical or any other kind of interaction) must present similar mechanical and electronical rupture distances.

On this basis, we have calculated the pure stretching potential energy curves for selected C-C bonds in a series of molecules (see Figure 3.1) and we have determined the distances at which the electronic and spinodal instability occur (see Table 3.1).

Table 3.1. Mechanical and electronic ruptures for the C-C bonds analysed in the molecules summarized in Figure 3.1. All units are in Å. r_{BET} and r_{LAP} stands for distance at the BET catastrophe and Laplacian sign change occurs. The ratio $(D_e/k_e)^{1/2}$ has been calculated from r_e and r_{sp} using eq. 3.1 (see text for discussion).

C-C Bond	r_e	r_{sp}	r_{BET}	r_{Lap}	$(D_e/k_e)^{1/2}$
Ethane	1.534	1.985	2.00	2.25	0.451
Cyclohexene	1.532	1.96	1.95	2.30	0.428
Cyclohexene-mod	1.534	1.98	2.00	2.25	0.446
$(F_3C)_2$	1.545	1.99	2.00	2.35	0.445
Cyclobutane	1.549	1.99	1.95	2.20	0.441
$(TercC)_2$	1.573	2.03	2.05	2.25	0.457
$(Cl_3C)_2$	1.579	2.03	2.10	2.30	0.451
$(Et_2MeC)_2$	1.601	2.05	2.05	2.25	0.449
$(Et_3C)_2$	1.635	2.08	2.10	2.40	0.445
Adamantane-Dim	1.675	2.13	2.15	2.30	0.455
Ph_3C	1.735	2.16	2.20	2.40	0.425

The spinodal distances, r_{sp}, were calculated from the condition of null second derivative of the pure stretching potential energy curves. The values of r_{sp} lie in the range 1.95-2.15 Å, in excellent agreement with the analysis of Isea [8], where compounds with C-C bonds lengths higher than 2.2 Å were never observed in a distance histogram. Notice that such a distance histogram is in fact a statistical representation of all the C-C bonds contained in the Cambridge Structural Database, and therefore it can be considered as an experimental evidence that no stable C-C bonds are experimentally found beyond these distances.

Likewise, the distances at which the BET catastrophe, which combines the topological analysis of ELF and catastrophe theory by Thom, lie within the 2.00-2.25 Å range, which matches that obtained applying the spinodal criteria. It is interesting to note that values of the Laplacian sign change at the critical point, r_{Lap} perfectly correlate with both r_{sp} and r_{BET}, although it typically happens at slightly (*ca.* 10%) larger distances. In any case, it must be emphasized that which, the Laplacian sign change at the critical point and the BET catastrophe are the indicators considered as a reference to detect covalent bond ruptures [23,24], and both quantities are pretty consistent with the range of spinodal distances found in our analysis.

The observed similarities between mechanical and electronical instability distances imply that the bond stability limit of the single C-C bond is an intrinsic property of the bond, which only depends on the C-C pairwise interaction and not on the type or nature of the external effects. This idea can be illustrated by thinking of all-fluorine (huge negative hyperconjugation effect) and the all-substituted tertbutyl derivate (stabilized by dispersive interactions) of ethane, or the highly strained cyclobutane molecule. If such dramatic interactions plays a dominant role, the electronic and mechanical rupture of the C-C bond will be of course influenced by these effects and will induce a different rupture mechanism, but the of the C-C bond will proceed in a similar fashion with similar rupture distances (within a difference of less than 0.1 Å).

In fact, the mechanical instability is accompanied by an electronic reorganization between a shared electron (shared shell character) regime to a radical like (open shell character) state that in some extent does not depend on the origin of surrounding interactions. Typically shared shell-open to shell electronic transitions indicate processes where bonding electrons evolve to form a radical or electrostatic type interaction, so the bond stability distance can also be understood as the threshold between covalent and non-covalent interactions [25,26].

That rupture distances depends only on covalent nature of the C-C bond implies that its equilibrium characteristics in a given chemical moiety must conform the constrains imposed by the mechanical stability limit. In this regard, a previous study (see Chapter 2) has demonstrated that the spinodal point, r_{sp}, depends on the equilibrium bond-strength properties through the relationship:

$$r_{sp} = r_e + (D_e/k_e)^{1/2} \tag{3.1}$$

where r_e, D_e and k_e are equilibrium quantities, namely distance, bond dissociation energy and stretching force constant, respectively. The spinodal distances calculated through the equation (1) perfectly matches those calculated numerically using the second derivate, as it can be confirmed from the values of $(D_e/k_e)^{1/2}$ presented in Table 1. Notice that this result implies that bond stability limits are produced as consequence of the equilibrium properties, therefore they not only constitute a distance stability limit, but also a mechanical energy limit. Interestingly, a detailed analysis of these data also reveals that the $(D_e/k_e)^{1/2}$ ratio is almost constant (0.45 ± 0.03) Å. Although we will thoroughly analyze this result in the next section, it is worth mentioning here that this constancy reinforces the idea that C-C covalent bonding can be universally described in terms of a universal potential energy function.

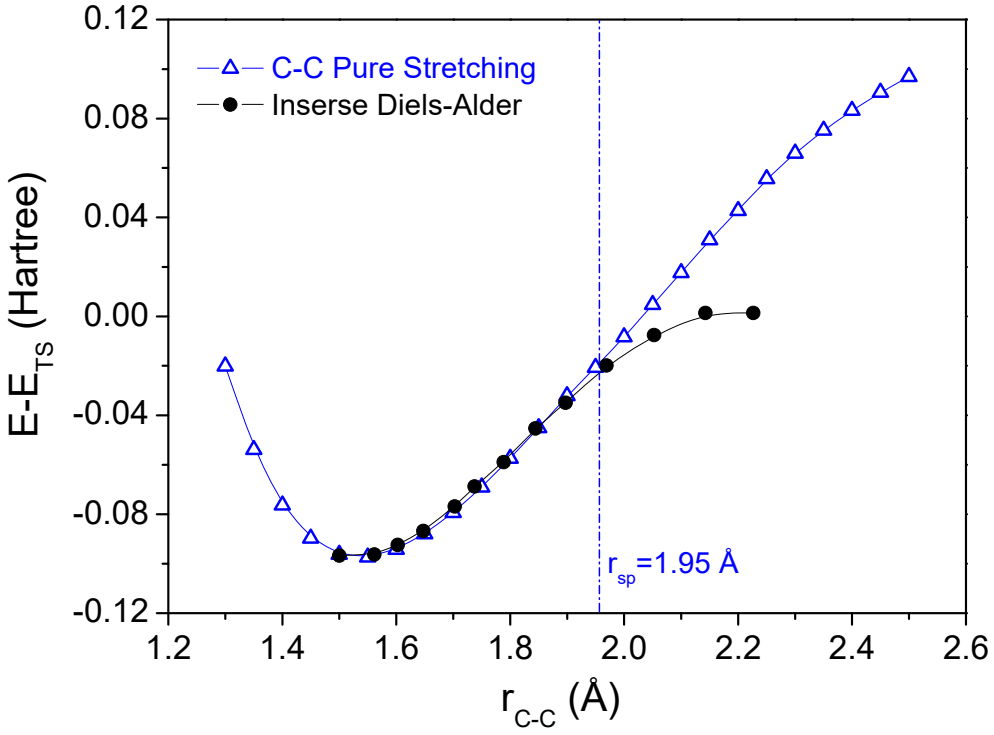

Figure 3.2. Relaxed stretching potential energy curve of the C-C bonds in cyclohexene produced during the Diels-Alder reaction (Blue triangles). Inverse reaction path of the Diels-Alder reaction between ethylene and butadiene (Black dots). The energies have been scaled respect to the transition state energy, E_{TS} = –234.616 Hartree.

We will attempt to outline the implications of the C-C bond universal stability limit in a reactive process. Up to now, we have defined the bond stability limits in terms of the maximum rupture force exerted on a given bond as

consequence of a pure elongation process. This description contrasts to the typical C-C reactions where the covalent bond is formed as consequence of the reagent's interactions. However, chemical reactions can be also understood in terms of a force picture where the bond forming also corresponds to the rupture of the inverse reaction[27-29]. The attractive or repulsive interactions during a chemical process are manifestations of a chemical force which induces a distortion of the bonds elongating or compression inducing the bond ruptures. Moreover, in as much the reaction coordinate is the same in the direct and inverse process of a given chemical reaction, the transition states are unchanged and therefore the bond rupture points of the chemical bonds correspond also to the bond formation.

In the latter reasoning we have considered that the forces are chemical in nature, but they can be also applied mechanically as for instance is done in mechanochemical experiments [30]. Indeed, in as much as these forces are applied along the same path there will be no difference between them, both will produce the same distorted states. Accordingly, the elongation of the chemical bonds along a reaction path can be assimilated to the its pure stretching potential curve. In this regard, we emphasize that models of reactivity, such as the acclaimed Marcus' kinetic theory, [31,32] have been already based on a similar hypothesis. In fact, if we compare the inverse Diels-Alder profile of the ethylene and butadiene with the stretching potential energy curve of the cyclohexane C-C bonds formed during the reaction as a function of the C-C distance, the pure stretching curve and the reaction profile are almost coincident up the spinodal point. The results are plotted in Figure 3.2, where the energy has been scaled and referenced to the transition state.

This transferability of the pure stretching potential energy curve to the reactive process implies that the bond stability conditions also hold in chemical reactions. At this point a nice interpretation of the constancy in the C-C bond forming reactions can be displayed. In as much as the spinodal distance represent the threshold limit for a mechanical breaking of a bond, it is clear that it also defines the point beyond which the bond will exhibit a negative stretching force constant leading to the formation of a transition state. In a similar way, such a point must be associated with an electronic instability that allows the formation of a bond or, in other words, the transition from an open-shell regime, representing the two methyl radical like character of ethane, to a closed shell regime, associated with the 2 electron 2 center C-C bond. Therefore, in spite of electronic substituents or the reaction conditions, all C-C forming and cleavage reactions will be produced at a

universal spinodal distance, which reflect both the bonding formation (rupture) and the mechanical-energetic limit able to produce a favorable (unfavorable) C-C covalent bond.

The latter is clearly evidenced in the Diels-Alder reaction and Cope rearrangements, where the transition state distances are very similar to the C- C bond stability limits. However, we want to emphasize that the spinodal point it is not necessary the same as the transition state. It represents a local stretching force constant which is not defined in the hessian matrix where the second derivates of the energy are performed respect to the normal mode displacement. Only in concerted mechanisms, as those previously discussed here, where the reaction coordinate highly depends on the bond stretching length, the spinodal point will be very close to the maxima in the reaction coordinate. Nonetheless, this is an appealing feature of our model. Transition states are produced in terms of the balance between the attractive and repulsive forces between the reagents and not necessary involve broken of forming bonds. On contrary bond stability model determines the forces, energetics and electronic process needed to produce the bond rupture or formation and only depends on the bond nature of the pairwise interaction. Therefore, the bond rupture or formation of given chemical bond in any chemical reaction will be always produced at the distances determined by the bond stability limits.

The reference C-C single bond. A Universal force constant and electron density distance model.

In the previous section we have evidenced that bond stability limits may constitute a universal criterion which only depends on the nature of the pairwise interaction. However, our ultimate goal is to provide the subjacent basis behind this universality as well as to extend the implications of this model into the C-C bond electronic and mechanical properties.

In this regard, during the C-C bond stability analysis, we realize that regardless the different external interactions produced in the compounds, the square root ratio between the dissociation energy and the equilibrium stretching force constant was quite consistent and approximately equal to 0.45 Å. This result was remarkable since the chemical effects included in our analysis produce a range of C-C equilibrium distances which goes from the standard 1.54 Å up to 1.74 Å, almost a 13% of elongation. Here, it is worth to recall that $(D_e/k_e)^{1/2}$ has been usually defined as the scaling length of the

typical covalent potential energy functions like the Morse and Rydberg ones[33,34]. Consider for example the Rydberg potential, the energy is expressed as

$$E/D_e = -(1 + a^*)e^{-a^*} \tag{3.2}$$

where a^* is a reduced distance defined as,

$$a^* = \frac{r - r_e}{(D_e/k_e)^{1/2}} \tag{3.3}$$

A constant value of the scaling length makes possible to define a common reference equilibrium distance. Otherwise it will be necessary to change r_e in other to accurately describe the stretching behavior of different bonds under this analytical form. As a result, the observed constancy in the C-C scaling length suggest that stable C-C bonds can be considered as fixed points along a reduced hypothetical universal potential energy curve of an isolated single covalent reference, which upon stretching behaves energetically and mechanically similar as the stable counterparts.

For an isolated C-C single covalent bond, the reference equilibrium bond length will correspond to the distance where the repulsive forces between two isolated C nuclei balance the attractive forces between them and the electrons concentrated in the internuclear region. At this respect, Ganguly [35,36] have demonstrated that the equilibrium distance of a bond in standard conditions (d_{MM}) can be expressed as the sum of two screened core lengths, defined in terms of the average orbital radii, plus a bonding transferable length equal to 0.74 Å. The latter was calculated assuming a Borh model for the hydrogen molecule and considering that the bond formation involves two states. One arising from the charge-transfer of a hole which defines the attraction of the electron to the nuclei, and the other from an electron transfer which accounts for the repulsion between the two shared electrons. Within this model the bond length will not depend neither in any experimental data or molecular properties but only on the characteristics of two interacting C atoms. Accordingly, the isolated C-C bond length can be estimated in 1.54 Å. This value is very close to the equilibrium bond length of the C-C in the ethane molecule, which typically has been considered as the reference single C-C covalent bond, and is also in agreement with the experimental sum of the covalent radii statistically determined by X-Ray diffraction [37,38] reinforcing the idea that our reference corresponds to the prototypical single C-C covalent bond.

On this basis, we can provide an explanation for the constancy in the C-C rupture distances. Using equation 1 with a scaling and equilibrium distances of 0.45 and 1.54 Å respectively, the C-C bond reference rupture will be produced at 1.99 Å. Here we want to emphasize that the latter calculation only depends on a reference equilibrium bond distance and on a scaling length determined from ab-initio calculations, and therefore barely depends on the assumed potential energy function, rather it is a consequence of the universal energy-distance dependence experimented by all the pairwise interactions. Consequently, this rupture point represents the bond stability limit of a generalized single covalent interaction and no matter how C-C bonds will be elongated (structure, electronic, interaction or reactive effects), close to this distance they will be always unstable.

The latter conclusion can be corroborated analyzing the dependence of the stretching force constant of the C-C bonds as a function the equilibrium distance. According to our reasoning, the force constant distance dependence of isolated C-C pairwise interaction must reproduce the experimental data and gradually decrease up to the spinodal point. As the C-C pairwise interaction corresponds to a hypothetical entity, it is necessary to assume a functional form to describe its force constant behavior. Considering a Rydberg type potential, the stretching force constant of our reference depends on the distance as

$$k = k_e(1 - a^*)e^{-a^*} \tag{3.4}$$

The scaled distance, a^*, is defined using the previous equilibrium and scaling lengths. In the case of k_e we have assumed that it is equal to the relaxed stretching force constant of the ethane (4.00 N cm^{-1}) which displays a similar equilibrium distance.

In Figure 3.3, we have represented the relaxed force constant data of the 70 single C-C bonds of several compounds studied by Markopoulos and Grunenberg[39]. As expected, our isolated reference accurately describes both the compressed and overlong C-C single bonds. Notice how in the logarithmic plot the experimental data consistently decrease following the curvature of the isolated C-C bond reference up to the spinodal point evidencing that all stable C-C bond will break at the C-C bond stability limit. Such a behavior clearly contrasts with other empirical laws proposed in the literature such as the Badger one[40,41]. The latter is based on inverse power law relationship and have accurately described the distance dependence of numerous bonds. However, it is important to highlight that this correlation (as well as other

such as the exponential ones) does not consider the bond cleavage, only at infinite distance they predict a zero stretching force constant.

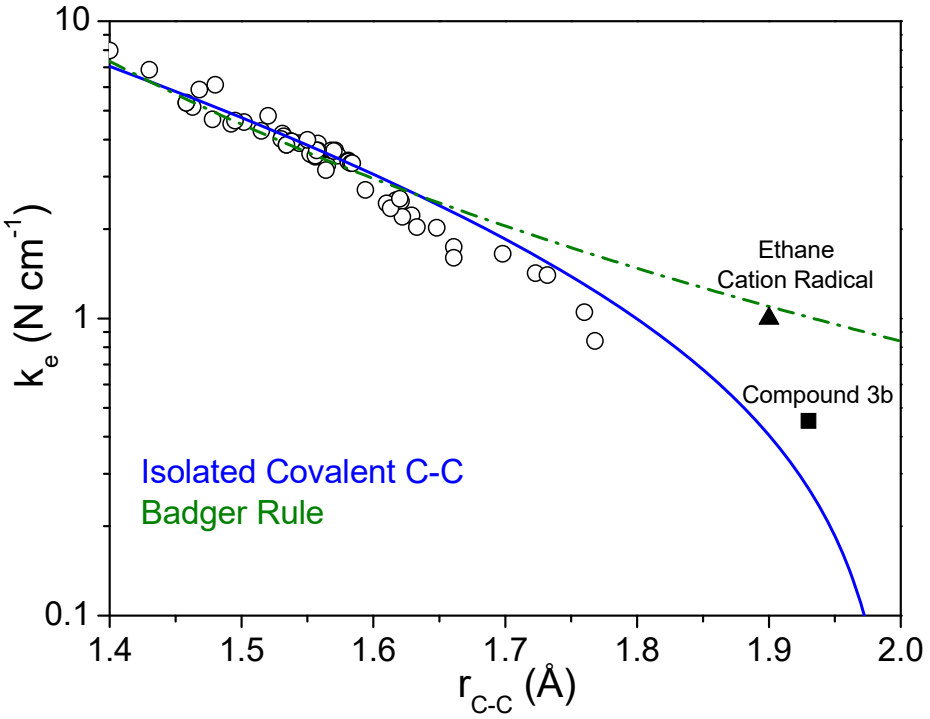

Figure 3.3. Equilibrium stretching force constant of 70 single C-C bonds from reference X (empty circles) against its equilibrium distance. The triangle and square points stand for the ethane cation radical and compound 3b. Blue line isolated C-C bond reference model of this work. Green dash-dot line Badger rule from reference [42].

The force constant distance dependence of C-C bonds has been –and still is– a fruitful debate topic [43,44]. Recently, Grunenberg [42] have demonstrated that C-C bond accomplish the Badger rule up to the distances of 1.90 Å if one considers the ethane cation radical. Including the proposed Badger rule in Figure 3.3, we see how the latter clearly deviates at distances larger than 1.6 Å, yet the ethane cation radical is accurately described under this model. At this respect we have calculated the stretching force constant of another overlong bond with a similar distance as the ethane cation radical, the cyclic C-C bond of the amino-o-carborane 3b compound[5]. Interestingly its stretching force constant clearly follows our isolated C-C single bond reference towards the bond rupture point. This discrepancy can be resolved recalling that the bond stability limit model is based on the assumption that the universal potential energy function corresponds to a single C-C covalent bond. When we analyze the electron localization function of the ethane cation

radical in the D_{3d} geometry, we obtain a population of 0.35 e^- for the C-C disynaptic basin with an electronic fluctuation variance of 0.276 e^-. According to this result, the latter corresponds to a charge-shift bond[45] where a high contribution of an ionic character is present in the wavefunction and therefore cannot be considered a covalent C-C interaction. This is not the case of the diamino borane compound, which as it has been demonstrated fulfills the conditions to be considered a covalent bond [5]. Interestingly, this interaction change is reflected in the mechanical properties as a deviation from the covalent pairwise interaction. This result points out that bond stability limits not only evidence the bond rupture but also variations in the nature on the interaction. The latter involve changes in mechanical properties of the bond and thus in its potential energy function. As we will see next, this result has important consequences in the chemical conception of C-C multiple bonds

The excellent agreement between the bond stability model and the force constant-distance data proves that an isolated pairwise interaction can provide fruitful chemical information about the bond properties. Moreover, reinforces the idea that the relationship between the spinodal distance and the equilibrium bond characteristics given by equation 1 can be of general applicability. This is a quite restrictive criteria, because given an equilibrium bond length, its dissociation energy and force constant must adjust in order to fulfill the universal bond stability limits of the isolated C-C pairwise interaction. Consider for example the all-meta-tert-butylhexaphenylethane compound. Many conventional computational methods fail to describe its dissociation energy, and London dispersion corrections have to be applied during the calculations in order to produce a stable interaction energy [46]. Using the computed data obtained by Wagner et al. [47] we obtain an equilibrium distance of 1.67 Å and a k_e value of 237.47 kcal mol^{-1} $Å^{-2}$. Readily we can say that this bond must be stable because is beyond the isolated C-C 2Å limit. Moreover, if we assume that the scaling length is equal to 0.45 Å, we predict a dissociation energy for this C-C bond of 48 kcal mol^{-1}, in fair agreement with the experimental one which ranges from 30 to 44 kcal mol^{-1} depending on the calculation method [3].

Finally, it is worth to analyze our isolated C-C bond reference in terms of an electron density perspective. Interestingly, the idea of an isolated C-C reference able to describe the properties of a given bond has been also present in this field. Several authors have demonstrated that the electron density at the bond critical point of different C-C bonds follows the same distance dependence as the promolecular reference [6,9]. Notice, that in this case the

electron density at a given distance is described in terms of the overlap of the electron density tails of the isolated atoms. The fact that two isolated C-C bond references accurately describes the mechanical-energetic and the electron density evolution of the C-C bond cannot be accidental. Indeed, in the well foundation basis of the density functional theory [48] the electron density is a functional of the energy, and therefore a model able to describe the energetic and mechanical properties of a bond must also reproduce its electron density behaviour.

Let us try to depict how our universal pairwise interaction can be related to the electron density characteristics. Using the well-known Pauling bond order relationship [49], the potential energy function of a covalent bond can be expressed in terms of a bond order coordinate, n,

$$n = e^{-(r-r_e)/b} \tag{3.5}$$

Apart from the controversial definition of the bond order, it is clear that expression 5 defines to some extend a reduced magnitude related to the electron density properties of the bond. Assume for a moment that the constant b in the previous formula is equal to our scaling distance $(D_e/k_e)^{1/2}$. Then, the energy can be expressed as

$$E/D_e = -[1 - ln(n)]n \tag{3.6}$$

Within this perspective, the mechanical properties are to some extend linked to the bond electronic behavior. Indeed, if we consider that the bond order can be defined as the ratio between the electron density at critical point (ρ) at a given distance r and the electron density at the equilibrium (ρ_e) [ref Bader],

$$n = \frac{\rho}{\rho_e} \tag{3.7}$$

We predict a exponential dependence of the electron density with the distance, in clear resemblance with the promolecular model

$$\rho = \rho_e e^{-(r-r_e)/(D_e/k_e)^{1/2}} \tag{3.8}$$

In the case of the isolated C-C bond, $(D_e/k_e)^{1/2}$must be equal to 0.45±0.03 Å and r_e =1.541 Å. Therefore, if our isolated C-C bond reference corresponds to the promolecular C-C bond, we must expect that expression 8 accurately describe the electron density of the different C-C bond. This view is confirmed in Figure 3.4, where we can see how using the value of ρ_e of the ethane

molecule (1.569 e^{-} $Å^{-3}$) to describe our isolated C-C bond, the electron density variation perfectly matches the value of the different single C-C bond in the compounds studied within the limits of error (All the data are collected in the supplementary material 3).Under this view, the isolated C-C bond potential energy curve constitutes the functional of the electron density of the promolecular bond. In principle such a relationship must hold for any pairwise interaction, and therefore the bond stability limits can be considered an inevitable consequence of the interaction shape which is applicable to all the bonds.

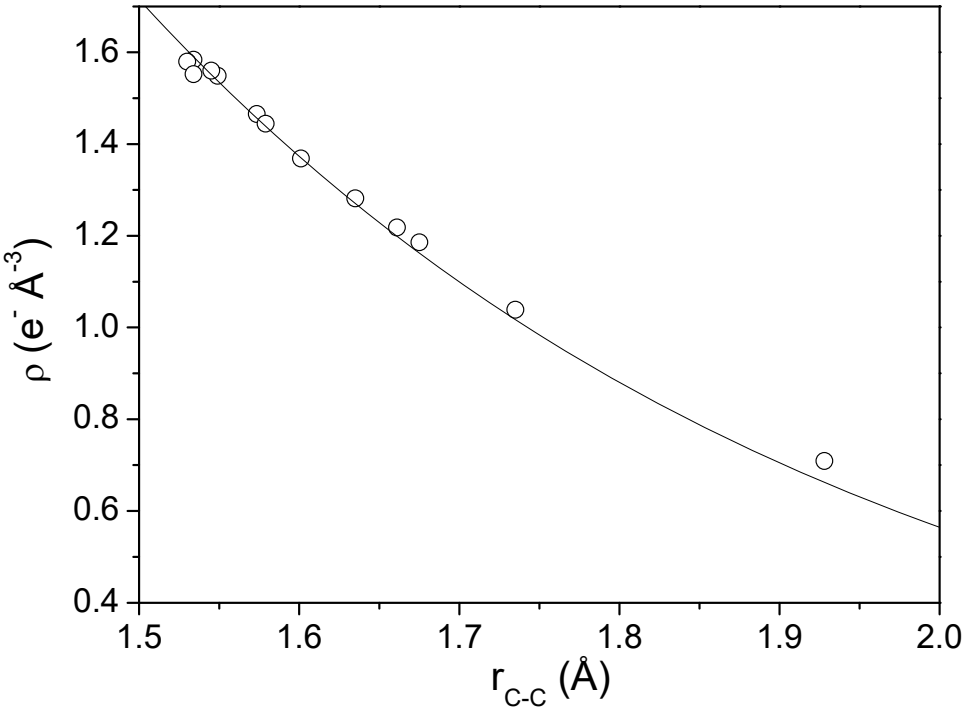

Figure 3.4. Electron density at the bond critical point against is equilibrium distance for the 11 C-C bonds studied in this work (empty circles). The black line corresponds to the isolated dependence given by expression 3.8.

To sum up, through this section we have carefully provided a reliable theoretical basis to the bond stability limits, demonstrating that bond ruptures are an inevitable consequence of the pairwise interaction nature between two atoms. Our results clearly evidence that bond ruptures are produced at specific distances independently the way they are produced and therefore imposes a quite restrictive criteria to the bond dissociation energy and stretching force constant values. This relationship may allow the calculation of vibrational and thermochemical data in complex systems knowing the value of the scaling length. Moreover, in addition to the ideas

previously discussed we have provided a direct link between the mechanical properties and the electron density distance dependences pointing out that interaction changes must produce modifications of the potential energy function.

Bond Stability Limits and interaction changes. The case of Multiple Bonds.

Finally, it is interesting to explore the implication of our model in C-C multiple bonds. Several well-known relationships such as the bond order-bond length correlations [50,51] have settled up the idea the multiple C-C bonds has can be considered as compressed analogues of the single ones, leading to the conception that the mechanical and electronic properties of all the C-C bonds gradually change with the distance. Although this view has proved to be very useful, in our opinion it is somewhat confusing, because implies that upon compression a single bond can become a multiple one and therefore display a similar chemical behaviour. This situation clearly contrasts with the theoretical perspective of the multiple bonds where the pi interactions are clearly differentiated from the sigma ones in its energy and electron density distributions.

In this regard, the previously discussed example of C-C bond in the ethane cation radical in the diamino-o-carborane 3b compound have evidenced that when the interaction type is modified its bond stability limits and thus its potential energy curve is also altered. Such a result is quite striking because it demonstrates that a change in the interaction type must produce abrupt transitions in the mechanical and energetic properties of the bonds. At this respect it is important to define what it is an interaction change. In our model we refer to it as any modification of the bond stability limit parameters which produce a different scaling length and therefore a different pairwise interaction reference. Notice that the interaction change also involves a modification in the promolecular reference and consequently in its electron density behaviour. Accordingly, if the chemical conception of a multiple bond it is correct, they will display the same bond stability limits as the single ones and therefore they will be described under the same universal potential energy curve. On this basis we have calculated the potential stretching curves of the ethane, ethylene and acetylene molecules, the three prototypical single, double and triple C-C bonds. As expected their bond ruptures consistently decrease from 1.99 Å in the ethane to 1.75 Å and 1.59 Å in the ethylene and acetylene respectively as well as their scaling lengths does from 0.45 Å to 0.42 Å and

0.38 Å, reinforcing the idea that triple, double and single bonds are completely different in nature. This view is even more clearly confirmed when we plot in Figure 3.5, the previously discussed single C-C bond force constant of Markopoulus [39], the force constant of some double and triple bonds [52,53] and the force constant distance variation of the ethane, ethylene and acetylene. Notice how all the data follow the distance dependence of its prototypical bond partner as well as they are systematically lower as the multiple bond character is increased. The electron density variation shows a similar flaw as the force constant data, and the acetylene and ethylene curves are systematically lower than the corresponding to the ethane (See Figure X of the supplementary material). As a result, the single to multiple bond transition does not involve a gradually change –not even the double and triple bonds can be considered as it–,rather they correspond to different pairwise interactions described by different potential energy curves. Under this view, the multiple to single transition must be considered as chemical reaction like process, where the two potential energy curve crosses defining a transition state.

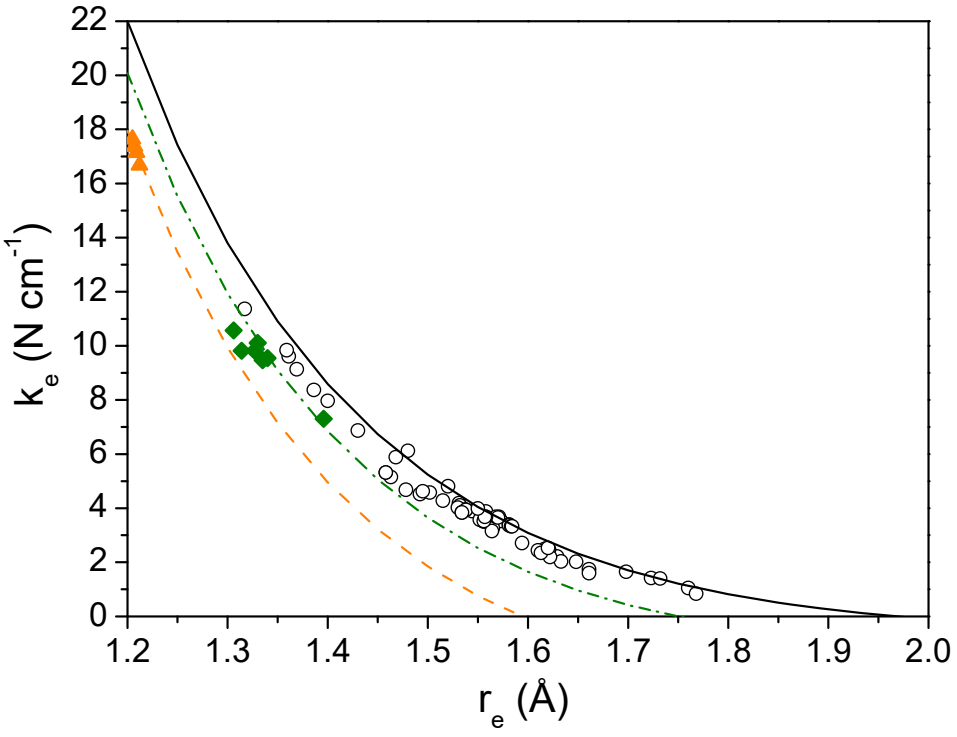

Figure 3.5. Distance dependence of the equilibrium stretching force constant for single (empty circles), double (green diamonds) and triple (orange triangles) C-C bonds. The stretching force constant variations for ethane, ethylene and acetylene are shown as black, green dash-dot and orange dash lines.

References

[1] G. Kaupp and J. Boy, Overlong C-C Single Bonds. *Angew. Chem. Int. Ed. Engl*, *36*, **1997**. DOI: https://doi.org/10.1002/anie.199700481.

[2] A. A. Fokin, L. V. Chernish, P. A. Gunchenko, E. Y. Tikhonchuk, H. Hausmann, M. Serafin, J. E. Dahl, R. M. Carlson, and P. R. Schreiner, Stable alkanes containing very long carbon-carbon bonds. *J Am Chem Soc*, *134*, 13641-13650, **2012**. DOI: https://doi.org/10.1021/ja302258q.

[3] P. R. Schreiner, L. V. Chernish, P. A. Gunchenko, E. Y. Tikhonchuk, H. Hausmann, M. Serafin, S. Schlecht, J. E. Dahl, R. M. Carlson, and A. A. Fokin, Overcoming lability of extremely long alkane carbon-carbon bonds through dispersion forces. *Nature*, *477*, 308-311, **2011**. DOI: https://doi.org/10.1038/nature10367.

[4] Y. Ishigaki, T. Shimajiri, T. Takeda, R. Katoono, and T. Suzuki, Longest C-C Single Bond among Neutral Hydrocarbons with a Bond Length beyond 1.8 Å. *Chem*, *4*, 795-806, **2018**. DOI: https://doi.org/10.1016/j.chempr.2018.01.011.

[5] J. Li, R. Pang, Z. Li, G. Lai, X. Q. Xiao, and T. Muller, Exceptionally Long C-C Single Bonds in Diamino-o-carborane as Induced by Negative Hyperconjugation. *Angew Chem Int Ed Engl*, *58*, 1397-1401, **2019**. DOI: https://doi.org/10.1002/anie.201812555.

[6] P. M. Dominiak, A. Makal, P. R. Mallinson, K. Trzcinska, J. Eilmes, E. Grech, M. Chruszcz, W. Minor, and K. Wozniak, Continua of interactions between pairs of atoms in molecular crystals. *Chem. Eur. J.*, *12*, 1941-1949, **2006**. DOI: https://doi.org/10.1002/chem.200500600.

[7] D. R. Huntley, G. Markopoulos, P. M. Donovan, L. T. Scott, and R. Hoffmann, Squeezing C-C bonds. *Angew Chem Int Ed Engl*, *44*, 7549-7553, **2005**. DOI: https://doi.org/10.1002/anie.200502721.

[8] R. Isea, What is the maximum stretching for the C-C single bond? *J. Mol. Struct.*, *540*, 131-138, **2001**. DOI: https://doi.org/10.1016/S0166-1280(00)00721-1.

[9] A. Costales, M. A. Blanco, A. Martín Pendás, P. Mori-Sánchez, and V. Luaña, Universal Features of the Topological Bond Properties of the Electron Density. *J. Phys. Chem. A*, *108*, 2794-2801, **2004**. DOI: https://doi.org/10.1021/jp037627z.

[10] K. Black, P. Liu, L. Xu, C. Doubleday, and K. N. Houk, Dynamics, transition states, and timing of bond formation in Diels-Alder reactions. *Proc*

Natl Acad Sci U S A, *109*, 12860-12865, **2012**. DOI: https://doi.org/10.1073/pnas.1209316109.

[11] L. R. Domingo, A new C–C bond formation model based on the quantum chemical topology of electron density. *RSC Adv.*, *4*, 32415-32428, **2014**. DOI: 10.1039/c4ra04280h.

[12] L. R. Domingo, E. Chamorro, and P. Perez, Understanding the mechanism of non-polar Diels-Alder reactions. A comparative ELF analysis of concerted and stepwise diradical mechanisms. *Org Biomol Chem*, *8*, 5495-5504, **2010**. DOI: 10.1039/c0ob00563k.

[13] J. Huang and M. Kertesz, Stepwise Cope Rearrangement of Cyclobiphenalenyl via an Unusual Multicenter Covalent π-Bonded Intermediate. *J. Am. Chem. Soc.*, *128*, 7277-7286, **2006**. DOI: https://doi.org/10.1021/ja060427r.

[14] O. Wiest, *IEncyclopedia of Computational Chemistry*, ed. W.C. Schleyer, Schleyer, Wiley: Chichester, Vol. 5, **1998**.

[15] G. W. T. M. J. Frisch, H. B. Schlegel, G. E. Scuseria, M. A. Robb, J. R. Cheeseman, G. Scalmani, V. Barone, G. A. Petersson, H. Nakatsuji, X. Li, M. Caricato, A. Marenich, J. Bloino, B. G. Janesko, R. Gomperts, B. Mennucci, H. P. Hratchian, J. V. Ortiz, A. F. Izmaylov, J. L. Sonnenberg, D. Williams-Young, F. Ding, F. Lipparini, F. Egidi, J. Goings, B. Peng, A. Petrone, T. Henderson, D. Ranasinghe, V. G. Zakrzewski, J. Gao, N. Rega, G. Zheng, W. Liang, M. Hada, M. Ehara, K. Toyota, R. Fukuda, J. Hasegawa, M. Ishida, T. Nakajima, Y. Honda, O. Kitao, H. Nakai, T. Vreven, K. Throssell, J. A. Montgomery, Jr., J. E. Peralta, F. Ogliaro, M. Bearpark, J. J. Heyd, E. Brothers, K. N. Kudin, V. N. Staroverov, T. Keith, R. Kobayashi, J. Normand, K. Raghavachari, A. Rendell, J. C. Burant, S. S. Iyengar, J. Tomasi, M. Cossi, J. M. Millam, M. Klene, C. Adamo, R. Cammi, J. W. Ochterski, R. L. Martin, K. Morokuma, O. Farkas, J. B. Foresman, and D. J. Fox, *Gaussian 09*, I. Gaussian, Wallingford CT, 2016

[16] T. H. Dunning, Gaussian basis sets for use in correlated molecular calculations. I. The atoms boron through neon and hydrogen. *J. Chem. Phys.*, *90*, 1007-1023, **1989**. DOI: https://doi.org/10.1063/1.456153.

[17] G. E. Scuseria, Analytic evaluation of energy gradients for the singles and doubles coupled cluster method including perturbative triple excitations: Theory and applications to FOOF and Cr2. *J. Chem. Phys.*, *94*, 442-447, **1991**. DOI: https://doi.org/10.1063/1.460359.

[18] Energy-Represented Direct Inversion in the Iterative Subspace within a Hybrid Geometry Optimization Method. *J. Chem. Theory Comput.*, *2*, 835-839, **2006**. DOI: https://doi.org/10.1021/ct050275a.

[19] Todd A. Keith, *AIMAll (Version 19.02.13)*, O.P.K. TK Gristmill Software, USA, aim.tkgristmill.com, 1995

[20] A. Otero-De-La-Roza, E. R. Johnson, and V. Luaña, Critic2: A program for real-space analysis of quantum chemical interactions in solids. *Computer Physics Communications*, *185*, 1007-1018, **2014**. DOI: https://doi.org/10.1016/j.cpc.2013.10.026.

[21] K. M. a. F. Izumi, VESTA 3 for three-dimensional visualization of crystal, volumetric and morphology data. *J. Appl. Cryst.*, *44*, 1272-1276, **2011**. DOI: https://doi.org/10.1107/S0021889811038970.

[22] E. F. Pettersen, T. D. Goddard, C. C. Huang, G. S. Couch, D. M. Greenblatt, E. C. Meng, and T. E. Ferrin, UCSF Chimera--a visualization system for exploratory research and analysis. *J Comput Chem*, *25*, 1605-1612, **2004**. DOI: https://doi.org/10.1002/jcc.20084.

[23] R. F. W. Bader, Definition of Molecular Structure: By Choice or by Appeal to Observation? *J. Phys. Chem. A*, *114*, 7431–7444, **2010**. DOI: https://doi.org/10.1021/jp102748b.

[24] X. Krokidis, S. Noury, and B. Silvi, Characterization of Elementary Chemical Processes by Catastrophe Theory. *J. Phys. Chem. A*, *101*, 7277-7282, **1997**. DOI: https://doi.org/10.1021/jp9711508.

[25] P. R. Mallinson, G. T. Smith, C. C. Wilson, E. Grech, and K. Wozniak, From Weak Interactions to Covalent Bonds: A Continuum in the Complexes of 1,8-Bis(dimethylamino)naphthalene. *J. Am. Chem. Soc*, *125*, 4259-4270, **2003**. DOI: https://doi.org/10.1021/ja029389b.

[26] E. Espinosa, I. Alkorta, J. Elguero, and E. Molins, From weak to strong interactions: A comprehensive analysis of the topological and energetic properties of the electron density distribution involving X–H···F–Y systems. *J. Chem. Phys.*, *117*, 5529-5542, **2002**. DOI: https://doi.org/10.1063/1.1501133.

[27] A. Toro-Labbe, S. Gutierrez-Oliva, J. S. Murray, and P. Politzer, The reaction force and the transition region of a reaction. *J Mol Model*, *15*, 707-710, **2009**. DOI: https://doi.org/10.1007/s00894-008-0431-8.

[28] A. Toro-Labbé, S. Gutiérrez-Oliva, J. S. Murray, and P. Politzer, A new perspective on chemical and physical processes: the reaction force.

Molecular Physics, *105*, 2619-2625, **2010**. DOI: https://doi.org/10.1080/00268970701604663.

[29] D. Yepes, J. S. Murray, P. Perez, L. R. Domingo, P. Politzer, and P. Jaque, Complementarity of reaction force and electron localization function analyses of asynchronicity in bond formation in Diels-Alder reactions. *Phys. Chem. Chem. Phys.*, *16*, 6726-6734, **2014**. DOI: 10.1039/c3cp54766c.

[30] R. Stevenson and G. De Bo, Controlling Reactivity by Geometry in Retro-Diels-Alder Reactions under Tension. *J. Am. Chem. Soc.*, *139*, 16768-16771, **2017**. DOI: https://doi.org/10.1021/jacs.7b08895.

[31] R. A. Marcus, Electron transfer reactions in chemistry. Theory and experiment. *Reviews of Modern Physics*, *65*, 599-610, **1993**. DOI: https://doi.org/10.1103/RevModPhys.65.599.

[32] I. Fernandez and F. M. Bickelhaupt, The activation strain model and molecular orbital theory: understanding and designing chemical reactions. *Chem Soc Rev*, *43*, 4953-4967, **2014**. DOI: 10.1039/c4cs00055b.

[33] J. Ferrante, H. Schlosser, and J. R. Smith, Global expression for representing diatomic potential-energy curves. *Physical Review A*, *43*, 3487-3494, **1991**. DOI: https://doi.org/10.1103/PhysRevA.43.3487.

[34] F. Wang, The invariant character of two-body binding potentials. *Journal of Molecular Structure: THEOCHEM*, *664-665*, 83-89, **2003**. DOI: 10.1016/j.theochem.2003.07.004.

[35] P. Ganguly, Relation between Interatomic Distances in Transition-Metal Elements, Multiple Bond Distances, and Pseudopotential Orbital Radii. *J. Am. Chem. Soc*, *17*, 2655-2656, **1995**. DOI: https://doi.org/10.1021/ja00114a033.

[36] P. Ganguly, Atom-Bond Transition: Transferability of Atomic Length Scales. *J. Phys. Chem. A*, *104*, 8432-8444, **2000**. DOI: https://doi.org/10.1021/jp001719w.

[37] B. Cordero, V. Gomez, A. E. Platero-Prats, M. Reves, J. Echeverria, E. Cremades, F. Barragan, and S. Alvarez, Covalent radii revisited. *Dalton Trans*, 2832-2838, **2008**. DOI: 10.1039/b801115j.

[38] P. Pyykko and M. Atsumi, Molecular single-bond covalent radii for elements 1-118. *Chem.: Eur. J.*, *15*, 186-197, **2009**. DOI: https://doi.org/10.1002/chem.200800987.

[39] G. Markopoulos and J. Grunenberg, Predicting kinetically unstable C-C bonds from the ground-state properties of a molecule. *Angew. Chem. Int. Ed. Engl.*, *52*, 10648-10651, **2013**. DOI: https://doi.org/10.1002/anie.201303821.

[40] R. M. Badger, A Relation Between Internuclear Distances and Bond Force Constants. *J. Chem. Phys.*, *2*, 128-131, **1934**. DOI: http://dx.doi.org/10.1063/1.1749433.

[41] J. Cioslowski, Guanghua Liu, and R. a. M. Castro, Badger's rule revisited. *Chem. Phys. Lett.*, *331*, 407-501, **2000**. DOI: https://doi.org/10.1016/S0009-2614(00)01209-4.

[42] J. Grunenberg, Comment on "The Nature of the Fourth Bond in the Ground State of C2: The Quadruple Bond Conundrum". *Chem.: Eur. J.*, *21*, 17126, **2015**. DOI: https://doi.org/10.1002/chem.201500130.

[43] W. Zou and D. Cremer, C2 in a Box: Determining Its Intrinsic Bond Strength for the X Ground State. *Chem.: Eur. J.*, *22*, 4087-4099, **2016**. DOI: https://doi.org/10.1002/chem.201503750.

[44] D. Danovich, P. C. Hiberty, W. Wu, H. S. Rzepa, and S. Shaik, The nature of the fourth bond in the ground state of C2: the quadruple bond conundrum. *Chem.: Eur. J.*, *20*, 6220-6232, **2014**. DOI: https://doi.org/10.1002/chem.201400356.

[45] S. Shaik, D. Danovich, B. Silvi, D. L. Lauvergnat, and P. C. Hiberty, Charge-shift bonding--a class of electron-pair bonds that emerges from valence bond theory and is supported by the electron localization function approach. *Chem. Eur. J.*, *11*, 6358-6371, **2005**. DOI: https://doi.org/10.1002/chem.200500265.

[46] S. Grimme and P. R. Schreiner, Steric crowding can stabilize a labile molecule: solving the hexaphenylethane riddle. *Angew Chem Int Ed Engl*, *50*, 12639-12642, **2011**. DOI: https://doi.org/10.1002/anie.201103615.

[47] J. P. Wagner and P. R. Schreiner, London dispersion in molecular chemistry--reconsidering steric effects. *Angew Chem Int Ed Engl*, *54*, 12274-12296, **2015**. DOI: https://doi.org/10.1002/anie.201503476.

[48] R. G. Parr and Y. Weitao, *Density-Functional Theory of Atoms and Molecules*, Oxford Univerty Press, Vol. 1, **1989**.

[49] L. Pauling, The Nature of the Chemical Bond and the Structure of Molecules and Crystals: An Introduction to Modern Structural Chemistry, Cornell University Press, 3rd ed., **1960**.

[50] J. Sedlar, I. Anđelić, I. Gutman, D. Vukičević, and A. Graovac, Vindicating the Pauling-bond-order concept. *Chem. Phys. Lett.*, *427*, 418-420, **2006**. DOI: https://doi.org/10.1016/j.cplett.2006.06.026.

[51] T. M. Krygowski and M. K. Cyranski, Structural Aspects of Aromaticity. *Chem. Rev.*, *101*, 1385−1419, **2001**. DOI: https://doi.org/10.1021/cr990326u.

[52] D. Cremer, A. Wu, A. Larsson, and E. Kraka, Some Thoughts about Bond Energies, Bond Lengths, and Force Constants. *J. Mol. Model*, *6*, 396 – 412, **2000**. DOI: https://doi.org/10.1007/PL00010739.

[53] W. Zou, R. Kalescky, E. Kraka, and D. Cremer, Relating normal vibrational modes to local vibrational modes with the help of an adiabatic connection scheme. *J. Chem. Phys.*, *137*, 084114, **2012**. DOI: https://doi.org/10.1063/1.4747339.

Supplementary Material Chapter 3

Table S.3.1. Potential energy curves for the different C-C bonds.

Ethane			
r (Å)	E (a.u.)	r (Å)	E (a.u.)
1.1	-79.39085	2	-79.55447
1.15	-79.4549	2.05	-79.54707
1.2	-79.50324	2.1	-79.5398
1.25	-79.53914	2.15	-79.53272
1.3	-79.56518	2.2	-79.52587
1.35	-79.5834	2.25	-79.51929
1.4	-79.59546	2.3	-79.51298
1.45	-79.60265	2.35	-79.50697
1.5	-79.60603	2.4	-79.50126
1.55	-79.60646	2.45	-79.49586
1.6	-79.60459	2.5	-79.49075
1.65	-79.60099	2	-79.55447
1.7	-79.59608	2.05	-79.54707
1.75	-79.59021	2.1	-79.5398
1.8	-79.58366	2.15	-79.53272
1.85	-79.57665	2.2	-79.52587
1.9	-79.56936	2.25	-79.51929
1.95	-79.56193	2.3	-79.51298

Cyclohexene			
r (Å)	E (a.u.)	r (Å)	E (a.u.)
1.3	-234.67447	1.9	-234.6806
1.35	-234.69143	1.95	-234.67401
1.4	-234.70263	2	-234.66743
1.45	-234.70937	2.05	-234.66121
1.5	-234.71262	2.1	-234.65554
1.55	-234.71314	2.15	-234.65008
1.6	-234.7116	2.2	-234.6450
1.65	-234.70849	2.25	-234.6401
1.7	-234.70419	2.3	-234.6356
1.75	-234.69902	2.35	234.6314
1.8	-234.69325	2.4	-234.6275
1.85	-234.68705	2.45	234.62405

Cyclohexene-mod			
r (Å)	E (a.u.)	r (Å)	E (a.u.)
1.3	-387.35789	1.9	-387.34801
1.35	-387.37263	1.95	-387.34063
1.4	-387.38188	2	-387.33325
1.45	-387.38687	2.05	-387.32592
1.5	-387.38854	2.1	-387.31871
1.55	-387.38766	2.15	-387.31165
1.6	-387.38484	2.2	-387.30477
1.65	-387.38056	2.25	-387.29808
1.7	-387.37519	2.3	-387.29161
1.75	-387.36904	2.35	-387.28535
1.8	-387.36234	2.4	-387.27931
1.85	-387.35528	2.45	-387.27349

Cyclohexene-mod			
r (Å)	E (a.u.)	r (Å)	E (a.u.)
1.3	-387.35789	1.9	-387.34801
1.35	-387.37263	1.95	-387.34063
1.4	-387.38188	2	-387.33325
1.45	-387.38687	2.05	-387.32592
1.5	-387.38854	2.1	-387.31871
1.55	-387.38766	2.15	-387.31165
1.6	-387.38484	2.2	-387.30477
1.65	-387.38056	2.25	-387.29808
1.7	-387.37519	2.3	-387.29161
1.75	-387.36904	2.35	-387.28535
1.8	-387.36234	2.4	-387.27931
1.85	-387.35528	2.45	-387.27349

$(CF_3)_2$			
r (Å)	E (a.u.)	r (Å)	E (a.u.)
1.1	-673.84118	1.75	-674.06311
1.15	-673.91047	1.8	-674.05635
1.2	-673.96304	1.85	-674.04905
1.25	-674.00233	1.9	-674.04138
1.3	-674.03107	1.95	-674.03351
1.35	-674.05141	2	-674.02555
1.4	-674.0651	2.05	-674.01761
1.45	-674.07352	2.1	-674.00976
1.5	-674.07781	2.15	-674.00207
1.55	-674.07884	2.2	-673.99458
1.6	-674.07737	2.25	-673.98733
1.65	-674.07395	2.3	-673.98033
1.7	-674.06908	2.35	-673.97362

Cyclobutane			
r (Å)	E (a.u.)	r (Å)	E (a.u.)
1.4	-156.72415	1.4	-156.72415
1.45	-156.73205	2	-156.69311
1.5	-156.73621	2.05	-156.68652
1.55	-156.73744	2.1	-156.68004
1.6	-156.73641	2.15	-156.67373
1.65	-156.73365	2.2	-156.66762
1.7	-156.7296	2.25	-156.66175
1.75	-156.7246	2.3	-156.65615
1.8	-156.71891	2.35	-156.65082
1.85	-156.71276	2.4	-156.64579
1.9	-156.70633	2.45	-156.64107
1.95	-156.69974	2.5	-156.63667

Cyclobutane			
r (Å)	E (a.u.)	r (Å)	E (a.u.)
1.4	-156.72415	1.4	-156.72415
1.45	-156.73205	2	-156.69311
1.5	-156.73621	2.05	-156.68652
1.55	-156.73744	2.1	-156.68004
1.6	-156.73641	2.15	-156.67373
1.65	-156.73365	2.2	-156.66762
1.7	-156.7296	2.25	-156.66175
1.75	-156.7246	2.3	-156.65615
1.8	-156.71891	2.35	-156.65082
1.85	-156.71276	2.4	-156.64579
1.9	-156.70633	2.45	-156.64107
1.95	-156.69974	2.5	-156.63667

$(TercC)_2$			
r (Å)	E (a.u.)	r (Å)	E (a.u.)
1.3	-315.71789	2.2	-315.72799
1.35	-315.74321	2.25	-315.72174
1.40	-315.76141	2.3	-315.71565
1.45	-315.77395	2.35	-315.70972
1.5	-315.78198	2.4	-315.70399
1.55	-315.78645	2.45	-315.69842
1.6	-315.78811	2.5	-315.69305
1.65	-315.78757	2.55	-315.68788
1.7	-315.78532	2.6	-315.68292
1.75	-315.78177	2.65	-315.67818
1.8	-315.77724	2.7	-315.67364
1.85	-315.77198	2.75	-315.6693
1.9	-315.7662	2.8	-315.66515
1.95	-315.76007	2.85	-315.66119
2.00	-315.75373	2.9	-315.65741
2.05	-315.74728	2.95	-315.65381
2.1	-315.7408	3.00	-315.65039
2.15	-315.73435	--	--

Adamantane-Dimer			
r (Å)	E (a.u.)	r (Å)	E (a.u.)
1.3	-1089.87885	1.9	-1089.93841
1.35	-1089.90101	1.95	-1089.93527
1.4	-1089.91732	2	-1089.9319
1.45	-1089.92872	2.05	-1089.92838
1.5	-1089.93679	2.1	-1089.92477
1.55	-1089.94203	2.15	-1089.92112
1.6	-1089.94507	2.2	-1089.91747
1.65	-1089.94639	2.25	-1089.91382
1.7	-1089.9464	2.3	-1089.91019
1.75	-1089.94538	2.35	-1089.90662
1.8	-1089.9436	2.4	-1089.9031
1.85	-1089.94122	--	--

$(Ph_3C)_2$			
r (Å)	E (a.u.)	r (Å)	E (a.u.)
1.3	-1089.87885	1.9	-1089.93841
1.35	-1089.90101	1.95	-1089.93527
1.4	-1089.91732	2	-1089.9319
1.45	-1089.92872	2.05	-1089.92838
1.5	-1089.93679	2.1	-1089.92477
1.55	-1089.94203	2.15	-1089.92112
1.6	-1089.94507	2.2	-1089.91747
1.65	-1089.94639	2.25	-1089.91382
1.7	-1089.9464	2.3	-1089.91019
1.75	-1089.94538	2.35	-1089.90662
1.8	-1089.9436	2.4	-1089.9031
1.85	-1089.94122	--	--

Table S 3.2. Electron density at critical point for the difference C-C bonds studied.

C-C Bond	r_e	r_{sp}
Ethane	1.534	1.58388
Cyclohexene	1.532	1.57995
Cyclohexene-mod	1.534	1.55244
$(F_3C)_2$	1.545	1.56053
Cyclobutane	1.549	1.54879
$(TercC)_2$	1.573	1.46559
$(Cl_3C)_2$	1.579	1.44442
$(Et_2MeC)_2$	1.601	1.36482
$(Et_3C)_2$	1.635	1.28148
Adamantane-Dim	1.675	1.1861
Ph_3C	1.735	1.0218
Compound-3b	1.928	0.70925

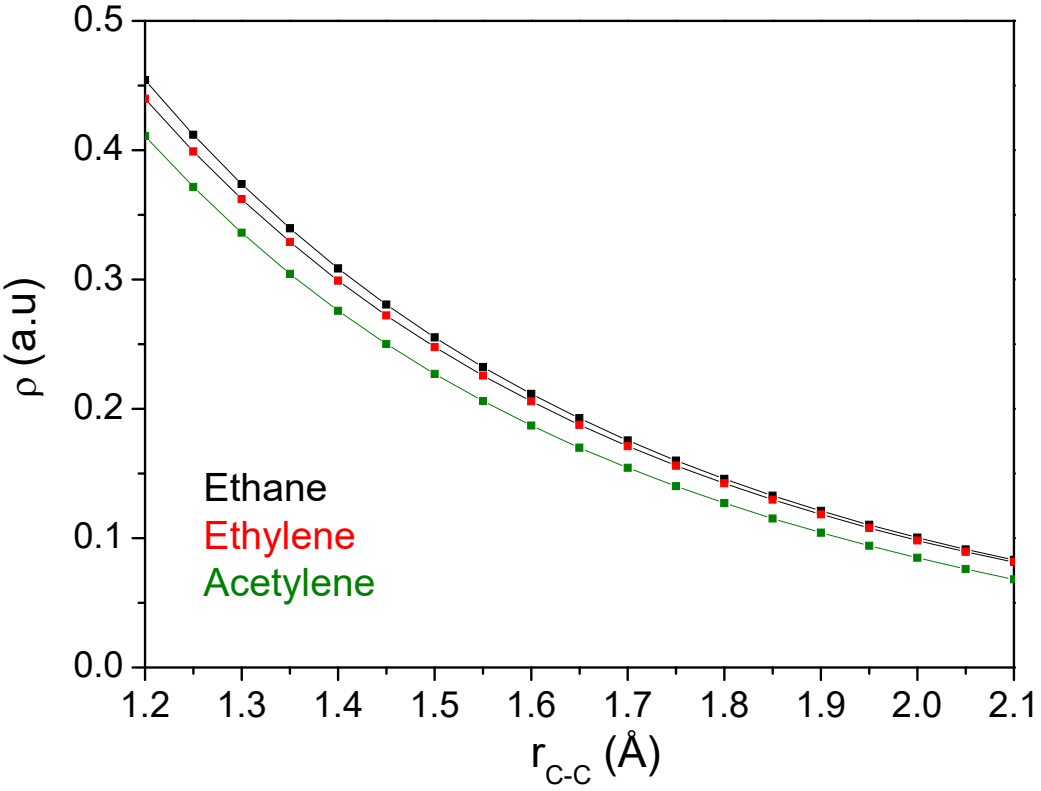

Figure S3.1. Distance dependence of the electron density at the C-C bond critical point for ethane (black squares), ethylene (red squares) and acetylene (green) C-C bonds.

Chapter 4

Chained Interaction Conjecture. The case of hydrogen bonds

Introduction

Among the non-covalent interactions, hydrogen-bonding is perhaps of the most popular one and it is usually considered as a reference of such kind of unions [1]. Its relatively directional and strong interaction combined with complex dynamic properties has played a key role in chemistry. Numerous examples ranging from biological reactions and life processes[2,3] to molecular recognition [4-6], or hydrogen transfer reactions are continuously subject of new investigations[7].

Nonetheless, the nature and definition of hydrogen bonding is still ill defined. [8-10]. The traditional Pauli definition based on electrostatic point of view has been overcame. New interactions like, dihydrogen [11], or blue-shifted hydrogen bonds (HBs) [12,13], have evidenced that such a non-covalent interaction extends from the covalent regime to the van der walls limit. [1,14-16] Of course such a broad range of interactions cause hydrogen bonding to be fundamental in chemistry, leading the possibility to stabilize transition states [17,18] or design new organic crystals [19], but also have opened several questions about the chemical connection between covalent and non-covalent interactions.

In this regard, the different definitions of hydrogen bonding display almost any chemical criteria available to define chemical bonding and binding. The most important, and perhaps the most applied one, is the so called geometric constrains. Accordingly, hydrogen bonding is produced when the interatomic atomic distances are shorter than those corresponding to the sum of their non bonded distances or Van der Waals radii. This definition was the result of the chemical knowledge that HBs display an intermedium character between the purely covalent interaction and the dispersive ones. Indeed, geometrical constrains found support on numerous statistical analysis of the Cambridge Structural Data Base (CCSD) where well defined maxima in between the covalent and van der Waals distances distributions appear. Nice chemical correlations between HBs lengths data and bond strengths [20-22], bond valences [23] or vibrational frequencies [24,25] have been obtained, supporting the chemical idea that structure and properties are connected. However, although these geometrical empirical laws have provided further insight on the properties of the HBs, they have not been able to reveal the nature of this interaction. Furthermore, geometric criteria have been widely criticized because weak HBs as C-H $\cdot$ O display interaction distances bigger than their van der Waals radii sum [26].

As in the case of covalent chemistry, energy has been also a criterion to distinguish the nature of HBs. Traditionally, HBs have been described as the sum of two potential energy functions, an electrostatic one, with a deeper and stepper curve, and a Van der Waals function [26] which reflects the intermediate character of this interaction. Indeed, as appeared in most common chemistry textbooks, HBs interaction energies are about 2-5 kcal mol^{-1}, in the middle range between covalent and Van der Waals limits. Nowadays, energy decomposition schemes [27,28] have been able to split up the interaction energies in different meaningful contributions evidencing that shorter HBs share common features with covalent bond whereas longer ones display an electrostatic/dispersive nature. Nonetheless energy criteria have not been able to explain why such an interaction can be spread in the range from covalent to van der Waals limits. Indeed, the well stablish chemical idea that each interaction can be represented by a characteristic potential energy function seem to disappear in favor of a continua energy change where the limits between covalent–electrostic–Van der Waals regimens are not clearly defined.

Finally, electron density has also played a key role in the classification of HBs. The analysis of the electronic distributions have stablished the idea that HBs display a continua of interactions.[14-16] Moreover, electronic properties have been able to reveal the existence of very weak hydrogen bonds ,such as dihydrogen bonds, where distances and energetic criteria do not suffice. Undoubtedly, charge distributions have become an invaluable tool in the modern classification of non-covalent interactions. However, it has to be mentioned that, as pointed out by Graboswky [8], electron density criteria also depend on the different values displayed by strong and weak hydrogen bonds. Additionally, electron charge distribution analysis it is usually combined with the previous energetic and geometric criteria, evidencing that a practical definition able to enclose the different HBs definitions is still lacking.

To this end, in this communication we provide an intuitive chemical model able to explain the distances at which HBs can produce an interaction change. Recovering the chemical idea that each potential energy function defines a given interaction, we will show how the covalent–electrostatic–Van der Waals regimens are chained through energetic constrains. Our model will be tested in the most widely studied hydrogen bond interaction, the O-H O system. Different criteria such as distances distributions, electron density and

energetic properties will be analyzed within this framework to prove its generality.

The Chained Interaction Conjecture

The different criteria to classify hydrogen bonds have manifested that the different interaction nature of a given pairwise interaction naturally evolves with this distance. For instance, short hydrogen bonds are classified as covalent bonds, and as the distance increase, they progressively go through an electrostatic and Van de Waals binding.

This view implies that regardless the compound, the hydrogen bond interaction between two atoms can be described as a result of three potential energy curves, one covalent and the other electrostatic and Van der Waals interactions. Notice that although this picture naturally emerges from the classification criteria, clearly contrast with the traditional view of hydrogen bonds. In the latter, they are usually considered as a triatomic system where their energetic behavior is described by the sum of two potential energy curves. However, the distance evolution analysis point towards a diatomic or pairwise description where the only control parameter is the distance between the X =(O,F,N…) atom and the H involved in the interaction.

At this point it is important to recall that despite its differences, the pairwise interaction model have found support in several electron density studies. Specifically, Espinosa et al. [16,29] in a series of works demonstrated that the electron density at the critical point, its Laplacian and even the energy density of O-H and F-H hydrogen bond follows the same dependence as their diatomic counterparts. As a result, they used the universal electronic evolution [30] presented by the diatomic reference, which experiences a covalent to electrostatic change as a consequence of a Laplacian sing change and a electrostatic to weak transition produced by an increase of the kinetic energy density, to define the critical distances at which hydrogen bonds interaction nature changes. Although this interaction sequence has been applied only to hydrogen bonds, we want to remark that is based on diatomic like bond and therefore can be considered as general applicability to any pairwise interaction type.

This view provides an interesting picture of the chemical properties and the atomic distances of hydrogen bonds. Given a distance between two atoms they can only interact according to the behavior displayed by its electron density characteristics. Moreover, as it has been demonstrated (See chapter 3) this electron density changes also modifies the characteristic of the pairwise

interaction potential energy curve. Therefore, the different covalent, electrostatic and Van der Waals potential energy functions used in chemistry to define the different chemical interactions must be joined in such a way that they reproduce the same behavior as the electron density does. At short distances a covalent type interaction will be main one, in agreement with the covalent character displayed by shortest HBs. As distance increases, the covalent contribution will be reduced, and the electrostatic binding will become predominant giving as a result the interaction displayed by the most common HBs. At this point if HBs length is further stretched, a new interaction will come in to play resulting in a Van der Waals potential energy function. The question remains if such a gradually change in the interaction type occur at a given distances. The question remains if such a hydrogen bond interaction transitions can be accurately described.

In this regard, it has been demonstrated that pair potential energy functions are characterized by two invariant points, which define the lower and the upper bounds at which a given interaction is stable.(See chapter 2) The first point also named hard sphere point (r_{hs}), represent the closest interatomic distance at which the atoms can approach maintaining their potential energy negative. Similarly, the upper distance limit, the spinodal one, is related to the mechanical breaking point of the system. These interaction stability limits are symmetrically disposed around the equilibrium distance and are related with the equilibrium properties of the potential energy curve through the following relationships

$$r_{sp} = r_e + (D_e/k_e)^{1/2} \tag{4.1}$$

$$r_{hs} = r_e - (D_e/k_e)^{1/2} \tag{4.2}$$

As a result, each hydrogen bond interaction will be defined by a scaling length equal to $(D_e/k_e)^{1/2}$ and a equilibrium bond length r_e which fix the maximum and minimum distances at they can be extend. Here, it is worth to recall that these potential energy functions stands for an universal potential energy curve able to describe all the different hydrogen bonds and therefore the equilibrium bond length must be understood as a reference length of an hypothetical isolated interaction which upon compression or elongation behaves energetically, mechanically similar as their counterparts in the compounds.

Accordingly, we can assume that when a covalent hydrogen bond elongates to it spinodal or equivalently to its breaking point, the formation of an electrostatic interaction must occur. Nonetheless, if instead of considering the

stretching behavior of the same bond, we examine the inverse evolution of the distance, the electrostatic HBs will be compressed up to the shortest possible distance (r_{hs}), where it will be unstable. This distance must coincide with the covalent spinodal limit since the system necessary will evolve to the previously regime. A similar reasoning can be applied to the electrostatic to van der Waals transition. In Figure 4.1 we have represented a schematic picture of this conjecture emphasizing that the spinodal point of previous interaction always coincides with the hard sphere distance of the next interaction producing a chain of interactions. This equality between the spinodal distance and hard sphere point of two consecutive interactions implies that the three different interactions are related to each other and therefore they will be distances where both interactions will be unstable. In similitude to the chemical processes where the cross between two potential energy curve crosses defined a transition state, we will refer hereafter to these unstable distances as a bond transition region.

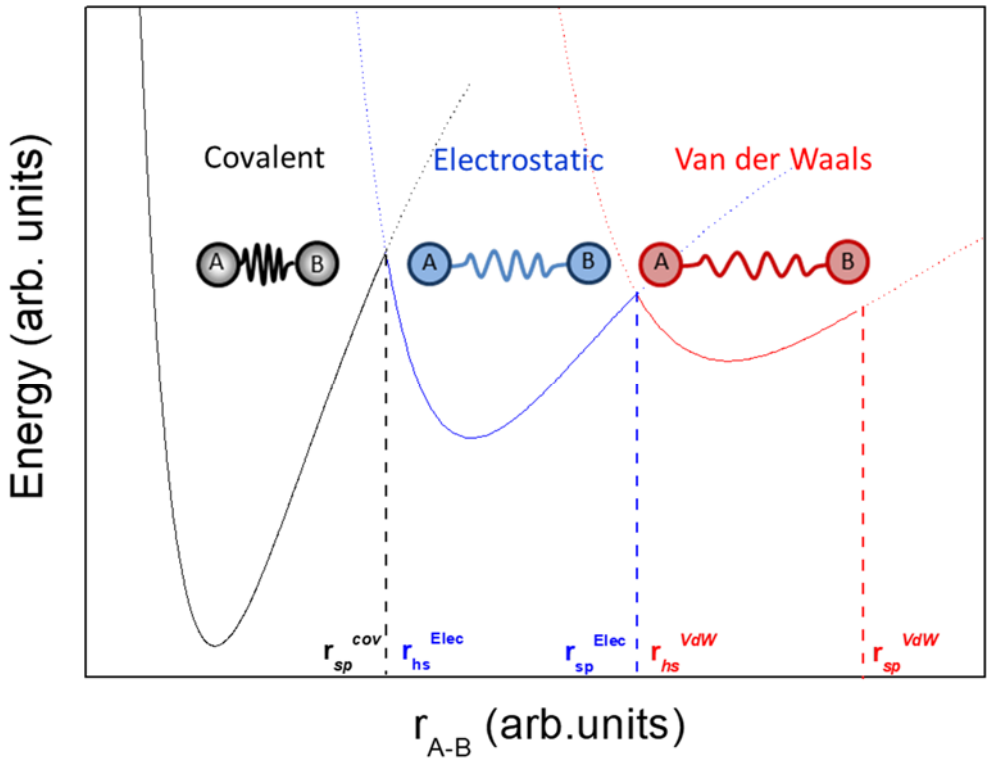

Figure 4.1. Schematic representation of the chained interaction conjecture. In black, the covalent interaction, blue and red represents the electrostatic and Van der Waals bonding respectively. Notice how the spinodal corresponds to the hard sphere distance of the next interaction. (See text for explanation)

The case of O-H Hydrogen bonds

According our chained interaction model, the different interactions are described in terms of three reference universal potential energy curves, which transform to each other through an unstable state. Let us now consider the experimental implications of our model. In a potential energy curve, the compression our elongation induces a destabilization of the bond reference. As a result, any bond in a compound which display a different bond length than the reference one will be destabilized up to the spinodal point or the hard sphere limit where it becomes completely unstable. Under this view, if we analyze a statistically significant sample of the number of X-Y bonds which display a given interaction distance, we should expect that they reproduce a well-defined pattern of maxima and minima reflecting the equilibrium and rupture distances of the different interactions.

In order to corroborate the latter hypothesis, we have calculated the O-H bond reference equilibrium and rupture distances. As it has been proved in a recent study (See chapter 3) the scaling length for a given interaction between the same atoms pairs is constant and can be determined from the experimental equilibrium properties of any of the stable compounds that represents. Accordingly using energetic and mechanical data and only one distance reference, we can calculate the rupture distances of the other interactions. The scaling length of the O-H covalent interaction can be obtained from the O-H stretching potential energy curve of the water molecule. A value of 0.37 Å is obtained using a D_e and k_e values of 118 kcal mol^{-1} and 6.1 mdyna Å^{-1} respectively. Likewise, for the electrostatic interaction we can use the water dimer potential energy curve. As this respect Mokomura et al. [27] calculated a D_e and k_e values of 5 kcal mol^{-1} and 0.197 mdyna Å^{-1}, giving as a result a value of 0.42 Å. Finally, the Van der Waals limits represent a rather weak interaction, where no much experimental data are available, therefore we have turned to the potential energy functions used in gas phase equation of state predictions. In this regard several potential energy functions such as the Stockmayer [31] potential includes a Lenard-Jones term responsible for the Van der Waals interaction plus an orientational dependent dipole or electrostatic contribution. According to the data provided by Hishfelder, and considering only the Lenard-Jones contribution the estimated the scaling length for this interaction is 0.32 Å.

In order to fix a one reference distance, we have considered that the covalent bond distance is 0.97 Å, which corresponds to the sum of the O and H covalent

radii provided by Pykko [32]. Using expression (1) the covalent rupture distance is predicted at 1.34 Å. As this distance corresponds to the hard sphere point of the electrostatic contribution, using expression (2) we predict an equilibrium distance for the electrostatic interaction of 1.76 Å. Applying the same procedure, the electrostatic rupture or equivalently the Van der Waals hard sphere limit will occur at 2.18 Å. Finally, the equilibrium bond length of the latter contribution can be estimated to be 2.50 Å.

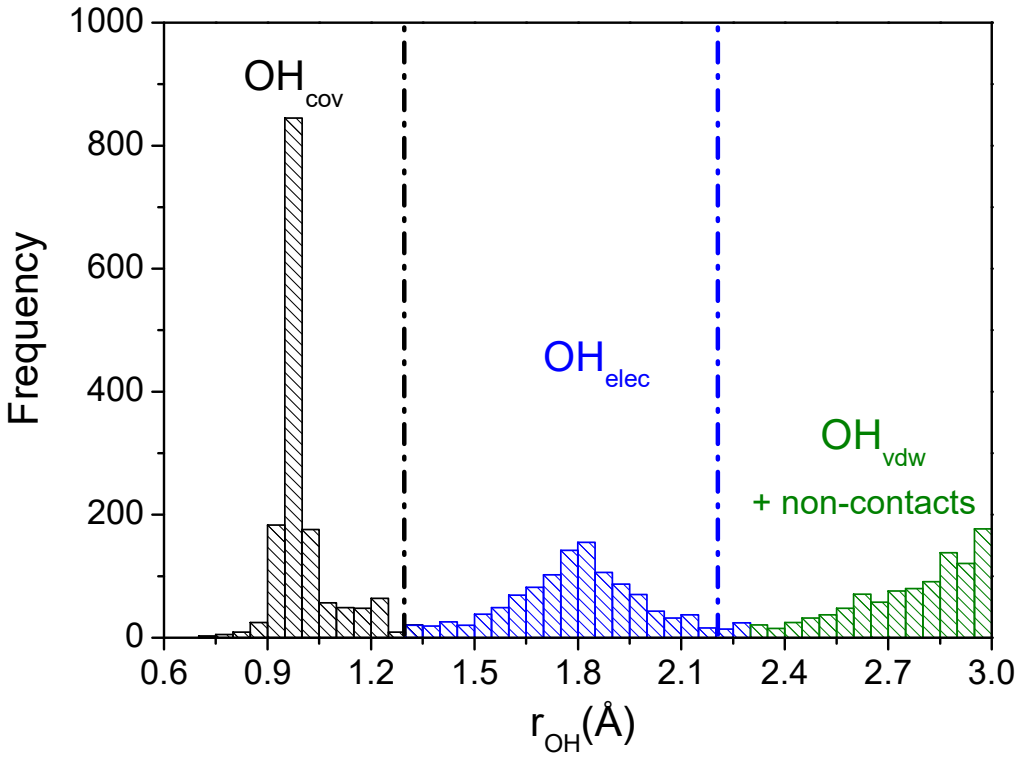

Figure 4.2. Distance histogram for the O-H contact. Covalent, electrostatic and Van der Waals contacts have been represented as black blue and green bins respectively.

In Figure 4.2, we have plotted the number of O-H constants as a function of the distance for all the compounds included in the crystallographic data base. We have considered only neutron diffraction data where the position of H atoms can be accurately defined. In order to facilize the discussion we have differenced the covalent contacts provided in the crystallographic data base (black bins) from those classified as non-contact interactions (Blue and green binds. As it can be expected because the Pykko covalent radii are determined from the distance histograms, our covalent reference distance coincides with the fist maxima in the distribution. More interestingly is the position of the first minima. It occurs in a range between 1.2 and 1.4 Å in clear agreement with our predicted covalent spinodal distance which is 1.34 Å. The number of

contacts produced at this distance is less than 20 units in more than 1000 compounds. Moreover, statistically this distance is not a favored one neither for covalent nor for electrostatic interactions. To the best of our knowledge the existence of such a minimum in the distance distributions has been considered as an experimental fact lacked from theoretical justification. However, when we realize that such a distance corresponds to the bond stability limits of the interactions, it is clear that few compounds can exhibit this distance, at this point covalent and hydrogen bonds are mechanically unstable and therefore compounds will avoid them because they will evolve to a more stable configuration.

According to our chained interaction model we should expect other maxima at the electrostatic reference length (1.76 Å). Again, the latter is clearly reproduced in the experimental pattern, which occurs between 1.75 and 1.85 Å. This electrostatic interaction was calculated only from the OH covalent reference distance and the dissociation energy and stretching force constant of the water dimer based on the assumption that the latter is constant for all O-H hydrogen bonds. Therefore, bond interaction between two atom pairs evolves with the distance in a chained way as imposed by the universal bond stability conditions. Notice that under this view hydrogen bonds are not so different from other chemical interaction. Indeed when we realize that the rupture distance of the electrostatic interaction is produced at 2.18 Å, again very close to the distance as the second minima in the distribution appears (2.1-2.4 Å) we can see that hydrogen bond classification is a natural consequence of the different interaction displayed between two atoms. Finally, our model predicts another maxima and rupture distance for a van der Waals interaction. The latter it is not observed in the distance diagram mainly because as it has been pointed out by several authors [33] [34] , it includes a monotonically increasing non-contact distance distribution which modify the statistics of this regimen. However, it is worthy to highlight that out chained interaction model predicts a Van der Waals spinodal distance of 2.85 Å, only 0.15 Å lower than the sum of the O and H Van der Waals radii predicted by Alvarez et al[33] and 0.4 Å larger than the estimations provided by electron density analysis [35].

An interesting feature of the model is the existence of bond transition regimes associated to the rupture and hard sphere points of the interactions. To the best of our knowledge such an idea of unstable distances has not been already reported although it can provide a huge information about chemical processes. Consider for example the bond transition distance between the covalent and

electrostatic interaction. At these points neither covalent (hydrogen) bonds nor electrostatic hydrogen bonds interaction can be stable, as a result it is expected that chemical compounds try to avoid this configuration. Consequently, knowing the rupture distances, we can predict chemical (un)stable compounds.

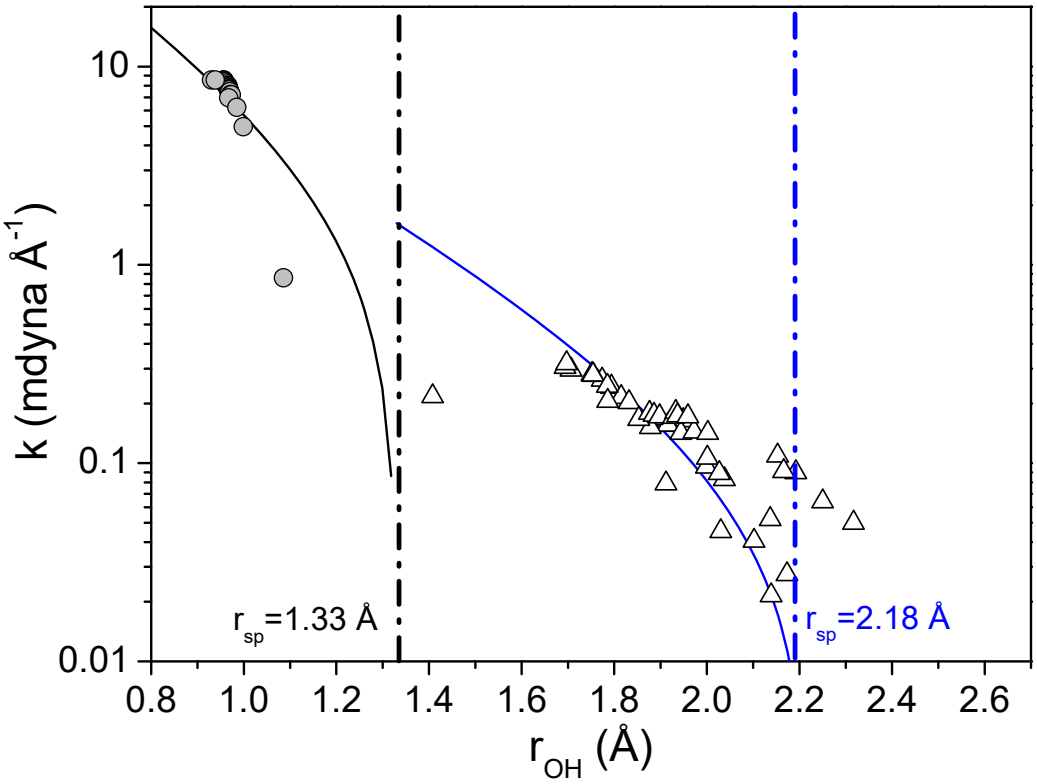

Figure 4.3. Stretching force constant data for covalent O-H bonds (grey symbols) and hydrogen bonds (non-filled triangles). Black and blue lines correspond to our force constant distance model for the O-H covalent reference bond and O · H electrostatic reference bond respectively.

Notice that the existence of this transition regimes implies that the electron density and force constant properties will not evolve continuously with the distance (See chapter 3). As the spinodal or rupture point is based on the condition of zero stretching force constant we will start analyzing this property. Notice that as we know the equilibrium distances and the scaling lengths, we can predict a dependence of the stretching force constant with the distance assuming an analytical potential energy function for the pairwise interaction. In this case we have selected the Morse potential,

$$U = D_e \left(1 - e^{\frac{-(r-r_e)}{b}}\right)^2 \tag{4.3}$$

where b is the softness parameter an it is related with the scaling length through the expression [36]

$$\left(\frac{D_e}{k_e}\right)^{1/2} = b\frac{\sqrt{2}}{ln\ (2)} \tag{4.4}$$

If we derivative twice this potential, the stretching force constant distance dependence read as,

$$k(r) = k_e\left(-1 + 2e^{\frac{-(r-r_e)}{b}}\right)e^{\frac{-(r-r_e)}{b}} \tag{4.5}$$

Where k_e represents the equilibrium stretching for constant of the reference bond. In our case we have assumed a value of 6.1 and 0.25 mdyna Å^{-1} for the covalent and electrostatic interactions. These values have been obtained from the average value of the bibliographic data of compounds with the same equilibrium distance as our reference bond length [37]. In Figure 4.3 we have plotted the predicted stretching force constant dependences for the covalent and electrostatic pairwise interaction along with several data for different covalent and hydrogen bonds [38,39]. Interestingly, two different trends are observed one for the covalent interaction and the other for the electrostatic ones. In each case the data follows our predicted potential models and consistently decrease towards the predicted rupture points evidencing a highly unstable state.

Regarding the electron density, several studies have considered that the dependence of this property with the distance is accurate described by a single exponential model [15] In contrast, the chained interaction model predicts a slope change of their convex behavior with the distance.

Indeed, as it has been demonstrated the electron density at the critical point can be expressed in terms of the scaling length of the potential as

$$\rho = \rho_e e^{-(r-r_e)/(D_e/k_e)^{1/2}} \tag{8}$$

Notice that an interaction change modifies the scaling length and therefore the exponential decay factor. In Figure 4.4 we have displayed the electron density behavior of several O-H bonds [39]. As expected, two different linear trends are observed with slopes equal to 0.35 and 0.42 Å in excellent agreement with the covalent and electrostatic scaling lengths of our chained interaction model.

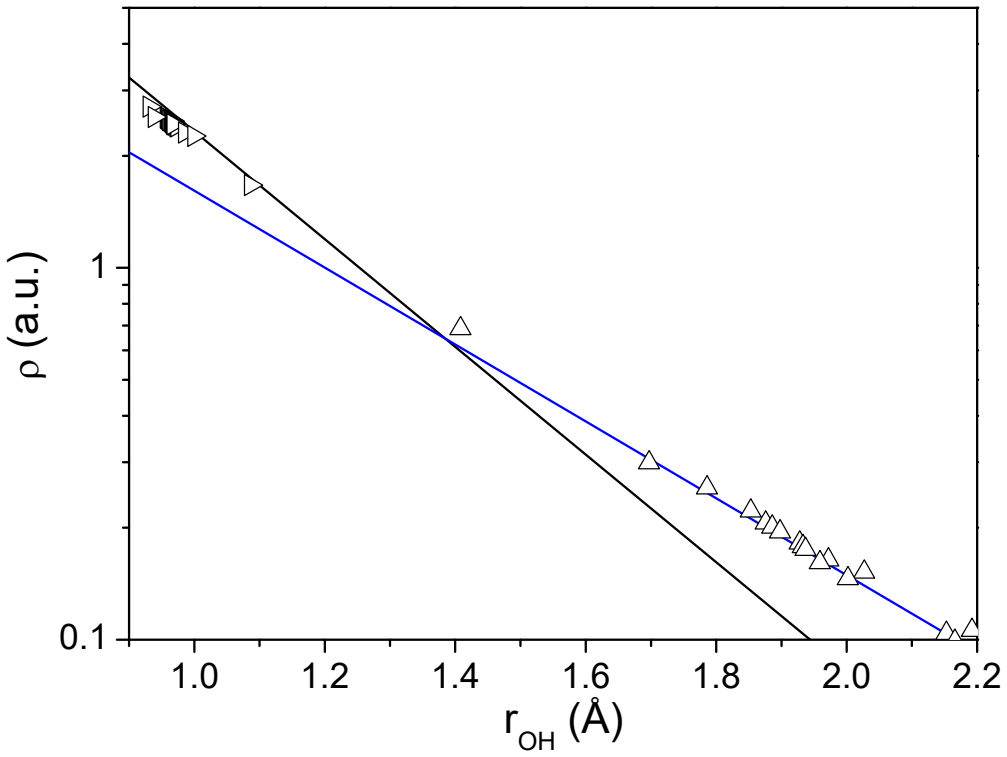

Figure 4.4. Electron density at the bond critical point for different O-h bonds. Black and blue lines correspond to the model proposed in this work. (See tect for an explanation)

References

[1] A. S. Mahadevi and G. N. Sastry, Cooperativity in Noncovalent Interactions. *Chem. Rev.*, *116*, 2775-2825, **2016**. DOI: https://doi.org/10.1021/cr500344e.

[2] J. Lehn, Perspectives in Supramolecular Chemistry-From Molecular Recognition towards Molecular Information Processing and Self-organization. *Angew Chem Int Ed Engl*, *29*, 1304-1319, **1990**. DOI: https://doi.org/10.1002/anie.199013041.

[3] J. Lehn, *M. Supramolecular Chemistry*, Verlag-Chemie, Weinheim, **1995**

[4] L. Leiserowitz, Molecular Packing Modes. Carboxylic Acids. *Acta Cryst. B*, *32*, 775-800, **1976**. DOI: https://doi.org/10.1107/S0567740876003968.

[5] J. D. Dunitz and A. Gavezzotti, Molecular recognition in organic crystals: directed intermolecular bonds or nonlocalized bonding? *Angew Chem Int Ed Engl*, *44*, 1766-1787, **2005**. DOI: https://doi.org/10.1002/anie.200460157.

[6] E. Fan, S. a. V. Arman, S. Kincaid, and A. D. Hamilton, Molecular Recognition: Hydrogen-Bonding Receptors That Function in Highly Competitive Solvents. *J. Am. Chem. Soc.*, *11*, 369-370, **1993**. DOI: https://doi.org/10.1021/ja00054a066.

[7] G. Zundel, *Advances in Chemical Physics*, Prigogine, I., Rice, S. A., Eds.; J. Wiley: New York, 2000; Vol. 111.,

[8] S. J. Grabowski and W. A. Sokalski, Different types of hydrogen bonds: correlation analysis of interaction energy components. *Journal of Physical Organic Chemistry*, *18*, 779-784, **2005**. DOI: https://doi.org/10.1002/poc.937.

[9] S. J. Grabowski, What is the covalency of hydrogen bonding? *Chem Rev*, *111*, 2597-2625, **2011**. DOI: https://doi.org/10.1021/cr800346f.

[10] V. L. Deringer, U. Englert, and R. Dronskowski, Covalency of hydrogen bonds in solids revisited. *Chem. Commun.*, *50*, 11547-11549, **2014**. DOI: 10.1039/c4cc04716h.

[11] R. Custelcean and J. E. Jackson, Dihydrogen Bonding: Structures, Energetics, and Dynamics. *Chem. Rev.*, *101*, 1963-1980, **2001**. DOI: https://doi.org/10.1021/cr000021b.

[12] P. Hobza and Z. Havlas, Blue-Shifting Hydrogen Bonds. *Chem. Rev.*, *100*, 4253-4264, **2000**. DOI: https://doi.org/10.1021/cr990050q.

[13] S. N. Delanoye, W. A. Herrebout, and B. J. V. D. Veken, Blue Shifting Hydrogen Bonding in the Complexes of Chlorofluoro Haloforms with Acetone-d6

and Oxirane-d4. *J. Am. Chem. Soc*, *124*, 11854-11855, **2002**. DOI: https://doi.org/10.1021/ja027610e.

[14] P. R. Mallinson, G. T. Smith, C. C. Wilson, E. Grech, and K. Wozniak, From Weak Interactions to Covalent Bonds: A Continuum in the Complexes of 1,8-Bis(dimethylamino)naphthalene. *J. Am. Chem. Soc*, *125*, 4259-4269, **2003**. DOI: https://doi.org/10.1021/ja029389b.

[15] P. M. Dominiak, A. Makal, P. R. Mallinson, K. Trzcinska, J. Eilmes, E. Grech, M. Chruszcz, W. Minor, and K. Wozniak, Continua of interactions between pairs of atoms in molecular crystals. *Chem. Eur. J.*, *12*, 1941-1949, **2006**. DOI: https://doi.org/10.1002/chem.200500600.

[16] E. Espinosa, I. Alkorta, J. Elguero, and E. Molins, From weak to strong interactions: A comprehensive analysis of the topological and energetic properties of the electron density distribution involving X–H···F–Y systems. *J. Chem. Phys.*, *117*, 5529-5542, **2002**. DOI: https://doi.org/10.1063/1.1501133.

[17] P. Gilli, V. Bertolasi, L. Pretto, and G. Gilli, Outline of a transition-state hydrogen-bond theory. *Journal of Molecular Structure*, *790*, 40-49, **2006**. DOI: https://doi.org/10.1016/j.molstruc.2006.01.024.

[18] Y. Zheng and T. C. Bruice, Is strong hydrogen bonding in the transition state enough to account for the observed rate acceleration in a mutant of papain? *Proc. Natl. Acad. Sci.*, *94*, 4285–4288, **1997**. DOI: https://doi.org/10.1073/pnas.94.9.4285.

[19] G. R. Desiraju, Reflections on the Hydrogen Bond in Crystal Engineering. *Crystal Growth & Design*, *11*, 896-898, **2011**. DOI: https://doi.org/10.1021/cg200100m.

[20] R. Y. Rohling, I. C. Tranca, E. J. M. Hensen, and E. A. Pidko, Correlations between Density-Based Bond Orders and Orbital-Based Bond Energies for Chemical Bonding Analysis. *J. Phys. Chem. C*, *123*, 2843-2854, DOI: https://doi.org/10.1021/acs.jpcc.8b08934.

[21] P. Gili, V. Bertolasi, V. Ferretti, and G. Gilli, Covalent Nature of the Strong Homonuclear Hydrogen Bond. Study of the O-H-O System by Crystal Structure Correlation Methods. *J. Am. Chem. Soc*, *116*, 909-915, **1994**. DOI: https://doi.org/10.1021/ja00082a011.

[22] H. Burgi, Stereochemistry of Reaction Paths as Determined from Crystal Structure Data-A Relationship between Structure and Energy. *Angew Chem Int Ed Engl*, *14*, 460-473, **1975**. DOI: https://doi.org/10.1002/anie.197504601.

[23] D. Brown, Recent Developments in the Methods and Applications of the Bond Valence Model. *Chem. Rev.*, *109*, 6858–6919, **2009**. DOI: https://doi.org/10.1021/cr900053k.

[24] M. A. Boyer, O. Marsalek, J. P. Heindel, T. E. Markland, A. B. Mccoy, and S. S. Xantheas, Beyond Badger's Rule: The Origins and Generality of the Structure-Spectra Relationship of Aqueous Hydrogen Bonds. *J Phys Chem Lett*, *10*, 918-924, **2019**. DOI: https://doi.org/10.1021/acs.jpclett.8b03790.

[25] G. C. Pimentel and A. L. Mcellan, Hydrogen Bonding. *Annu. Rev. P. Chem.*, *22*, 347-385, **1971**. DOI: https://doi.org/10.1146/annurev.pc.22.100171.002023.

[26] L. Sobczyk, S. J. Grabowski, and T. M. Krygowski, Interrelation between H-Bond and Pi-Electron Delocalization. *Chem. Rev.*, *105*, 3513−3560, **2005**. DOI: https://doi.org/10.1021/cr030083c.

[27] K. Morokuma, Why Do Molecules Interact? The Origin of Electron Donor-Acceptor Complexes, Hydrogen Bonding, and Proton Affinity. *Acc. Chem. Res.*, *10*, 294-320, **1977**. DOI: https://doi.org/10.1021/ar50116a004.

[28] A. Martin Pendas, M. A. Blanco, and E. Francisco, The nature of the hydrogen bond: a synthesis from the interacting quantum atoms picture. *J. Chem. Phys.*, *125*, 184112, **2006**. DOI: https://doi.org/10.1063/1.2378807.

[29] E. Espinosa and E. Molins, Retrieving interaction potentials from the topology of the electron density distribution: The case of hydrogen bonds. *J. Chem. Phys.*, *113*, 5686-5694, **2000**. DOI: 10.1063/1.1290612.

[30] A. Costales, M. A. Blanco, A. Martín Pendás, P. Mori-Sánchez, and V. Luaña, Universal Features of the Topological Bond Properties of the Electron Density. *J. Phys. Chem. A*, *108*, 2794-2801, **2004**. DOI: https://doi.org/10.1021/jp037627z.

[31] M. E. Van Leeuwen, Deviation from corresponding-states behaviour for polar fluids. *Molecular Physics*, *82*, 383-392, **2006**. DOI: https://doi.org/10.1080/00268979400100294.

[32] P. Pyykko and M. Atsumi, Molecular single-bond covalent radii for elements 1-118. *Chem.: Eur. J.*, *15*, 186-197, **2009**. DOI: https://doi.org/10.1002/chem.200800987.

[33] S. Alvarez, A cartography of the van der Waals territories. *Dalton Trans*, *42*, 8617-8636, **2013**. DOI: 10.1039/c3dt50599e.

[34] I. Dance, Distance criteria for crystal packing analysis of supramolecular motifs. *New Journal of Chemistry*, *27*, 22-27, **2003**. DOI: 10.1039/b206867b.

[35] M. Rahm, R. Hoffmann, and N. W. Ashcroft, Atomic and Ionic Radii of Elements 1-96. *Chem. Eur. J.*, *22*, 14625-14632, **2016**. DOI: https://doi.org/10.1002/chem.201602949.

[36] F. Wang, The invariant character of two-body binding potentials. *Journal of Molecular Structure: THEOCHEM*, *664-665*, 83-89, **2003**. DOI: 10.1016/j.theochem.2003.07.004.

[37] Y. Tao, W. Zou, J. Jia, W. Li, and D. Cremer, Different Ways of Hydrogen Bonding in Water - Why Does Warm Water Freeze Faster than Cold Water? *J Chem Theory Comput*, *13*, 55-76, **2017**. DOI: https://doi.org/10.1021/acs.jctc.6b00735.

[38] M. Majumder and S. Manogaran, Redundant internal coordinates, compliance constants and non-bonded interactions – some new insights. *J. Chem. Sci.*, *125*, 10-14, **2013**. DOI: https://doi.org/10.1007/s12039-012-0357-7.

[39] M. Freindorf, E. Kraka, and D. Cremer, A comprehensive analysis of hydrogen bond interactions based on local vibrational modes. *Int. Journal of Quantum Chemistry*, *112*, 3174-3187, **2012**. DOI: https://doi.org/10.1002/qua.24118.

Chapter 5

Chemical Pressure Chemical Knowledge: Squeezing Bonds and Lone Pairs within the Valence Shell Electron Pair Repulsion Model

A. Lobato, H. H. Osman, M. A. Salvadó, M. Taravillo, V. G. Baonza and J. M. Recio

The Valence Shell Electron Pair Repulsion (VSEPR) model is a demanding testbed for modern chemical bonding formalisms. The challenge consists in providing reliable quantum mechanical interpretations of how chemical concepts such as bonds, lone pairs, electronegativity or hyper-valence influence (or modulate) molecular geometries. Several schemes have been developed so far to visualize and characterize these effects but, to the best of our knowledge, none has yet incorporated the analysis of the premises derived from the ligand close-packing (LCP) extension of VSEPR model. Within the LCP framework, the activity of the lone pairs of the central atom and the ligand-ligand repulsions constitute the two key features necessary to explain some controversial molecular geometries that do not conform the VSEPR rules. Considering the dynamical picture obtained when electron local forces at different nuclear configurations are evaluated from first principles calculations, we explore the chemical pressures distributions in a variety of molecular systems, namely: electron deficient

molecules (BeH_2, BH_3 and BF_3), several AX_3 series (A: N, P, As; X: H, F, Cl), SO_2, ethylene, SF_4, ClF_3, XeF_2, and non-equilibrium configurations of water and ammonia. Our chemical pressure maps clearly reveal space regions totally consistent with the molecular and electronic geometries predicted by VSEPR and provide a quantitative correlation between the lone pair activity of the central atom and the electronegativity of the ligands in agreement with the LCP model. Moreover, the analysis of the kinetic and potential energy contributions to the chemical pressure allows us to provide simple explanations on the connection between ligand electronegativity and the electrophilic/nucleophilic character of the molecules, with interesting implications in their potential reactivity. NH_3, NF_3, SO_2, BF_3, and the inversion barrier of AX_3 molecules are selected to illustrate our findings.

Phys. Chem. Chem. Phys. DOI: a10.1039/C9CP00913B

Introduction

From the very beginning, chemists have been trying to predict molecular geometry without any other knowledge than the constituent atoms, being conscious of the fact that molecular geometry eventually determines the molecular properties. From the old Lewis's eight electron rule,[1] several concepts such as bond pairs, lone pairs, electronegativity, or hypervalency have emerged in chemistry, allowing the description and rationalization of bonding, structure, and reactivity of molecules and solids.

Although these concepts play a key role in recent chemistry, they are not always unequivocally defined and are usually the focus of modern chemical bonding formalisms, looking for a rigorous physicochemistry basis of such concepts. In this regard, the topological analysis of scalar fields related to electron density and its derivatives have demonstrated that a reliable connection between chemical intuition and quantum mechanical laws is feasible.[2] Indeed, the valence shell electron pair repulsion (VSEPR) theory, which is perhaps the chemical model that has demonstrated the most invaluable capability to predict molecular geometry,[3,4] has become a demanding testbed example for such formalisms. Based on Pauli's exclusion principle, VSEPR describes the molecular and electronic geometries as those that have valence electrons distributed in pairs, minimizing Pauli's repulsion. Indeed, identifying such electron pairs as bond and lone pairs and using chemical concepts such as the number of electrons per bond and electronegativity, Gillespie ordered the electronic repulsions leading to three well-known rules that govern molecular structures.[5,6] Such rules can be summarized in terms of the so-called electron pair domains where their size and shape determine the magnitude of repulsion between the electron pairs. The VSEPR theory reveals that chemical concepts affect molecular geometries and must be somehow described as objects within modern chemical bonding formalisms.[7]

In particular, approaches based on the analysis of local properties of electronic media, such as electron localization function (ELF),[8] Laplacian of electron density,[9] or molecular electrostatic potential (MEP)[10] have been –and still are– applied to determine rigorous connections between quantum mechanical laws and chemical concepts emerging from the VSEPR model. For example, in 1998, Bader et al. analyzed the Laplacian of the electron density of prototypical VSEPR molecules for this purpose.[11,12] They found that the local maxima of this scalar field replicate the positions of the electron pairs

because of the spatial localization of the Fermi hole, thereby establishing one of the first evidences of the deep connection between VSEPR chemical concepts and quantum mechanics. Later, Savin[13] and Silvi[14] demonstrated that ELF basins define space regions that are associated with bonding, nonbonding, and lone electron pairs. The analysis of MEP has also been used as the criterion to describe lone pairs and how the VSEPR model can be suitably reproduced within this methodology.[15,16] A different, but related, approach has been made from the point of view of valence bond (VB) and molecular orbital (MO) theories. Based on an orbital description, these theories have demonstrated that electron pairing reveals a localized–delocalized picture capable of linking the VSEPR domains with chemical entities (such as hybrid orbitals).[17] Nonetheless, VSEPR has its own drawbacks. Some geometries resist following the arrangement according to the minimization of the principle of electron pair repulsions of VSEPR when lone pairs are involved. For example, AX_2E_2 and AX_3E molecules exhibiting bond angles greater than 109.5^0 do not follow the VSEPR rules and need to be explained by the weak activity of the A lone pairs due to the low electronegativity of the ligands.[18,19] This is very well explained within the ligand closepacking [20,21] (LCP) ideas presented by Gillespie and Robinson as an extension of VSEPR. Ligand–ligand repulsions also dominate the controversial trends in the bond angles of the AX_3E series (A: N, P; X: F, Cl, H), where, although F and Cl are more electronegative than H, the bond angles follow the electronegativity sequence in NX_3 but not in PX_3.[22] AX_6E molecules (BrF_6^-, $SeCl_6^{2-}$) lead to non-VSEPR octahedral geometries that the LCP model explains again in terms of the impossibility of an active role for the lone electron pair of the central atom. These and other molecular geometry exceptions in the angles and distances have been and still being explored and characterized in an attempt to prove and rationalize the influence of both the Pauli's exclusion principle and the ligand–ligand repulsions in molecular charge organization. Indeed, the description and quantification of lone pairs as real quantities is still a worthwhile topic of discussion.[23-27] Because of its generic applicability, addressing the combined VSEPR-LCP model as a whole constitutes a pertinent challenge for these modern chemical bonding formalisms.[28,29] Not only electron pair domains have to be identified, but also the ligand–induced effect on the activity of lone pairs should be determined.

Chemical pressure (CP) is a scalar field that is able to describe chemical interactions in terms of electronic pressure exerted by the molecular charge distributions. Based on the quantum stress density formalism within the

framework of density functional theory (DFT), CP provides a dynamical picture of how local forces (CPs) are distributed around the nuclei. Indeed, CP has been successfully applied to describe several chemical phenomena, such as chemical bonding,[30] bond breaking[31] or size effects in intermetallic compounds.[32] Nonetheless, despite its capabilities, CP formalism has never been applied to systematically study how the local pressures distributed around the chemical entities affect molecular geometries.

In this article, we apply CP formalism to several VSEPR prototypical molecules that appear in most common chemistry textbooks. Through the analysis of CP maps, we shall show how regions of positive and/or negative CP enclosed by zero–value isolines are totally consistent with the positions of chemical bonds and lone pairs predicted by the VSEPR model. Interestingly, a straightforward correlation between the electronegativity of ligands (as compared with that of the central atoms) and the value of the CP associated with the central atom lone pairs can be easily derived. The more negative the CP value at the lone pair domain, the higher is the effect of this lone pair on molecular geometry. This is an appealing result within the spirit of the LCP model.

Since CP maps are formulated from the balance between the kinetic and potential energy contributions, a richer chemical interpretation of the concepts involved in the VSEPR-LCP model can be derived. In particular, we are interested in illustrating how: (i) our approach allows us to extend the conclusions on the structural role played by the ligand electronegativity of the chemical activity of the central atom identifying its electrophilicity /nucleophilicity character; (ii) antibonding regions naturally emerge in our maps too, providing the necessary support to the LCP model in its explanation of VSEPR exceptions such as angle trends found in molecules along the PX_3 series (X: F, Cl, H); and (iii) CP maps of some nonequilibrium geometries (linear water, planar ammonia) draw interesting conclusions on the interconnection between the VSEPR entities, LCP geometries, and molecular reactivity.

In addition, some potential drawbacks of the CP-DFT approach will also be pointed out as we introduce and apply it to our set of selected molecules within the context of the VSEPR model. In particular, special care has to be taken when selecting adequate parameters illustrating the VSEPR domains in 2D and 3D maps. Other limitations are related to the impossibility of separate s and p interactions in multiple bonding molecules or the difficulties to differentiate each of the lone pairs associated with the ligands. We will see

that none of these limitations avoid extracting new chemical information regarding the molecular geometries in terms of the calculated local pressures. This paper is organized in three sections. In the next section, methodological and computational details of our CP-DFT approach are presented. Section 3 contains the results and discussion and is further divided in four subsections. The first one contains the description of the VSEPR prototypical molecules in the light of the CP approach. This is followed by the study of some VSEPR exceptions and their explanation using LCP ideas supported by CP formalism. In the third subsection, we show how the analysis of the kinetic and potential energy contributions of the CPs in the lone and bond pair regions provides valuable information on the chemical (electrophilic/nucleophilic) activity of the selected molecules. In the last subsection, ammonia and water nonequilibrium configurations are examined to illustrate how their CP maps are consistent with non-VSEPR geometries anticipated by the LCP model. Energetic inferences on the inversion barrier of AX_3E molecules are given. The paper concludes with a summary of the main conclusions of our investigation.

Chemical Pressure Methodology

In the CP formalism the total DFT energy of the system is expressed as an integral all over the space of the energy density ρ_{Energy}

$$E_{DFT} = \int \rho_{Energy}\, d\tau \tag{1}$$

In analogy with the thermodynamic macroscopic pressure, CP is thus defined as the derivative of the local energy with respect to the local volume, where the local energy ε_{Voxel} is calculated in each of the small parallelepipeds (voxels) of V_{Voxel}volume in which the 3D space is divided:

$$p_{Voxel} = -\frac{\partial \varepsilon_{Voxel}}{\partial V_{Voxel}} \tag{2}$$

In order to perform such a derivative, we adopt the procedure proposed by Fredrickson in which the energy density is calculated in the real space and then, we perform numerically the derivative with respect to the volume. Technical details about the procedure can be found in Ref. [33] and references therein. The energy density is obtained as the sum of the kinetic (KE) (expressed in its positive definite form), Hartree, local pseudopotential (PSP), and exchange-correlation (EXC) energy densities. Other terms contributing to the total energy, are treated simply as a homogeneous background energy ($\rho_{Remainder}$):

$$\rho_{Energy} = \rho_{KE} + \rho_{Hartree} + \rho_{PSP} + \rho_{EXC} + \rho_{Remainder} \quad (3)$$

By including all of them, the integral in Eq. (1) gives the correct total energy. Such an energy decomposition allows us to map each of the contributions or compute the total CP. The later approach is very appealing since within this definition, a CP map will contain information not only about the kinetic energy density, and so about the electron pair localization, but also about the electrostatic and exchange-correlation terms. Therefore, CP analysis will give a global picture both in a qualitative and quantitative manner of the chemical interactions. Moreover, our previous detailed discussion of the kinetic and potential energy contributions to the total CP in molecules and solids (see Ref. 30) reveals that the regions associated with bonds and lone pairs are much better identified when the total CP is depicted than when particular contributions are considered.

Recalling the definition of pressure, it is easy to realize the connection between this atomic level and the macroscopic realms. Being pressure the force exerted per unit area, we see that positive values are associated with compressed zones where in order to relax, the system must expand. On the other hand, negative pressure values represent space regions where the energy lowers if the volume is reduced. Equivalently, CP reveals in the microscopic realm the capability of electronic domains to accept or repel electron density when an electronic reorganization induced by an isotropic strain occurs in the chemical system. Positive pressure values represent potential expansions in the electron density distribution, thus, they are associated with repulsive interactions or antibonding regions. On the other hand, negative CP values represent space regions of cohesion where the electron density will tend to be accumulated (compressed) in order to lower the energy of the system, i.e. bonding regions or attractive interactions.

Computational details

Calculations have been performed according to the following procedure. First, in order to have a good starting geometry for CP analysis, molecular geometries have been optimized at MP2/6-311G* level of calculation using gaussian09 (g09) program.[34] Next, DFT geometry optimizations were carried out using the ABINIT software package[35,36] under the LDA approximation. All ABINIT calculations have been done using HGH pseudo-potentials[37] and ecut values selected from convergence studies (differences between cycles were less than 10^{-5} hartree). 10x10x10 $Å^3$ unit cells were used

to ensure that calculations represent an isolated molecule. The optimizations were stopped when forces were less than $5 \cdot 10^{-5}$ hartree/bohr. Using the optimized coordinates, three single point ABINIT calculations corresponding to equilibrium, expanded and contracted volumes (0.5% respect to the equilibrium one) were performed to obtain the necessary input for the CP program.[38]

In order to assure that convergence has achieved, we have checked that negligible modifications are obtained when lower expansion/contraction percentages are used. In all the cases, the core unwarping procedure was used to reduce the strong features around the cores. Two different types of CP maps will be used to illustrate our results. Both are designed using the VESTA program.[39] The best way to describe the topology of the chemical pressure field, i.e. how the values of CP are distributed around the nuclei of the molecule, is by means of 2D and 3D maps. 2D maps are the common so-called heat-maps where a color code evolves from low to high values of chemical pressure. Of course, as with other scalar fields, one has freedom to select which are the relevant planes to visualize. Usually, if the number of atoms is not high, as it occurs in this study, symmetry planes or those containing molecular nuclei are natural options for the 2D maps. In this representation, a zero chemical pressure isoline depicted in solid black will be of utmost importance since it separates, and many times encloses, meaningful regions of positive and negative chemical pressures. In the case of 3D maps, isosurfaces represent the spatial distribution of chemical pressure. We select particular positive (white) and negative (black) isovalues with the aim of enclosing and differentiating regions containing local extrema of chemical pressure. For this purpose, the CP values of the 2D maps are very helpful. Although, in general, this can be a tedious task when the number of these critical points of the chemical pressure field is high, we have seen that it has not been the case in this VSEPR study.

Molecules Studied

Molecules studied are summarized in Table 1 along with their molecular geometry and their VSEPR nomenclature (A, X, and E stand, respectively, for the central atom, the ligands, and the lone pairs). Bond lengths and bond angles along with computational details are available for all of them in the supporting information file. In the text, only those molecules more relevant to highlight the connection between CP and chemical concepts will be described in detail. We notice that it is in molecules with lone electron pairs

where geometry departs from ideal symmetry and VSEPR rules may not be fulfilled needing LCP explanations.

Table 5.1. Molecules, VSEPR nomenclature and geometry.

Molecule	VSEPR Nomenclature	Geometry
BeH_2	AX_2	Linear
BF_3, BH_3	AX_3	Trigonal Planar
Ethylene	AX_3, AX_3	Trigonal Planar
SO_2, H_2O	AX_2E_2	Bent
NH_3, NF_3, PH_3,PF_3,PCl_3, AsH_3	AX_3E	Trigonal Pyramidal
SF_4	AX_4E	Seesaw
ClF_3	AX_3E_2	T-Shaped
XeF_2	AX_2E_3	Linear

Towards VSEPR Model

Let us start our discussion describing the CP distribution of an electron deficient molecule with no lone pairs, BeH_2. Each of the two differentiated negative CP regions displayed in Figure 5.1 appears in each of the zones corresponding to Be-H bonds.

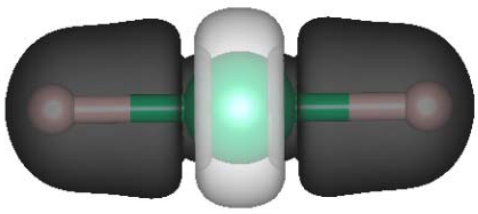

Figure 5.1. 3D isosurfaces of CP distributions within the BeH_2 molecule. Isosurface values: CP = +0.00417 (white) and –0.0016 (black). Green and gray spheres indicate beryllium and hydrogen atoms, respectively.

This feature clearly agrees with chemical intuition, where we expect that a reduction in the volume will lower the energy of the system as a consequence of the charge density accumulation produced by the attractive interaction between the Be and H atoms. Further, we observe a toroid-like positive CP

isosurface around the Be atom representing the shape of its core region where the electron density is willing to expand. In terms of the VSEPR model, the negative CP lobes resemble the tendency of charge density accumulation produced by the bond electron pairs, which are distributed in a 180^0 disposition as expected from an AX_2 molecule. Similarly, the electron-deficient BH_3 molecule shows an equivalent pattern with a positive p-like isosurface around the B nucleus and negative CP lobes along the B–H bonds (see Fig. S5.1 in the Supplementary Material 5).

To continue with our discussion, Figure 5.2 shows how CP describes ammonia, a molecule with just a single lone pair. Evidently, three negative CP regions appear in the zones corresponding to three N–H covalent bonds. Again, these features indicate the charge density accumulation produced by the attractive interaction between the N and H nuclei. Further, we observe a positive CP isosurface along the C3 rotation axis associated with the position of the N lone pair. This positive CP isosurface does not show any space division, highlighting that there is only one lone pair. Furthermore, its positive value reflects the fact that this lone pair tends to spread out in space, and therefore, any charge density accumulation in this region would increase the interelectronic repulsion. This is a clear sign of the expected chemical (re)activity of this center, as discussed later. Further, we notice that this result correlates with the fact that H is a weak electronegative ligand in this molecule, inducing a loose lone pair in N.

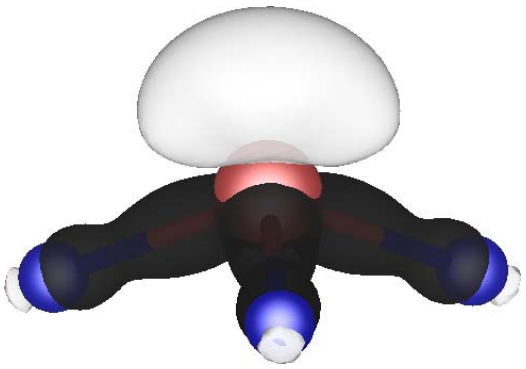

Figure 5.2. 3D isosurfaces of chemical pressure (CP) distributions within the NH_3 molecule. Isosurface values: CP=+0.028 (white) and -0.045 (black). Brown and blue spheres indicate nitrogen and hydrogen atoms, respectively.

Nevertheless, using the VSEPR language, our results support the fact that repulsions involving the lone pair are greater than those between bond pairs, as revealed by the bond angle being slightly below 109.5^0. Overall, the distribution of CPs in an ammonia molecule leads to a set of four CP lobes,

three associated with N–H bonds and one associated with the lone pair, which is in complete agreement with the electron pair domains defined by the VSEPR theory.

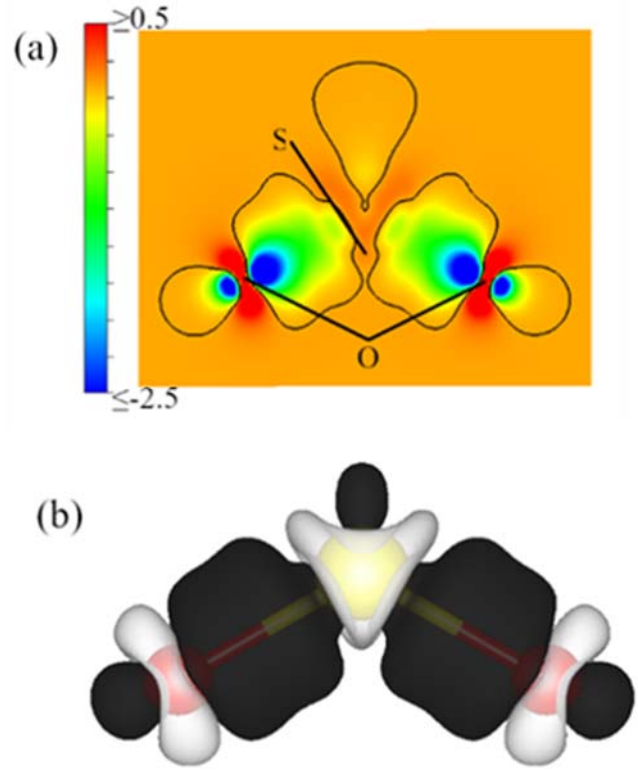

Figure 5.3. CP analysis of SO_2 molecule (yellow = S; red = O). (a) 2D map of the plane containing S and O nuclei. Black curves: CP = 0 isolines. (b) 3D isosurfaces with CP = +0.08 (white) and CP = 0.04 (black).

In the case of SO_2 (Figure 5.3a), a molecule with one lone pair but also with multiple bonds, we obtain three different CP regions surrounding the central atom, as expected for a molecule with AX_2E stoichiometry. Two are associated with the S–O bonds and one corresponds to the S lone pair. As depicted in the heat map along the plane that contains the SO_2 molecule (Figure 5.3b), bond regions have CP values ranging from 1.5 to 1.0 a.u., whereas the S lone pair has CP values from 0.15 to 0.0 a.u. Contrary to the NH_3 molecule, S lone pair is characterized by a negative CP value. It should be noted that in this molecule, oxygen is a strong electronegative ligand inducing a clear lone pair in S. Although we will later comprehensively explain why the CP sign of lone pair changes and how it is related to chemical concepts, it is worth mentioning here that CP values in the lone pair regions are always less negative (or positive) than those in the bonding regions. Once again, such values of CP denote that lone pairs are less attracted to the nucleus, and therefore, occupy

larger volume regions than bonds. All these facts support the idea that the VSEPR rule of lone pair repulsions are greater than those of the bonding pairs.

The two oxygen lone pairs are clearly enclosed in a single region of negative CP. Although this result is not transcendent in the VSEPR discussion, it should be noted that the CP analysis is not able to clearly identify different lobules for the lone pairs of the ligands. Nevertheless, it is noteworthy that a positive CP region with a shape resembling a p-like orbital can be observed at the oxygen positions. These positive CP values indicate that the accumulation of charge density in the regions perpendicular to the bond axis produces an expansion of the electron density distribution, resulting in the weakening of the S=O bond. In the molecular orbital language, this feature would be called an antibonding region.[40] Incidentally, such CP features are not exclusive to S–O double bonds, but they are a general characteristic of the inherent chemical information contained in the CP analysis of multiple bonds.

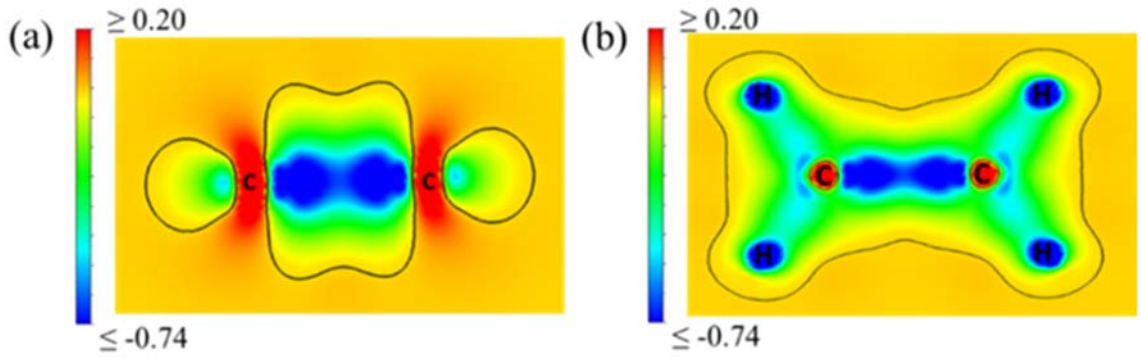

Figure 5.4. Chemical pressure heat-maps of the ethylene molecule. Cross sections are shown for (a) the plane containing C atoms and perpendicular to the molecular plane and (b) the molecular plane containing all C and H atoms. Black curves: CP = 0 contour.

For instance, in the prototypical ethylene molecule, a similar pattern associated with the double bond is displayed. In Figure 5.4a, we observe a similar p-like shape with a positive CP value emerging perpendicular to the bond axis and out of the molecular plane. In addition, zero CP isolines enclose three negative pressure regions in this plane. Two of them are equivalent and are not chemically meaningful as they originate from the projections of the negative CP values associated with the C–H bonds that will be discussed later. The third region between the C atoms can be used as a signature of a multiple bond in the CP framework and is associated with the charge density

accumulation resulting from the existence of the C–C double bond. The strength of this interaction is exhibited by the low values of CP along the C–C bond axis (dark blue) and above and below the molecular plane (green and yellow). Although a similar bonding pattern is observed between the two C atoms when the CP is depicted in the plane containing the molecule (see Fig. 4b), here, only one region of negative CP is obtained. C–H and C–C bonds are not differentiated in this plane by zero CP isolines, but they can be clearly identified by the particular negative values of CP along the C–H (light blue) and C–C (dark blue) directions. At this point, it should also be noted that our CP analysis does not reveal the differences between s and p contributions to the C–C bond as far as the two 2D maps of the ethylene molecule are concerned. This seems to be a limitation of our study, which necessitates further studies in other molecules exhibiting multiple bonds.

Amore comprehensive topological analysis in progress, and out of the scope of this VSEPR study, would allow us to characterize the double bond in a quantitative manner. With regard to a lone pair system, another interesting question worth addressing is the nonequivalence of the axial and equatorial positions in the AX_4E geometries. The VSEPR theory postulates that there exists lower repulsion at the equatorial plane of the trigonal bipyramid than that at the axial one.[7] Therefore, if the CP formalism is consistent with the VSEPR model, our CP maps should reflect the different behavior of such positions. It should be noted that we do not pursue to provide a rigorous proof, but only formulate a test on the reliability of our approach since we are investigating the equilibrium geometry of the molecule. In order to illustrate if there is a preference between the two planes for the electron density to be located, Figure 5.5 shows the CP heat maps of the axial and equatorial planes of the SF_4 molecule. Both contain two S–F bonds and the region associated with the lone electron pair. As the electron density is more comfortable in such molecular regions with negative CP values, we expect to see wider zones with lower CP values in the 2D equatorial map. Indeed, this is observed in Figure 5.5(a) and (b). Whereas S–F axial bonds are characterized by less negative pressure, indicated by an almost uniform green color in the heat map, equatorial bonds exhibit a dark blue-green pattern. Moreover, the region of the lone pair with low negative CP values is

asymmetrically distributed along the axial and equatorial planes, showing bigger extension of the equatorial plane.

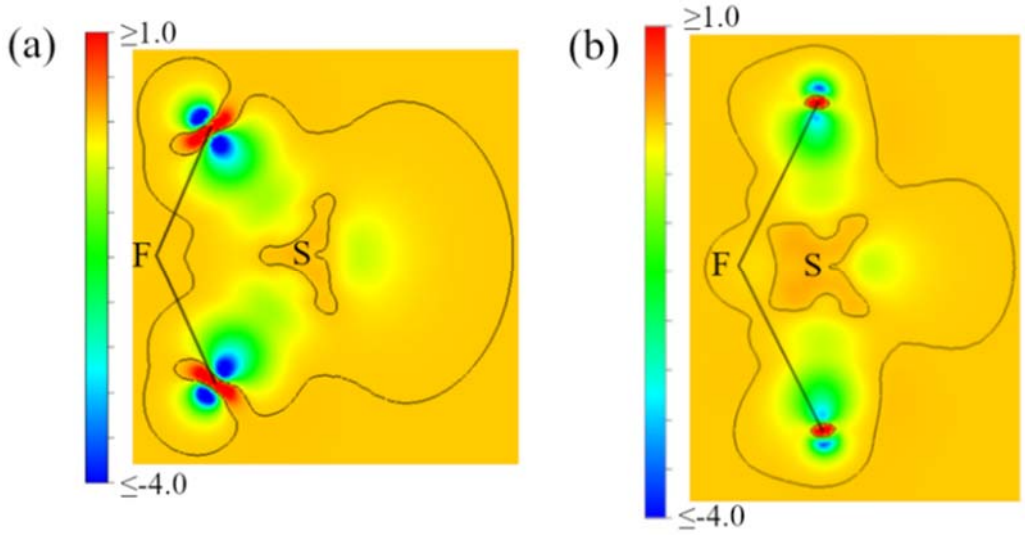

Figure 5.5. CP heat maps of the SF_4 molecule. Cross sections are shown for the (a) equatorial and (b) axial planes containing S and F atoms. Black curves: CP = 0 contour. Pressures are expressed in atomic units.

In the light of these results, several compelling conclusions can be drawn. First, this lone pair asymmetry is due to a larger size of the lobe along the equatorial plane, and consequently, these negative CP values indicate that electron density tends to accumulate around these positions. This is in agreement with the VSEPR model: the equatorial plane is the one where the electronic repulsions between the lone pairs and bond pairs are minimized. A second unequivocal conclusion emerges when hypervalency is invoked to explain the bonding pattern in the SF_4 molecule. According to our calculations, all S–F bonds exhibit well-defined and equivalent CP covalent profiles.[30] This is in agreement with the work of Noury, Silvi, and Gillespie.[41] These authors found the same ELF basin populations of two electrons in all the bonds involving hypervalent atoms. Our results confirm the similarity of all the bonds as well as their covalent character, regardless of the hypervalence of the S atom in the SF_4 molecule. These results highlight the capability of the CP formalism to describe bonds in molecules with hypervalent atoms, although we believe that a more comprehensive analysis is necessary to explain the role of other factors, such as retrodonation and d character, which are usually invoked to explain these molecules. To continue through this CP analysis of the VSEPR molecules, we will now examine how this formalism can describe molecules with more than one lone electron pair.

Figure 5.6a shows the CP isosurfaces and heat map along the plane that contains the nuclei of ClF_3, an AX_3E_2 molecule. As that in the previous cases, negative CP appears again around the Cl–F bonds, with values ranging from 5 to 2 a.u., whereas the lone pairs exhibit fewer but negative values (from 0.6 to 0.0 a.u.). We notice again that these values correlate with a stronger electronegative ligand (F).

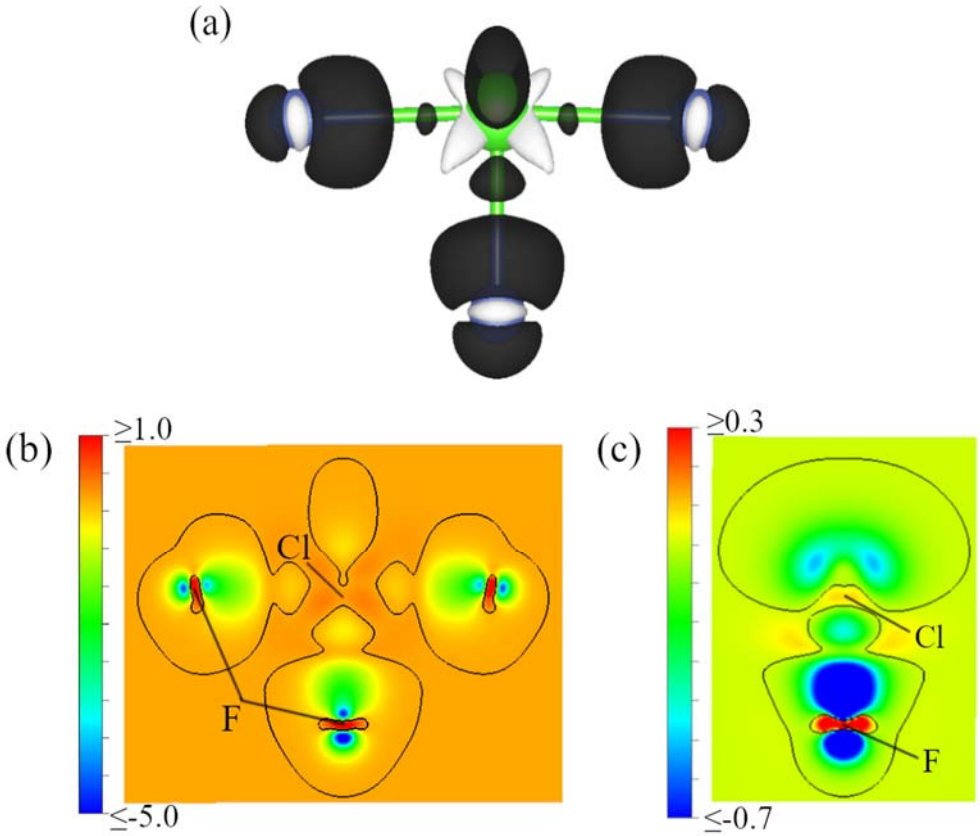

Figure 5.6. Chemical pressure plots of molecular ClF3. (a) 3D isosurfaces with CP = +0.096 (white) and CP = −0.14 (black). Green and violet spheres indicate chlorine and fluorine atoms, respectively. (b) 2D map of the (100) plane containing Cl and F atoms. (c) 2D map of the (110) plane containing the lone pairs. Black curves: CP = 0. Pressures are given in atomic units.

From the color map representation along the plane perpendicular to the one that contains the molecule, the lone pair plane (Figure 5.6b) exhibits two minima of CP at a separation of 120^0 (blue regions), suggesting the most likely positions of the Cl lone pairs. Such a result shows, one more time, the agreement with the VSEPR theory, which describes the AX_3E_2 molecules as having T-shaped morphology and the lone pairs are set at disposition of 1201 in order to minimize Pauli repulsion.

A final challenging example with multiple lone electron pairs (AX_2E_3) concerns the linear XeF_2 molecule. The spatial positions of these pairs are not well reproduced by the VSEPR model and it is, therefore, interesting to investigate the results from our CP approach. The CP isosurfaces of the XeF_2 molecule shown in Figure 5.7 clearly reveal that Xe lone pairs are distributed on a torus (doughnut-like) region of negative CP around the central atom.

This topological feature agrees with Linnet's theory,[42] which establishes that in the case of linear molecules, contrary to the VSEPR model, lone pairs are not presented as opposite spin pairs but they rather have their most probable locations equally distributed around the molecular axis. A further examination of the XeF_2 CP heat map (Figure 5.7) reveals that the torus surrounding the Xe atom has four minima equally distributed along the zero pressure isobar. Similar features have been observed in the topology of ELF and Laplacian of electron density,[7] which highlight the capability of CP formalism to reveal the electronic and geometrical structures of such molecules. Incidentally, the existence of an antibonding p-like region of positive CP at the F position and perpendicular to the Xe–F bond should be noted, which is similar to the one discussed in the SO_2 molecule. These regions are responsible for repulsions between the ligands, as discussed later.

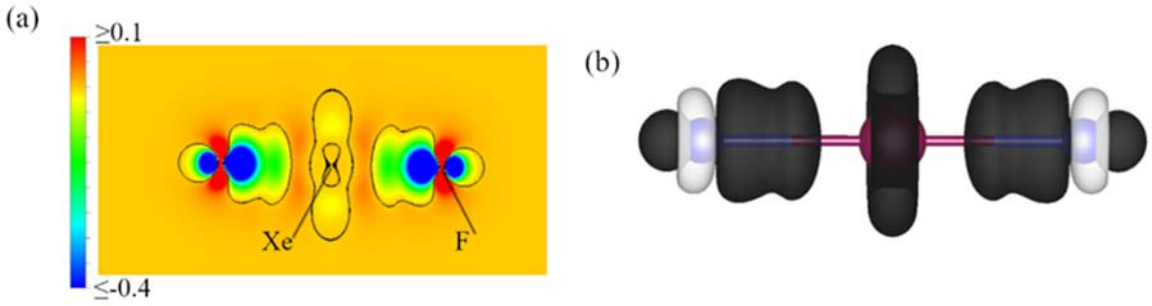

Figure 5.7. Chemical pressure analysis of XeF_2. (a) Cross section along the (100) plane. Black curves: CP = 0 isolines. (b) 3D isosurfaces of CP = +0.05 (white) and CP = − 0.01 (black).

Rationalization of VSEPR and LCP results: Exceptions in the light of CP formalism

One of the VSEPR rules asserts that as the central atom's electronegativity decreases in a series of molecules with a common ligand, bond–pair repulsions also decrease because the valence electrons of the central atom are less attached to the nucleus. Therefore, lone pair domains increase their activity, forcing bond angles to decrease in order to minimize the lone pair–bond pair

repulsions. To test how our approach describes this trend, we have calculated the CP maps of a series of molecules with a common ligand and different central atoms of decreasing electronegativity. In Figure 5.8a, the CP heat maps of the XH_3 molecules (X: N, P, and As) are shown.

Clearly, a sequence in the colors of the bonding and lone pair regions is detected. However, CP values for the bonds increase from higher to lower negative values; in the case of lone pairs, these values decrease from being positive to slightly negative. Such a behavior indicates a correlation between the difference in the electronegativity between the ligand and central atom because of the lone pair, which becomes more active as its CP value decreases. This correlation between the activity of the lone pair that we detect in terms of low (negative) CP values and the electronegativity of the ligands is in accordance with the LCP model. In NH_3, the ligand-induced activity of the lone pair is not important as H is a weak electronegative ligand (as compared to N). This is revealed by the positive CP values at the N lone pair positions and a decrease in the bond angle from the ideal tetrahedral value of less than 31. In contrast, the electronegativity of H is higher than that of As; as evident from the small region of negative CP associated with the As lone pair, it leads to a bond angle of only 90.6^0. Contrary to this well-behaved trend, one of the drawbacks of the VSEPR theory was the inability to explain why although F and Cl are more electronegative than H, the angles in the PH_3 molecule are smaller than those in PF_3 and PCl_3. Gillespie and Robinson also realized that ligand repulsions play a key role in molecular geometry, and therefore, the VSEPR theory must consider ligands as a part of bond pair domains [19].

Ligand repulsions can be considered as repulsive noncovalent interactions, and therefore, are difficult to characterize using the ELF and Laplacian of electron density. However, a simple interpretation of the CP maps of these three molecules provides a coherent explanation of the observed trend. We associate an increase in the activity of the corresponding lone pair along the PH_3, PCl_3, and PF_3 series with lower and negative CP regions at the P lone pair positions, which is in agreement with the correlation established above. It should be noted that this activity results in lower bond angles in PH_3 than those in NH_3 or lower in PF_3 than those in PCl_3; however, this does not explain why the bond angle in PH_3 is lower than that in PF_3 or PCl_3. The consideration of the ligand–ligand repulsions needs to be taken into account, too. Figure 5.8b shows a positive CP p-like region around the F and Cl nuclear positions in PF_3 and PCl_3, respectively; however, in PH_3, this feature is absent. These positive CP values, representing space regions where the electron density

tends to expand, were previously associated with antibonding interactions. Here, this feature highlights the higher electrostatic repulsions of the F and Cl ligands (as compared to H), and therefore, serves to explain the angle trend found in these molecules.

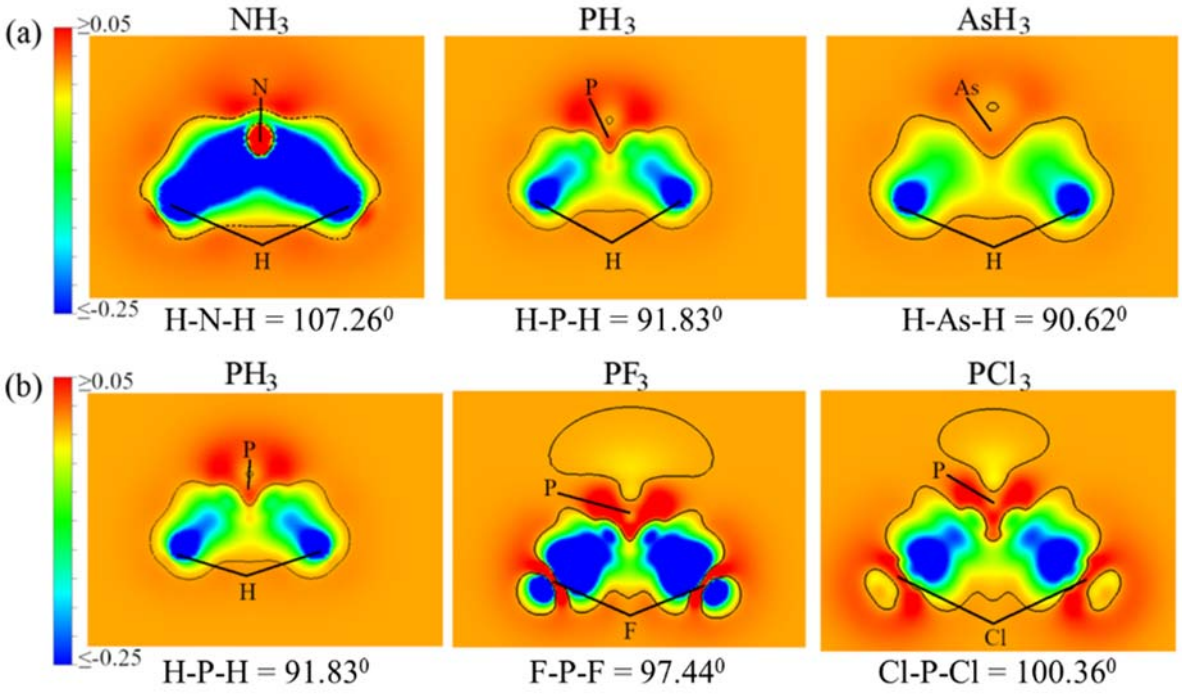

Figure 5.8. CP 2D heatmaps containing the nuclei of (a) XH3 hydrides, where X = N, P, and As, and (b) PX_3 halides, where X = H, F, and Cl. Black curves: CP = 0 isolines are shown in all the panels.

Recovering chemical concepts from CP formalism

In the previous sections, we have shown how CP values and isosurfaces can recover space regions that resemble the electron pair domains defined in the VSEPR theory. These features are associated with the kinetic and potential energy pressure contributions, which, as demonstrated by the ELF, ELI, or quantum electronic pressure defined by Tao,[43-45] contain information about electron pair localization. However, some other striking aspects have appeared through the previous analysis of the CP maps. For example, earlier cases have shown that the CP sign changes from positive to negative, with lone pairs having positive or less negative values than those of bond pairs. One would expect, as that with NH_3, that lone pairs would be characterized by positive pressure isosurfaces because they represent space regions where an

accumulation of charge density would increase the electronic repulsion between them (lone pairs are only attached to one core nucleus). However, since CP formalism also comprises the potential electrostatic pressure, its sign also depends on the partial charges of the atoms, and therefore, on the electronegativity difference between the central atom and ligands.

When electronegative ligands or double bonds are attached to the central atom, their force distribution tends to partially delocalize. Therefore, an excess of positive charge is set on this atom and this can accumulate, lowering the energy and increasing the charge density. Such a simple reasoning is also valid for understanding why CP values of lone pairs are always less negative than those of bond pairs. Although lone pairs can accumulate a certain amount of charge density, their electron repulsion prevents its considerable accumulation as compared to that in bond pairs. To highlight how much chemical information can be gained from the combined analysis of the potential and kinetic pressures, we have compared the CP maps of NF_3 and NH_3 molecules. This comparison also allows us to extend our conclusions beyond the correlation previously proposed within the LCP model. NF_3 and NH_3 are excellent examples to illustrate these ideas. Although NH_3 is a well-known basic and nucleophilic compound, NF_3 does not exhibit any basic properties (under extreme conditions, it behaves as a Lewis acid) and has been characterized as an electrophilic molecule. As shown in Figure. 5.9, the substitution of H ligands by F ligands produces a change in the sign of the CP isosurface associated with the lone pairs. This is the expected behavior after our analysis of ligands with different electronegativities. Now, the conclusions regarding the chemical activity of the molecule can also be derived.

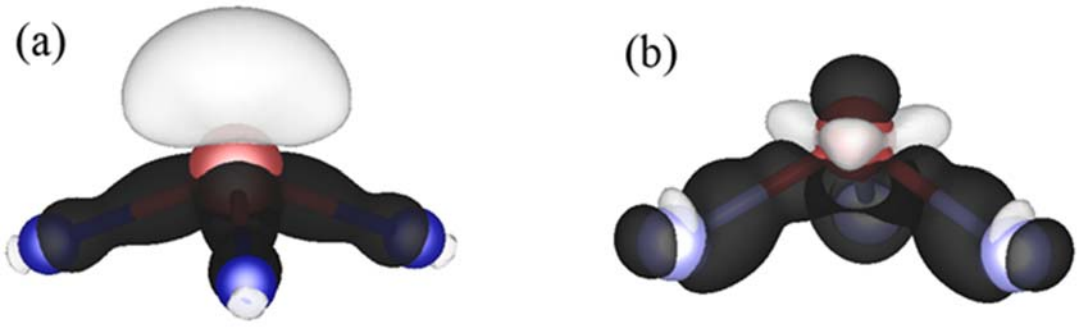

Figure 5.9. CP distributions visualized with 3D isosurfaces with (a) CP = +0.028 (white) and CP = –0.045 (black) for the NH_3 molecule and (b) CP = +0.05 (white) and CP = –0.045 (black) for the NF_3 molecule, both at their corresponding equilibrium geometries.

CP formalism can not only reveal the static electronic structure involved in the bonding pattern of the molecules, but also can be dynamically related with chemical reactivity. As positive CP values correspond to space regions where electrons tend to expand, and consequently, yield regions in which the electron density could be shared with other chemical species, their presence reveals basic or nucleophilic regions. In the case of negative values, they indicate space regions in which the charge density tends to accumulate, and therefore, should be related to acidic or electrophilic behavior. Therefore, our analysis is in tune with the chemical activity of NH_3 and NF_3 molecules. To further illustrate this result, we choose a prototypical Lewis acid molecule with empty orbitals capable to accept electron pairs (e.g., BF_3). It is also a deficient electron molecule within the VSEPR context. As explained above, we should expect a negative CP distribution around the B atom, suggesting a preferred region to host electron pairs. Such an expectation is confirmed through the analysis of the 3D CP distribution in the BF_3 molecule, where a negative pressure isosurface surrounds the B atom (Figure 5.10). In addition, in Figure S5.2 (Supplementary Material 5), we include a 2D CP map of the molecular plane of BF_3. Only a very small region of positive CP associated with the core of B appears subsumed inside the domain of negative CP corresponding to the B–F bonds. The absence of an external positive CP region at the B position, as those in the other electron-deficient molecules explored earlier (BeH_2 and BH_3), is justified here due to the strength of the B–F bonds, and this is in accordance with the high electronegativity of F.

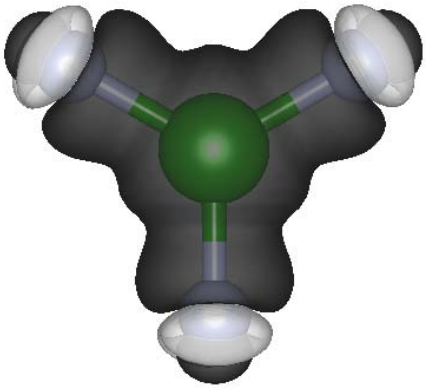

Figure 5.10. Chemical pressure distributions visualized with 3D isosurfaces with (a) CP = +0.03 (white) and CP = −0.04 (black) for the BF_3 molecule.

Bearing in mind these ideas, we can extend our discussion to some other features that have been overlooked in the previous sections. For example, regarding SF_4 and SO_2 molecules, we can see that the value of CP minima of

the S lone pair is around 0.5 a.u. in SF_4, whereas its value decreases to 0.15 a.u. in the case of SO_2. In accordance with the LCP model, such a difference is due to the electronegativity difference between the F and O atoms and illustrates (which is in agreement with chemical intuition) that SF_4 is a stronger Lewis acid than SO_2. A correlation between the CP values at the minima is associated with the central atom lone pair and the acid–base character is, therefore, disclosed. Moreover, it is well known that SO_2 can also behave as a Lewis base, while SF_4 does not. Such a result is not surprising considering that the CP values of lone pairs of SO_2 are relatively close to zero. We can propose that SO_2 can act as both an acid as well as a base depending on the CP values of the molecule with which it reacts. If the approaching molecule exhibits lower (greater) CP values than SO_2, then SO_2 is expected to behave like a base (acid).

At this point, another interesting and related concluding thought can be pointed out. As the CP values describe the local forces on atoms through the balance of the potential and kinetic energy pressure, both highly positive and highly negative pressure values indicate that strong forces are needed to either increase or decrease the electron density. Therefore, most likely interactions with other approaching molecules will be those that balance the pressure difference or, in other words, those that equalize the CPs. This simple reasoning is fairly similar to the analysis of hard–soft interactions,[46] where it is concluded that hard acids prefer hard bases and vice versa. Indeed, such a result is not surprising if we recall that the concept has been widely reviewed through the analysis of molecular electrostatic potential,[47,48] which actually is also somehow encoded in CP formalism.

Local pressures in nonequilibrium geometries

To the best of our knowledge, the influence of electronic structure domains within the VSEPR and LCP models into nonequilibrium geometries has not been studied yet, and it could provide simple chemical rules that can predict chemical reactivity. Only a few attempts of potential applications of VSEPR model in this regard have been described in the literature. For example, Naleway et al.[49] studied the energy and electron density distributions of the molecular orbitals of water for different H–O–H angles within the range from 90^0 to 180^0. Their results showed that deformations of the electron density can be rationalized in terms of the VSEPR theory, although these authors were more focused on the understanding of the water equilibrium geometry

rather than the implications of the VSEPR theory in nonequilibrium geometries.

It was not until 2016 that, for the first time, Andres et al.[26] explicitly analyzed the implications of the VSEPR model on chemical reactivity and nonequilibrium geometries. By means of ELF and bonding evolution theory, they analyzed the electron density transfer in chemical reactions. According to their work, two scenarios in chemical reactivity can be presented. With regard to VSEPR compliance, the electron density transfer induces the evolution of one structural stability domain into another through the reorganization of the electronic domains of the valence shell. In the other, the molecule remains in the same structural stability domain in a nonequilibrium configuration called VSEPR defective. In the latter case, the authors explain that VSEPR rules are not fulfilled.

For example, repulsion between the bonding domains is greater than the repulsions between the nonbonding domains as that in the case of the inversion of ammonia, where a trigonal bipyramid arrangement is preferred. VSEPR-defective configurations would lead to unstable structures, and therefore, they are expected to be chemically reactive. The spirit of the VSEPR model lies in the minimum repulsion principle of the valence shell domains, leading to rules wherein nonbonding domain repulsions are greater than those between bonding domains for molecules at equilibrium. However, when equilibrium geometry is distorted, it is always followed by electron density reorganization; hence, a modification of the shape and volume of the pair domains is induced. In such situations, the previous rules cannot be applied, and more generic ones are necessary. Given the capacity of CP formalism for providing the reactivity information of molecules because of the combination of kinetic and potential energy pressures, it is interesting to explore if further insight can be gained on the interaction rules of nonequilibrium geometries through the analysis of these local pressures. In order to analyze how local pressures are distributed in nonlocal geometries, we shall start our discussion with a well-known example: the inversion of NH_3. During planarization, N atoms go from sp^3 to sp^2 hybridization; as a consequence, the $2p_z$ atomic orbital of N does not participate in the formation of N–H bonds and formally hosts the lone pair electrons. Figure 5.11 shows the CP maps of the NH_3 molecule in the equilibrium (C_{3v}) and planar (D_{3h}) configurations.

In this case, D_{3h} bond lengths were obtained from the optimized transition states of inversion, as provided by Xu et al.[50] Clearly, when the H–N–H

angle increases toward the value of 120^0 of a planar configuration, it is evident that the positive pressure isosurface associated with the lone pair spreads out in a direction perpendicular to the molecular plane, shaped in a p-like orbital in the D_{3h} geometry, thereby increasing the participation of the $2p_z$ N orbital as a nonbonding orbital. Furthermore, a detailed analysis of the CP maps also reveals that such a change is accompanied by an increase in the lone pair pressure from 0.4 to 0.6 a.u.

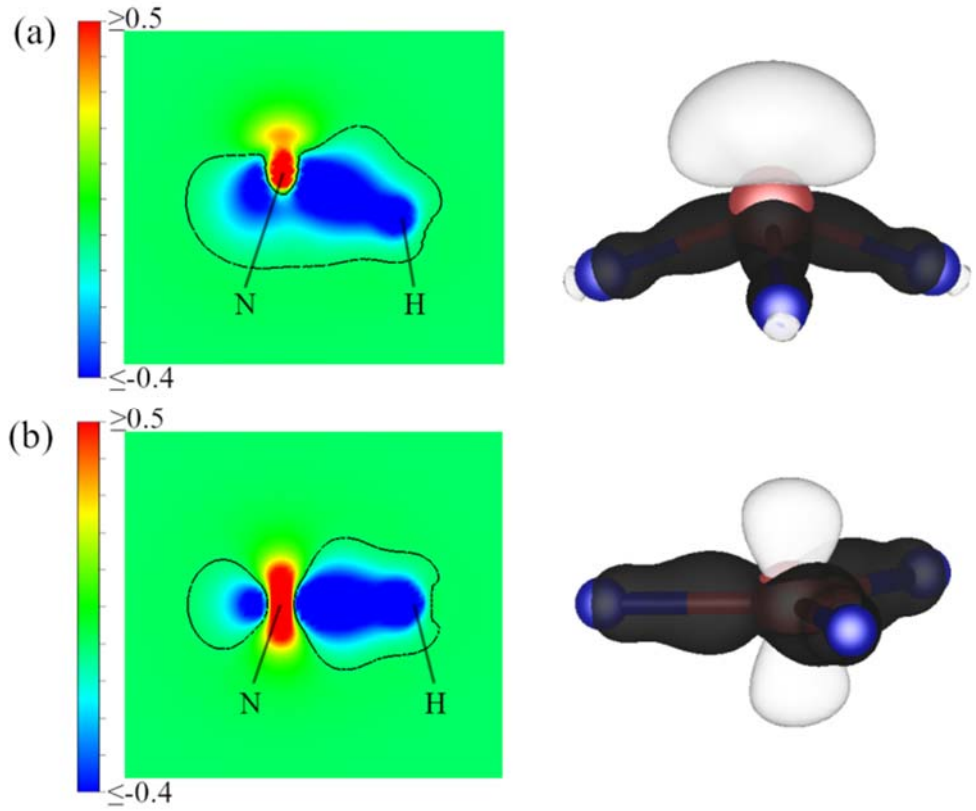

Figure 5.11. CP 2D heat maps of NH3 molecule with different configurations. (a) Cross section along the (110) plane containing the N–H bond with angular geometry. (b) Cross section along the (100) plane with planar geometry. 3D isosurfaces of CP are shown in both the panels for the two geometries. CP = +0.028 (white) and CP = –0.045 (black). (Brown = N; blue = H). Black curves: CP = 0 isolines are shown in the 2D panels.

At this point, it is interesting to recall the definition of pressure. This quantity is defined as minus the derivative of energy with respect to the volume, an increase in the CP value reveals that during inversion, the lone pair energy increases and volume of the lone pair decreases simultaneously. Such a volume reduction can only be explained if we realize that when planarization occurs, the electron density associated with the lone pair of N occupies a p_z orbital

perpendicular to the molecular plane. This fact formally implies that, on average, one electron is above and one electron is below the molecular plane; consequently, in terms of the Pauli's exclusion principle, the electrons are less repelled, and therefore, occupy less volume. Immediately, such a volume reduction displayed by the CP formalism allows us to conclude that in the planar configuration of NH_3, bond pair repulsions are stronger than lone pair–bond pair repulsions. This is contrary to the standard VSEPR rules for equilibrium configurations, but in agreement with the conclusions by Andres et al.[26] Moreover, as demonstrated through the analysis of AX_3E molecules in the section "Towards the VSEPR Model", the increase in the positive CP value of the N lone pair is associated with a weakening of the lone pair activity on the geometry of the molecule, leading to the ideal 120^0 angle of the D_{3h} geometry. Such a conclusion agrees well with the idea that planar ammonia formally has, in VSEPR and LCP nomenclatures, the expected geometry from an AX_3 molecule, where the absence of lone pairs in the valence shell can be understood in planar NH_3 as a result of the compensation of one electron above and one electron below the molecular plane. Interestingly, this result also allows us to draw a conclusion about the inversion barriers of AX_3E molecules: the more active the lone pair, the more energetic is the inversion transition.

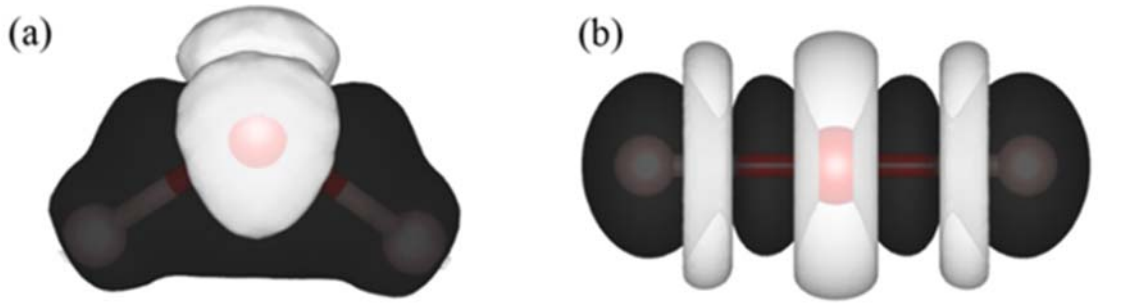

Figure 5.12. 3D isosurfaces of the chemical pressure distribution within H_2O molecule. Isosurfaces of CP = +0.04 (white) and CP= −0.02 (black) are visualized for (a) the equilibrium geometry (b) the linear configuration. Pressures are given in atomic units.

For example, as evident before (Figure 5.8), the CP associated with the lone pair region is lower in PH_3 than that in NH_3, and consequently, PH_3 lone pair is more active. Such a result unequivocally implies that P lone pairs occupy bigger volumes than those by N lone pairs. Therefore, in D_{3h} geometry, the P valence shell exhibits stronger directionality, and therefore, stronger lone pair–bond pair repulsions than those in NH_3, leading to a larger inversion

barrier. Such a conclusion becomes even more categorical when we collate the experimental energetic barriers, which is about 5 kcal mol^{-1} for NH_3 and 34 kcal mol1 for PH_3.[50] From Figure 5.12, changes in the CP distribution around the O–H lone pairs are evident. In particular, the two positive isosurfaces observed in the equilibrium configuration become a positive CP isosurface with a torus shape surrounding the O atom at 180^0 as expected for a linear configuration. As compared to the linear XeF_2 molecule discussed earlier, this lone pair region presents a positive CP isovalue indicating that, besides the constraint imposed by linear geometry, the low electronegativity of H induces weak activity to the O lone pairs.

Indeed, when we analyze the 1D-CP profiles along the O–H bond for the two configurations (Figure 5.13), it is evident that the CP minima located around 0.15 Å from the O nucleus decrease from the equilibrium configuration to a linear one. Such a minimum corresponds to the lowest pressure associated with the O atom. Therefore, as the negative pressure represents attractive interactions, such a value indicates the maximum attraction of electrons, and therefore, it is related with the electron density accumulated around oxygen. Consequently, the decrease in the minimum CP indicates that the O–H bond increases their ionic character, which is in agreement with the classical picture provided by the valence bond and molecular orbital theories where the transition from an angular (sp^3-like) configuration to a linear (sp-like) one reflects an increase in the s character of the O–H covalent bonds. Furthermore, in the 3D representation of the linear configuration, a positive pressure isosurface around the O–H bonds (Figure 5.12) is observed, which does not appear in the angular ones. Such positive isosurfaces, associated with an expansive zone, confirm the latter results and reveal that the electron density tends to accumulate close to the O nucleus rather than that in the bond region. Interestingly, the CP representation of the H_2O bond distortion provides further insight into the validity of the VSEPR and LCP theories to study nonequilibrium results. As discussed, the linearization of the H_2O molecule is accompanied by a decrease in the lone pair activity, as evidenced by the increase in the ionic character of the O–H bond. Such a result is in agreement with the examples given by Gillespie in their study of AX_2E_2 molecules, where oxygen was the central atom. In the case of highly electronegative and small ligands, the bond angle is lower than the tetrahedral ideal one, as that in the case of equilibrium OF_2 and H_2O molecules, evidencing strong directionality of the O lone pairs. On the contrary, the presence of low electronegative ligands, such as Li in Li_2O, leads to an almost

anion-type spherical distribution of the valence shell electron of the O with a bond angle of 180^0, which is higher than the tetrahedral ideal one.

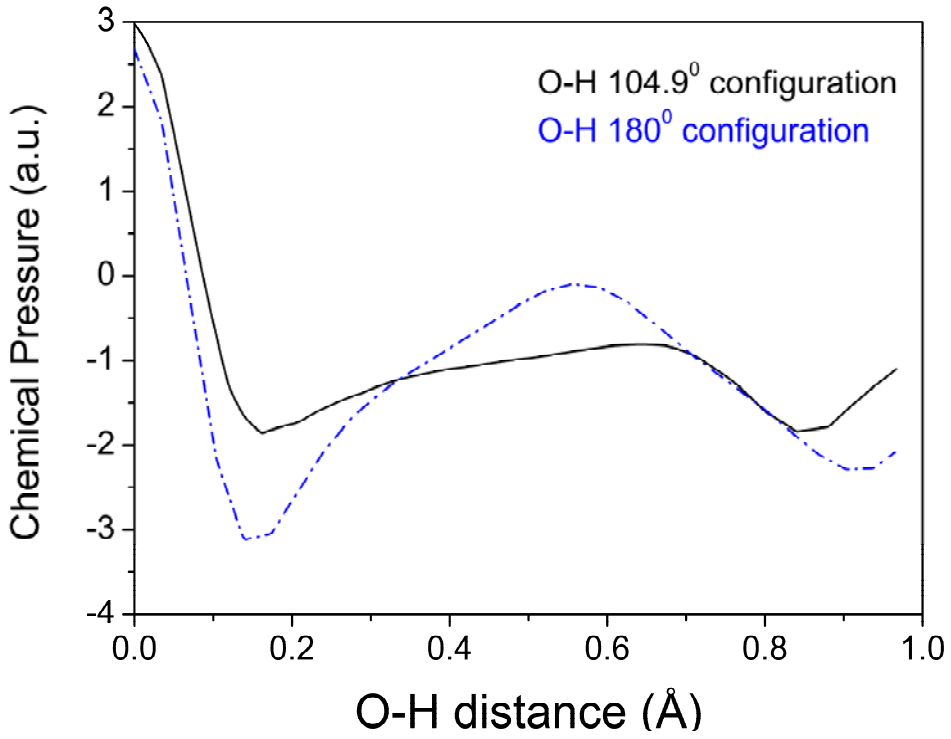

Figure 5.13. 1D CP profiles along the O–H bond of H_2O molecule. Blue dashdot line at 180^0 configuration; black line: equilibrium geometry. All the values are expressed in atomic units.

Conclusions

For the first time, CP formalism, a full stress tensor methodology comprising all the energetic contributions (kinetic, Coulombic, and exchange correlation), has been applied to systematically study certain prototypical molecules within the VSEPR model taking into account the premises of the LCP model, too. Potential difficulties in the selection of appropriate parameters for formulating illustrative 2D and 3D CP heat maps can be overcome in these simple molecules using molecular and symmetry planes. Other limitations of the CP-DFT formalism have been pointed out in the manuscript (impossibility of separation of s- and p-type interactions or single domains containing multiple lone pairs in ligands), but none of them deter the successful interpretation of the molecules within the VSEPR-LCP model. We have demonstrated that the CP is distributed along the molecules, revealing the positions of bonds and lone electron pairs (VSEPR) and providing correlations between the relative strength of the ligand and effect of the central atom lone pair in the molecular

geometry (LCP). Indeed, recalling that negative pressures are associated with space regions where the electron density tends to accumulate and positive ones with expansive zones of the electron density, we have recovered nonbonding and antibonding regions associated with the size of the ligands that explain some non-VSEPR trends in the bond angles of AX_3 molecules, as well as the nonequivalence of the axial and equatorial regions in SF_4. As the CP formalism also comprises potential energy contributions, we have demonstrated and quantified how the sign and value of pressure in the lone pair regions of the central atom are related not only with its effect on the molecular geometry, but also with the nucleophilic (base) and electrophilic (acid) character of the molecule. Furthermore, as CP is related with the tendency of the electron density to expand and contract, we have rationalized why SO_2 can act as both an acid and base depending on the CP values of the molecule with which it reacts. Our results have led to the conclusion of the well-known chemical analogy that like dissolves like or the hard–soft scenario: most likely interactions between molecules will be those which balance the pressure difference, i.e., those which equalize the CPs. Finally, we have applied the CP formalism to nonequilibrium geometries. Analyzing both planarization and linearization of NH_3 and H_2O molecules, we have intuitively correlated the CP topology and values with the activity of the central atom lone pairs and energetic barrier of inversion in AX_3 molecules, respectively. Such results reveal the capability of CP to provide information regarding reactive processes.

References

[1] G. N. Lewis, The atom and the molecule. *J. Am. Chem. Soc.*, *38*, 762-785, **1916**. DOI: https://doi.org/10.1021/ja02261a002.

[2] P. L. A. Popelier, Quantum Chemical Topology in The Chemical Bond II: 100 Years Old and Getting Stronger, Springer International Publishing, Vol. 115, **2005**.

[3] R. J. Gillespie and E. A. Robinson, Electron Domains and the VSEPR Model of Molecular Geometry. *Angew. Chem. Int. Ed. Engl.*, *35*, 495-514, **1996**. DOI: https://doi.org/10.1002/anie.199604951.

[4] R. J. Gillespie, *Molecular Geometry*, Van Nostrand Reinhold, **1972**.

[5] A. Schmiedekamp, D. W. J. Cruickshank, S. Skaarup, P. Pulay, I. Hargittai, and J. E. Boggs, Basis of the Valence Shell Electron Pair Repulsion Model by ab Initio Calculation of Geometry Variations in a Series of Tetrahedral and Related Molecules. *J. Am. Chem. Soc.*, *101*, 2002-2010, **1979**. DOI: https://doi.org/10.1021/ja00502a013.

[6] I. Hargittai and B. Chamberland, The VSEPR Model of Molecular Geomatry. *Comp. & Maths. with Appls.*, *12B*, 1021-1038, **1986**.

[7] R. J. Gillespie, Fifty years of the VSEPR model. *Coord. Chem. Rev.*, *252*, 1315-1327, **2008**. DOI: https://doi.org/10.1016/j.ccr.2007.07.007.

[8] A. D. Becke and K. E. Edgecombe, A Simple measure of Electron Localization in Atomic and Molecular Systems. *J. Chem. Phys.*, *92*, 5397-5403, **1990**. DOI: http://dx.doi.org/10.1063/1.458517.

[9] R. F. W. Bader, *Atoms in Molecules A Quantum Theory*, Oxford University Press, New York, **1994**.

[10] M. Leboeuf, A. M. Köster, K. Jug, and D. R. Salahu, Topological analysis of the molecular electrostatic potential. *J. Chem. Phys.*, *111*, 4893-4905, **1999**. DOI: http://dx.doi.org/10.1063/1.479749.

[11] R. F. W. Bader, P. J. Macdougall, and C. D. H. Lau, Bonded and Nonbonded Charge Concentrations and Their Relation to Molecular

Geometry and Reactivity. *J. Am. Chem. Soc.*, *106*, 1594-1605, **1984**. DOI: https://doi.org/10.1021/ja00318a009.

[12] R. F. W. Bader, R. J. Gillespie, and P. J. Macdougall, A Physical Basis for the VSEPR Model of Molecular geometry. *J. Am. Chem. Soc.*, *110*, 7329-7336, **1988**. DOI: https://doi.org/10.1021/ja00230a009.

[13] A. Savin, R. Nesper, S. Wengert, and T. E. Fassler, ELF: The Electron Localization Function. *Angew. Chem. Int. Ed. Engl.*, *36*, 1808-1832, **1997**. DOI: https://doi.org/10.1002/anie.199718081.

[14] B. Silvi, The Spin-Pair Compositions as Local Indicators of the Nature of the Bonding. *J. Phys. Chem. A*, *107*, 3081-3085, **2003**. DOI: https://doi.org/10.1021/jp027284p.

[15] N. O. J. Malcolm and P. L. A. Popelier, The full topology of the Laplacian of the electron density: scrutinising a physical basis for the VSEPR model. *Faraday Discuss.*, *124*, **2003**. DOI: 10.1039/b211650m.

[16] A. Kumar, S. R. Gadre, N. Mohan, and C. H. Suresh, Lone pairs: an electrostatic viewpoint. *J. Phys. Chem. A*, *118*, 526-532, **2014**. DOI: https://doi.org/10.1021/jp4117003.

[17] P. C. Hiberty and B. Braïda, Pleading for a Dual Molecular-Orbital/Valence-Bond Culture. *Angew. Chem. Int. Ed. Engl.*, *57*, 5994-6018, **2017**. DOI: https://doi.org/10.1002/anie.201710094.

[18] R. J. Gillespie and E. A. Robinson, A Ligand Close Packing Model. *Adv. Mol. Struct. Res.*, *4*, 1-41, **1998**.

[19] R. J. Gillespie, Improving our understanding of molecular geometry and the VSEPR model through the ligand close-packing model and the analysis of electron density distributions. *Coord. Chem. Rev.*, *197*, 51-69, **2000**. DOI: https://doi.org/10.1016/S0010-8545(99)00199-X.

[20] L. S. Bartell, A structural chemist's entanglement with Gillespie's theories of molecular geometry. *Coord. Chem. Rev.*, *197*, 37-49, **2000**. DOI: https://doi.org/10.1016/S0010-8545(99)00233-7.

[21] E. A. Robinson and R. J. Gillespie, Ligand Close Packing and the Geometry of the Fluorides of the Nonmetals of Periods 3, 4, and 5. *Inorg. Chem.*, *42*, 3865−3872, **2003**. DOI: https://doi.org/10.1021/ic030024h.

[22] E. A. Robinson, S. A. Johnson, T.-H. Tang, and R. J. Gillespie, Reinterpretation of the Lengths of Bonds to Fluorine in Terms of an Almost Ionic Model. *Inorg. Chem.*, *36*, 3022-3030, **1997**. DOI: https://doi.org/10.1021/ic961315b.

[23] A. Martín Pendás, E. Francisco, and M. A. Blanco, Electron–electron interactions between ELF basins. *Chem. Phys. Lett.*, *454*, 396-403, **2008**. DOI: https://doi.org/10.1016/j.cplett.2008.02.029.

[24] R. F. W. Bader, Definition of Molecular Structure: By Choice or by Appeal to Observation? *J. Phys. Chem. A*, *114*, 7431–7444, **2010**. DOI: https://doi.org/10.1021/jp102748b.

[25] M. Rahm and K. O. Christe, Quantifying the nature of lone pair domains. *Chem. Phys. Chem.*, *14*, 3714-3725, **2013**. DOI: https://doi.org/10.1002/cphc.201300723.

[26] J. Andres, S. Berski, and B. Silvi, Curly arrows meet electron density transfers in chemical reaction mechanisms: from electron localization function (ELF) analysis to valence-shell electron-pair repulsion (VSEPR) inspired interpretation. *Chem. Commun.*, *52*, 8183-8195, **2016**. DOI: 10.1039/c5cc09816e.

[27] D. B. Chesnut, An Electron Localization Function Study of the Lone Pair. *J. Phys. Chem. A*, *104*, 11644-11650, **2000**. DOI: https://doi.org/10.1021/jp002957u.

[28] A. J. Proud, B. J. H. Sheppard, and J. K. Pearson, Revealing Electron-Electron Interactions within Lewis Pairs in Chemical Systems. *J. Am. Chem. Soc.*, *140*, 219-228, **2018**. DOI: https://doi.org/10.1021/jacs.7b08935.

[29] L. S. Bartell, A personal reminiscence about theories used and misused in structural chemistry. *Struct. Chem.*, *22*, 247–251, **2011**. DOI: https://doi.org/10.1007/s11224-010-9693-8.

[30] H. H. Osman, M. A. Salvadó, P. Pertierra, J. Engelkemier, D. C. Fredrickson, and J. M. Recio, Chemical Pressure Maps of Molecules and Materials: Merging the Visual and Physical in Bonding Analysis. *J. Chem. Theory Comput.*, *14*, 104-114, **2018**. DOI: https://doi.org/10.1021/acs.jctc.7b00943.

[31] H. H. Osman, J. Andrés, M. A. Salvadó, and J. M. Recio, Chemical Bond Formation and Rupture Processes: An Application of DFT–Chemical Pressure Approach. *J. Phys. Chem. C*, *122*, 21216-21225, **2018**. DOI: https://doi.org/10.1021/acs.jpcc.8b06947.

[32] D. C. Fredrickson, Electronic Packing Frustration in Complex Intermetallic Structures: The Role of Chemical Pressure in Ca_2Ag_7. *J. Am. Chem. Soc.*, *133*, 10070–10073, **2011**. DOI: https://doi.org/10.1021/ja203944a.

[33] K. P. Hilleke and D. C. Fredrickson, Discerning Chemical Pressure amidst Weak Potentials: Vibrational Modes and Dumbbell/Atom Substitution in Intermetallic Aluminides. *J. Phys. Chem. A*, *122*, 8412−8426, **2018**. DOI: https://doi.org/10.1021/acs.jpca.8b07419.

[34] G. W. T. M. J. Frisch, H. B. Schlegel, G. E. Scuseria, M. A. Robb, J. R. Cheeseman, G. Scalmani, V. Barone, G. A. Petersson, H. Nakatsuji, X. Li, M. Caricato, A. Marenich, J. Bloino, B. G. Janesko, R. Gomperts, B. Mennucci, H. P. Hratchian, J. V. Ortiz, A. F. Izmaylov, J. L. Sonnenberg, D. Williams-Young, F. Ding, F. Lipparini, F. Egidi, J. Goings, B. Peng, A. Petrone, T. Henderson, D. Ranasinghe, V. G. Zakrzewski, J. Gao, N. Rega, G. Zheng, W. Liang, M. Hada, M. Ehara, K. Toyota, R. Fukuda, J. Hasegawa, M. Ishida, T. Nakajima, Y. Honda, O. Kitao, H. Nakai, T. Vreven, K. Throssell, J. A. Montgomery, Jr., J. E. Peralta, F. Ogliaro, M. Bearpark, J. J. Heyd, E. Brothers, K. N. Kudin, V. N. Staroverov, T. Keith, R. Kobayashi, J. Normand, K. Raghavachari, A. Rendell, J. C. Burant, S. S. Iyengar, J. Tomasi, M. Cossi, J. M. Millam, M. Klene, C. Adamo, R. Cammi, J. W. Ochterski, R. L. Martin, K. Morokuma, O. Farkas, J. B. Foresman, and D. J. Fox, *Gaussian 09*, I. Gaussian, Wallingford CT, 2016

[35] F. J. X. Gonze, F. Abreu Araujo, D. Adams, B. Amadon,, C. A. T. Applencourt, J. M. Beuken, J. Bieder,, E. B. A. Bokhanchuk, F. Bruneval, D. Caliste,, F. D. M. Coˆ Te´, F. Da Pieve, M. Delaveau, M. Di Ennaro,, C. E. B. Dorado, G. Geneste, L. Genovese, A. Gerossier,, Y. G. M. Giantomassi, D. R. Hamann, L. He, G. Jomard,, S. L. R. J. Laflamme Janssen, A. Levitt, A. Lherbier, F. Liu,, A. M. I. Lukacˇ Evic´, C. Martins, M. J. T. Oliveira, S. Ponce´,, T. R. Y. Pouillon, G. M. Rignanese, A. H. Romero,, O. R. B. Rousseau, A. A. Shukri,M. Stankovski, M. Torrent,, B. V. T. M. J. Van Setten, J. M. Verstraete, D. Waroquiers,, and B. X. J. Wiktor, A. Zhou and J. W. Zwanziger, Recent developments in the ABINIT software package. *Comput. Phys. Commun.*, *205*, 106-131, **2016**. DOI: https://doi.org/10.1016/j.cpc.2016.04.003.

[36] B. A. X. Gonze, P. M. Anglade, J. M. Beuken, F. Bottin,, F. B. P. Boulanger, D. Caliste, R. Caracas, M. Coˆ Te´,, L. G. T. Deutsch, P. Ghosez, M. Giantomassi,, D. R. H. S. Goedecker, P. Hermet, F. Jollet, G. Jomard,, M. M. S. Leroux, S. Mazevet, M. J. T. Oliveira, G. Onida,, T. R. Y. Pouillon, G.M. Rignanese, D. Sangalli, R. Shaltaf,, and J. M. V. M. Torrent, G. Zerah and J. W. Wanziger,, ABINIT: First-principles approach to material and nanosystem properties. *Comput. Phys. Commun.*, *180*, 2582-2615, **2009**. DOI: https://doi.org/10.1016/j.cpc.2009.07.007.

[37] S. G. C. Hartwigsen, And J. Hutter, Relativistic separable dual-space Gaussian pseudopotentials from H to Rn. *Phys. Rev. B*, *58*, 3641-3662, **1998**. DOI: https://doi.org/10.1103/PhysRevB.58.3641.

[38] V. M. Berns, J. Engelkemier, Y. Guo, B. J. Kilduff, and D. C. Fredrickson, Progress in Visualizing Atomic Size Effects with DFT-Chemical Pressure Analysis: From Isolated Atoms to Trends in AB5 Intermetallics. *J. Chem. Theory Comput.*, *10*, 3380-3392, **2014**. DOI: https://doi.org/10.1021/ct500246b.

[39] K. M. a. F. Izumi, VESTA 3 for three-dimensional visualization of crystal, volumetric and morphology data. *J. Appl. Cryst.*, *44*, 1272-1276, **2011**. DOI: https://doi.org/10.1107/S0021889811038970.

[40] V.-A. Glezakou, S. T. Elbert, S. S. Xantheas, and K. Ruedenberg, Analysis of Bonding Patterns in the Valence Isoelectronic Series O3,S3,SO2, and OS2 in Terms of Oriented Quasi-Atomic Molecular Orbitals†. *J. Phys. Chem. A*, *114*, 8923–8931, **2010**. DOI: https://doi.org/10.1021/jp105025d.

[41] S. Noury, B. Silvi, and R. J. Gillespie, Chemical Bonding in Hypervalent Molecules: Is the Octet Rule Relevant? *41*, 2164−2172, **2002**. DOI: https://doi.org/10.1021/ic011003v.

[42] J. W. Linnett, *The Electronic Structure of Molecules*, Wiley, New York, **1964**.

[43] J. S. M. Anderson, P. W. Ayers, and J. I. R. Hernandez, How Ambiguous Is the Local Kinetic Energy? *J. Phys. Chem. A*, *114*, 8884–8895, **2010**. DOI: https://doi.org/10.1021/jp1029745.

[44] F. R. Wagner, V. Bezugly, M. Kohout, and Y. Grin, Charge decomposition analysis of the electron localizability indicator: a bridge between the orbital and direct space representation of the chemical bond. *Chem. Eur. J.*, *13*, 5724-5741, **2007**. DOI: https://doi.org/10.1002/chem.200700013.

[45] J. Tao, S. Liu, F. Zheng, and A. M. Rappe, Quantum pressure and chemical bonding: Influence of magnetic fields on electron localization. *Phys. Rev. B*, *92*, 060401-060405, **2015**. DOI: https://doi.org/10.1103/PhysRevB.92.060401.

[46] P. K. Chattaraj, H. Lee, and R. G. Parr, HSAB Principle. *J. Am. Chem. Soc.*, *113*, 1855-1856, **1991**. DOI: https://doi.org/10.1021/ja00005a073.

[47] P. Sjoberg and P. Politzer, Use of the Electrostatic Potential at the Molecular Surface To Interpret and Predict Nucleophilic Processes. *J. Phys. Chem.*, *94*, 3959-3961, **1990**. DOI: https://doi.org/10.1021/j100373a017.

[48] P. Politzer and D. G. Truhlar, Chemical Application of Atomic and Molecular Electrostatic Potential, Springer, New York, **1981**.

[49] C. A. Naieway and M. E. Schwartz, Consideration of the VSEPR Model by a Localized Molecular Orbital Study of the Geometry of H_2O. *J. Am. Chem. Soc.*, *95*, 8235-8241, **1973**. DOI: https://doi.org/10.1021/ja00806a005.

[50] L. T. Xu, T. Y. Takeshita, and T. H. Dunning, Why edge inversion? Theoretical characterization of the bonding in the transition states for inversion in F n NH(3−n) and FnPH(3−n) (n=0–3). *Theoretical Chemistry Accounts*, *133*, **2014**. DOI: https://doi.org/10.1007/s00214-014-1493-6.

Supplementary Material Chapter 5

Computational details of studied molecules

Table S5.1: Calculation details and geometrical parameters of the molecules studied.

Molecule	ecut (ha)	k-points	nfft grid	Bond Length (Å)	Bond Angle (deg)
H_2O	270	1x1x1	288x288x288	d(O-H) = 0.97120	α(H-O-H) = 104.92
NH_3	220	1x1x1	256x256x256	d(N-H) = 1.0217	α(H-N-H) = 107.26
NF_3	300	1x1x1	300x300x300	d(N-F) =1.37301	α(F-N-F) = 101.70
NF_3	300	1x1x1	300x300x300	d(N-F) =1.37301	α(F-N-F) = 101.70
AsH_3	280	1x1x1	288x288x288	d(As-H) =1.52132	α(H-As-H) =90.62
PH_3	240	1x1x1	270x270x270	d(P-H) =1.42719	α(H-P-H) = 91.83
PF_3	290	1x1x1	300x300x300	d(P-F) =1.56403	α(F-P-F) = 97.44
PCl_3	270	1x1x1	290x290x290	d(P-Cl) =2.03959	α(Cl-P-Cl) = 100.36
SO_2	260	1x1x1	288x288x288	d(S-O) = 1.4281	α(O-S-O) = 119.54
SF_4	280	1x1x1	290x290x290	$d(S\text{-}F)_{ax}$ =1.6482 $d(S\text{-}F)_{eq}$ =1.5541	$\alpha(F\text{-}S\text{-}F)_{ax}$ = 173.07 $\alpha(F\text{-}S\text{-}F)_{eq}$ = 100.61
ClF_3	360	1x1x1	324x324x324	$d(Cl\text{-}F)_{ax}$ =1.6921 $d(Cl\text{-}F)_{eq}$ =1.6026	$\alpha(F\text{-}Cl\text{-}F)_{ax}$ = 176.9 $\alpha(F\text{-}Cl\text{-}F)_{eq}$ = 88.19
XeF_2	380	1x1x1	340x340x340	d(Xe-F) = 2.0084	α(F-Xe-F) = 179.99
BeH_2	290	1x1x1	290x290x290	d(Be-H) = 1.3167	α(H-Be-H) = 179.99

Molecule	ecut (ha)	k-points	nfft grid	Bond Length (Å)	Bond Angle (deg)
BeH_2	290	1x1x1	290x290x290	d(Be-H) = 1.3167	α(H-Be-H) = 179.99
BH_3	280	1x1x1	280x280x280	d(B-H) = 1.1983	α(H-B-H) = 120.00
BF_3	320	1x1x1	320x320x320	d(B-F) =1.3104	α(F-B-F) = 119.99
Ethylene	300	1x1x1	300x300x300	d(C-C) =1.3309 d(C-H) =1.0852	α(H-C-H) = 119.49

Chemical Pressure distribution in BH_3 Molecule

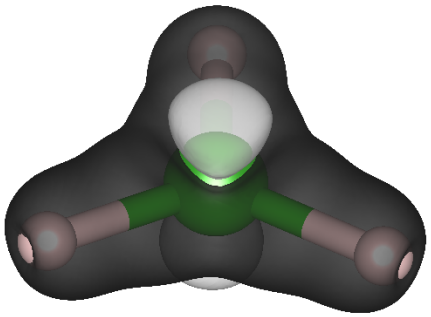

Figure S5.1. 3D isosurfaces of chemical pressure (CP) distributions within the BH_3 molecule. Isosurface values: CP=+0.013 (white) and –0.013 (black). Green and white spheres indicate boron and hydrogen atoms, respectively.

Chemical Pressure distribution in BF_3 Molecule

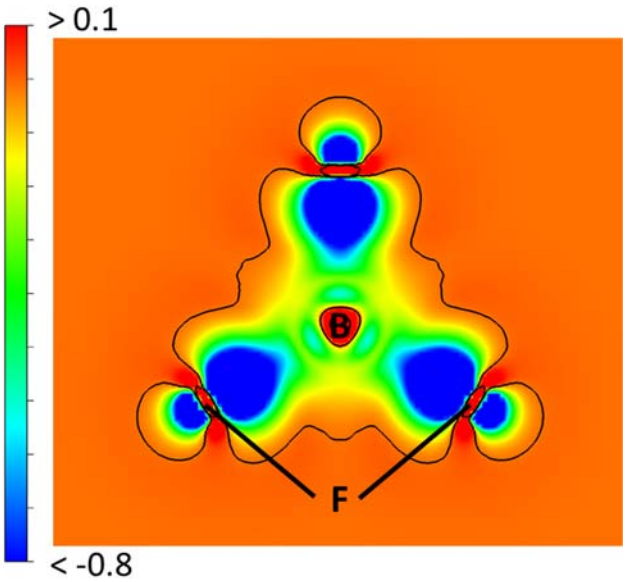

Figure S5.2. Chemical pressure heat-maps of the BF_3 molecule along the molecular plane. Black curves: CP = 0 contour.

Chapter 6

Generalized Stress-Redox Equivalence: A Chemical Link between Pressure and Electronegativity in Inorganic Crystals

A. Lobato, H. H. Osman, M. A. Salvado, P. Pertierra, Á. Vegas, V. G. Baonza and J. M. Recio

The crystal structure of many inorganic compounds can be understood as a metallic matrix playing the role of a host lattice in which the nonmetallic atomic constituents are located, the Anions in Metallic Matrices (AMM) model stated. The power and utility of this model lie in its capacity to anticipate the actual positions of the guest atoms in inorganic crystals using only the information known from the metal lattice structure. As a pertinent test-bed for the AMM model, we choose a set of common metallic phases along with other nonconventional or more complex structures (face-centered cubic (fcc) and simple cubic Ca, CsCl-type BaSn, hP4-K, and fcc-Na) and perform density functional theory electronic structure calculations. Our topological analysis of the chemical pressure (CP) scalar field, easily derived from these standard first-principles electronic computations, reveals that CP minima appear just at the precise positions of the nonmetallic elements in typical inorganic crystals presenting the above metallic subarrays: CaF2, rock-salt and CsCl-type phases of CaX (X = O, S, Se, Te), BaSnO3, K2S, and NaX (X = F, Cl, Br, I). A theoretical basis for this correlation is provided by exploring

the equivalence between hydrostatic pressure and the oxidation (or reduction) effect induced by the nonmetallic element on the metal structure. Indeed, our CP analysis leads us to propose a generalized stress-redox equivalence that is able to account for the two main observed phenomena in solid inorganic compounds upon crystal formation: (i) the expansion or contraction experienced by the metal structure after hosting the nonmetallic element while its topology is maintained and (ii) the increasing or decreasing of the effective charge associated with the anions in inorganic compounds with respect to the charge already present in the interstices of the metal network. We demonstrate that a rational explanation of this rich behavior is provided by means of Pearson-Parr's electronegativity equalization principle.

Inorg. Chem. DOI: https://doi.org/10.1021/acs.inorgchem.9b01470

Introduction

The literature on the theories and formalisms describing chemical bonding in inorganic crystal structures is very extensive,[1-6] and the models can typically be classified into either classical or quantum types. Among them, the approach of Pauling has been the paradigm for describing and rationalizing the crystal structures of ionic compounds over the last century [1,7,8]. The limitations of the ionic model, which have also led to a number of misconceptions about the crystal structure and the bonding network, were discussed by O'Keeffe and Hyde using alternative approaches [9,10]. These authors put the emphasis on the description of the structures of oxides as oxygen-stuffed alloys, since their cationic sublattices adopt the structures of either elements or simple alloys. Interestingly, this concept can also be applied to the naked metallic structure if the valence electrons localized in the empty spaces of the structure are conceived as coreless pseudoanions. In fact, the term electride was introduced after an extensive quantum-mechanical treatment of a high-pressure modification of metallic cesium that led to denote this phase as $Cs^{+}e^{-}$ [11]. Prior to these calculations, Schubert already proposed that the valence electrons might be well-located at the voids of the metals/alloys structures [12]. This idea was also applied by Vegas et al. in a more recent work[13].

The consideration of the metallic matrix of a compound as a host lattice for nonmetallic atoms was indeed formalized later by Vegas et al. [14,15] in the so-called anions in metallic matrices (AMM) model. According to the AMM model, the electronic structure and the atomic arrangement of the metallic sublattice induce the equilibrium positions of the nonmetallic atoms in the crystal. This idea culminated a wide variety of studies that take into account not only a dense packing of atoms, as in metals and/or alloys, but also more open metal skeletons such as those present in AlX_3 structures (X = F, Cl, OH)[15]. The AMM model found support from several theoretical calculations in a variety of systems including the AlX_3 crystals, boron phosphide in the zinc blende phase, and high-pressure phases of Na and K, to cite a few [16-18]. Topological analyses of the electron density of these structures reveal that the valence electrons of the metal are found to be localized in interstitial positions, where anions are found in inorganic compounds, or close to the sites of bonding and lone electron pairs. These electronic domains were named pseudoanions and preceded the concept of Interstitial Quantum-Atoms later introduced by Miao and Hoffmann [19,20]. In other examples (face centered

cubic (fcc) and simple cubic (sc) phases of Ca), the topology of the electron localization function (ELF) was also evaluated to reveal the correlation between the interstitial positions of ELF attractors in the corresponding unit cells and the positions of the oxygen atoms in the rock-salt and CsCl-type phases of CaO [21]. The same result is obtained when the ELF topology in the high-pressure CsCl-type phase of BaSn alloy is evaluated to anticipate the preferential positions of oxygen in the perovskite $BaSnO_3$. 21 In all these cases, the topological evidence appears and/or is enhanced when the metal is explored in the actual strained configuration presented at the equilibrium structure of the inorganic crystal. The enhanced effect induced by the nonmetallic atom is an inherent feature of the AMM model that corresponds to the concept of pressure-oxidation equivalence and requires further exploration[22].

This equivalence between chemical oxidation and external macroscopic pressure was proposed by Martínez-Cruz et al. [23] and more exhaustively illustrated for a large set of compounds by Vegas and Jansen [14,23]. Cations are not independent chemical entities filling voids in the corresponding anionic subarrays as usually described by the ionic model. They are instead arranged keeping the same lattice structure as in the isolated metals but showing strained unit cells induced by the embedding of nonmetallic atoms. If the effect of the nonmetallic atom is strong enough, the metallic sublattice in the inorganic crystal may display a structure not stable at its equilibrium conditions but another one among those present in the metal/alloy phase diagram. To cite a couple of examples that will be analyzed later in this work, the potassium sublattice in K_2S is the hP_4 phase found in metallic K at very high pressure,[18] and BaSn alloy in $BaSnO_3$ presents the high pressure CsCl-type structure to which the CaSi-type zero pressure structure transforms. The physical principle or explanation behind this behavior has not been reported, to the best of our knowledge.

Recently, a simple implementation of the quantum–mechanical stress density formalism has been developed, [24-28] the chemical pressure (CP) approach [29]. This new scheme provides bonding patterns in which the various types of interatomic interactions (ionic, covalent, metallic, H-bond, dispersion) are clearly differentiated [30] and can also be used to track the bond formation and rupture processes in crystalline solids [31]. The CP method is now widely applied for analyzing the atomic size effects and the corresponding interactions with the surrounding atoms in the solid state [32-35]. For our purposes, the exploration of two-dimensional (2D) and three-dimensional (3D)

CP maps in metals and inorganic crystals is especially convenient, since those regions in the maps with low chemical pressure are identified with unit cell positions showing a preference for electron density accumulation. In addition, since the CP field is not a scaled property (as it happens, e.g., with the ELF), variations of CP values either induced by hydrostatic pressure or by the presence of other chemical elements provide useful information about the observed correlation between these two effects that deserves further investigation.

In this Article, our first goal is to examine whether or not the CP formalism supports the AMM model. To this end we choose a research test bed involving metal structures of different complexity as the fcc- and sc-Ca, CsCl-type BaSn, hP4-K, and fcc-Na lattices. Once the assessment of the AMM model is verified, our next focus will be to explain why the positions of the anions in a given inorganic crystal can be anticipated just resorting to its subjacent metallic sublattice. Plausible answers associate these positions to particular topological features in the electron density, the ELF, or the CP maps of the metallic structures. However, our challenge here is to find an underlying justification to account for both the positive and negative strains experienced by the metallic sublattices as a result of the effect induced by the nonmetallic guest elements. We show that atomic sizes do not necessarily account for the observed distortions and that a more profound explanation in terms of the host and guest capacity to attract/donate electron density is needed. The goal will be accomplished after proposing a generalized stress-redox equivalence, which is further supported by Pearson-Parr's electronegativity equalization principle [36-38]. In essence, by modifying the size of the metallic lattice, the charge located at the interstice positions changes in a way that correlates with the electronegativity of the nonmetallic element occupying those positions. This reasoning will be illustrated using density functional theory (DFT) CP results on the metallic lattices collected above and on a number of halide and chalcogenide inorganic crystals containing these metallic arrays.

The Article is divided into four more sections plus a supplementary material 6. Computational details of the electronic structure calculations and the CP approach are presented in the following section. In Section 3, the AMM model is checked in the light of the DFT-CP approach using a number of metal (alloy)/inorganic crystal couples. Section 4 contains the results of the new generalized stress-redox correlation with a discussion guided by the electronegativity equalization principle. The Paper ends with a summary of our findings and the most relevant conclusions of our study. In the

Supplementary Material 6, we included some technical details about the calculations together with the CP analysis of fcc- and sc-Mg and the electronegativity-CP correlations for fcc-Mg and fcc-Na. A brief description of the unit cell of the structures discussed in the main text is also provided.

Computational Details

DFT-chemical pressure calculations were performed on the pair systems Ca/CaO, BaSn/$BaSnO_3$, K/K_2S, and Na/NaX (X = F, Cl, Br). The local density approximation (LDA) exchange-correlation functional of Goedecker, Teter, and Hutter [39] and Hartwigsen-Goedecker-Hutter norm-conserving pseudopotentials [40] were used under the formalism of DFT as implemented in the ABINIT software package [41-43]. The semicore electrons of all the metals were included in the calculations. The geometrical optimization of the unit cells was performed with the Broyden-Fletcher-Goldfarb-Shanno minimization algorithm. Further details regarding cutoff energies and Monkhorst−Pack k-point [44] grids are collected in the Supplementary Material 6.

In the Chemical Pressure formalism, the total DFT energy of the system is expressed as an integral all over the space of the energy density (ρ_{Energy}):

$$E_{DFT} = \int \rho_{Energy}\, d\tau \tag{6.1}$$

In analogy to the thermodynamic macroscopic pressure, a microscopic chemical pressure (p_{Voxel}) is defined as the derivative of the local energy with respect to a volume voxel V_{Voxel}, where the local energy ε_{Voxel} is calculated in each of the small parallelepipeds (voxels) in which the 3D space is divided:

$$p_{Voxel} = -\frac{\partial \varepsilon_{Voxel}}{\partial V_{Voxel}} \tag{6.2}$$

To perform such a derivative, we adopt the procedure proposed by Fredrickson in which the energy density (ρ_{Energy}) is calculated in the real space, and then we perform numerically the derivative with respect to the volume. Further details are given elsewhere [32-35,45]. To apply the same scheme to all the systems reported in this work, three single-point calculations were always performed over a volume change of 0.5% around the corresponding equilibrium unit cell volumes using the Fredrickson group CP package [29]. In all the cases, the core unwarping method was used to reduce the strong features around the cores as explained in our previous works [29,35].

The above computational details define the standard DFTCP scheme followed in previous papers (see, e.g., refs [30] and [45] and refs therein). Nonetheless, we checked that differences are not meaningful when CP maps obtained with the standard procedure followed in this paper are compared with those obtained from generalized gradient approximation (GGA) calculations (computational details and maps are collected in the Supplementary Material 6). The CP maps were then rendered using the VESTA program [46]. Pressure values are given throughout the manuscript in atomic units unless otherwise specified (1 au = 29421 GPa). Bader atomic charges [47] and electron density integrations in the positive pressure regions enclosed by CP = 0 contour isosurfaces were performed using Critic2 code [48] with the Yu−Trinkle integration method [49].

Assessment of the anions in metallic matrices model

The basic premise of the AMM model states that the metallic arrangement and its electronic structure reveal the specific positions of the anions in the corresponding inorganic crystals [50]. In this section, we aim to illustrate whether the CP formalism is able or not to support the basis of the AMM model. Bearing in mind this idea, we selected several common metallic phases along with other nonconventional or more complex structures (fcc and sc-Ca, CsCl-BaSn, hP_4-K, and fcc-Na), where nonmetallic elements such as chalcogenides and halides form typical inorganic crystals as CaF_2, CaX (X = O, S, Se, Te), $BaSnO_3$, K_2S, and NaX (X = F, Cl, Br, I). This selection constitutes a large enough number of examples going from stable zero pressure to high pressure phases, displaying different guest positions and allowing us to finally address the linking between the effect of mechanical pressure and chemical oxidation.

Let us start describing the main features emerging from the application of the CP formalism to the fcc structure of Ca. This is the stable phase of Ca at zero pressure and low temperature with a lattice parameter of a = 5.588 Å. Figure 6.1a shows the 2D CP map of the fcc-Ca unit cell in which intense positive CP features (red) around the nucleus reflect the semicore [$3s^2 3p^6$] electrons of the Ca atom. This positive CP gradually and radially decreases as we move from the nuclear position toward the neighboring atoms through a plateau region of negative CP (blue). In addition, each atomic position is surrounded by a contour line (black) of zero chemical pressure, which turns to be of a spherical shape in the 3D space and contains the atomic nucleus and the core

electron pressure of the metallic atom. Such CP features are common to all results hereafter. This is in concordance with the so-called free electron model of metals [51,52]. According to the CP formalism, [30] positive values indicate that, in these regions, a decrease of the volume will increase the energy. Therefore, they are associated with repulsive regions, where the electron density tends to expand. In contrast, the negative CP background, representing the delocalized sea of valence electrons, is associated with the cohesion of the nuclei, because in these regions the electron density looks for a reduction of volume to decrease its energy as dictated by eq 6.2.

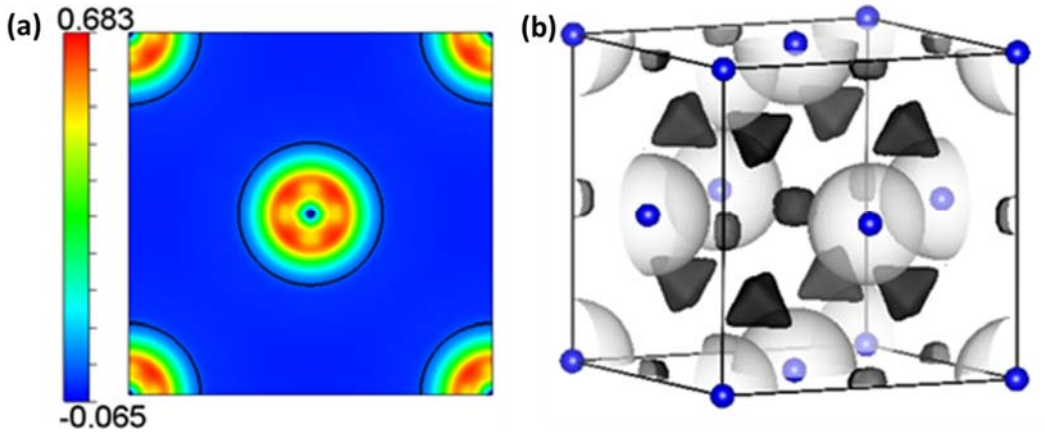

Figure 6.1. CP analysis of fcc-Ca at equilibrium conditions. (a) Cross section along the (001) plane containing the Ca atoms. The CP = 0 contour is shown with a black solid line. (b) 3D isosurfaces with CP= +0.001 (white) and CP = −0.0274 (black). Pressures are given in atomic units.

However, a closer analysis of the negative background reveals inhomogeneities in the local CP distribution that are crucial to validate the AMM model, as we will show in the ongoing discussion. By selecting appropriate negative and positive values, with the purpose of representing regions enclosing CP minima and maxima, the 3D CP plot of fcc-Ca can be constructed (see Figure 6.1b). Two nonequivalent isosurfaces of negative (black) pressures clearly appears in the unit cell. One of those negative CP isosurfaces is located at the tetrahedral 8c sites (1, 1, 1), with a CP value of −0.0278 au, whereas the other appears at the 4b positions with a value of −0.0275 au. In agreement with the AMM model, these are exactly the coordinates where fluoride atoms in the archetypical fluorite structure and chalcogenide elements in the rock-salt structure are situated, respectively.

Indeed, equivalent features have been observed by the ELF analysis in fcc-Ca [21]. In their paper, Vegas and Mattessini revealed the presence of an ELF

attractor at the (1/2, 1/2, 1/2) position, whereas in the case of the (1, 1, 1) position the situation was not so evident. In this regard, the CP formalism provides a neat picture for the potential guest positions in the fcc-Ca lattice. But what we would like to emphasize here is that the CP approach offers an extra insight about these preferential positions in the lattice informing when an accumulation of the electron density available for the anion formation is favored. For example, when pressure is applied to the fcc-Ca phase to achieve its volume in the rock-salt phase of CaO, the CP minima at the 8c and 4b positions decreases to −0.0422 and −0.0424 au, respectively. Such a decrease in the CP minima values can be attributed to an increase in the electron density accumulated through the interstitial positions. Although this feature will be discussed later, we want to remark that this behavior is a general result for the metallic phases and has a strong correlation with the rationalization of inorganic structures in the light of the AMM model.

To continue with the link between the CP formalism and the privileged positions for the anions in the metallic matrices, we applied the previous strategy to the simple cubic sc-Ca phase. This is one of the high-pressure phases found in the polymorphic sequence of metallic Ca (see, e.g., ref [53] for a thorough study of the experimental phase diagram of Ca).

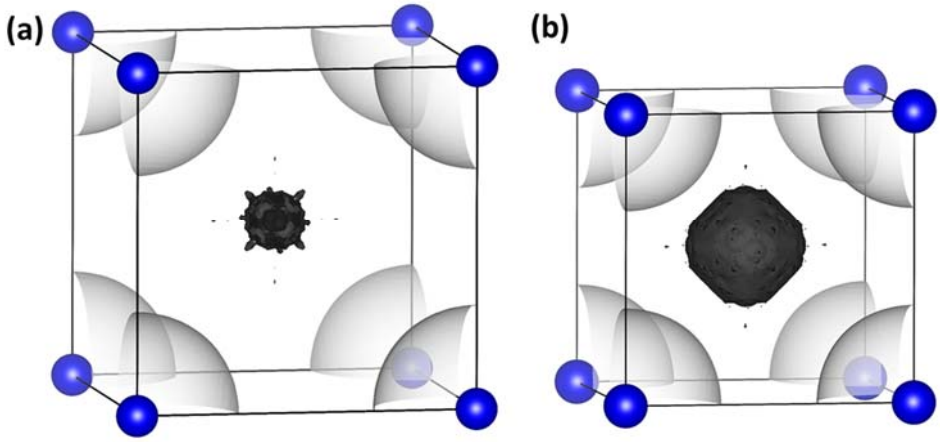

Figure 6.2. 3D CP isosurfaces of sc-Ca crystal at (a) the equilibrium volume with CP = +0.001 (white) and CP = −0.032 (black) and (b) the volume of the CsCl-CaO crystal with CP = +0.001 (white) and CP = −0.066 (black). Pressures are given in atomic units.

Indeed, the more open sc phase displays a valence band with a greater d-band character than the low-pressure structures, as discussed by Errandonea et al [54]. and Rahm et al [55]. Therefore, this is an excellent example to test if the proposed methodology can support the AMM model in a different scenario.

At 39 GPa, sc-Ca presents a lattice parameter of 2.62 Å. In this structure, only one CP minimum appears in the unit cell at (1/2, 1/2, 1/2) suggesting this preferential position for the nonmetallic element. In fact, in the high-pressure CsCl phases of CaX (X = O, S, Se, Te) crystals, X^{2-} anions are situated at this same precise position identified by the CP formalism (see Figure 6.2).

Once we have considered simple examples of a pure metal, let us explore how the CP analysis performs in the binary BaSn alloy. At high pressure, BaSn transforms from the CaSi-type to the CsCl-type structure [56], which can be considered as the metallic skeleton of the well-known $BaSnO_3$ perovskite. Successfully, the 3D CP isosurfaces of the CsCl-type structure of BaSn, calculated at the equilibrium volume of the perovskite BaSnO3 phase (a = 4.1168 Å), display six regions enclosing CP minima at the centers of the faces of the cubic cell forming an octahedral environment around the Sn atom (see Figure 6.3). The positions of these localized regions of negative CP coincide with the coordinates where O atoms are located in the perovskite structure of $BaSnO_3$ in concordance also with the ELF topological analysis of Vegas and Mattesini [21].

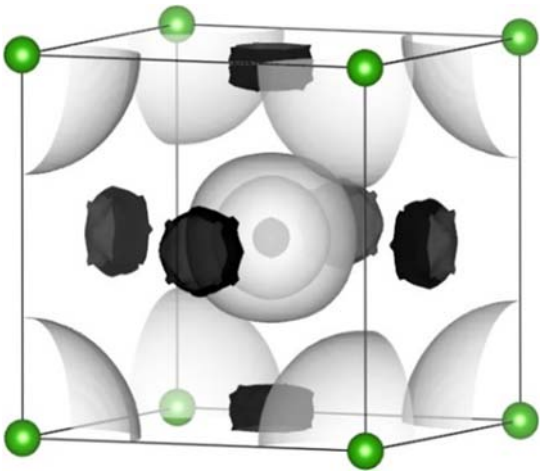

Figure 6.3. 3D CP isosurfaces of BaSn lattice (Ba = green, Sn = blue) at the equilibrium volume of $BaSnO_3$. White and black isosurfaces are of CP = +0.001 and CP = −0.0125 au, respectively.

In the same way, metallic K adopts an hP_4 phase at very high pressure analogous to the K-substructure of the Ni_2In type phase of K_2S obtained under pressure[57]. This K phase has been extensively studied, since Marques et al. [18] demonstrated that the topologies of the electron density and the ELF show local attractors at the unoccupied 2d (1/3, 2/3, 3/4) positions leading

to the consideration of this K phase as an electride. Showing the preference for these positions by means of the CP analysis is challenging given the low symmetry and the extreme conditions needed for the stabilization of this structure. Our CP results of the hP4-K phase show negative CP regions centered at the same positions where electrons in the electride and anions in the Ni_2In-type structures of several dialkali-metal monochalcogenides such as Na_2S, Rb_2Te and K_2SO_4 are found (see Figure 6.4).

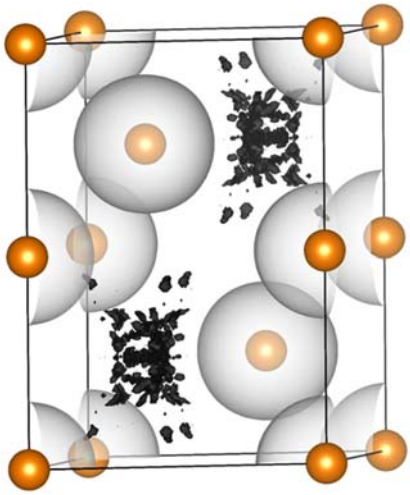

Figure 6.4. 3D CP isosurfaces in the hP4 phase of metallic K at the volume of K_2S compound. White and black isosurfaces are of CP = +0.001 and CP = −0.043 au, respectively.

We now turn to the fcc structure of Na to complete our CP analysis of metallic lattices. Although body-centered cubic (bcc) Na is the stable phase at room conditions, the fcc structure is the one present in the low-pressure rock-salt phases of NaX crystals (X = F, Cl, Br). Our expectation from the CP analysis of these fcc-Na lattices at the different equilibrium dimensions of the corresponding halides would be at least the presence of negative CP regions at the 4b (1/2, 1/2, 1/2) positions, since these are the coordinates of the X halides in their rock-salt phase. In fact, these positions clearly appear in the 3D CP representations shown in Figure 6.5. In addition, as in the first example discussed in this section (fcc-Ca), eight minima also appear at the (1/4,1/4,1/4) coordinates. We propose that these positions are potential sites for a hypothetical anion, although the stoichiometry requires a fractional negative charge of $-0.5e^-$ given the multiplicity of this position. Nevertheless, evidence of the preference of electrophilic entities for this position are provided when examining the minimum energy diffusion path of negative defects, which go through this position [58,59]. It is interesting to notice that the same

qualitative view is obtained regardless of the dimensions of the unit cell. The global analysis of the CP maps of the metallic sublattices of NaF, NaCl, and NaBr gives the following values for the black isosurfaces located at the expected 4b (1/2, 1/2, 1/2) positions of the anions: −0.0443, −0.0212, and −0.0172 au for NaF (2.31 Å), NaCl (2.56 Å), and NaBr (2.64 Å), respectively, while the CP minima at the 8c sites (1/4,1/ 4,1/4) are −0.0439, −0.0210, and −0.0170 au for the same latter crystals. Such a trend in the CP values points toward a relationship between the nature of the anion and the size of the metallic unit cell, supporting not only the AMM model but also pointing to the connection between oxidation and pressure that we will examine in the following section.

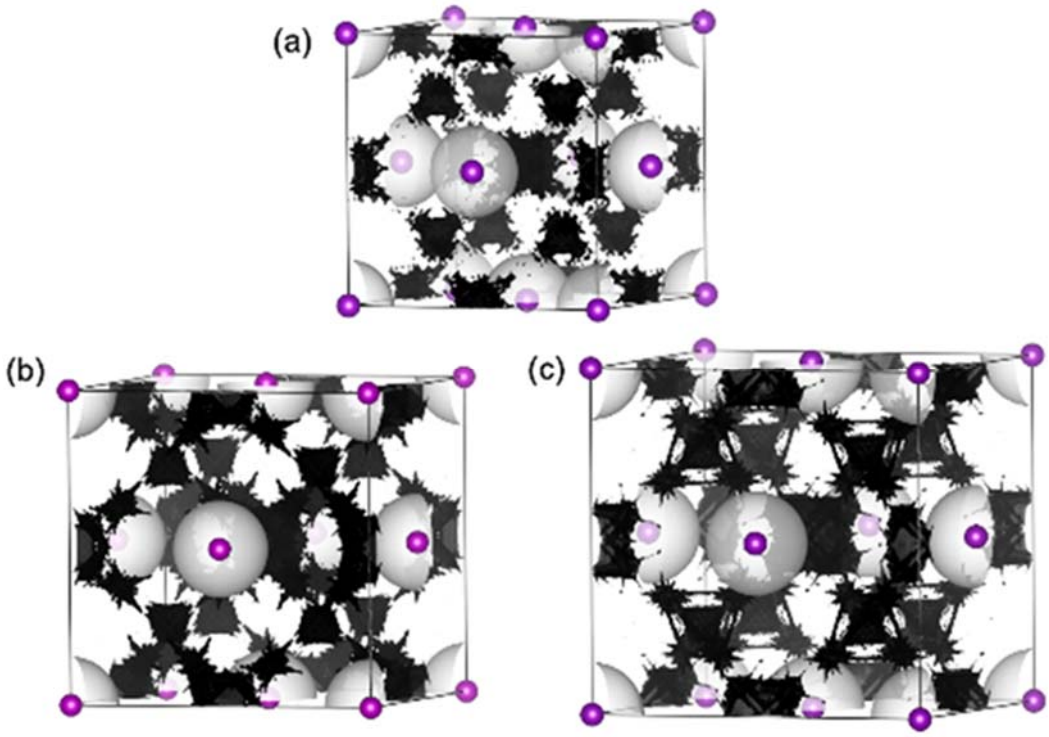

Figure 6.5. 3D CP analysis of the fcc-Na sublattices at the equilibrium volume of (a) NaF (CP = −0.044 au), (b) NaCl (CP = −0.021 au), and (c) NaBr (CP = −0.017 au). White isosurfaces are of CP = +0.001.

To sum up, through this section of the paper we carefully depicted the CP description of a number of metallic structures. Our results clearly demonstrate that CP minima reveal positions in the unit cell totally consistent with those that occupy nonmetallic elements in the inorganic compounds. Moreover, in addition to the ideas previously derived by the electron density and ELF analysis, CP provides a direct support to the AMM model in terms of

energetic considerations and electron density accumulations that will be disclosed in the next section.

The pressure-oxidation equivalence in the light of the chemical pressure formalism

4.1. Proving the Pressure-Oxidation Equivalence

Pressure-oxidation equivalence is based on empirical evidence showing that nonmetallic elements induce similar stress in the metallic sublattices where they are hosted as hydrostatic pressure does on the isolated metal structure [21]. As an example, the lattice parameter of fcc-Ca at 12 GPa is the same as the lattice parameter of the rock-salt CaO phase at zero pressure. Therefore, it can be understood that the effect of oxygen in the fcc-Ca sublattice of rock-salt CaO is equivalent to the mechanical compression shown by the metal structure at 12 GPa. If the pressure exerted by the nonmetal guest is high enough, the metal sublattice can eventually undergo a phase transition to a high-pressure structure, as in the case of the K_2S crystal previously discussed. Extending this view to cases where the metal sublattice is expanded would lead to consider the effect of the nonmetallic atom as that of a negative pressure.

To illustrate this apparent link between generalized stress and the redox state in a given structure under a broader perspective, we plot in Figure 6.6 the energy−volume equations of state of the fcc phases of Mg, Ca, and Sr metals emphasizing the pressures associated with the volumes of these lattices in the rock-salt phases of MgX, CaX, and SrX (X: O, S, Se, and Te) crystals. Our calculated values are in good agreement with the available experimental data of ref [53]. We assume that these pressures are induced in the metallic sublattices by the presence of the nonmetallic element. Whereas oxides are always in the repulsive part of the metal potential energy curves, thus indicating that the anion induces a compressive stress in the lattice, sulfides, selenides, and tellurides are always in the attractive regime, and therefore this fact could be viewed in these cases as a negative tensile stress (expansion) on the metallic lattice. Moreover, the expansion and contraction strains induced by the nonmetal guests seem to affect the different metallic lattices in an opposite direction. If we consider the oxygen anion, we can see how the compression effect increases from Mg to Sr; however, with the expansive anions the stretching behavior increases from Sr to Mg. These trends claim

for the existence of a generalized pressure-oxidation correlation, which actually depends on the metal and the nonmetallic element.

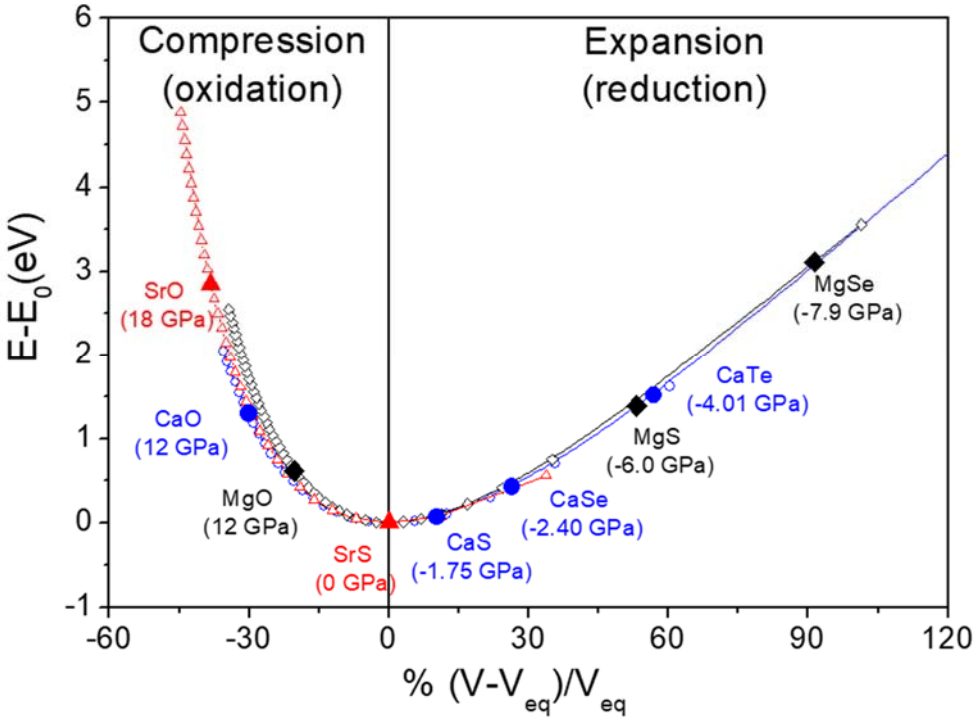

Figure 6.6. Energy−Volume equation of state curves for fcc-metallic Mg (black), Ca (blue), and Sr (red) along with the pressures associated with the volumes of the metallic sublattices in the corresponding MX (X = O, S, Se, Te) zero-pressure crystals. MgX (black), CaX (blue), and SrX (red).

Interestingly, similar trends are found when we analyze the evolution of the CP minima of the metallic lattices with volume. For instance, we display in Figure 6.7 how the CP minima found in the fcc-Ca structure increases monotonically with the lattice parameter. Using a simple Thomas-Fermi model, we can easily understand the obtained sublinear behavior. As in this framework the energy depends on the electron density to the 2/3 power, the CP (see eq 6.2) should correlate with the lattice parameter as the power of −5, in fair agreement with the results displayed in Figure 6.7. The labels are located at the cell parameters of metallic fcc-Ca, where the equilibrium structures of their corresponding CaX compounds are found. Notice that the lowest minima CP values are obtained in the fcc-Ca structures with a reduced volume (positive-pressure regime induced by compressive guest elements), whereas the higher CP minima values correspond to expanded lattices (negative-pressure regime induced by expansive guest elements).

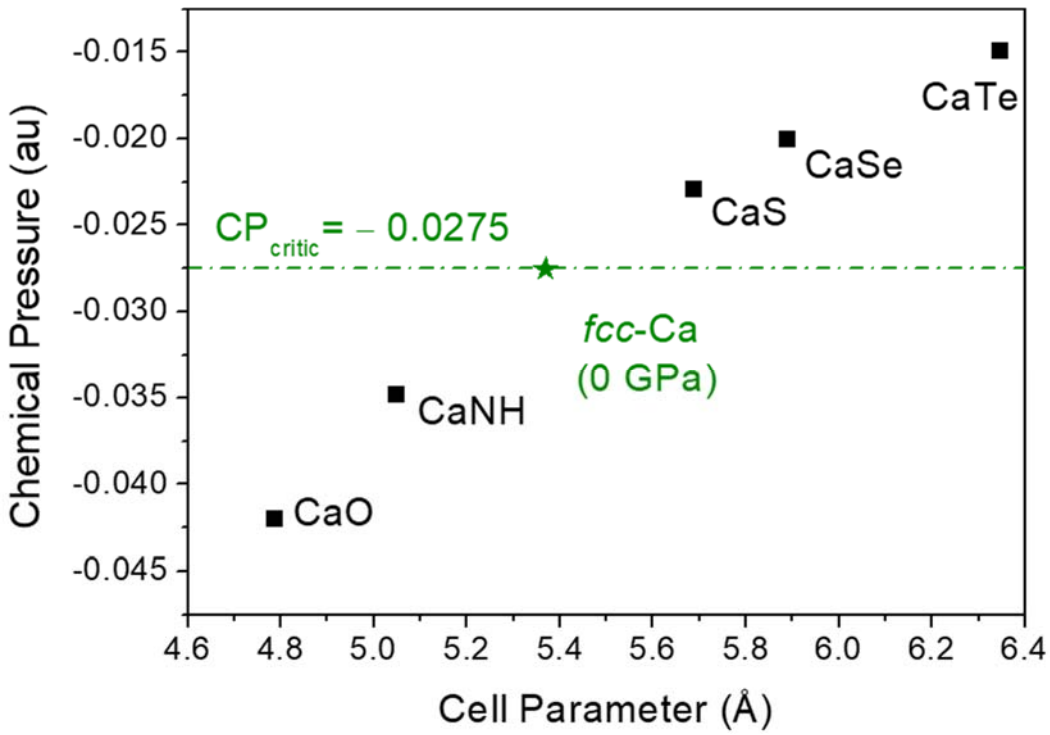

Figure 6.7. CP values at 4b (1/2, 1/2, 1/2) positions of metallic fcc-Ca at the different equilibrium lattice parameters of their corresponding CaX inorganic crystals. The green star represents the fcc-Ca CP value at zero pressure (reference value). Dash dotted line represents the critical chemical pressure, CPcritic, splitting the compressive (oxidation) and expansive (reduction) regimes.

From this analysis, a critical value for the CP at the minima can be defined considering the value of the fcc-Ca metal at zero pressure ($CP_{critic} = -0.0275$). This value serves to define a boundary between nonmetallic elements inducing compression or expansion on the metallic lattice. Moreover, the observed trend points toward a relationship between the oxidation capacity of the nonmetallic element, the CP at the minima, and the pressure (positive or negative) exerted on the lattice. This connection supports us in using the CP formalism in what follows as a way to prove the equivalence between effective stress and the redox state.

Under the CP scheme, we can infer a correlation between these two quantities by analyzing the changes in the CP distribution in the unit cell of the fcc-Ca at zero pressure either by the application of external pressure or by the presence of nonmetallic elements leading to the rock-salt CaX phase. The comparison of the CP cross sections along the (001) plane of the rock-salt CaO structure (a = 4.829 Å) and the CP distributions of fcc-Ca at the same volume (p = 12 GPa) is shown in Figure 6.8. CP features around the Ca cores are mostly maintained, reflecting that the core−shell structure is essentially

preserved during the electron density reorganization induced by pressure or by oxidation. Negative CP values out of the core positions are also very similar in both Figure 6.8 a,b, except, of course, at the positions where oxygen atoms are located.

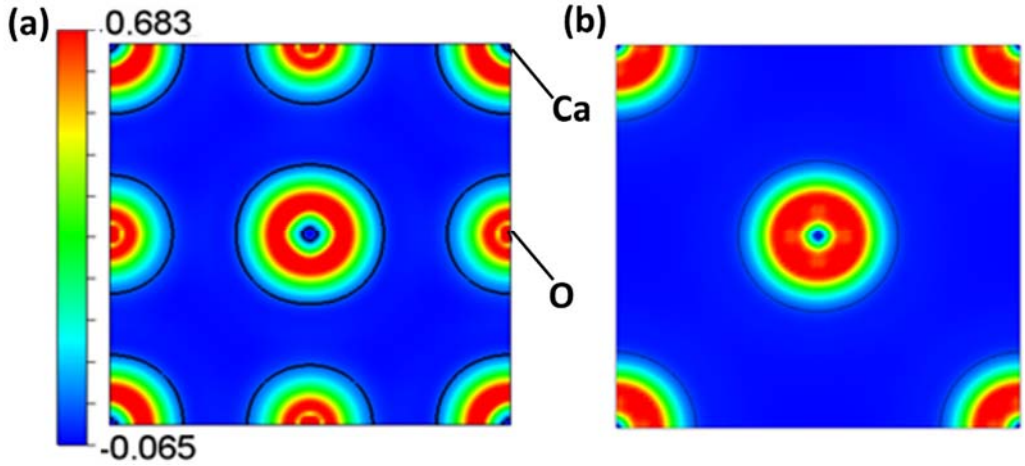

Figure 6.8. 2D CP cross sections along the (001) plane of (a) rock-salt CaO crystal and (b) fcc-Ca at the same lattice parameter than the rock-salt CaO. Black lines correspond to the CP = 0 isoline. Pressures are given in atomic units.

A more detailed analysis is provided in Figure 6.9 from the plot of the one-dimensional (1D) CP profiles along the Ca—Ca path in the fcc-Ca lattices at 0 and 12 GPa, and at zero pressure in the rock-salt CaO phase. It can be seen that both pressure and oxidation increase the CP maxima located at the core region from +0.6028 au in the zero-pressure metallic Ca to +0.7125 and +0.8571 au, respectively. This effect is accompanied by a lowering of the negative CP along the intermediate region of the interatomic path. Consequently, both positive pressure and oxidation lead to similar CP features in the core region and in the interstices. Therefore, CP indicates that electron density accumulation produced by the oxidation is also produced by the compression of the lattice in the line of the claimed pressure oxidation equivalence.

Nonetheless the slight differences in the CP values reflect that such an effect is similar but not equal. Such differences can be attributed to the fact that, in the oxide Ca, atoms formally transfer two electrons to O forming Ca^{2+} and O^{2-} ions, whereas in the case of fcc-Ca at 12 GPa such an electron transfer is not formally produced, at least to the same extend, because valence electrons are partially delocalized.

When compared with the 1D Ca—Ca profile in fcc-Ca at the same volume of the CaSe equilibrium structure (p = −2.40 GPa), an opposite effect is observed. A reduction of the CP values at the core regions and an increase at the interstitial voids are produced. As a result, the pressure-oxidation state principle seems to hold again. However, in this case this behavior is associated with a depletion (reduction) of the electron density at the interstices toward the nuclei positions due to the expansion of the lattice induced either by the nonmetallic atom or the (negative) pressure.

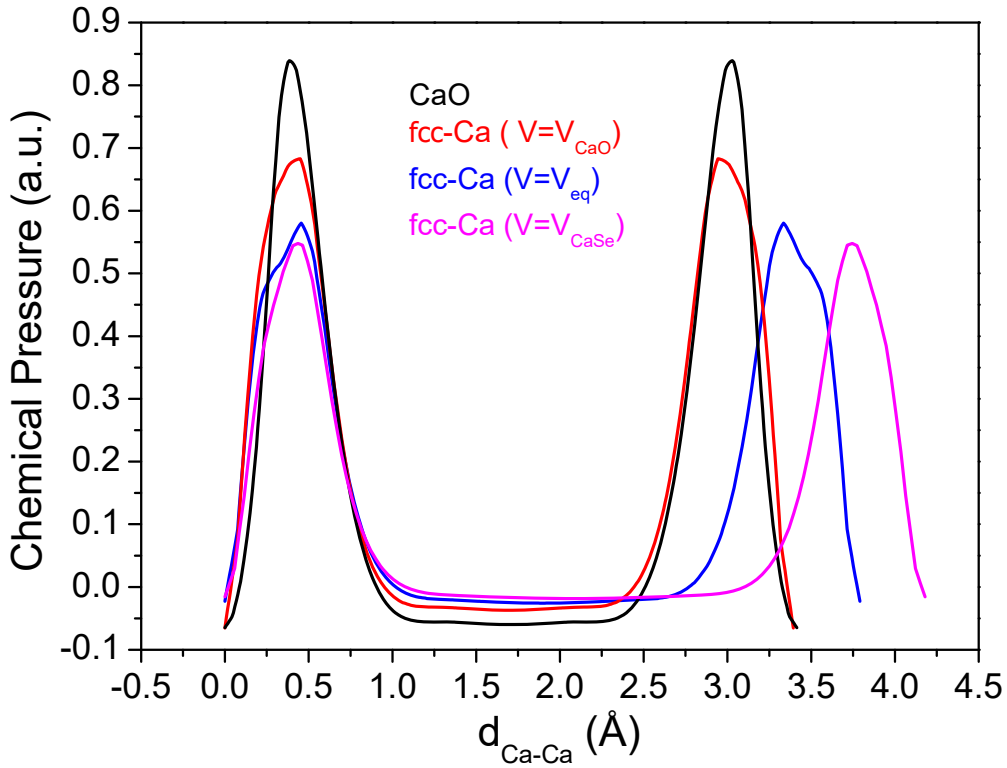

Figure 6.9. 1D Ca—Ca CP profiles of metallic fcc-Ca at its equilibrium volume (blue line), metallic fcc-Ca at the equilibrium volume of the rock-salt CaO crystal (red line), metallic fcc-Ca at the equilibrium volume of the rock-salt CaSe crystal (magenta line), and within the rock-salt CaO crystal at its equilibrium volume (black line).

Linking Pressure and Oxidation through Atomic Electronegativity

So far, we demonstrated that metal oxidation induced by nonmetallic atoms and hydrostatic pressure lead to similar structural effects. Our ultimate goal is to seek for a chemical basis for this correlation. Traditionally, size effects have been invoked to explain the compressive or expansive behavior of the metallic sublattices in inorganic compounds [7,8]. We can apply this idea using

Shannon radii [60] for O, S, Se, and Te (1.40, 1.84, 1.98, and 2.21 Å, respectively) and the metallic radii of fcc Mg, Ca, and Sr (1.60, 2.00, and 2.15 Å, respectively). For instance, on the one hand, considering CaX compounds as a test, an increase in the lattice parameter is predicted along the O, S, Se, and Te series, following the same trend as the ionic radii. On the other hand, only the Ca sublattice in CaTe should suffer an expansion effect, since Te radius is the only one greater than that of Ca in the fcc structure at equilibrium. However, this is not the observed result, as demonstrated in Figures 6.6 and 6.7, where the Ca sublattice in CaS and CaSe is also observed to show a larger lattice parameter than in fcc-Ca. Similar flaws of this purely geometric reasoning are also found for the Mg and Sr series.

Analogously, the amount of charge density transferred from the metallic atoms to the guest elements could also be used as a means to throw light into the pressure-oxidation correlation, since cation/anion charges can inform on the oxidation strength of the nonmetallic element. By means of the Atoms in Molecules formalism, we calculated the following Bader charges for Ca in CaO, CaS, CaSe, and CaTe: 1.445, 1.423, 1.395, and 1.374, respectively. As expected, such a decrease in the charge of Ca correlates with a decrease in the oxidation power of the guest element and also with an increase in the lattice parameter. However, nothing can be inferred regarding the contraction /expansion observed in the zero−pressure pure metallic Ca lattice upon crystal formation. In the case of a pure metal, Bader charges are always zero regardless the pressure (or volume) applied on the unit cell. In this sense, all the guest elements formally oxidize the submetal lattice, and therefore, it is not possible to prove if pressure regulates the amount of charge accumulated in the interstice voids of the pure metal.

Consequently, we have to recall to further elaborated arguments to explain both the expansive and compressive regimes. For this, we will again invoke the Vegas' hypothesis [15] on the equivalence between oxidation and pressure at the microscopic level, based on the fact that pressure induces an accumulation of electron density in the interstices of the metallic lattice. This is in concordance with the emergence of non-nuclear maxima [61] and the existence of electrides at high pressure [18-20]. According to this view, when the nonmetallic element is hosted just at the same positions in an unstressed metal, a similar effect on the electron density of the metal is expected. Whereas this result seems to hold in the compressive regime, this rule must be carefully applied when the metal subarray suffers an expansion induced by the nonmetallic atom. In such cases, the increased metal−metal interatomic

distances lead to a reduction of the electron density in the voids, which may be regarded as somewhat contradictory from the perspective of an oxidation process. Furthermore, according to the free electron model [48,49], metallic atoms transfer its valence electrons to the lattice interstices acquiring formally an oxidized state already in the zero-pressure metallic phase.

This view can be quantitatively confirmed through the evaluation of the number of core electrons of the metal at different pressure (volume) conditions. As we saw in the previous sections, the CP = 0 contour in metallic Ca defines a boundary between the positive CP zone representing a sphere corelike region and the negative-pressure background associated with the delocalized sea of electrons (see, e.g., Figure 6.1a). A measure of the number of core electrons (ne), and therefore an estimation of the amount of charge transferred to the metal voids, can be given by integrating the electron density within this positive chemical pressure region. Values are collected in Table 6.1, where we selected the zero-pressure metallic phase as our reference within the AMM model for the ongoing discussion.

Table 6.1. Lattice Parameters (a), Pressures (p), Radii (Rcore), and Number of Electrons (n_e) of the Core-like Region of *fcc*-Ca at Its Zero Pressure Equilibrium Volume and at the Corresponding Volumes of Different CaX Compounds (X =O, S, Se, Te). Δn_e stands for the difference between the number of electrons in the corelike region of *fcc*-Ca at different pressures with respect to the zero-pressure value.

	a (Å)	**p (GPa)**	**R_{Core}(Å)**	**n_e**	**Δn_e**
fcc-Ca (V_{CaO})	4.787	12	0.955	7.181	-0.216
fcc-Ca (V_{Caeq})	5.410	0	1.007	7.397	0
fcc-Ca (V_{CaS})	5.689	-1.75	1.043	7.520	0.123
fcc-Ca (V_{CaSe})	5.916	-2.40	1.065	7.585	0.188
fcc-Ca (V_{CaTe})	6.348	-4.01	1.119	7.714	0.317

Indeed, when we compared the number of core-like electrons in the pure fcc-Ca metal at the zero-pressure equilibrium volume with those corresponding to the volumes of their CaX compounds (see Table 1), then the generalized stress-redox relationship is clearly illustrated. For instance, in the case of Ca, an estimation of the redox effect induced in the pure metallic lattice as a consequence of the structural distortions associated with the guest elements (O, S, Se Te) is given by the number of core-like electrons transferred Δn_e. The latter quantity is calculated as the difference between the number of core-like electrons of the pure metal Ca metal at the volumes of the respective CaX

compounds and the value of pure Ca metal at zero pressure (see Table 1). In the case of O atom, it exerts a pressure of 12 GPa on the lattice, which induces a core electron transfer of −0.215 to the interstitial voids producing an oxidation effect in the metallic lattice. On the contrary, the expansion effect induced by S, Se, and Te exerts −1.75, −2.40, and −4.01 GPa on the sub-metal lattice, which corresponds to an electron core increase of 0.123, 0.193, and 0.317 au, respectively. Such an increase in the number of core electrons clearly manifests that S, Se, and Te induce a reduction effect on the lattice (previous to the oxidation produced by the formation of their respective anions). In summary, although in the global process the metal is formally oxidized, if we take the zero-pressure metal as a reference state, we can distinguish nonmetallic atoms behaving either as oxidizing or reducing agents. These redox processes are unequivocally manifested through the volume change of the metal sublattice providing further support to the pressure-oxidation equivalence, which should be more appropriately renamed as general stress-redox correspondence, as we advanced in the previous section.

The fundamental basis behind this general stress-redox equivalence is provided by the Pearson-Parr's electronegativity equalization principle.37,38 This principle explains not only the failure of the radius ratio rule but also the observed contraction−expansion trends. Accordingly, the electron density transferred from the metallic atoms to the guest element should correlate with the difference between the electronegativity of the nonmetallic element and the capacity of the metal to donate electron charge to the anion position. The latter can be either quantified by the value of the CP at the minima located at that 4b position, as we saw in the previous sections, or by the number of core electrons transferred Δn_e.

Since both quantities increase (decrease) monotonically with the volume (pressure) of the metal phase, we can understand that the metal array fits its lattice parameter to fulfill the equalization principle. If this lattice parameter is fixed, then only nonmetallic elements within a narrow range of electronegativity values could be hosted by the metallic lattice. Under the equalization principle scheme, this electronegativity range would ideally be a narrow one with just the value that perfectly matches the metal capability to accumulate electron density at the anion position, which we demonstrated that can be quantitatively associated with the CP minimum value and/or the number of the core electrons transferred.

This view is confirmed when we plot the CP values at the 4b positions and Δn_e of the fcc-Ca structure using the volumes of the respective CaX

compounds (X: O, S, Se, Te) with respect to the Pauling electronegativity of the different X atoms (see Figure 6.10). The linear correlations observed in Figure 6.10 seem to be quite general and support the generalized stress-redox correlation as a general principle. Following a referee recommendation, we would like to be very clear at this respect.

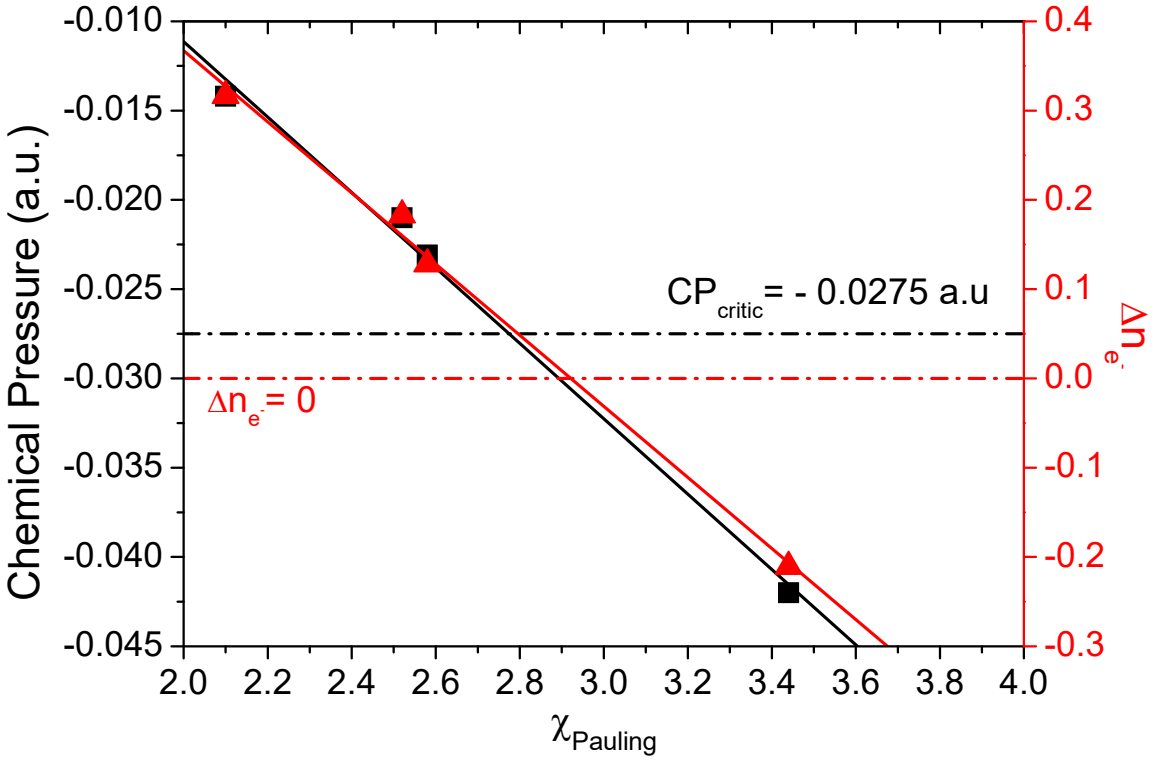

Figure 6.10. Metallic fcc-Ca CP values at the 4b position (squares) and number of core-like electrons transferred Δn_e (triangles) for the different CaX (X = O, S, Se, Te) compounds against the Pauling electronegativity of the corresponding X atom. Black and red straight lines correspond, respectively, to the linear fittings of the CP data, CP = 0.0311−0.0211 $\chi_{Pauling}$., and ne data, Δn_e = 1.164−0.0398 $\chi_{Pauling}$.

By "quite general" we mean that this type of linear trend also holds in other metals. For example, in the ones explored in this work (see, e.g., the plots for Na and Mg collected in the Supplementary Material 6 file) linear fittings of similar quality were obtained. It should be also pointed out that CP-χ values obviously depend on the metal and the particular structure, since the reference redox state varies from lattice to lattice. As a corollary, we can state that the Pearson-Parr's equalization principle is the driving force expanding or compressing the metal structure to equalize the electronegativity of the guest element with the CP at the metal voids (or equivalently its charge), leading the formation of the inorganic crystal.

From the plot of Figure 6.10, a quite high value of 2.78 is obtained for the electronegativity of the zero pressure fcc-Ca lattice acting on the 4b position. Such a value does not represent the actual electronegativity of isolated Ca but a local value, which evidences that voids are preferred positions of the structure where formally the metal electron density is accumulated.

From the plot of Figure 6.10, a quite high value of 2.78 is obtained for the electronegativity of the zero pressure fcc-Ca lattice acting on the 4b position. Such a value does not represent the actual electronegativity of isolated Ca but a local value, which evidences that voids are preferred positions of the structure where formally the metal electron density is accumulated.

Interestingly enough, this linear trend also provides a way to infer either the electronegativity of the nonmetallic atom (group) located at the Ca 4b position or, alternatively, the equilibrium lattice parameter of an unknown CaX compound. For instance, in the case of the CaNH crystal we propose a Pauling electronegativity value for the NH group of 3.11 based on its lattice parameter of 5.05 Å. Using this value of electronegativity for the NH group, we can now estimate the lattice parameter of the hypothetical rock-salt MgNH compound by means of the CP-lattice parameter correlation of Mg depicted in Figures S6.4 and S6.5 of Supplementary Material 6. A value of 4.18 Å is obtained, which is not too far from the value of 4.35 Å derived for a cubic lattice assuming the same volume as the experimental zero pressure value determined for the hexagonal MgNH phase.[62] This result points to the transferability between the guest electronegativities obtained in this work but also highlights the potential of the chemical pressure to anticipate lattice parameters of unknown phases. Obviously, this feature has nothing to do with the possible determination of the stable phase of the compound at given p, T conditions (that requires the evaluation of the Gibbs energy), which up to now is in general far to be foreseen under the CP-AMM scheme.

As negative CP and atom electronegativity represent the capability of the electron density to be accumulated, respectively, in the metal voids and in the nonmetallic atom, compressive effects will result when the atom capability is higher than that of the corresponding metal, whereas expansive effects will result from an excess of the electron density in the metal voids compared to one that the nonmetallic atom can attract. From another perspective, such a capability can be interpreted as the oxidation potential. Therefore, on the one hand, if the guest atom has a higher oxidation potential than the corresponding metal, a compressive effect (positive pressure) must be applied to equalize its capability. On the other hand, in the case of a lower oxidation

potential, the metal must move to the negative-pressure regime (expansion) to reach the oxidation state of the anion.

Table 6.2. Total CP and Potential CP Contribution at the 4b Position of the Metallic fcc-Ca Structure at Different Pressures Corresponding to the Equilibrium Volumes of CaX (X = O, S, Se, Te) Compounds. The CP value at zero pressure is included for reference.

	a (Å)	**p (GPa)**	**CP(4b) (au)**	**CP_{Pot} (au)**
fcc-Ca (V_{CaO})	4.787	12	-0.0421	-0.0619
fcc-Ca (V_{Caeq})	5.410	0	-0.0207	-0.0406
fcc-Ca (V_{CaS})	5.689	-1.75	-0.0229	-0.0341
fcc-Ca (V_{CaSe})	5.916	-2.40	-0.0200	-0.0310
fcc-Ca (V_{CaTe})	6.348	-4.01	-0.0149	-0.0208

Finally, as the CP formalism allows us to decompose chemical pressure into different meaningful contributions, [28] it is interesting to evaluate the contribution coming from the potential energy term, which is described in the CP program as the local pseudopotential (PSP) contribution. This is mainly responsible for the nucleus−electron interaction, and so it is connected to the tendency of a given unit cell position to attract the electron density, which we ultimately associate with the total electronegativity at that point. In Table 6.2, we collected the total CP and the potential energy CP contribution at the 4b positions of *fcc*-Ca at pressures corresponding to the equilibrium volumes of different CaX (X = O, S, Se, Te) compounds. The potential energy pressure is by far mainly responsible for the overall negative pressure at such positions indicating that electronegativity dominates the guest insertion on the lattice.

Furthermore, the more the pressure is applied on the structure the more is the potential contribution in absolute value. To further illustrate this behavior, we plotted in Figure 6.11 the potential energy contribution to CP (CP_{Pot}) against the number of core electrons transferred Δn_e for fcc-Ca at the different volumes of the CaX compounds. As we have previously seen, Δn_e represents the amount of charge transferred from the Ca cores to the interstitial voids and, therefore, in analogy with Bader charges in ionic compounds, can be used as an estimation of the electronegativity changes in the metal. Interestingly, a linear trend between potential energy CP and Δn_e is observed, thus evidencing that the increase of the potential energy CP (in absolute value) is ultimately related to the decreasing of the electronegativity of the metal, in total concordance with the clarifying analysis of a recent

publication of Rahm et al. [55] Furthermore, such a result leads us to propose that the expansion and the contraction of the unit cell are intrinsic mechanisms of the metal lattice to regulate its potential energy pressure and therefore its local electronegativity at the relevant interstitial positions.

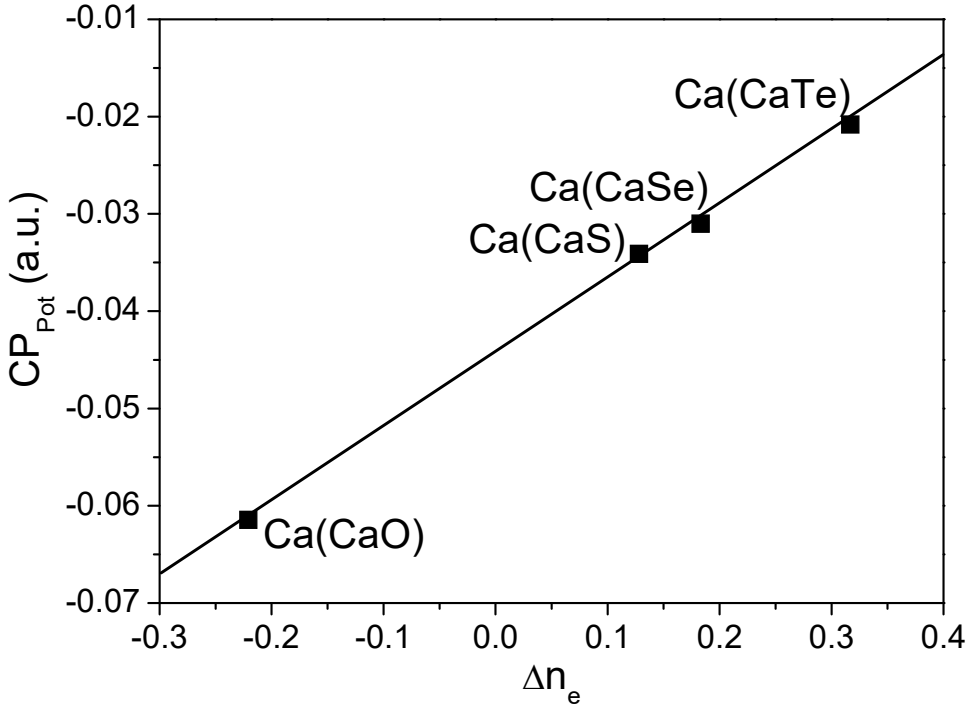

Figure 6.11. Potential energy contribution to CP (CP_{Pot}) against the number of core electrons transferred Δn_e for fcc-Ca at the different volumes of the CaX compounds.

Conclusions

Throughout this Manuscript, we have tried to take some steps forward in the understanding of inorganic crystalline structures. First, the DFT-CP approach has proved to be an efficient verifier of the premises of the AMM model. Minima of CP are clearly identified in a collection of metallic structures just at the precise positions where nonmetallic elements are situated in the corresponding inorganic crystalline compounds. Second, the pressure-oxidation equivalence inherent to the AMM model has been explained and consequently generalized finding a robust support in the Pearson-Parr's electronegativity equalization principle. Our results provide a clear conclusion on the structures of inorganic crystals. Ionic compounds are formed through the distortion of their underlying metal sublattice in such a way that the metallic structure adjusts its volume leading a value for the potential energy

chemical pressure (local electronegativity) at the relevant interstice positions to formally host the nonmetallic element with the same electronegativity. As far as we know, this is the first time that a clear connection between a local electronegativity acting on a specific position of a metal lattice is correlated to the formation of the corresponding ionic compound.

References

[1] L. Pauling, The Nature of the Chemical Bond and the Structure of Molecules and Crystals: An Introduction to Modern Structural Chemistry, Cornell University Press, 3rd ed., **1960**.

[2] C. Gatti, Chemical bonding in crystals: new directions. Z. Kristallogr. - Cryst. Mater., 220, 399, **2005**. DOI: https://doi.org/10.1524/zkri.220.5.399.65073.

[3] F. Weinhold and C. R. Landis, Valency and Bonding: A Natural Bond Orbital Donor-acceptor Perspective, **2005**.

[4] G. Frenking and S. Shaik, The Chemical Bond: Fundamental Aspects of Chemical Bonding, Vol. 1, **2014**.

[5] M. W. Schmidt, J. Ivanic, and K. Ruedenberg, The Chemical Bond. Fundamental Aspects of Chemical Bonding, **2014**.

[6] G. N. Lewis, Valence and the structure of atoms and molecules, **1966**.

[7] L. Pauling, The Principles Determining the Structure of Complex Ionic Crystals. J. Am. Chem. Soc., 51, 1010-1026, **1929**. DOI: https://doi.org/10.1021/ja01379a006.

[8] L. Pauling, The Nature of the Chemical Bond, **1939**.

[9] M. O'keeffe and B. Hyde, An alternative approach to nonmolecular crystal structures with emphasis on the arrangements of cations., In Cation Ordering and Electron transfer; Springer: Berlin, Germany ; Vol. 61, pp 77−144., **1985**.

[10] M. O'keeffe and B. G. B.G. Hyde, The Role of Nonbonded Forces in Crystals. , In Structure and Bonding in Crystals; Academic Press: New York; Vol. 1, pp 227−253., **1981**.

[11] H. G. Von Schnering and R. Nesper, How Nature Adapts Chemical Structures to Curved Surfaces. Angew. Chem., Int. Ed. Engl., 26, 1059-1063, **1987**. DOI: https://doi.org/10.1002/anie.198710593.

[12] K. Schubert, Kristallstrukturen Zweikomponentiger Phasen, **1964**.

[13] Á. Vegas and L. A. Martínez-Cruz, A study of cation arrays in MB2, MB4 and MB6 borides. Part II. Cluster formation and bonding aspects. Z. Kristallogr. - Cryst. Mater., 210, 581, **1995**. DOI: https://doi.org/10.1524/zkri.1995.210.8.581.

[14] Á. Vegas and M. Jansen, Structural relationships between cations and alloys: an equivalence between oxidation and pressure. Acta Crystallogr., Sect. B, B58, 38-51, **2002**. DOI: https://doi.org/10.1107/S0108768101019310.

[15] Á. Vegas, D. Santamaría-Pérez, M. Marqués, M. Flórez, V. Garcia Baonza, and J. M. Recio, Anions in metallic matrices model: application to the aluminium crystal chemistry. Acta Crystallogr., Sect. B, 62, 220-235, **2006**. DOI: https://doi.org/10.1107/S0108768105039303.

[16] M. Marqués, M. Florez, J. M. Recio, D. Santamaría, A. Vegas, and V. Garcia Baonza, Structure, Metastability, and Electron Density of Al Lattices in Light of the Model of Anions in Metallic Matrices. J. Phys. Chem. B, 110, 18609-18618, **2006**. DOI: https://doi.org/10.1021/jp063883a.

[17] P. Mori-Sánchez, Á. M. Pendás, and V. Luaña, Polarity inversion in the electron density of BP crystal. Phys. Rev. B: Condens. Matter Mater. Phys., 63, 125103, **2001**. DOI: https://doi.org/10.1103/PhysRevB.63.125103.

[18] M. Marqués, G. J. Ackland, L. F. Lundegaard, G. Stinton, R. J. Nelmes, M. I. Mcmahon, and J. Contreras-García, Potassium under Pressure: A Pseudobinary Ionic Compound. Phys. Rev. Lett., 103, 115501, **2009**. DOI: https://doi.org/10.1103/PhysRevLett.103.115501.

[19] M. M. Miao and R. Hoffmann, High Pressure Electrides: A Predictive Chemical and Physical Theory. Acc. Chem. Res., 47, 1311-1317, **2014**. DOI: https://doi.org/10.1021/ar4002922.

[20] M. M. Miao and N. Hoffmann, High Pressure Electrides: the Chemical Nature of Interstitial Quasi-atoms. J. Am. Chem. Soc., 137, 3631-3637, **2015**. DOI: https://doi.org/10.1021/jacs.5b00242.

[21] Á. Vegas and M. Mattesini, Towards a generalized vision of oxides: disclosing the role of cations and anions in determining unit-cell dimensions. Acta Crystallogr., Sect. B, B66, 338-344, **2010**. DOI: https://doi.org/10.1107/S0108768110013200.

[22] Á. Vegas, Concurrent Pathways in the Phase Transitions of Alloys and Oxides: Towards an Unified Vision of Inorganic Solids. Struct. Bonding

(Berlin, Ger.), 138, 133-148, **2011**. DOI: https://doi.org/10.1007/430_2010_38.

[23] L. A. Martínez-Cruz, Á. Ramos-Gallardo, and Á. Vegas, MSn and MSnO3 (M = Ca, Sr, Ba): New Examples of Oxygen-Stuffed Alloys. J. Solid State Chem., 110, 397-398, **1994**. DOI: https://doi.org/10.1006/jssc.1994.1186.

[24] A. Filippetti and V. Fiorentini, Theory and applications of the stress density. Phys. Rev. B: Condens. Matter Mater. Phys., 61, 8433-8455, **2000**. DOI: https://doi.org/10.1103/PhysRevB.61.8433.

[25] C. L. Rogers and A. M. Rappe, Geometric formulation of quantum stress fields. Phys. Rev. B: Condens. Matter Mater. Phys., 65, 224117, **2002**. DOI: https://doi.org/10.1103/PhysRevB.65.224117.

[26] M. J. Godfrey, Stress field in quantum systems. Phys. Rev. B: Condens. Matter Mater. Phys., 37, 10176-10181, **1988**. DOI: https://doi.org/10.1103/PhysRevB.37.10176.

[27] O. H. Nielsen and R. M. Martin, Quantum-mechanical theory of stress and force. Phys. Rev. B: Condens. Matter Mater. Phys., 32, 3780, **1985**. DOI: https://doi.org/10.1103/PhysRevB.32.3780.

[28] P. Ziesche, J. Gräfenstein, and O. H. Nielsen, Quantum-mechanical stress and a generalized virial theorem for clusters and solids. Phys. Rev. B: Condens. Matter Mater. Phys., 37, 8167, **1988**. DOI: https://doi.org/10.1103/PhysRevB.37.8167.

[29] D. C. Fredrickson, DFT-Chemical Pressure Analysis: Visualizing the Role of Atomic Size in Shaping the Structures of Inorganic Materials. J. Am. Chem. Soc., 134, 5991-5999, **2012**. DOI: https://doi.org/10.1021/ja300685j.

[30] H. H. Osman, M. A. Salvadó, P. Pertierra, J. Engelkemier, D. C. Fredrickson, and J. M. Recio, Chemical Pressure Maps of Molecules and Materials: Merging the Visual and Physical in Bonding Analysis. J. Chem. Theory Comput., 14, 104-114, **2018**. DOI: https://doi.org/10.1021/acs.jctc.7b00943.

[31] H. H. Osman, J. Andrés, M. A. Salvadó, and J. M. Recio, Chemical Bond Formation and Rupture Processes: An Application of DFT-Chemical Pressure Approach. J. Phys. Chem. C, 122, 21216-21225, **2018**. DOI: https://doi.org/10.1021/acs.jpcc.8b06947.

[32] D. C. Fredrickson, Electronic Packing Frustration in Complex Intermetallic Structures: The Role of Chemical Pressure in Ca2Ag7. J. Am. Chem. Soc., 133, 10070-10073, **2011**. DOI: https://doi.org/10.1021/ja203944a.

[33] M. V. Berns and D. C. Fredrickson, Structural Plasticity: How Intermetallics Deform Themselves in Response to Chemical Pressure, and the Complex Structures That Result. Inorg. Chem., 53, 10762-10771, **2014**. DOI: https://doi.org/10.1021/ic5020412.

[34] J. Engelkemier, V. M. Berns, and D. C. Fredrickson, First-Principles Elucidation of Atomic Size Effects Using DFT-Chemical Pressure Analysis: Origins of Ca36Sn23's Long-Period Superstructure. J. Chem. Theory Comput., 9, 3170-3180, **2013**. DOI: https://doi.org/10.1021/ct400274f.

[35] J. Engelkemier and D. C. Fredrickson, Chemical Pressure Schemes for the Prediction of Soft Phonon Modes: A Chemist's Guide to the Vibrations of Solid State Materials. Chem. Mater., 28, 3171-3183, **2016**. DOI: https://doi.org/10.1021/acs.chemmater.6b00917.

[36] P. K. Chattaraj, H. Lee, and R. G. Parr, HSAB Principle. J. Am. Chem. Soc., 113, 1855-1856, **1991**. DOI: https://doi.org/10.1021/ja00005a073.

[37] R. G. Pearson, Absolute Electronegativity and Hardness: Application to Inorganic Chemistry. Inorg. Chem., 27, 734-740, **1988**. DOI: https://doi.org/10.1021/ic00277a030.

[38] R. G. Parr and R. G. Pearson, Absolute Hardness: Companion Parameter to Absolute Electronegativity. J. Am. Chem. Soc., 105, 7512-7516, **1983**. DOI: https://doi.org/10.1021/ja00364a005.

[39] S. Goedecker, M. Teter, and J. Hutter, Separable Dual-space Gaussian Pseudopotentials. Phys. Rev. B: Condens. Matter Mater. Phys., 54, 1703-1708, **1996**. DOI: https://doi.org/10.1103/PhysRevB.54.1703.

[40] C. Hartwigsen, S. Goedecker, and J. Hutter, Relativistic Separable Dual-space Gaussian Pseudopotentials from H to Rn. Phys. Rev. B: Condens. Matter Mater. Phys., 58-86, 3641, **1998**. DOI: https://doi.org/10.1103/PhysRevB.58.3641.

[41] X. Gonze, F. Jollet, F. Abreu Araujo, D. Adams, B. Amadon, T. Applencourt, C. Audouze, J. M. Beuken, J. Bieder, A. Bokhanchuk, E. Bousquet, F. Bruneval, D. Caliste, M. Côté, F. Dahm, F. Da Pieve, M.

Delaveau, M. Di Gennaro, B. Dorado, C. Espejo, G. Geneste, L. Genovese, A. Gerossier, M. Giantomassi, Y. Gillet, D. R. Hamann, L. He, G. Jomard, J. Laflamme Janssen, S. Le Roux, A. Levitt, A. Lherbier, F. Liu, I. Lukačević, A. Martin, C. Martins, M. J. T. Oliveira, S. Poncé, Y. Pouillon, T. Rangel, G. M. Rignanese, A. H. Romero, B. Rousseau, O. Rubel, A. A. Shukri, M. Stankovski, M. Torrent, M. J. Van Setten, B. Van Troeye, M. J. Verstraete, D. Waroquiers, J. Wiktor, B. Xu, A. Zhou, and J. W. Zwanziger, Recent developments in the ABINIT software package. Comput. Phys. Commun., 205, 106-131, **2016**. DOI: https://doi.org/10.1016/j.cpc.2016.04.003.

[42] X. Gonze, B. Amadon, P. M. Anglade, J. M. Beuken, F. Bottin, P. Boulanger, F. Bruneval, D. Caliste, R. Caracas, M. Côté, T. Deutsch, L. Genovese, P. Ghosez, M. Giantomassi, S. Goedecker, D. R. Hamann, P. Hermet, F. Jollet, G. Jomard, S. Leroux, M. Mancini, S. Mazevet, M. J. T. Oliveira, G. Onida, Y. Pouillon, T. Rangel, G. M. Rignanese, D. Sangalli, R. Shaltaf, M. Torrent, M. J. Verstraete, G. Zerah, and J. W. Zwanziger, ABINIT: First-principles Approach to Material and Nanosystem Properties. Comput. Phys. Commun., 180, 2582-2615, **2009**. DOI: https://doi.org/10.1016/j.cpc.2009.07.007.

[43] X. Gonze, G. M. Rignanese, M. Verstraete, J. M. Beuken, Y. Pouillon, R. Caracas, J. Y. Raty, V. Olevano, F. Bruneval, L. Reining, R. Godby, G. Onida, D. R. Hamann, and D. C. Allan, A Brief Introduction to the ABINIT Software Package. Z. Kristallogr. - Cryst. Mater., 220, 558, **2005**. DOI: https://doi.org/10.1524/zkri.220.5.558.65066.

[44] H. Monkhorst and J. Pack, Special Points for Brillouin-zone Integrations. J. Phys. Rev. B, 13, 5188-5196, **1976**. DOI: https://doi.org/10.1103/PhysRevB.13.5188.

[45] K. P. Hilleke and D. C. Fredrickson, Discerning Chemical Pressure amidst Weak Potentials: Vibrational Modes and Dumbbell/Atom Substitution in Intermetallic Aluminides. J. Phys. Chem. A, 122, 8412-8426, **2018**. DOI: https://doi.org/10.1021/acs.jpca.8b07419.

[46] K. M. a. F. Izumi, VESTA 3 for three-dimensional visualization of crystal, volumetric and morphology data. J. Appl. Cryst., 44, 1272-1276, **2011**. DOI: https://doi.org/10.1107/S0021889811038970.

[47] R. F. Bader, Atoms in Molecules. Acc. Chem. Res., 18, 9-15, **1985**. DOI: https://doi.org/10.1021/ar00109a003.

[48] A. Otero De La Roza, E. R. Johnson, and V. Luaña, Critic2: A program for real-space analysis of quantum chemical interactions in solids. Comput.

Phys. Commun., 185, 1007-1018, **2014**. DOI: https://doi.org/10.1016/j.cpc.2013.10.026.

[49] M. Yu and D. R. Trinkle, Accurate and efficient algorithm for Bader charge integration. J. Chem. Phys., 134, 064111, **2011**. DOI: https://doi.org/10.1063/1.3553716.

[50] A. Vegas, Structural Models of Inorganic Crystals, Universitat Politecnica de Valencia, **2018**.

[51] P. Drude, Zur Elektronentheorie der Metalle. Ann. Phys., 306, 566-582, **1900**. DOI: https://doi.org/10.1002/andp.19003060312.

[52] A. Sommerfeld, Zur Elektronentheorie der Metalle auf Grund der Fermischen Statistik. Eur. Phys. J. A, 47, 1-32, **1928**. DOI: https://doi.org/10.1007/BF01391052.

[53] S. Anzellini, D. Errandonea, S. G. Macleod, P. Botella, D. Daisenberger, J. M. De'ath, J. Gonzalez-Platas, J. Ibáñez, M. I. Mcmahon, K. A. Munro, C. Popescu, J. Ruiz-Fuertes, and C. W. Wilson, Phase diagram of calcium at high pressure and high temperature. Phys. Rev. Materials, 2, 083608, **2018**. DOI: https://doi.org/10.1103/PhysRevMaterials.2.083608.

[54] D. Errandonea, R. Boehler, and M. Ross, Melting of the alkaline-earth metals to 80 GPa. Phys. Rev. B: Condens. Matter Mater. Phys., 65, 012108-012128, **2001**. DOI: https://doi.org/10.1103/PhysRevB.65.012108.

[55] M. Rahm, R. Cammi, N. W. Ashcroft, and R. Hoffmann, Squeezing All Elements in the Periodic Table: Electron Configuration and Electronegativity of the Atoms under Compression. J. Am. Chem. Soc., 141, 10253-10271, **2019**. DOI: https://doi.org/10.1021/jacs.9b02634.

[56] H. P. Beck and G. Lederer, Thermische Dilatation und Hochdruckverhalten der Zintl-Phasen CaSn und BaSn. Z. Anorg. Allg. Chem., 619, 897, **1993**. DOI: https://doi.org/10.1002/zaac.19936190516.

[57] Á. Vegas, A. Grzechnik, M. Hanfland, C. Mühle, and M. Jansen, Antifluorite to Ni2In-type phase transition in K2S at high pressures. Solid State Sci., 4, 1077-1081, **2002**. DOI: https://doi.org/10.1016/S1293-2558(02)01360-2.

[58] E. H. Megchiche, M. Amarouche, and C. Mijoule, First-principles calculations of the diffusion of atomic oxygen in nickel: thermal expansion

contribution. J. Phys.: Condens. Matter, 19, 296201-296219, **2007**. DOI: https://doi.org/10.1088/0953-8984/19/29/296201.

[59] J. Kim, S. H. Shin, J. A. Jung, K. J. Choi, and J. H. Kim, First-principles study of interstitial diffusion of oxygen in nickel chromium binary alloy. Appl. Phys. Lett., 100, 131904-131925, **2012**. DOI: https://doi.org/10.1063/1.3696079.

[60] R. D. Shannon, Revised Effective Ionic Radii and Systematic Studies of Interatomic Distances in Halides and Chalcogenides. Acta Crystallogr., Sect. A, 32, 751-767, **1976**. DOI: https://doi.org/10.1107/S0567739476001551.

[61] A. M. Pendás, M. A. Blanco, A. Costales, P. M. Sánchez, and V. Luaña, Non-nuclear Maxima of the Electron Density. Phys. Rev. Lett., 83, 1930-1933, **1999**. DOI: https://doi.org/10.1103/PhysRevLett.83.1930.

[62] F. Dolci, E. Napolitano, E. Weidner, S. Enzo, P. Moretto, M. Brunelli, T. Hansen, M. Fichtner, and W. Lohstroh, Magnesium Imide: Synthesis and Structure Determination of an Unconventional Alkaline Earth Imide from Decomposition of Magnesium Amide. Inorg. Chem., 50, 1116-1122, **2011**. DOI: https://doi.org/10.1021/ic1023778.

Supplementary Material Chapter 6

Computational Details

Parameters used in the LDA-DFT calculations with ABINIT and the total energy of the crystalline solids studied are shown in Table S1.

Table S6.1. Computational parameters and electronic energies per formula unit (f.u.) of the crystals calculated with ABINIT.

Structure	E_{cutoff} (Ha)	*k*-point grid	FFT grid	E/f.u. (Ha)
fcc-Ca	190	6×6×6	128x128x128	-36.73850
sc-Ca	120	8×8×8	80x80x80	-36.67165
fcc-Mg	220	6×6×6	240x240x240	-252.52650
sc-Mg	180	6×6×6	200x200x200	-63.11237
fcc-Na	340	4×4×4	162x162x162	-45.70505
BaSn (CsCl-type)	60	6×6×6	52x52x52	-29.19013
*hP*4-K	100	6×6×4	72x72x100	-56.46768
B1- CaO	300	6×6×6	144x144x144	-52.91820

GGA-LDA Comparison of chemical pressure maps

GGA calculations have been performed using PBE functional from the reference Perdew, J. P.; Burke, k.; Ernzerhof, M. Generalized Gradient Approximation Made Simple, Phys. Rev. Lett. 1996, 77, 3865-3868. Same number of k points and FFT grid has been used in order to facilitate the CP maps comparison. As in the case of the LDA calculations, HGH pseudopotentials have been also used, but adapted to GGA calculation level as described in reference Krack, M; Pseudopotentials for H to Kr optimized for gradient-corrected exchange-correlation functionals, Theor. Chem. Acc. 2005 114, 145.

- fcc-Ca at zero pressure

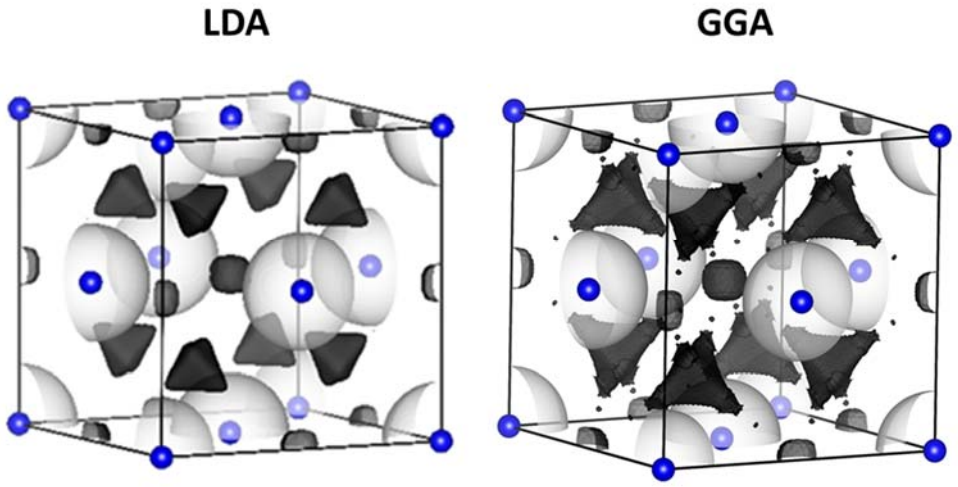

Figure S6.1. 3D CP isosurfaces of fcc-Ca crystal at equilibrium volume with CP= +0.001 (white) and CP = 0.0274 (black) at LDA and GGA calculation levels.

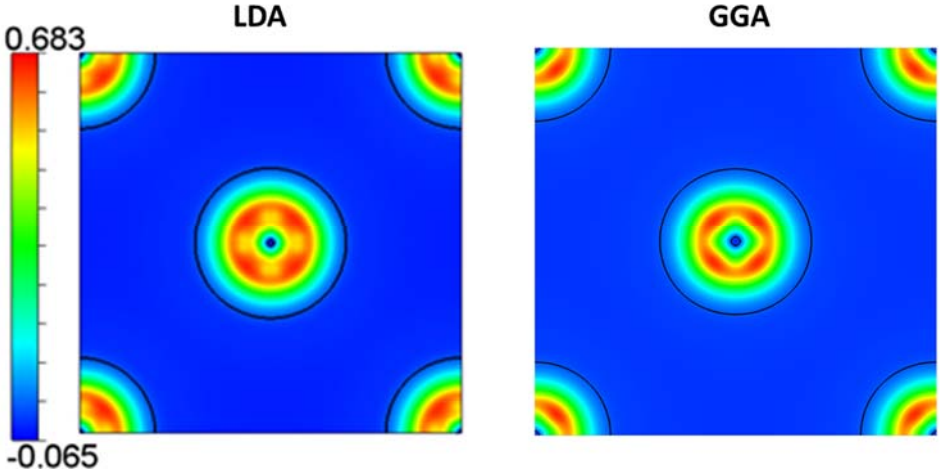

Figure S6.2. LDA and GGA Cross-section along the (001) plane containing the Ca atoms for the fcc-Ca at zero pressure. The CP = 0 contour is shown with a black solid line.

- fcc-Ca at the equilibrium volume of the CaO

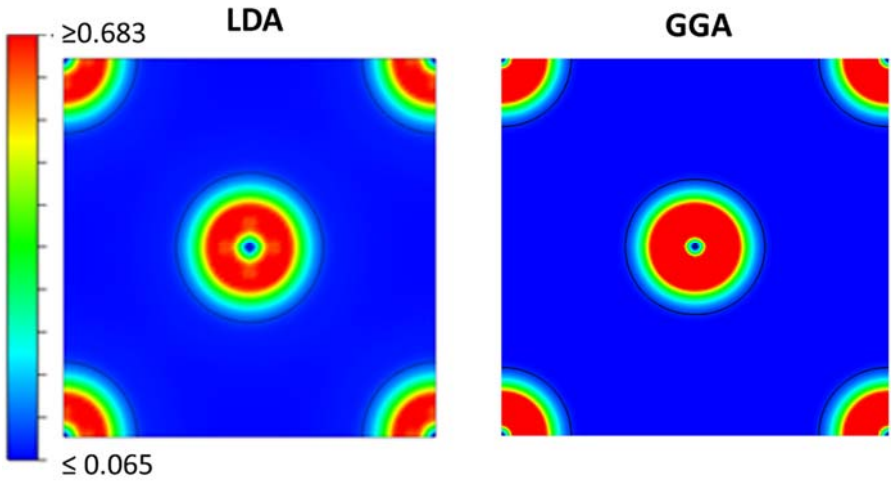

Figure S6.3. LDA and GGA Cross-section along the (001) plane containing the Ca atoms for the fcc-Ca at zero pressure. The CP = 0 contour is shown with a black solid line. The chemical pressure at the 4b position in the GGA level is -0.04226 whereas in the case of the LDA level is -0.04212.

Chemical pressure distribution in fcc and sc-Mg crystal

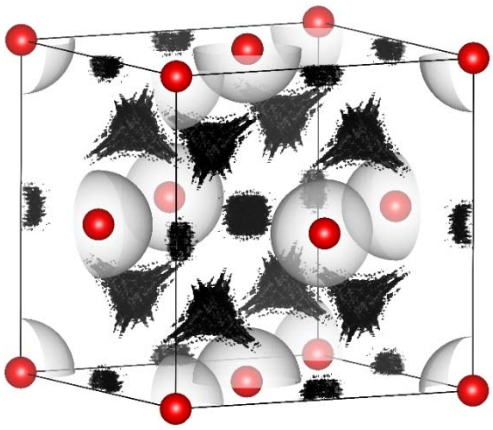

Figure S6.4. 3D CP isosurfaces of fcc-Mg crystal at equilibrium volume with CP= +0.001 (white) and CP = 0.062 (black). Mg nuclei are represented by red spheres.

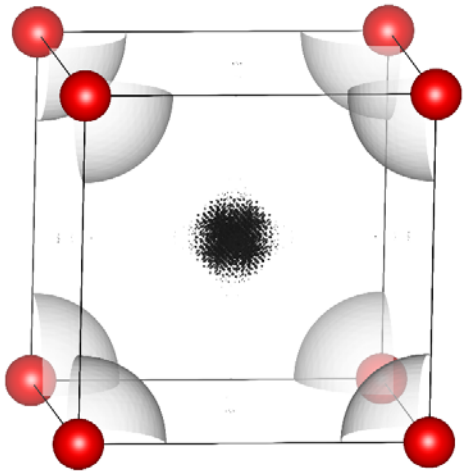

Figure S6.5. 3D CP isosurfaces of sc-Mg crystal at equilibrium volume with CP= +0.001 (white) and CP = 0.046 (black). Mg nuclei are represented by red spheres.

Chemical Pressure Minima-Electronegativity correlations for *fcc*-Na crystal

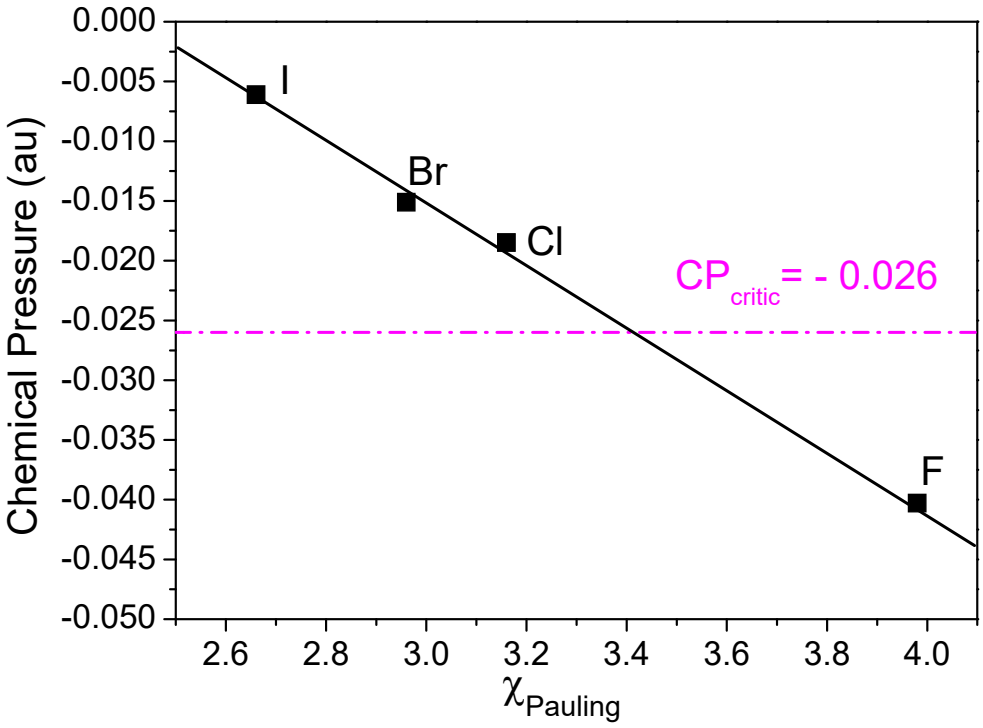

Figure S6.6. Metallic fcc-Na CP value at the 4b position for the different NaX (X = F, Cl, Br, I) compounds against the Pauling electronegativity of the corresponding X atoms (black solid squares). Magenta dash dot line, CP critic value of fcc-Na crystal. Black line corresponds to the linear fit of the data, CP=0.06174–0.0256 $\chi_{Pauling}$.

Chemical Pressure Minima-Electronegativity correlations for and *fcc*-Mg crystal

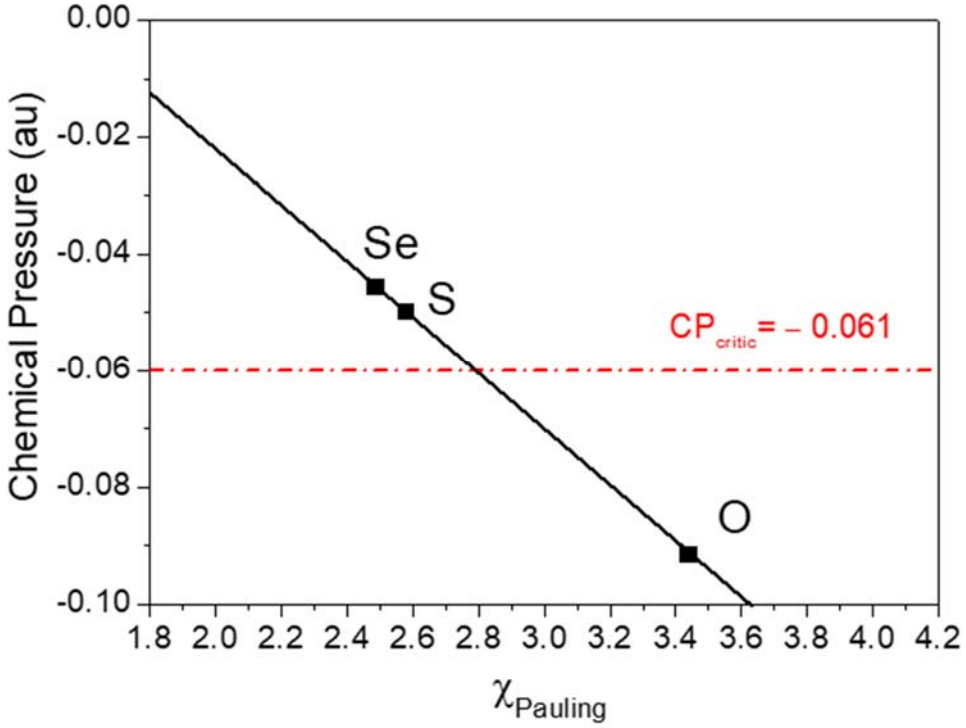

Figure S6.7. Metallic fcc-Mg CP value at the 4b position for the different MgX (X = O, S, Se) compounds against the Pauling electronegativity of the corresponding X atoms (black solid squares). Red dash dot line, CP critic value of fcc-Mg crystal. Black line corresponds to the linear fit of the data, CP=0.0748 – 0.04838$\chi_{Pauling}$.

Chemical Pressure minima-lattice parameter correlation for fcc-Mg phase

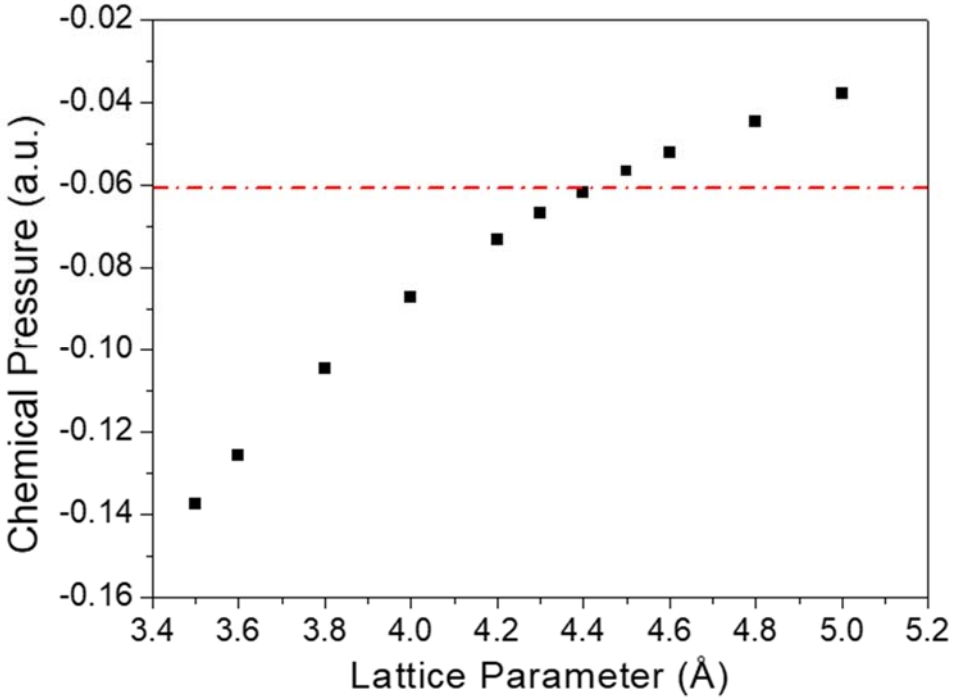

Figure S6.8. CP values at 4b (½, ½, ½) positions of metallic fcc-Mg at different lattice parameters. Dash dotted line represents the critical chemical pressure, CP_{critic}, splitting the compressive (oxidation) and expansive (reduction) regimes.

Description of metal structures

- *fcc*-structure (Ca, Na, Mg)

fcc is a cubic structure belonging to the space group Fm-3m. It contains 4 atoms per unit cell located on the 4a sites at the (0,0,0) position.

- *sc*-structure (Ca at high pressure)

sc is a cubic structure belonging to the space group Pm-3m. This cubic phase contains 1 atom per unit cell located on the 1a sites at the (0,0,0) position.

- CsCl structure (BaSn at high pressure)

CsCl is a cubic structure belonging to the space group Pm-3m with 2 atoms per unit cell located on the 1a and 1b sites. Their positions are (0,0,0) and (1/2,1/2,1/2) respectively.

- hP4 structure (K at high pressure)

hP4 is a hexagonal structure belonging to the space group P63/mmc with 4 atoms per unit cell located on the 2a and 2c sites at (0,0,0) and (1/3, 2/3,1/4) respectively.

Description of inorganic structures.

- rock-salt structure. CaX (X = O, S, Se, Te), NaX (X = F, Cl, Br, I), MgX (X = O, S, Se)

rock salt is a cubic structure belonging to the space group Fm-3m. with 4 formula units per unit cell. Cations are located on the 4a sites at the (0,0,0) position, whereas anions are located on the 4b sites at the (1/2,1/2,1/2) position.

- Fluorite structure (CaF_2)

Fluorite is a cubic structure belonging to the space group Fm-3m. with 4 formula units per unit cell. Cations are located on the 4a sites at the (0,0,0) position, whereas anions are located at the 8c sites at the (1/4,1/4,1/4) and positions.

- Perovskite structure ($BaSnO_3$)

Perovskite is a cubic structure belonging to the space group Pm-3m. Ba are located at 1a sites at the (0,0,0). Sn are located at 1b sites, whose position is (1/2,1/2,1/2). O are located at 3d sites with positions located at (1/2,0,0).

- CsCl structure (CaX (X = O, S, Se) and NaX (X = F, Cl, Br, I) at high pressure)

CsCl is a cubic structure belonging to the space group Pm-3m with 2 atoms per unit cell. Cations are located on the 1a and anions on 1b sites. Their positions are (0,0,0) and (1/2,1/2,1/2) respectively.

Chapter 7

Conclusions

The purpose of this chapter is to summarize the main contributions of this Thesis, as well as to highlight those ideas that may lead to new research lines.

Already from the introduction, we have demonstrated how a pairwise interaction formalism allows us to transfer some concepts well stablished in the high-pressure field to the molecular one, and vice versa. This transferability recalls in the fact that the shape of the potential energy curve can be considered universal and, therefore, the interaction between two atoms either in a molecule or in a crystalline solid –or in any other condensed phase– is described by the same distance–energy relationship. This idea constitutes itself the first contribution of the PhD Thesis, where we have demonstrated that the bulk modulus of a crystal directly depends on the stretching force constant of its diatomic analogues. It is worth mentioning that the bulk modulus constitutes a fundamental parameter in the development of equations of state and, its value is usually considered as a criterion in the synthesis of super– and ultra–hard materials. Our model successfully reproduces the experimental data of ionic, covalent, and even metallic solids, and establish a theoretical framework about the bond characteristics needed to obtain materials with highest compression resistance possible. This is an interesting feature of our model with potential applications in material sciences, however the latter has not been completely developed here in order to maintain the focus of this PhD Thesis.

Indeed, it is the relationship between the bulk modulus and the force constant what led us to consider that the spinodal criterion, or mechanical stability limit, can also be applied to chemical interactions. Up to now, the mechanical stability limit had been exclusively defined as the thermodynamic condition at which the bulk modulus of a macroscopic system is zero, thus determining the maximum negative pressure that bonds in a solid can withstand without breaking, or in the case of liquid phases, to split up. Nonetheless, our results evidenced that in one dimension, it corresponds to the distance where interaction stretching force constant is zero. This analogy also suggested that pressure and volume would scale with force and distance in one dimension respectively, leading to the definition of a spinodal force and spinodal distance.

In order to proof this hypothesis, we have analyzed a classic example in solid state physics: the frequency–temperature dependence (*i.e.* energy) of the longitudinal optical phonon (ωLO, *i.e.* force constant) of some diatomic solids. According to the Born-von Karman model, the frequency ωLO can be directly calculated through the stretching force constant of its pairwise interaction, and as we have shown, this can be expressed as the ratio between the spinodal

force and the difference of equilibrium and spinodal distances. To determine the temperature dependence of the ωLO phonon, we assume that both the spinodal force and the distance difference vary with the temperature as the pressure and volume on the crystal do using the volumetric (thermodynamic) equation of state. Our model excellently reproduces the experimental results in prototypical crystals such as diamond and silicon and allow to separate the so-called extrinsic and intrinsic temperature contributions to the phonon frequency, a problem that had been extensively discussed in the literature in terms of thermal expansion and anharmonic interactions in the crystal. Moreover, thee spinodal concept allows to evaluate the variation of the phonon frequencies using a purely mechanical criterion through the variation of the shape of the interaction curve, and question if it is lawful to separate the intrinsic and extrinsic variations in the crystal.

The previous results point out that the spinodal criterion is also fulfilled in one dimension and, therefore, can be used to determine the conditions in which the rupture (or formation) of a chemical bond occurs. The demonstration of this fact through different examples and methodologies has been the leitmotif of this PhD Thesis, and we can conclude that it has been successfully completed with examples of the C-C and O-H archetypical bonds.

Using theoretical methodologies based on the topological analysis of electron density and related scalar fields, we have demonstrated how the mechanical stability limit is reflected as bonding electronic changes. Specifically, for covalent bonds, the distances at which mechanical instability occurs corresponds to a transition between a shared electrons regimen to radical like atoms state. Based on these results, we have defined the stability limits of a chemical bond. In addition, considering that bond are pairwise interactions, we have evidenced that these limits can be determined from experimentally accessible equilibrium properties: the dissociation energy and the stretching force constant at the equilibrium distance.

The chemical implications of this idea have strong impact in diverse fields, including the nature of the chemical bond, reactivity, mechanochemistry, or synthesis of novel materials by predicting which compounds can be synthesized or not, and the conditions under they would be (meta)stable. However, we want to remark that these conditions represent mechanical instabilities and drastic electronic changes in the molecular bonds, therefore very few experimental results are available to generalize the validity of our hypothesis. As a result, in this thesis we have only been able to analyze in an exhaustive way the C-C and O-H bond, where there are enough transition-

state data, frequencies and computational studies in a enough range of distances to analyze the rupture and formation of these bonds.

Specifically, in the case of CC bond, we realized that different criteria, such as distance histograms, the Laplacian sign change of electron density and CC distances in the transition states of typical CC forming reactions evidences that CC covalent interactions are broken or formed over a similar distance (~ 2Å). In this regard, we performed an analysis of the spinodal criteria of different CC bonds in stable compounds ranging from the typical of 1.54 Å of the ethane to 1.8 Å in the adamantane dimer. Interestingly, the stability limits of this bonds always occur in a narrow range of distances between 1.95 and 2.15 Å. These results imply that the rupture of the C-C bond does not depend on external chemical factors, such as dispersive or hyperconjugative effects, and therefore neither should depend on how the stretching (chemically or mechanically) occurs. Comparing the potential energy curve of the C-C cyclohexene bonds with the analogous profile of the Diels-Alder reaction we evidenced how these were almost coincident to the spinodal point. The constancy in the C-C distances of the transition states was only because these bonds are mechanically unstable close to the spinodal distance.

The latter should not be considered a specific characteristic of the C-C, but rather an intrinsic property of any interaction which only depends on its bonding nature. Moreover, assuming that there is a universal reference for the simple covalent C-C bond, we established a force constant model that perfectly reproduce the experimental results and predict a rupture distance of 2 Å. When compared with other bibliographic models, we realize that when the nature of the interaction is modified, so are its spinodal references and therefore, the spinodal criterion may be used discriminate different chemical interactions.

We want to be clear at this respect, we mean as an interaction change to any modification between the atoms that modify their stability conditions and therefore their electronic distributions. The latter include multiple bonds and, continuing with the same example above, they cannot be considered as distance analogs of its respectively single bonds, that is, a compressed single C-C bond is not a double bond. From this point of view, we believe that several correlations between the bond order, or the electronic density and the distance described in the literature should be reviewed and reconsidered.

Based on the hypothesis that the spinodal criterion may be a criterion to detect interaction changes between two atoms –that is, in their bonding

nature– in this PhD Thesis we have proposed the Chained Interaction Conjecture. Essentially, it establishes that the mechanical and electronic stability conditions of the successive interactions are overlapped giving rise to a covalent–electrostatic–van der Waals sequence of interactions, similar as the one described by the electronic density. As a result, using only a reference equilibrium distance and the values of dissociation energies and stretching force constants (accessible by spectroscopic data or from equations of state in condensed phase), we are able to calculate the breaking points of the various interactions and, what is more suggestive from the chemical point of view, classify and determine the optimal distances to stabilize them. It should be remarked that this conjecture predicts transition distances between interactions in which any kind of union between the atoms is unstable. Accordingly, if a statistically significant sample of distances between two atoms in a collection of compounds were available, we should observe a sequence of maxima and minima associated with the equilibrium points and the transition distances of the successive interactions. Our hypothesis has been successfully validated by analyzing the OH distance histograms, which contains multitude of structural results. Its distance distribution clearly displays two maxima, associated with the most common distances of covalent and electrostatic interactions, and two minima, where less than 50 compounds are described in a sample of more than 10,000. The latter occur at the same distances as the bonding transitions and clearly determine the interaction changes.

We would like to emphasize that, under this point of view, hydrogen bond is not an interaction that depends on the presence of another atom, that is, it is not a triatomic interaction as generally considered in chemistry, but a natural consequence that two atoms, at a given distance, interact according to the most favorable form in terms of its mechanical stability and depending on their electronic distributions. Interestingly, an experimental demonstration of this fact, stated here in molecular terms, is provided by the high–pressure phase of ice (ice X), in which the hydrogen atom is located at the midpoint between two oxygen atoms. This example evidences how the pressure effect would be equivalent to the presence of a third atom of different electronegativity than H.

All the results summarized above and based on the spinodal hypothesis, have underlaying evidenced that the effects exerted by a chemical or mechanical interaction are essentially analogous, that is, both modify the distance between two atoms and, consequently, the conditions of mechanical stability

of the bonds. In other words, there is an equivalence between the mechanical and chemical forces. Within this perspective we can rationalize the chemical effects in terms of pressures, or forces, as well as to understand the phenomena of high pressure as a modification of the chemical interactions. In recent years, our group, in collaboration with the University of Oviedo, has been involved in the development and interpretation of a new quantum formalism named as DFT-Chemical Pressure. Essentially, this formalism uses the latter hypothesis to describe the chemical properties at the atomic level. As a result, we have completed this PhD thesis, applying this methodology to two apparently very different problems, but which clearly illustrate what a pressure perspective can contribute to the atomic-molecular field.

The first one, discusses how local pressures in molecules define regions totally consistent with the molecular bond and lone pairs, in clear analogy with the valence shell electron pair repulsion theory. Indeed, considering that a positive pressure is like a repulsion and a negative like an attraction, we have quantified the activity of the solitary pairs, and related them to the electronegativity of the atom to which they are attached. Our result gives a simple explanation to the electrophilic and/or nucleophile character displayed by some molecules. Likewise, we have studied several non-equilibrium geometries, demonstrating how a change in geometry varies the local distribution of pressures and, therefore, the activity of solitary pairs.

In the final example of this PhD thesis, we have shown how the equivalence between mechanical and chemical pressure is able describe inorganic structures. Some previous studies had evidenced that anions in inorganic compounds induced an effect similar as the pressure does in the metal sublattice. However, to the best of our knowledge, this pressure-oxidation correspondence has relied only on empirical evidences and structural correlations. By means of a Chemical Pressure analysis, we have shown that CP minima appear just at the precise positions where the nonmetallic elements in typical inorganic crystals are hosted. Our results reveal that, when positive pressure is applied to metal sublattice, the pressure minima of these position decreases (becomes more negative), while increases (becomes less negative) under the effect of tensile macroscopic pressures. This analysis has led us to propose a generalized redox-stress equivalence that that is able to account for the two well stablish phenomena observed in solid state chemistry: (i) the expansion or contraction experienced by the metal structure after hosting the nonmetallic element while its topology is maintained and (ii) the increasing or decreasing of the effective charge associated with the anions in

inorganic compounds with respect to the charge already present in the interstices of the metal network Both are intrinsic mechanisms to the metal sublattice and can be understood as an equalization of the electronegativity between the metal subnet and the anion.

Capítulo 7

Conclusiones

El propósito de este capítulo es resumir las principales contribuciones de esta Tesis Doctoral, así como resaltar aquellas ideas que abren futuras vías de trabajo.

Ya en el capítulo introductorio hemos demostrado como el formalismo de las interacciones interatómicas en términos de un potencial de pares permite vincular y transferir algunos conceptos propios del campo de la alta presión al campo molecular, y viceversa. Esta transferibilidad reside en el hecho de que la forma de la curva de energía potencial se puede considerar prácticamente universal y, por tanto, la interacción entre dos átomos -ya sea en una molécula o en un sólido cristalino, o en cualquier otra fase condensada está descrita por la misma dependencia entre la distancia y la energía potencial de interacción. Esta premisa constituye en sí misma la primera contribución de esta Tesis Doctoral, con la demostración de que el valor del módulo de compresión volumétrico de un cristal correlaciona directamente con la constante de fuerza de sus análogos diatómicos. Cabe mencionar que el módulo de compresión volumétrico constituye uno de los parámetros fundamentales en el desarrollo de ecuaciones de estado y que su valor sirve de criterio en la síntesis de materiales super- y ultra-duros. Nuestro modelo reproduce con éxito los valores experimentales de sólidos iónicos, covalentes, e incluso metálicos, estableciendo así una referencia teórica de cuáles son las características que deben presentar los enlaces para obtener materiales con la mayor resistencia posible, lo que da lugar a interesante transferencia hacia la ciencia de materiales, aunque esta transferencia no se haya desarrollado aquí en toda su extensión para mantener el enfoque de esta Tesis Doctoral.

Precisamente, esta relación entre el módulo de compresibilidad y la constante de fuerza de un enlace es la que nos llevó a plantearnos que el criterio espinodal, o de límite de estabilidad mecánica, puede aplicarse también a una interacción típicamente química. Hasta la fecha, la idea de estabilidad mecánica había sido definida exclusivamente como la condición termodinámica a la cual se anula el módulo de compresión de un sistema macroscópico, y determina la máxima presión negativa que podía soportar dicho sistema sin que se produjese la ruptura de sus enlaces en el caso de un sólido, o la disgregación en moléculas en el caso de un líquido. No obstante, nuestros resultados demuestran que, en una dimensión, dicho límite de estabilidad se corresponde unívocamente con la distancia donde se anula la constante de fuerza en una interacción interatómica. Dicha analogía también sugería que la presión y el volumen escalarían, respectivamente, con la fuerza y la distancia en una dimensión, desembocando en la definición de la fuerza

espinodal y la distancia espinodal. Para demostrar la validez de esta hipótesis, analizamos un ejemplo clásico en física del estado sólido: la dependencia con la temperatura (i.e. energía) que presenta la frecuencia del fonón longitudinal óptico (ω_{LO}, i.e. constante de fuerza) de algunos sólidos diatómicos modelo. Acudiendo al modelo clásico de Born-von Karman, la frecuencia ω_{LO} puede calcularse directamente a través de la constante de fuerza de una interacción par, y aquí hemos demostrado que dicha constante de fuerza par depende directamente de la ratio entre la fuerza espinodal y la diferencia de distancias de equilibrio y espinodal. Para determinar la dependencia de ω_{LO} con la temperatura, asumimos que éstas varían de manera análoga a como lo hacen la presión y el volumen en el cristal, utilizando la ecuación de estado volumétrica (termodinámica) para evaluar dichas dependencias. El modelo propuesto predice de manera excelente los resultados experimentales de cristales como el diamante y el silicio y permite además discriminar las denominadas contribuciones extrínseca e intrínseca a la variación de la frecuencia fonónica, un problema que se había discutido extensamente en la literatura en términos de la expansión térmica e interacciones anarmónicas en el cristal. Estos resultados indican que el concepto espinodal permite evaluar la variación de las frecuencias fonónicas utilizando un criterio puramente mecánico a través de la variación de la forma de la curva de interacción, y cuestionan hasta qué punto es lícito separar las variaciones intrínseca y extrínseca en el cristal.

Los resultados anteriores demostraban que el criterio espinodal se cumple también en una dimensión y, por tanto, puede utilizarse para determinar las condiciones en las que se produce la ruptura (o formación) de un enlace químico. La demostración de este hecho a través de diferentes ejemplos y metodologías ha sido el *leitmotiv* de esta Tesis Doctoral, y podemos concluir que se ha cumplido con éxito.

Así, utilizando metodologías teóricas basadas en el análisis topológico de la densidad electrónica y campos escalares derivados, hemos analizado cómo la estabilidad mecánica se refleja en los cambios electrónicos. En concreto, para los enlaces covalentes, las distancias a las cuales se produce la inestabilidad mecánica llevan asociadas una transición entre un régimen de electrones compartidos a un estado de átomos radicalícos. Estos resultados nos han permitido definir los límites de estabilidad de un enlace químico. Además, considerando una interacción par para el enlace químico hemos demostrado que dichos límites pueden determinarse a partir de propiedades de equilibrio

accesibles experimentalmente: la energía de disociación y la constante de fuerza a la distancia de equilibrio.

Las implicaciones en la Química de esta idea abarcan temas tan diversos como la naturaleza del enlace, la reactividad, la mecanoquímica o incluso, la posibilidad de delimitar qué compuestos son sintetizables o no, y en qué condiciones serían (meta)estables. No obstante, dado que éstas condiciones reflejan situaciones de inestabilidad mecánica y cambios electrónicos drásticos, hay muy pocos resultados experimentales que permitan generalizar la validez de nuestra hipótesis. Por ello, en esta tesis hemos podido únicamente analizar de forma exhaustiva los enlaces C-C y O-H donde hay datos de estados de transición, frecuencias y estudios computacionales en un rango de distancias suficientes como para analizar la ruptura y formación de estos enlaces.

En concreto, para el caso de los enlaces C-C, nos dimos cuenta de que diferentes criterios, como los histogramas de distancia, el cambio de signo de la laplaciana de la densidad electrónica y las distancias C-C en los estados de transición de las reacciones de formación CC típicas, indican que las interacciones covalentes C-C se rompen o se forman en una distancia similar (~ 2Å). Por ello realizamos un análisis del criterio espinodal de diferentes enlaces C-C en compuestos estables que abarcaban distancias desde la típica de 1.54 Å hasta 1.8 Å y concluimos que el límite de estabilidad de este enlace ocurría siempre en un estrecho rango de distancias comprendidas entre 1.95 y 2.15 Å. Estos resultados implican que la ruptura del enlace C-C no dependen de factores químicos externos, tales como efectos dispersivos o hiperconjugativos, y que por lo tanto tampoco debían de depender de cómo se produce la elongación. Comparando la curva de energía potencial de los enlaces C-C de ciclohexeno con el perfil análogo de la reacción de Diels-Alder vimos como estos eran prácticamente coincidentes hasta el punto espinodal. La constancia en las distancias C-C de los estados de transición se debía únicamente a que estos enlaces son mecánicamente inestables en el entorno de la distancia espinodal.

Este hecho no se debe considerar especifico de los C-C, sino más bien una propiedad intrínseca de cualquier interacción que solo depende de la naturaleza del enlace. Es más, suponiendo que existe una referencia universal para el enlace C-C covalente simple establecimos un modelo de constante de fuerza que reproducía perfectamente los resultados experimentales y predecía un punto de ruptura para estos enlaces alrededor de 2 Å. Al compararlo con otros modelos descritos en la literatura, vimos que, cuando la naturaleza de la interacción se modifica, también lo hacen sus referencias espinodales y, por

lo tanto, desde este punto de vista, el criterio espinodal permite discriminar entre las diferentes interacciones químicas.

En este sentido queremos dejar claro que nos referimos como cambio de interacción a cualquier modificación entre los átomos que altera sus condiciones de estabilidad y por tanto su distribución electrónica. Esto incluye a los enlaces múltiples y, continuando con el ejemplo anterior, no se pueden considerar como una evolución continua en función de la distancia, es decir un enlace C-C simple comprimido no es un enlace doble. Desde este punto de vista, creemos que varias de las correlaciones del orden de enlace, o la densidad electrónica, con la distancia descritas en la bibliografía deberían ser ampliamente revisadas y reconsideradas.

Basándonos en la hipótesis de que el criterio espinodal debe servir de criterio para detectar cambios en el tipo de interacción entre dos átomos -esto es, en la naturaleza de su enlace- en esta Tesis Doctoral hemos propuesto la conjetura de interacciones encadenadas (*Chained Interaction Conjecture*). En esencia, ésta establece que se produce un solapamiento en las condiciones de estabilidad mecánica y electrónica de las sucesivas interacciones, dando lugar a una secuencia covalente-electrostática-van der Waals similar a la descrita por la densidad electrónica. De esta forma, conociendo únicamente una distancia de equilibrio y valores de energías de disociación y constantes de fuerza (accesibles mediante resultados espectroscópicos o a partir de ecuaciones de estado en fase condensada), nuestra aproximación permite calcular los puntos de ruptura de las diversas interacciones y, lo que es más sugerente desde el punto de vista químico, clasificarlas y determinar las distancias óptimas para estabilizarlas. Cabe destacar que esta conjetura predice distancias de transición entre interacciones en las cuales cualquier tipo de unión entre los átomos es inestable. Esto quiere decir que, si se dispusiese de una muestra estadísticamente significativa de distancias entre dos átomos en una colección de compuestos, deberíamos observar una secuencia de máximos y mínimos asociadas, respectivamente, a los puntos de equilibrio y las distancias de transición entre las sucesivas interacciones. Nuestra hipótesis se ha validado con éxito mediante el análisis de los histogramas de distancias OH, que sí están disponibles a partir de multitud de resultados estructurales, donde claramente hay dos máximos, asociados a las distancias más comunes de las interacciones covalentes y electrostáticas, y dos mínimos, donde hay descritos menos de 50 compuestos en una muestra de más de 10,000. Estos últimos ocurren a las mismas distancias que las zonas de transición entre enlaces y claramente determinan los cambios de interacción. Nos gustaría

señalar que, desde este punto de vista, el enlace de hidrogeno no es una interacción que dependa de la presencia de otro átomo, es decir, no es una interacción triatómica como generalmente se ha considerado en química, sino una consecuencia natural de que dos átomos, a una distancia dada, interaccionan de acuerdo a la forma más favorable, desde el punto de vista de la estabilidad mecánica, en función de sus distribuciones electrónicas. La demostración experimental de este hecho, formulado aquí en términos moleculares, la proporciona la fase X de alta presión del hielo, en la que el átomo hidrógeno se sitúa exactamente entre dos átomos de oxígeno, lo que demuestra que un puro efecto de presión sería equivalente a la presencia de un tercer átomo de diferente electronegatividad que el H.

Todos estos resultados basados en la hipótesis espinodal han evidenciado de manera subyacente que los efectos ejercidos por una interacción química o mecánica son en esencia análogos, esto es, que ambos modifican la distancia entre dos átomos y, en consecuencia, las condiciones de estabilidad mecánica de su enlace. O, dicho de otro modo, hay una equivalencia entre la fuerza mecánica y química. Esta visión permite entender los efectos químicos en términos de presiones, o fuerzas, así como entender los fenómenos de alta presión como una modificación de las interacciones químicas. En los últimos años, nuestro grupo, en colaboración con la universidad de Oviedo, ha estado involucrado en el desarrollo y la interpretación del formalismo cuántico denominado *Presión Química-DFT*, que en esencia utiliza esta hipótesis para describir las propiedades químicas a nivel atómico. Por ello esta Tesis Doctoral se completa aplicando está metodología a dos problemas aparentemente muy dispares, pero que ilustran claramente qué puede aportar la variable presión al ámbito atómico-molecular.

En el primero de ellos se discute como las presiones locales en moléculas permiten definir regiones totalmente consistentes con los pares de enlace y pares solitarios de las moléculas, en evidente analogía con la teoría de repulsión de pares de electrones de valencia. Así, considerando que una presión positiva constituye una repulsión y una presión negativa una atracción, hemos cuantificado la actividad de los pares solitarios, y la hemos relacionado con la electronegatividad del átomo al que están unidos, dando una explicación sencilla al carácter electrófilo y/o nucleófilo que presentan algunas moléculas. Así mismo, hemos estudiado varias geometrías de no equilibrio, demostrando cómo un cambio de la geometría varía la distribución local de presiones y, por tanto, la actividad de los pares solitarios.

En el último ejemplo de esta Tesis Doctoral hemos demostrado cómo la equivalencia entre la presión mecánica y la presión química permiten describir las estructuras inorgánicas. Algunos estudios previos habían propuesto que los aniones en compuestos inorgánicos inducían un efecto similar al de la presión en la subred metálica. Sin embargo, hasta donde nosotros sabemos, dicha correspondencia presión-oxidación estaba basada únicamente en evidencias empíricas y correlaciones estructurales. Aquí hemos demostrado, mediante un análisis de Presión Química, que los mínimos de presión negativa aparecen precisamente en las posiciones cristalográficas donde se alojan los aniones. Nuestros resultados indican que, al aplicar una presión positiva a la subred metálica, los valores de presión en los mínimos aumentaban, mientras que éstos disminuyen tras la aplicación de presiones negativas. Este análisis nos ha llevado a proponer una equivalencia redox-estrés generalizada que explica dos fenómenos bien conocidos en química estructural: (i) una sub-estructura metálica, manteniendo su topología, se expande o contrae después de alojar el elemento no metálico, y (ii) la carga efectiva de los aniones en las estructuras inorgánicas es diferente a la que ya está presente en los intersticios de la subred metálica. Ambos son mecanismos intrínsecos a la subred metálica y pueden entenderse como una ecualización de la electronegatividad entre la subred metálica y el anión.

Chapter 8

Perspectives

The contributions developed in this PhD Thesis provides some directions for future work that worth to be explored in length. The purpose of this chapter is to summarize some of them, as well as to show their potential implications. We want to remark here that we have already several preliminary results, and some of them will be presented and discussed in this final section.

- One of the ideas that this PhD Thesis has evidenced is that the application of pressure (positive or negative) may lead to effects like those resulting from chemical interactions. In this regard, the understanding of pressure effects in molecules can provide fruitful information about chemical processes as well as to understand the transformations (phase transitions or chemical reactions) observed in high pressure experiments. Unfortunately, a difficulty arises to calculate the pressure in molecules because the molecular volume is ill-defined. However, according to our Chained Interactions Conjecture, any interaction cannot be extended far beyond the van der Waals limit of stability, and any space excluded from this region should have negligible effects in the molecule. Under this assumption, the van der Waals surface constitutes a reliable limit of the effective molecular volume. As pointed by several authors, the van der Waals volume can by determined integrating the space region enclosed by the electron density isovalue of $1 \cdot 10^{-3}$ a.u. Within this approximation, we have performed several calculations in adamantane by contracting all the bonds of this highly symmetric molecule from its equilibrium configuration. These calculations allow us to obtain pairs of (energy-van der Waals volume) data, from which the pressure can be estimated by applying directly the thermodynamic definition: the derivative of the energy respect to the volume. To check the validity of our approach, we have selected the adamantane molecule because it can be considered the smallest cluster of diamond preserving the local symmetry. With this in mind, we compare our calculated pressures in the adamantane molecule with those provided by the diamond equation of state in Figure 8.1, together with the equation of state of solid adamantane for the sake of comparison. Let us emphasize that compressing an isolated adamantane molecule in an experiment is virtually an impossible task, even in the solid phase, because the local pressure acting on the molecule is not known. As demonstrated in Figure 8.1, applying an external hydrostatic pressure to solid adamantane leads to a drastic reduction of the van der

Waals volume, but the pressure acting over the adamantane molecules is less than one order of magnitude.

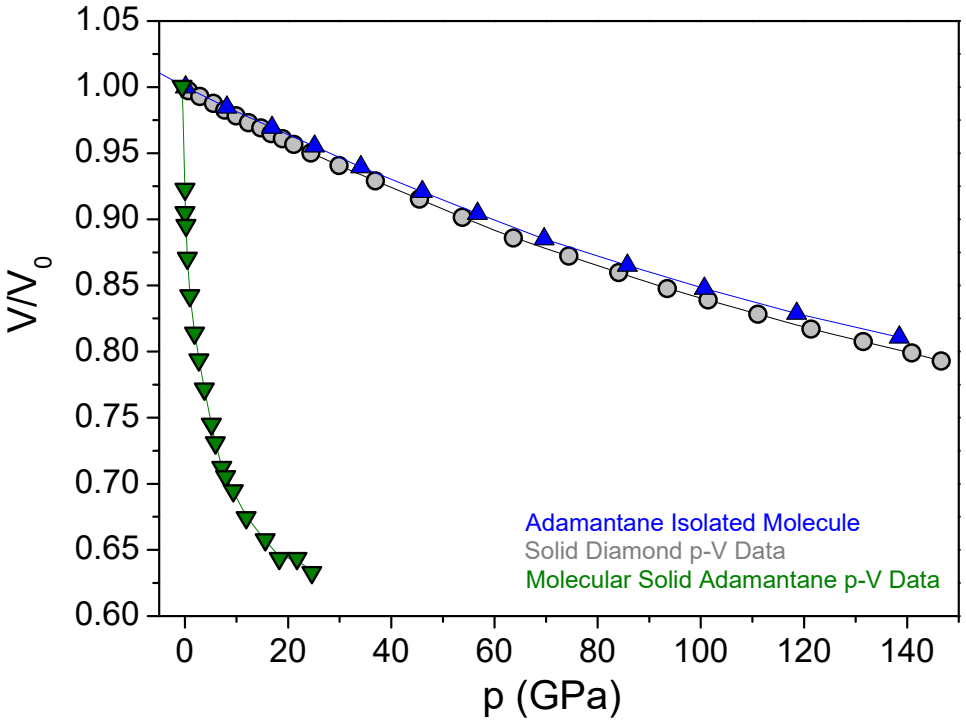

Figure 8.1. Pressure-Volume equation of state: Experimental data for diamond (grey dots), Experimental data for adamantane (green down triangles), and van der Waals volume of the adamantane molecule (blue up triangles, see text for explanation).

On the other hand, the striking agreement between the equation of state of diamond and the (pressure, van der Waals volume) data of the adamantane molecule demonstrates that we are in the right way for predicting the effect of pressure in the length of the chemical bonds, a long-standing challenge in the high pressure field, where only few theoretical models are available. See for example reference [https://doi.org/10.1107/S0108768103010474].

The huge difference in the pressure response of an adamantane molecule either isolated or in the molecular solid indicates that our previous approach can be very useful to study the effect of pressure in non-covalent interactions. Such weak interactions are strongly modified by the application of moderate pressures, leading to sequential phase transitions and, ultimately, novel chemical reactivity. The validity of our model in this kind of interactions is shown in Figure 8.2, where we have estimated how distance between the two molecules in a benzene

dimer distance varies with pressure. Again, compared to the bibliographic data reported by R. Bini et al. our results are in excellent agreement. [https://doi.org/10.1038/nmat1803]

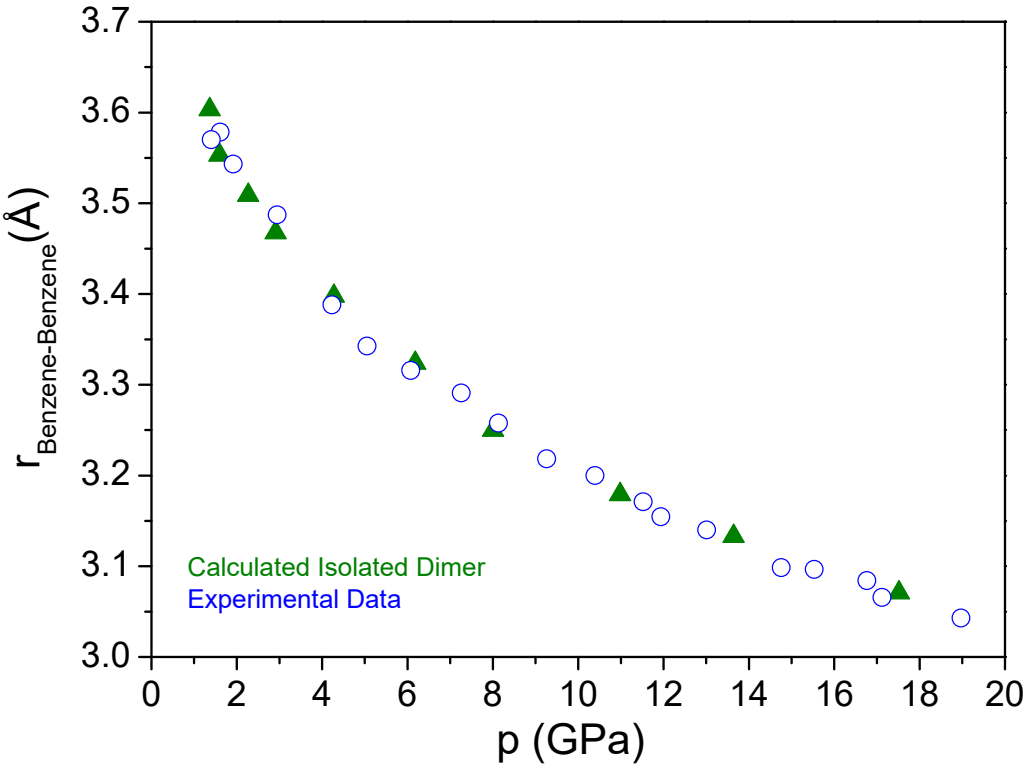

Figure 8.2. a) Calculated distance between the two molecules in a benzene dimer (green triangles), and b) Experimental data from the solid phase (https://doi.org/10.1038/nmat1803).

- Special attention deserves the idea that chemical reactions can be understood in terms of mechanical forces (pressures). Indeed, understanding the reaction mechanism from a combined electronic and mechanical perspective can provide a valuable information about the transition states and how to reduce the activation energy or even how to produce new reaction products. In this regard we have begun to develop chemical pressure calculations in non-hydrostatic conditions, where the volume modification is defined as the variation of van der Waals volume along the intrinsic reaction coordinate. Of course, the interpretation of this pressures recalls directly in the spinodal criteria as the maximum negative pressure which bonds can withstand.

- Another issue that deserves to be explored is the fact that pressures can provide reliable basis to understand atomic and molecular properties such as the electronegativity and lone pair activity. We are already exploring the possibility to integrate the chemical pressure field in the basins provided by the topological analysis of the electron density and the electron localization functions. The latter defines atomic regions, bond and lone pairs, where the integration of the chemical pressure can provide a quantitative account of the forces exerted by the atoms. The impact of these studies includes identification of inactive lone pairs, bond strength measurements, electronegativity estimations, and changes in the chemical interactions under pressure. As an example, we show in Figure 8.3, the variation of the local pressures of the Mg and O atoms in the MgO crystal as calculated from the integration of the chemical pressure in the Bader basins.

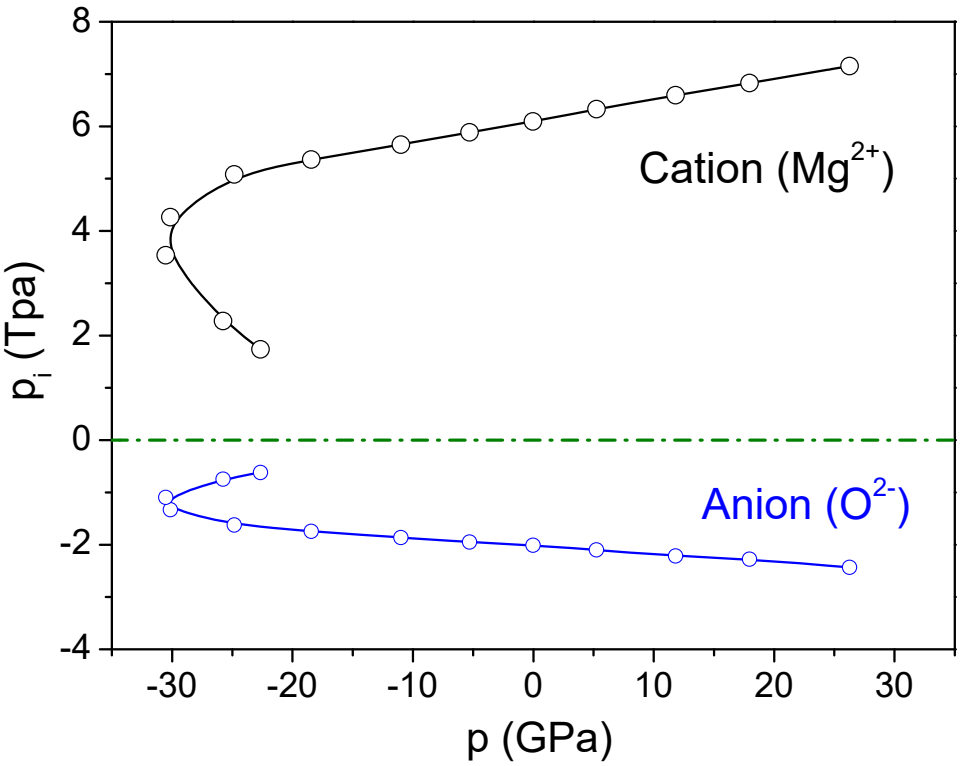

Figure 8.3. Local pressures (p_i) for the cation (black dots) and the anion (blue dots) at different pressures in the MgO crystal.

Firstly, note that at zero pressure neither the pressure of the cations nor the one of the anions are zero, which can be understood as a consequence of the ionic interaction displayed by the charged species in MgO that induce a non-zero force in their electronic distributions.

Indeed, the pressure of the oxygen (anion) is negative whereas the cation is positive, thus reflecting the intuitive chemical idea that anions are those who tend to accumulate electron density and therefore are more compressible than the cations. As a result, the MgO structure at equilibrium results from an equilibration of the ionic pressures. Interestingly, when we analyze the effect of the compression on the crystal, we observe that the pressure of the cation is increased, while the pressure of the anion is reduced. This is in excellent agreement with our results displayed in chapter 6 and evidences an accumulation of the charge in the oxygen atoms resulting from a volume reduction. Based on our results of this PhD, we can state that the electronegativity of the oxygen is increased whereas that for Mg is decreased.

- Finally, from the methodological point of view, up to now the DFT-Chemical Pressure methodology was only available for *Abinit* software, a program devoted to calculations in crystals. *Abinit* uses periodic boundary conditions and pseudopotentials, which clearly limits the calculation methods and the potential systems which can be studied. So that, we are currently developing new code to calculate the chemical pressure distributions in molecules directly from all-electron first principles calculations. Specifically, our program uses the wavefunction file from gaussian 09 and the potential energy maps calculated with the *critic2* code.